TRIAXIAL EFFECTS IN

CONCRETE-FILLED TUBULAR STEEL COLUMNS

A Thesis presented for the degree of

Ph.D. (Engineering)

in the University of London

by

Hirak Kumar Sen, B.C.E. (Hons.), M.Tech.

Imperial College of Science and Technology

London

July, 1969

T O M Y P A R E N T S

ABSTRACT

The work described in this thesis consists of three phases:

Phase I - Uniaxial analysis: A computer program has been written in a form suitable for calculating the failure loads for a large number of eccentrically-loaded, circular or rectangular concrete-filled columns, using the uniaxial material properties and the part cosine-wave assumption.

The experimental failure loads of 22 eccentrically-loaded square and rectangular columns are compared with the computed loads, and a satisfactory agreement is found, i.e. triaxial effects are negligible for the columns tested.

Phase II - Stub columns: The elasto-plastic biaxial stresses in the steel are calculated from observed strains for 14 of the available tests on concentrically-loaded stub columns, using the generalised flow-law for plastic solids. The triaxial stresses in the concrete are then calculated from simple statics. It is found that near failure the longitudinal compression in the steel is approximately equal to three-quarters of the uniaxial yield stress, and the hoop tension is half the longitudinal compression in magnitude, while the longitudinal compression in the concrete core is twice the strength of uncontained concrete.

The equivalent longitudinal 'stress-strain relationships' for the steel and concrete are represented by equations, and a formula is given for predicting the failure load of concentrically-loaded stub columns.

Phase III - Triaxial analysis: Moment-load-curvature characteristics

are experimentally determined for 35 circular columns comprising 7 tube thicknesses with 5 levels of axial load for each thickness. Triaxial effects are found to be insignificant when the axial load is less than 40 per cent of the sum of the uniaxial compressive strengths of the steel and concrete. For higher axial loads, triaxial effects are taken into account by using the equivalent stress-strain relationships of Phase II in a semi-rational analysis.

All the experimental moment-load-curvature characteristics are numerically simulated on a digital computer.

ACKNOWLEDGEMENTS

The author wishes to express his gratitude and appreciation to the following people:

Dr. J. C. Chapman, who supervised this work, for his guidance and encouragement

Professor S. R. Sparkes, for his permission to pursue the work at Imperial College

The Commonwealth Scholarship Commission, for the award of their scholarship

The Construction Industry Research and Information Association (CIRIA), The International Committee for the Study and Development of Tubular Structures (CIDECT) and Messrs. Stewarts and Lloyds Ltd., for their joint financial help

Mr. P. J. D. Guile of the Structures Laboratory at Imperial College, for conducting many of the moment-curvature experiments and being mainly responsible for the design of the bending and axial compression rig

The management of the Imperial College Computer Centre, for their generous provision of free computer time

The staff and postgraduate students of the Structures Section, in particular Dr. P. K. Neogi, Dr. E. H. Brown and Dr. A. K. Basu, for their valuable discussions

Miss J. Clarke for typing the thesis.

CONTENTS

NOTATION

A_c, A_s	cross-sectional areas of the concrete and steel;
A_{ci}, A_{si}	areas of the concrete and steel in a strip;
b	breadth of a rectangular tube;
d, d_i	external and internal diameter or depth;
E_c, E_s	Young's moduli of the concrete and steel;
E_{Tc}, E_{Ts}	tangent-moduli of the concrete and steel;
e	end eccentricity of the load;
e_i	elastic component of strain;
e_{major}, e_{minor}	eccentricities about the major- and minor-axis;
e_o	fictitious end eccentricity representing initial out-of-straightness;
f	yield function;
f_{cu}, f_{cy}	cube and cylinder strength of the concrete;
G_i	distance from the centroidal axis of the cross-section to the centre of a strip;
I_c, I_s	moments of inertia of the concrete and steel;
k	radius of gyration;
L	half cosine wave length;
l	effective length of the column;
M_c, M_T	maximum calculated and test moments;
M_{eo}, M_{io}	external and internal moments at the mid-height section of the column;
M_i	internal moment;
m	modular ratio $(= E_s/E_c)$
P_{ax}, P_{ay}	failure loads of a concentrically-loaded column about the major- and minor-axis;
P_c, P_s	loads carried by the concrete and steel;
P_H	failure load of a concentrically-loaded concrete-filled stub column;

P_i internal axial force;

P_L nominal squash load = $A_s\sigma_y + A_c\sigma_m$;

P_m calculated maximum load of an eccentrically-loaded column;

P_T test failure load;

P'_T load up to which strain readings are available (Chapter 3);

P_u approximate failure load of a concentrically-loaded stub column (Chapter 5);

P_w working load;

P_x, P_y calculated failure loads under uniaxial bending about the major- and minor-axis respectively (Chapter 2);

P_{xy} calculated failure load under biaxial bending;

P_y load on a concentrically-loaded stub column at the first yield of the steel (Chapter 3);

p_i plastic component of strain;

$Q_1, Q_2, \ldots, Q_n$ generalised stress components;

t thickness of the tube wall;

W_e work done by the external agency during a cycle of loading and unloading;

W_T total work done;

Y distance of the neutral axis from the centroidal axis;

Y_i distance from the centroidal axis to the centre of a strip;

Y_o value of Y at the mid-height section of the column;

y total deflection;

y_o total deflection at the mid-height section;

y_{oc} initial central deflection;

α $-1/\gamma$

β σ_{sH}/σ_{sL}

β_1 $\sqrt{1 - \beta + \beta^2}$

δ additional deflection under the load;

δ_o	value of δ at the mid-height section;
δ_1, δ_2, δ_3	deflections at points 1, 2 and 3 (Figure 4.2A);
ε	strain;
ε_c	maximum compressive strain in the concrete of an eccentrically-loaded column under the maximum load;
ε_{cL}, ε_{cR}	longitudinal and radial strains in the concrete;
ε_{cv}	volumetric strain in the concrete;
ε_i	strain at the centre of a strip;
ε_m	strain corresponding to the peak stress in the concrete under uniaxial compression or flexure (Figure 2.2);
ε_{sH}, ε_{sL}	hoop and longitudinal strains in the steel;
ε^e_{sH}, ε^p_{sH}, ε^e_{sL}, ε^p_{sL}	elastic and plastic components of the hoop and longitudinal strains in the steel;
ε_y	yield strain of steel;
ε_1, ε_2, ε_3, ε_4	strains in gauges 1, 2, 3 and 4 (Figure 4-2B);
η	initial imperfection parameter;
γ	$(2\sigma_{sL} - \sigma_{sH})/(2\sigma_{sH} - \sigma_{sL})$;
γ_c, γ_s	material-factors for the concrete and steel;
λ	a constant used in the failure criteria for concrete (equation 3.21);
ν_c, ν_s	Poisson's ratios for the concrete and steel;
ρ	curvature;
ρ_o	curvature at the mid-height section;
ρ_{oc}	initial central curvature;
σ	stress;
σ_{ci}, σ_{si}	stresses in the centre of the i-th strip for the concrete and steel;
σ_{cL}, σ_{cR}	longitudinal and radial stresses in the concrete;
σ_{cv}	$\sigma_{cL} + 2\,\sigma_{cR}$;
σ_m	peak stress in the concrete under uniaxial compression or flexure;

σ_{sH}, σ_{sL}	hoop and longitudinal stresses in the steel;
σ_y	yield stress in the steel;
σ_1, σ_2, σ_3	principal stresses;
τ	shear stress;
τ_c	shear stress in the concrete.

CHAPTER 1

INTRODUCTION

1.1 GENERAL

Tubular sections, either empty or filled with concrete, are being increasingly used as structural members. The recent uses include the roofing of sports buildings in France [1.1], the Boeing 747 hangar at London Airport [1.2], port installations, domes and bridges in Italy [1.3], masts, towers, signal gantries [1.4] and a 32-storeyed building [1.5] in Belgium, piers for a four-level motorway interchange [1.6] in England, etc.

When a tube is acting as a compression member, filling the tube with concrete is advantageous because it increases the load-carrying capacity without increasing the size of the column. The tube shutters the concrete, and protects the surface from damage. The concrete inhibits wrinkling of the tube.

Due to the large strain capacity of filled tubes there may be applications where seismic loading can occur. The filled tube also appears to offer some advantages in piling.

However, for application in building, the fire resistance of filled tubes needs to be established, and there is at present conflicting evidence as to the increase of resistance afforded by the filling. The possibility of the tube bursting due to fire or due to freezing needs further investigation.

For small diameter tubes there may be some difficulty in ensuring that no voids occur and for this reason factory-filled tubes appear advantageous. For bridge columns the diameter may be such as to allow full site inspection.

The exterior of a filled tube is exposed to the same corrosive action as any other steel structure, and requires similar protection [1.7].

The design of joints with columns of the adjoining floor and with beams is being studied at the present [1.8].

In this country, tubular columns received increased attention following a decision (1963) to use this type of column in the multi-level interchange between motorways M4 and M5 at Almondsbury [1.6]. There was no suitable Code of Practice, and 35 concrete-filled columns were designed and constructed on the basis of exploratory tests [1.9] conducted at the Building Research Station and Imperial College. A programme of research was then initiated at Imperial College to provide design data in respect of tubular columns. Considerable work has since been done at Imperial College on composite columns in general, in connection with the preparation of CP 117 (Part 3) - Composite Columns [1.10]. The current investigation forms part of the overall programme.

Before the programme of research may be discussed it is necessary to give a brief description of the structural behaviour of concrete-filled tubular columns. This may best be done by taking the two limiting cases of eccentrically-loaded columns, namely (i) a short length ($l/d \leq 5$, say) of filled tube, called a stub column, subjected to concentric loading only, and (ii) a filled tube of any length subjected to bending alone.

In the first limit, when a stub column is loaded concentrically, in the early stages of loading the Poisson's ratio for concrete is lower than

for steel, and the steel has no restraining effect on the concrete core. As the longitudinal strain increases, however, the lateral expansion of uncontained concrete gradually becomes greater than that of steel. A radial pressure therefore develops at the steel-concrete interface, thereby restraining the concrete core and setting up a hoop tension in the tube. At this stage the concrete is stressed triaxially and the steel biaxially. As the hoop tension increases the longitudinal compression in the steel decreases while that in the contained concrete increases. The failure load of all practical stub columns is considerably greater than the sum of the uncontained compressive strengths of the steel and concrete, because the loss of longitudinal compression in steel is more than compensated by the augmentation of the strength of concrete.

In the second limit, when the filled tube is acting like a beam, a large part of the concrete is cracked and triaxial effects are negligible. Therefore the behaviour of a filled tube under bending alone, may be calculated from the uniaxial stress-strain properties of the steel and concrete.

Thus the concentrically-loaded stub column shows the maximum triaxial effects while the beam has no triaxial effects. Any intermediate case of of a beam-column, i.e. eccentrically-loaded columns or long columns, has an amount of beneficial triaxial effects dependent primarily on the length and eccentricity.

The overall programme of research into the behaviour of filled tubes was planned at Imperial College in three phases:

Phase I: Uniaxial analysis - The failure load of eccentrically-loaded columns was to be calculated from uniaxial material properties both by determining the exact deflected shape and by assuming this shape to be part of a cosine-wave [1.11]. These loads would then be compared with

experimental failure loads to confirm the theory and to establish the slenderness and eccentricity beyond which triaxial effects are negligible.

Phase II: Stub columns - A series of tests on concentrically-loaded stub columns was planned to study and analyse the maximum triaxial effects that may occur in a filled tube.

Phase III: Triaxial analysis - The comparison of experiments with the uniaxial analysis may determine the slenderness and eccentricity below which triaxial effects are significant. However, the difficulties inherent in a triaxial analysis of an eccentrically-loaded concrete-filled tube, where the cross section is subjected to non-uniform longitudinal compression, can be appreciated. In such an analysis the column must be treated as a three-dimensional continuous medium, with appropriate boundary conditions. For concrete-filled tubes the medium is not homogeneous, consisting as it does of the concrete core and the steel shell. The problem is further complicated by the absence of any suitable theory for the inelastic deformation of concrete under three unequal principal stresses.

From the above considerations, a rigorous triaxial analysis seemed impracticable, and it was intended to account for triaxial effects in eccentrically-loaded columns by incorporating experimentally determined moment-load-curvature relationships in the column analysis. It was anticipated that the knowledge of triaxial effects in stub columns (Phase II) would assist the numerical simulation of the experimental moment-curvature relationships.

Prior to this investigation, in Phase I, 18 eccentrically-loaded circular columns were tested at Imperial College, and it was shown [1.12,1.13] from the results of these experiments and of experiments conducted elsewhere [1.14, 1.15, 1.16] that the uniaxial failure load is in good

agreement with the experimental load for columns with l/d ratios greater than 15, and that for shorter columns with nearly concentric loading triaxial effects may be significant. It was also shown that the part cosine-wave assumption greatly simplfies the analysis and gives failure loads up to only 5 per cent less than the failure loads computed by the exact approach. However, a computer program suitable for calculating a large number of failure loads, and data on square and rectangular columns were not available at the onset of this investigation.

In Phase II, 22 concentrically-loaded stub columns were tested at Imperial College [1.12], and similar tests were done elsewhere [1.17,1.18].

It was at this stage that the present investigation was started, and its objectives are discussed below.

1.2 PURPOSE OF THIS THESIS

Phase I: Uniaxial analysis - Since only those columns which have l/d ratios less than 15 and nearly concentric loading, show significant triaxial effects, it was decided to develop a computer program suitable for the production of failure load tables for a comprehensive range of sections, based on the uniaxial material properties and the part cosine-wave assumption. These tables would give an accurate estimate of the failure load where triaxial effects are negligible, and would give an interim, but conservative estimate where triaxial effects are significant. When the triaxial analysis (Phase III) is complete it is intended to replace the tabulated uniaxial loads by the augmented loads wherever necessary.

Phase I also included the testing of square and rectangular columns for a confirmation of the computed load, so that the tables could include square and rectangular sections as well.

Phase II: Stub columns - The biaxial stresses in the steel were to be calculated from experimentally observed strains, throughout the elasto-plastic range, for a selection of existing stub column tests. The calculation of the post-elastic biaxial stresses in steel, from known load-strain relationships, is not straightforward; this was to be accomplished by using the generalised flow-law for plastic solids.

Once the stresses in the steel are known from experimental load-strain relationships, the stresses in concrete may be calculated from simple statics. This would give the 'equivalent' relationship between the longitudinal stress and longitudinal strain for the biaxially stressed steel and the triaxially stressed concrete. It was anticipated that these equivalent stress-strain relationships would be of use in Phase III for numerically simulating the experimental moment-load-curvature characteristics.

Phase III: Triaxial analysis - The objective of this investigation in Phase III, was to test a number of sections under fixed axial loads and increasing end moments in order to determine the load-moment-curvature characteristics. The objective also included the numerical simulation of the experimental moment-load-curvature characteristics on a digital computer.

The method of predicting the failure loads, for a given length and eccentricity, from predetermined moment-load-curvature characteristics of the section is well known [1.20]. This thesis presents a method of generating moment-load-curvature relationships in agreement with experiments, therefore it is now possible, in principle, to predict the failure loads of eccentrically-loaded columns, taking triaxial effects into account. The reason why this final objective is not fulfilled, as a part of the present investigation, is discussed later.

CHAPTER 2

FAILURE LOADS BASED ON UNIAXIAL MATERIAL PROPERTIES

2.1 INTRODUCTION

Neogi, Sen and Chapman [2.1] showed that failure loads of circular columns, calculated on the basis of the part-cosine wave assumption and the uniaxial stress-strain relationships for the steel and concrete were in good agreement with the test loads of slender columns ($l/d \geq 15$). For shorter columns the test load may be greater than the failure load, because of the augmentation in the strength of concrete due to triaxial containment. The difference between the test load and calculated load of short columns was found to vary inversely with the eccentricity. For example, for 4 circular columns with l/d varying between 8.8 and 10.4 and e/d between 0.2 and 0.6, this difference was insignificant, whereas for 10 columns with l/d between 4.4 and 10.4 and e/d between 0.001 and 0.01, the said difference varied between 0.34 and 0.13 of the calculated load. Thus columns which show appreciable triaxial effect have small l/d and nearly concentric loading.

It was decided to produce failure load tables for a comprehensive range of circular sections using the uniaxial material properties, because for many practical columns it is unnecessary to take triaxial effects into account. A computer program was developed, as a part of the present investigation, in a form suitable for calculating the failure loads for

a large number of eccentrically-loaded, circular or rectangular columns.

Although the computer program was designed to deal with square and rectangular sections, production of failure load tables for these sections could not be undertaken because experimental evidence was not available. Therefore, 4 series of tests comprising 22 specimens were planned. The tests were sponsored by the International Committee for the Study and Development of Tubular Structures (CIDECT), and the specimens were manufactured and tested by Guiaux and Dehousse [2.2] at Liege University. The test loads were found to agree well with calculated failure loads, and it was resolved to produce failure load tables for a range of square and rectangular sections as well.

The development of the computer program, tests on square and rectangular columns and the influence of various parameters on the behaviour of the column are described in this chapter. Long-term loading and initial imperfection have been taken into account in the calculation of failure loads. The failure load tables are with the printer at the time of writing this thesis, and are expected to be published in the near future as a separate document. This chapter contains sample tables for one column section only.

Failure loads for all 35 of the concrete-filled columns now in service at the Almondsbury Interchange [2.3] are calculated and the load factors are tabulated in section 2.10.

2.2 COMPUTER PROGRAM

2.2.1 Theoretical assumptions

The assumptions on which the computation is based are listed below:

(1) Uniaxial stress-strain relationships are used for the steel and concrete, i.e., the triaxial effects, if any, are neglected. The concrete takes no tension and the steel has identical stress-strain properties in tension and compression.

(2) Both stress-strain curves are reversible.

(3) Complete interaction takes place between the steel tube and the concrete core, and plane sections remain plane after bending.

(4) Failure due to local buckling or due to shearing does not occur.

(5) The column bends in the form of a part-cosine wave.

(6) The peak of the load-deflection curve for the mid-height section of the column is taken as the failure load of all eccentrically-loaded columns and of axially-loaded columns with initial out-of-straightness.

(7) Practical columns have a sinusoidal imperfection.

2.2.2 Uniaxial stress-strain relationship for steel

The assumed uniaxial stress-strain relationship for steel is shown in Figure 2.1. The curve is a second degree parabola tangential to both straight lines. The stress-strain relationships are given below:

$$\text{when } o \leq \varepsilon \leq k\varepsilon_y \qquad \sigma = E_s \cdot \varepsilon \tag{2.1}$$

It can be shown that $\varepsilon_t = \varepsilon_y (2 - k)$, and

$$\text{when } k\varepsilon_y \leq \varepsilon \leq \varepsilon_t$$

$$\sigma = k\sigma_y + E_s (\varepsilon - k\varepsilon_y) \left[1 - \frac{(\varepsilon - k\varepsilon_y)}{4 (1 - k) \varepsilon_y} \right] \tag{2.2}$$

$$E_{Ts} = \frac{d\sigma}{d\varepsilon} = E_s \left[1 - \frac{(\varepsilon - k\varepsilon_y)}{2 (1 - k) \varepsilon_y} \right] \tag{2.3}$$

$$\text{and when } \varepsilon \geq \varepsilon_t \qquad \sigma = \sigma_y \tag{2.4}$$

Equations 2.1 to 2.4 are valid for all values of k excepting k = 1, when $\varepsilon_t = \varepsilon_y$ and only equations 2.1 and 2.4 are used.

By varying the value of k the effect of residual stress may be taken into account and actually rounded stress-strain relationships approximated. k is taken as unity throughout this investigation unless otherwise stated.

2.2.3 Uniaxial stress-strain relationship for concrete

The stress-strain relationship for concrete is expressed in the polynomial form originally used by Basu [2.4].

$$\frac{\sigma}{\sigma_m} = 2.41 \left(\frac{\varepsilon}{\varepsilon_m}\right) - 1.865 \left(\frac{\varepsilon}{\varepsilon_m}\right)^2 + 0.5 \left(\frac{\varepsilon}{\varepsilon_m}\right)^3 - 0.045 \left(\frac{\varepsilon}{\varepsilon_m}\right)^4 \tag{2.5}$$

A plot of equation 2.5 is shown in Figure 2.2. Beyond $\frac{\varepsilon}{\varepsilon_m} = 4$, $\frac{\sigma}{\sigma_m}$ rapidly drops to a negative value. However, such a high strain never occurs in practice. This is discussed later in section 2.9. The rising part of the curve is close to Hognestad's parabolic stress-strain relation, and the entire curve is a good approximation of the

experimental curves obtained by Barnard [2.6] in a series of recent tests at Cambridge.

One advantage of equation 2.5 is that ε_m may be given any chosen numerical value. ε_m does not seem to alter significantly with the cube strength, and a value of 0.0025 is chosen for short-term loading, after studying Barnard's experimental curves. It is shown later in section 2.7 that a variation of ε_m within certain limits has a relatively small effect on the maximum load of a column.

$\sigma_m = 0.8 f_{cu}$ gives good agreement with experiments [2.1], and this value is used in all computations.

2.2.4 Part-cosine deflected shape

The column is assumed to deflect in a part-cosine curve shown in Figure 2.3 and given by

$$y = y_o \cos \left(\frac{\pi z}{L}\right) \tag{2.6}$$

and the curvature ρ at a point z is given by

$$\rho = - \frac{\pi^2}{L^2} y_o \quad \text{Cos} \quad \left(\frac{\pi z}{L}\right) \tag{2.7}$$

At $z = 0$

$$\rho_o = - \frac{\pi^2}{L^2} \cdot y_o \tag{2.8}$$

and at $z = \frac{1}{2}$

$$y = e = y_o \cdot \text{Cos} \left(\frac{\pi 1}{2L}\right)$$

$$\text{whence } L = \frac{\pi 1}{2 \text{ Cos}^{-1} \left(\frac{e}{y_o}\right)} \tag{2.9}$$

substituting 2.9 in 2.8

$$\rho_o = -\frac{4}{l^2}\left[\cos^{-1}\left(\frac{e}{y_o}\right)\right]^2 \cdot y_o \qquad (2.10)$$

Equation 2.10 gives the relation between the total central deflection y_o ($= e + \delta_o$) and the central curvature ρ_o.

In Figure 2.3 the initial shape of the column is shown straight. The case of an initially bent column is dealt with later in section 2.6.

2.2.5 Force and moment for a given strain distribution

The linear strain distribution across a section may be specified by the curvature ρ and the distance Y of the neutral axis from the centroidal axis. To obtain the internal force and moment, P_i and M_i, by a simple, repetitive, numerical approach the steel in the section is divided into $j + k$ strips and the concrete in k strips (Figure 2.4). The areas of the strips may be calculated by simple algebra. Strain at the centre of the ith strip is given by $\varepsilon_i = \rho . Y_i$, the corresponding stress σ_{si} (or σ_{ci}) may then be calculated from the relevant stress-strain relationship. It follows that

$$P_i = \sum_{i=i}^{j+k} A_{si}\,\sigma_{si} + \sum_{i=i}^{k} A_{ci}\,\sigma_{ci} \qquad (2.11)$$

Assuming that the internal force in each strip acts through the middle of the strip (which, in case of a circular tube, is not identical with the centroid),

$$M_i = \sum_{i=i}^{j+k} A_{si}\,G_i\,\sigma_{si} + \sum_{i=i}^{k} A_{ci}\,G_i\,\sigma_{ci} \qquad (2.12)$$

$j = 10$ and $k = 20$ are found to give values of P_i and M_i close to values calculated by rigorous integration. The merit of the strip-method

lies in its repetitiveness and its ability to accommodate any stress-strain relationship without involving complicated algebra.

2.2.6 Numerical steps

The computational procedure consists of calculating the loads corresponding to successively increasing pre-selected deflections, and then by locating the failure load as the maximum ordinate of the load-deflection curve (Figure 2.5). The steps are as follows:

(1) Choose an initial value of the total central deflection y_o.

(2) Calculate the corresponding central curvature ρ_o from equation 2.10.

(3) Select a trial value of Y_o.

(4) Using the values of ρ_o and Y_o, calculate P and M_{io} as described in subsection 2.2.5.

(5) If the calculated value of M_{io} satisfies the equilibrium condition $M_{io} = M_{eo} = P.y_o$, proceed to step (6). Otherwise modify the value of Y_o and repeat step (4) until this condition is satisfied to a pre-assigned tolerance.

(6) By successively incrementing the value of y_o and repeating steps (2) to (5) for each value of y_o, calculate points on the load-deflection curve until the current P is less than the previous P. (This ensures that the peak of the curve is passed).

(7) Select three successive points a, b and c, so that, $P_a < P_b > P_c$ (Figure 2.5).

(8) Repeat steps (2) to (5) to calculate loads corresponding to two deflections $(y_a + y_b)/2$ and $(y_b + y_c)/2$.

(9) Repeat steps (7) and (8) until P_a and P_c are within 1 per cent of P_b. The load for b is the failure load, i.e., $P_m = P_b$.

Regarding step (5) two important observations may be made:

(i) The equilibrium condition should be accurately satisfied. The pre-assigned tolerance used is:

$$\text{ABSOLUTE} \quad \left(\frac{M_{io} - M_{eo}}{M_{io}}\right) \leqslant 0.0001$$

A less rigorous check may give inaccurate values of P_m. For example, a check of 0.01 may introduce up to $\pm$ 5 per cent error in P_m.

(ii) In order that the equilibrium condition may be satisfied accurately, the successive trial values of Y_o must be controlled cautiously, so that the iteration procedure converges to the true solution. This is achieved by selecting (from approximate elastic calculations) a starter value of Y_o close enough to the true value and by using a careful combination of the methods of "successive bisection" and "Newton-Rhapson" [2.7] for progressive improvement of the starter value.

2.2.7 General structure of the computer program

The computer program is written expressly for large scale runs needed to produce a design manual. The aim is to keep the input to a minimum for the maximum amount of output. This is fulfilled by forming a nest of six repetitive loops, called 'DO-LOOPS' in the FORTRAN-IV language,

one corresponding to each of the six parameters defining a load case, namely, d, t, σ_y, f_{cu}, l and e, the last one being the innermost loop.

Input consisting of fifteen punched cards is enough to generate thousands of load cases for the manual. The following example clarifies the point:

$$\begin{bmatrix}\text{d cases}\\ =4\end{bmatrix} \times \begin{bmatrix}\text{t cases}\\ =4\end{bmatrix} \times \begin{bmatrix}\sigma_y \text{ cases}\\ =2\end{bmatrix} \times \begin{bmatrix}f_{cu} \text{ cases}\\ =3\end{bmatrix} \times \begin{bmatrix}\text{l cases}\\ =15\end{bmatrix} \times \begin{bmatrix}\text{e cases}\\ =7\end{bmatrix}$$

= total number of load cases = 10,080.

On an average, each load case takes 0.9 sec on an IBM 7094 computer.

2.3 TESTS ON SQUARE AND RECTANGULAR COLUMNS

2.3.1 Background

Furlong [2.8] reported five tests on axially-loaded square columns with d = 4 to 5 in, t = 0.084 to 0.189 in, and l = 28 to 34 in. Test conditions did not allow rotations at the end.

There was a lack of experimental evidence on eccentrically-loaded square and rectangular sections. A programme of 22 tests was therefore prepared to check the reliability of the computed failure loads. These tests were sponsored by the International Committee for the Study and Development of Tubular Structures (CIDECT) at the University of Liege. Preparation of the test specimens, design and construction of the loading rig and testing of the main and control specimens were done by Guiaux and Dehousse [2.2]. In the following sub-sections the tests are briefly described and the experimental loads are compared with failure loads calculated by the computer program.

2.3.2 Description of the tests

The tests were divided into three series:

(1) Series A - 5 tests on major-axis bending of rectangular columns; this series was planned to study the interaction between minor- and major-axis bending while the load was eccentric only about the major-axis.

(2) Series B - 6 tests on minor-axis bending of rectangular columns; this series was planned to examine the validity of the computer program for rectangular columns. An identical set of 6 empty tubes was tested to study any premature failure due to local wrinkling of the tube wall.

(3) Series C - 5 tests on eccentrically-loaded square columns; this series was planned to check the applicability of the program to square columns.

Dimensions and material properties of the test specimens are given in Table 2.1. d and b are average values of 5 sets of measurements along the length of each column. The tabulated t is calculated from d, b, length, average measured wall thickness and the weight of the empty tube. l represents the distance between the centres of rotation of the top and bottom bearings. The measured initial central deflection y_{oc} is given. σ_y is the average value of four tensile coupon tests, and f_{cu} is the average value of 3 20 cm cubes.

The main feature of the loading rig was a pair of hemispherical oil-film bearings, which allowed the column-ends a free rotation of up to 6°. In the acceptance test, the bearings were shown to be practically frictionless for loads up to 300 tonf. The load was applied by using a 500 ton Amsler machine.

Tests were of short duration, occupying not more than half an hour.

2.3.3 Comparison between experimental and calculated failure loads

Experimental failure loads (P_T) are given in Table 2.1. The test on column A5 could not be completed because of difficulties with the connection of one of its ends with the bearing. Three columns, BE1, BE2 and BE3, in the empty tube group failed by local wrinkling of the tube wall. Column C1 failed due to bulging at the upper end. The remaining 17 columns failed due to overall bending.

Cosine wave failure loads (P_m) are tabulated. These are calculated by using the computer program described in the previous section. In the computation the end eccentricity is taken as $e + 0.9\ y_{oc}$ (Table 2.1), in order to account for the initial central deflection. The reason for this is discussed in section 2.6.

Series A comprises five concrete-filled rectangular columns loaded eccentrically about the major-axis. In Table 2.1 two calculated failure loads are given, the one in parenthesis being the minor-axis failure load with $e_{minor} = 0.9\ y_{oc}$. The smaller of the two values is used to calculate the ratio P_T/P_m. This series was planned to study the interaction between major- and minor-axis bending when the loading is eccentric about the major-axis only. This is discussed in section 2.5.

In series BE, six empty tubes were tested. All had a nominal d/t ratio equal to 37 and e/d ratio equal to 0.3. The 1/d ratio varied from 7 to 36. The steel had a yield strain of 2241 $\mu\varepsilon$. The strains at failure on the interior face of the tube wall are calculated. On the concave side, these strains are 7360 $\mu\varepsilon$, 4000 $\mu\varepsilon$, 3250 $\mu\varepsilon$, 2390 $\mu\varepsilon$, 2190 $\mu\varepsilon$ and 2130 $\mu\varepsilon$ for columns BE1 - BE6 respectively. Columns

BE1 - BE3 failed at 90 per cent of the calculated failure load, the premature failure being caused by local buckling of the tube wall. Columns BE4 - BE6 failed by overall bending, and excellent agreement is obtained between calculated and experimental failure loads. The American Iron and Steel Industry [2.9] recommends $d/t \not> 3300/\sigma_y$ (where σ_y is in ksi) for slender circular columns, so that local buckling does not occur, but it appears from the test results that l/d and e/d values have also to be considered. Further work is necessary in this direction.

Satisfactory correlation is obtained between the calculated and experimental loads of the columns in series BF and C. For these 11 columns, the ratio P_T/P_m varies between 1.004 and 1.083 with an arithmetic mean of 1.037, and a standard deviation of 0.025. It may therefore be inferred that for the range of columns tested in series BF and C, triaxial effect was insignificant. (Only column C1 gives an indication of incipient triaxial action). Further tests on short columns with small eccentricity are necessary to understand any beneficial triaxial effects that may occur in these two types of columns. In the meantime the computer program may be used with confidence to predict the failure loads of filled rectangular columns loaded eccentrically about the minor-axis and of all square columns.

2.4 BIAXIAL BENDING

Bresler [2.10] suggested the following interaction relation for a reinforced concrete column under axial load and biaxial bending, the column being sufficiently short for the influence of deflexion on moment to be neglected.

$$\frac{1}{P_{xy}} = \frac{1}{P_x} + \frac{1}{P_y} - \frac{1}{P_L} \qquad (2.13)$$

where P_{xy} = load carrying capacity under compression and biaxial bending.

P_x and P_y = load carrying capacities under compression with uniaxial eccentricities about the major- and minor-axis respectively.

and P_L = load carrying capacity under pure compression

$= A_s \sigma_y + A_c \sigma_m$

For short reinforced concrete columns Bresler found that P_{xy} was in excellent agreement with calculated theoretical values and with test results, the maximum deviation being 9.4 per cent, and average deviation being 3.3 per cent. A relation similar to 2.13 is given in the Russian specification (2.11).

Basu and Somerville (2.12) have recently proposed an equation similar to 2.13 for long columns:

$$\frac{1}{P_{xy}} = \frac{1}{P_x} + \frac{1}{P_y} - \frac{1}{P_{ax}} \qquad (2.14)$$

where P_{ax} = failure load under nominally zero eccentricity with artificial restraints against minor-axis buckling.

Equation 2.14 is conjectural. In the absence of experimental and theoretical data on biaxial bending, the validity of equation 2.14 cannot be checked. However, it can also be derived from the linear interaction relation currently in use for steel columns.

Analytical and experimental research into this problem is being planned at Imperial College.

2.5 MAJOR-AXIS BENDING

A rectangular column loaded eccentrically about the major-axis may, depending on the amount of eccentricity, fail by minor-axis buckling. This will occur when $P_x > P_{ay}$ where, P_{ay} is the minor-axis buckling load with $e_{minor} = 0$. In this case the column bends about both axes and the actual failure load may be less than P_{ay}.

When $P_x < P_{ay}$ there would still be some interaction between minor-axis bending caused by initial imperfection and the predominant major-axis bending. The actual failure load in this case may be less than P_x. If the bending about the minor-axis is ignored, the actual failure load should be the same as P_x; this is supported by test results for columns A3 and A4 (Table 2.1). However, the upper bound value P_x cannot be accepted as the true failure load on the basis of two experiments.

Equation 2.14 may be used to determine the true failure load for major-axis bending. In this case P_y is equal to P_{ay}:

$$\frac{1}{P_{xy}} = \frac{1}{P_x} + \frac{1}{P_{ay}} - \frac{1}{P_{ax}} \qquad (2.14a)$$

Equation 2.14a is used to calculate the failure load P_{xy} of columns A1 - A5. These are compared with experimental failure loads in Table 2.2. It may be seen that P_{xy} is conservative, whereas the upper bound calculated values (i.e. the smaller of P_x and P_{ay}) give closer agreement with test results.

However, in the absence of analytical results and further experimental evidence, equation 2.14a may be used.

2.6 INITIAL IMPERFECTION

The load-carrying capacity of a column is reduced by initial imperfections, such as, initial out-of-straightness, residual stress and unintentional end eccentricity.

BS 4[2.13] specifies that the initial out-of-straightness should not exceed 1/600 at the centre of any length of hollow section. This corresponds to a maximum initial central deflection of 0.2 in for a 10 ft long column.

In this investigation only hot-finished seamless tubes are considered. The amount of residual stress that exists due to differential cooling across the thickness, is small, and is ignored.

Unintentional end eccentricity (due to setting error of the bearing, for example) may be arbitrarily included in a lumped initial imperfection parameter together with the initial out-of-straightness.

A numerical value for the initial out-of-straightness has to be chosen. BS 449 [2.14] recommends an initial imperfection parameter $\eta = 0.00003\ l^2/k^2$, where k is the radius of gyration, for steel columns under nominally axial loading. For axially-loaded columns initially bent in a part-cosine wave, it may be shown that

$$\eta = y_{oc} \cdot \frac{d}{2k^2} \text{ , whence } y_{oc} = 0.00006\ l^2/d$$

Observations by the Column Research Council [2.9] on steel columns without residual stresses show that the BS 449 recommendation is conservative. However, it would be even more conservative for the majority of columns ($l/d < 28$) to take the manufacturer's tolerance $y_{oc} = 1/600$.

Considering the above, and assuming that a filled column has the same initial out-of-straightness as an empty one, the BS 449 recommendation ($y_{oc} = 0.00006\ l^2/d$) is adopted as initial imperfection.

It now remains to be seen how y_{oc} may actually be incorporated in the calculation. For concentrically-loaded columns initially bent in a part-cosine wave with $y_{oc} = 0.00006\ l^2/d$, the initial curvature ρ_{oc} is 0.00059/d. Therefore either y_{oc} or ρ_{oc} may be deducted from y_o or ρ_o in the calculation of the P - y_o relationship. But in eccentric loading cases, the deduction of a constant value of y_{oc} from y_o amounts to the deduction of a progressively decreasing value of ρ_{oc} from ρ_o (and vice-versa) as e and y_o increase.

In the computer program, therefore, the initial imperfection is represented by an initial eccentricity e_o, taken as a fraction of y_{oc}, i.e., $e_o = r.y_{oc}$. r = 0.833 is reasonable for elastic buckling of steel columns. But for elasto-plastic behaviour of filled tubes a proper value of r has to be found out. Table 2.3 shows the influence of r on P_m. P_1 is the failure load of the axially-loaded column with an initial central deflection $y_{oc} = 0.00006\ l^2/d$. P_2, P_3 and P_4 are the failure loads of the equivalent straight column with e = 0 and $e_o = r.y_{oc}$, where r = 1.0, 0.9 and 0.8 respectively. Comparing P_1 with P_2, P_3 and P_4, r = 0.9 seems to be the most suitable value. This is adopted for all values of e.

Thus in all computation initial imperfection is taken as an initial end eccentricity e_o ($= 0.9 \times 0.00006\ l^2/d$).

Figure 2.6 shows the effect of e_o on P_m. The reduction in P_m due to e_o is greatest (maximum 30 per cent) for small values of e. It increases with l/d up to a certain point and then starts decreasing. This agrees with Johnston's [2.9] observation on steel columns:

"The effects of initial crookedness and residual stress may be compared with the idealized strength if both crookedness and residual stress were absent. Such a comparison shows that the maximum effect of either residual stress or initial crookedness, alone or in combination, always occurs when the slenderness parameter λ equals unity, where $\lambda = \frac{\ell}{k} \cdot \frac{1}{\pi}\sqrt{\frac{\sigma_y}{E_s}}$. For values of λ greater than this the effects of initial curvature gradually diminish."

2.7 LONG-TERM LOADING

A load acting continuously for a long period has two effects on concrete: (i) strain corresponding to the same stress is increased, i.e., E_{Tc} diminishes, and, (ii) σ_m is reduced; consequently, there is an increment in deflection and a reduction in the failure load.

Mauch [2.15] and Manuel and MacGregor [2.16] calculated the long-term strength of rectangular reinforced concrete columns taking proper account of the creep behaviour. It seems possible to extend these methods to concrete-filled tubular columns. However, a simpler semi-empirical method used by Broms and Viest [2.17] for reinforced concrete columns, is adopted. The reduction of concrete stiffness E_{Tc} is taken into account by doubling the short-term value of ε_m, i.e. $\varepsilon_m = 2 \times 0.0025 = 0.005$ for long-term loading. The reduction in σ_m caused by long-term loading is small and is ignored.

All loads tabulated in the design manual are calculated for $\varepsilon_m = 0.005$. It may be recalled here that the computer program has been checked only against short-term ($\varepsilon_m = 0.0025$) experiments. Results of long-term loading tests on concrete-filled columns are not available,

therefore loads calculated on the basis of $\varepsilon_m = 0.005$ cannot be verified.

$P_m - \varepsilon_m - l$ and $P_m - \varepsilon_m - \frac{e}{d}$ relationships are shown in Figures 2.7 and 2.8. It may be seen that the influence of ε_m on P_m increases with l up to a point and then remains virtually constant. The influence decreases with increasing e/d, becoming negligible at $e/d > 0.5$.

Short-term loading calculations are based on $\varepsilon_m = 0.0025$. Available experimental $\sigma - \varepsilon$ relations [2.6] suggest values of ε_m between 0.0020 and 0.0030. It may be seen from Figures 2.7 and 2.8 that by choosing a mean value of 0.0025 the maximum possible error in P_m is 7 per cent.

Long-term loading calculations are based on $\varepsilon_m = 0.005$. This may be regarded as a rate-of-creep calculation with a single time-increment for the entire duration of loading. Rusch [2.18] reported $\varepsilon_m = 0.008$ for concrete under sustained loading of long duration, if this value is used in the present 'single time-increment' calculation then P_m would be conservative [2.16]; (the maximum difference between the two values of P_m corresponding to $\varepsilon_m = 0.005$ and 0.008, being 15 per cent of the greater value (Figure 2.7). Therefore it does not seem unreasonable to use $\varepsilon_m = 0.005$ in the present single time-increment calculation of the long-term load.

A comparison between the short-term ($\varepsilon_m = 0.0025$) and long-term ($\varepsilon_m = 0.005$) failure loads is made in Figure 2.9. The maximum reduction is 11 per cent. However, for a column with a high value of $\frac{d}{t} \times \frac{f_{cu}}{\sigma_y}$, the reduction in P_m may be as high as 21 per cent (Figure 2.7).

The period during which a load must act continuously in order to be classified as long-term load, is not clearly established. Several foreign codes define this period as three days [2.17]. In the present calculation

the entire load is considered as 'long-term'. It is believed that this conservative assumption compensates for the inadequacy, if any, of the notional assumption that $\varepsilon_m = 0.005$ leads to the true long-term load.

2.8 DESIGN MANUAL

2.8.1 Background

Failure loads for a range of concrete-filled tubular columns are tabulated in a design manual [2.19]. The work has been done as a part of this investigation, but all the tables are not included in this thesis, instead sample tables for one diameter are shown (Tables 2.4 to 2.9).

The computer program described in section 2.2 has been used for the preparation of the tables. Initial imperfection equivalent to that assigned in BS 449 [2.14] is incorporated in the computation (as discussed in section 2.6). Creep is taken into account by the approximate method described in the previous section.

2.8.2 Scope

Failure loads are tabulated for the following ranges of hot-finished seamless tubes:

circular sections	4 1/2 in to 18 in
square sections	4 in to 16 in
rectangular sections (about both axes)	5 in x 3 in to 18 in x 14 in
thickness	All the manufactured thicknesses for square and rectangular sections and 40 out of 59 manufactured thicknesses for circular sections.

steel	steels to BS 4360 [2.20]: grades 43C (σ_y = 16 tonf/in^2) and 50C (σ_y = 23 tonf/in^2)
concrete	f_{cu} = 3000, 6000 and 9000 lbf/in^2
effective length	6 ft to 40 ft (or 40 diameter/depth whichever is less)
eccentricity	seven values of e/d between 0 and 1.0

Squash loads ($P_L = A_s \sigma_y + A_c \sigma_m$) are given.

The true major-axis bending loads may be obtained by substituting the tabulated failure loads in equation 2.14a. Equation 2.14 may be used for calculating the load carrying capacity under axial compression and biaxial bending. The tables do not cover unequal end eccentricities.

2.8.3 Influence of parameters on the failure loads

Yield strength: Failure loads are tabulated for σ_y = 16 and 23 tonf/in^2. Figure 2.10, in which loads are plotted for intermediate values of σ_y, shows that from the tabulated load values for σ_y = 16 and 23 tonf/in^2, loads can be linearly interpolated or extrapolated without significant error, for any value of σ_y between 13.9 (= 16/1.15) and 23 tonf/in^2.

Young's modulus: The variation of P_m with E_s is shown in Table 2.10, an empty tube being chosen to demonstrate the maximum effect. It may be seen that for all practical columns ($l/d < 24$), a change of E_s from 12000 to 14000 tonf/in^2 increases P_m by less than 1 per cent. However, for very long columns the increase in P_m with increasing E_s may be appreciable, the corresponding figure being 12 per cent at $l/d = 72$.

Loads are tabulated for $E_s = 13000$ tonf/in^2 which is generally recommended by the manufacturers.

Cube strength: Figure 2.11 shows that P_m varies linearly with f_{cu}, so that linear interpolation or extrapolation may be used for values of f_{cu} which are not tabulated. It should be noted however, that for the empty tube ($f_{cu} = 0$), the possibility of a premature failure due to local wrinkling of the tube-walls should be considered. This has been discussed in sub-section 2.3.3.

ε_m: E_{Tc} may be varied by using different values of ε_m in equation 2.5. The influence of ε_m on P_m is shown in Figures 2.7 and 2.8, and has been discussed in section 2.7. Failure loads are tabulated for $\varepsilon_m = 0.005$.

Thickness: The variation of the failure load with d/t is shown in Figure 2.12; an empty tube is chosen to study the maximum variation. It may be seen that by tabulating failure loads for one intermediate and two extreme thicknesses, a linear interpolation gives loads for other thicknesses without appreciable error.

Length: P_m is plotted against 1/d in Figure 2.13 for 10 values of e/d. The influence of 1/d on P_m decreases, as may be expected, with increasing e/d. Figure 2.13 shows that linear interpolation between tabulated values (marked by vertical grid lines) gives the failure load for any intermediate length with negligible error.

Eccentricity: Figure 2.14 is complementary to Figure 2.13 and shows the influence of e/d on P_m. Again, linear interpolation between tabulated values is shown to be satisfactory.

2.8.4 Choice of load factors and material factors

CP 117 (Part 3) [2.21] and the new Bridge specification [2.22] will recommend partial load factors for composite columns. The draft Unified Code [2.23] recommends 1.6 and 1.4 for live and dead load respectively, when there is no wind loading. BS 449 [2.14] and CP 114 [2.24] recommend overall load factors of 1.7 and 2.0 for steel and reinforced concrete columns respectively.

CP 114 implies a material factor of 1.5 for concrete. The Unified Code in its present form, suggests material factors of 1.5 for concrete and 1.15 for steel.

The second interim report [2.25] of the CIRIA Study Committee on Structural Safety gives a comprehensive account of limit states and suggests suitable partial load factors.

The alternative recommendations are quoted above, and the choice is left to the designer. That is why ultimate load values based on material factors = 1.0 are tabulated.

2.8.5 Effective length

The question of effective length is being considered by the drafting committees of CP 117 (Part 3) [2.21] and the new Bridge specifications [2.22].

BS 449 [2.14] gives effective lengths which are substituted in the Perry-Robertson formula to determine the yield loads of axially-loaded columns. These loads are then divided by 1.7 to obtain the working load. A straight line interaction relation is suggested for end moment.

Failure loads have been calculated for a range of practical empty tubes by using the computer program. These loads have been compared

with 1.7 x (the corresponding BS 449 working load)(Table 2.11). The comparison shows that the two values are within 4 per cent for axially-loaded tubes and within 14 per cent for eccentrically-loaded tubes.

Since the loads calculated by the computer program are of the same order as 1.7 x (BS 449 working load), it does not seem unreasonable to use the BS 449 effective length rules in conjunction with these tables. It is worth mentioning that the BS 449 recommendation for the sway-case may be unsafe.

2.8.6 Working load

Problem: what is the working load of a column of the following description:

Geometry:

d = 14 in

t = 3/8 in

l = 11 ft 3 1/16 in = 11.25 ft/say

e = 1.58 in

Material:

Steel to BS 4360 [2.20], grade 43C

Concrete: works minimum cube strength at 28 days = 5700 lbf/in^2

Material factors:

for Steel $\gamma_s = 1.15$

for Concrete $\gamma_c = 1.5$

Load factors:

Dead 1.4

Live 1.6

Load ratio - Dead load:Live load :: 4:1

Solution: Using the material factors, the reduced material properties are:

$$\sigma_y/\gamma_s = 16/1.5 = 13.91 \text{ tonf/in}^2$$

$$f_{cu}/\gamma_c = 5700/1.5 = 3800 \text{ lbf/in}^2$$

The above two reduced values of σ_y and f_{cu} and the given values

of l and e do not coincide with the values for which loads are tabulated. The load case of the problem has to be found by linear interpolation (extrapolation for σ_y) from sixteen values taken from Tables 2.6 and 2.7 and quoted below for ready reference:

		f_{cu} = 3000 lbf/in^2		f_{cu} = 6000 lbf/in^2	
		e = 1.4in	e = 2.8in	e = 1.4 in	e = 2.8in
σ_y = 16 tonf/in^2	l = 10 ft	281	233	371	303
	l = 12 ft	268	222	351	286
σ_y = 23 tonf/in^2	l = 10 ft	362	297	452	368
	l = 12 ft	346	283	427	348

Ultimate load in tonf (d = 14 in, t = 3/8 in)

After doing the interpolations the required ultimate load is found to be 266 tonf.

Working load calculation:

$$P_w = \frac{P_m}{\text{overall load factor}}$$

For the given dead and live load factors and the load ratio:

$$\text{overall load factor} = \frac{4 \times 1.4 + 1 \times 1.6}{4 + 1} = 1.44$$

$$\therefore \quad \text{Required working load} = \frac{266}{1.44} = 185 \text{ tonf}$$

2.8.7 Choice of section

The designer's usual problem is to find compatible values of d, t, f_{cu} and σ_y for known values of P_m, l and e. He may select a set of

trial values, use the tables, interpolate where necessary and calculate P_m. If the calculated P_m is lower or excessively higher than the desired P_m, the values of d, t, f_{cu} and σ_y may be improved in successive trials till the two values of P_m are acceptably close.

2.8.8 Deflexion

Elastic methods, exact or approximate, may be used to calculate the deflexion at working load. For example, the exact elastic formula for the common case of a column under an axial load P_w and equal end moments M is:

$$\delta_w = \frac{M.\ h^2}{8(EI)_t} \quad \frac{2(1 - \text{Cos } u)}{u^2 \text{ Cos } u}$$

where h = true length of column

$(EI)_t$ = stiffness of the transformed section

$= E_c I_c + E_s I_s$

$$u = \frac{h}{2}\sqrt{\frac{P_w}{(EI)_t}}$$

The value of I_c based on the total area of filling and that of I_s are tabulated. E_s may be taken as 13000 tonf/in^2. $E_c = E_s/m$, the long-term value of m as recommended by the draft Unified Code may be used.

The approximate method (2.26) consists of calculating the deflexion for end moments only, taking the true length of the column. The effect of axial load is then taken into account by multiplying this deflexion by an approximate magnification factor

$$1/(1 - P_w/P_E) \quad \text{where } P_E = \text{Euler load} = \frac{\pi^2 (EI)_t}{l^2}$$

where l = effective length

2.9 MAXIMUM STRAIN IN CONCRETE

Let ε_c be the strain at the concave face of the concrete-core while the filled-tube is subjected to the maximum load P_m. $\varepsilon_c/\varepsilon_m$ is plotted in Figure 2.15 against e/d for 4 values of l and for both the short- and long-term values of ε_m. $\varepsilon_c/\varepsilon_m$ decreases significantly with increasing length, 1.5 being the maximum value for the shortest length. With e/d varying from 0 to 1.0, the value of $\varepsilon_c/\varepsilon_m$ is spiky in nature. For values of e/d greater than 1.0, $\varepsilon_c/\varepsilon_m$ remains virtually constant.

The long-term $\varepsilon_c/\varepsilon_m$ curve runs below and parallel to the short-term curve, except for very short columns. The constant difference between the two curves is approximately 0.15.

It has been mentioned in sub-section 2.2.3 that equation 2.5 for the stress-strain relationship of concrete, gives spurious values of σ/σ_m for $\varepsilon/\varepsilon_m >> 4$. This does not cause any concern because $\varepsilon/\varepsilon_m$ never exceeds 4 in concrete-filled columns under the maximum load (Figure 2.15).

2.10 AN IMPORTANT APPLICATION

The multi-level motorway interchange at Almondsbury is an important example of the use of concrete-filled columns in this country. 35 columns were designed and constructed on the basis of semi-rational formulae [2.3] and exploratory tests [2.27]. The columns are analysed here by the computer program for both short- and long-term loading. The load factors are given in Table 2.12. It may be seen that all the columns have adequate safety margin.

2.11 CONCLUDING REMARKS

A computer program is now available for predicting the failure load of circular, square or rectangular tubular columns, either filled with concrete or empty. Failure loads of circular or rectangular reinforced concrete columns may also be calculated by the same program. Equal end eccentricities about one axis are considered, and uniaxial stress-strain properties for the steel and concrete are used, i.e. triaxial effects, if any, are neglected. Long-term loading may be taken into account by the approximate method of doubling the concrete strain at all stress levels. Initial imperfection may be incorporated as an end eccentricity or as a central deflexion or as a central curvature.

Failure load tables [2.19] have been prepared for a comprehensive range of tubular sections under axial compression and uniaxial bending. Loads are tabulated for two steel strengths, three concrete strengths, seven eccentricities and up to fifteen lengths; intermediate cases may be obtained by linear interpolation without appreciable error. Initial imperfection equivalent to that assigned in BS 449 is incorporated, and creep in concrete is approximately accounted for. Failure loads are given for material factors = 1.0 and $\sigma_m/f_{cu} = 0.8$, but loads may be be obtained for other values of material factors and σ_m/f_{cu} by linear interpolation from the same tables.

It does not seem unreasonable to use BS 449 recommendations on effective length in conjunction with the tables.

Load carrying capacity under axial compression and biaxial bending may be calculated by substituting relevant tabulated loads in equation 2.14. Equation 2.14a may be used for major-axis bending to take the interaction with probable minor-axis bending into account.

2.12 SUGGESTION FOR FUTURE WORK

Future theoretical works should include:

(i) biaxial bending; and

(ii) proper step-by-step creep analysis.

Further experiments are necessary to cover:

(i) short square and rectangular columns under nearly concentric loading;

(ii) biaxial bending;

(iii) unequal end eccentricities

(iv) long-term loading; and

(v) local buckling of the tube wall.

CHAPTER 3

TRIAXIAL EFFECTS IN CONCENTRICALLY-LOADED CIRCULAR STUB COLUMNS

3.1 INTRODUCTION

The structural behaviour of concentrically-loaded stub columns is largely influenced by the difference between the values of Poisson's ratio of steel and concrete. The Poisson's ratio of concrete ν_c may increase from 0.11 [3.1] to the order of 0.75 [3.2] with increasing longitudinal strain. Thus in the early stages of loading of a stub column when $\nu_c < \nu_s$, the steel has no restraining effect on the concrete core and bond must exist to prevent separation at the interface. As the longitudinal strain increases, however, ν_c gradually becomes greater than ν_s thereby setting up a radial pressure at the interface. At this stage the concrete is under triaxial compression and the steel is under longitudinal compression and hoop tension. This stage is usually reached after the steel has yielded biaxially. As the hoop tension increases the longitudinal compression in steel is reduced while the radial pressure on concrete increases, and as a result the longitudinal strength of the contained concrete is increased. The failure load of all practical stub columns is considerably more than the sum of the uniaxial compressive strengths of the steel and concrete, because the loss of longitudinal compression in steel is more than compensated for by the augmentation of the strength of concrete.

At the outset of this investigation the magnitude of the longitudinal and the hoop stress in steel were not known in the post-elastic range. The assumption had been made that at failure the steel yields in the hoop direction and carries no stress in the longitudinal direction, i.e. $\sigma_{sH} = -\sigma_y$ and $\sigma_{sL} = 0$ (3.3, 3.4). For such a state of stress the radial pressure on concrete σ_{cR} (Figure 3.1) is given by:

$$\sigma_{cR} = -\sigma_{sH} \times \frac{2t}{d-2t} = \sigma_y \frac{2t}{d-2t} \qquad (3.1)$$

From the failure criterion of triaxially contained concrete (3.5) the longitudinal stress in concrete σ_{cL} at failure was taken (3.3, 3.4) as:

$$\sigma_{cL} = \sigma_m + 4.1\,\sigma_{cR} \qquad (3.2)$$

The longitudinal stress in steel being zero, the failure load P_H was calculated as:

$$P_H = A_c\,\sigma_{cL} = A_c\left(\sigma_m + \frac{4.1\,\sigma_y \times 2t}{d - 2t}\right) \qquad (3.3)$$

Neogi (3.3) obtained reasonable correlation between experimental failure loads and loads calculated from equation 3.3. Gardner and Jacobson (3.4) used the same equation with less success.

The computation of the post-elastic biaxial stresses in steel from experimentally determined load-strain relationships is not straightforward; in this chapter a method is given by which this can be accomplished. The method is based on the generalised flow-law for plastic solids. 14 tests conducted at Imperial College are chosen, and steel stresses σ_{sL} and σ_{sH} are calculated from measured strain values ε_{sL} and ε_{sH} for small increments of strain up to failure. Once the stresses in the steel are known those in the concrete are calculated from simple statics.

The relationship between the longitudinal stress and strain for the

biaxially stressed steel and for the triaxially stressed concrete is plotted for all the 14 columns. These curves may be looked upon as equivalent longitudinal stress-strain relationships for the steel tube and the concrete core; the mean curves are used in chapter 5 to predict moment-curvature relationships taking triaxial effects into account.

The stresses in the concrete are compared with existing failure criteria, and a failure criterion is suggested for the concrete core.

A new equation is proposed in place of equation 3.3.

3.2 CALCULATION OF BIAXIAL STRESSES IN STEEL FROM MEASURED STRAINS

3.2.1 Uniaxial stress-strain relationship and biaxial yield criterion

The uniaxial stress-strain relationship of steel is assumed to be elastic - perfectly plastic.

The Hencky-von Mise's yield criterion is the most accurate one for ductile materials [3.7], and for biaxial stresses in the steel tube it may be written as:

$$\sigma_{sL}^2 + \sigma_{sH}^2 - \sigma_{sL}\ \sigma_{sH} = \sigma_y^2 \qquad (3.4)$$

3.2.2 Elastic biaxial stress-strain relationship

As long as the stress-point is within the yield surface defined by equation 3.4, the following relations are applicable:

$$\sigma_{sL} = \frac{E_s}{(1 - \nu_s^2)} \cdot (\varepsilon_{sL} + \nu_s\ \varepsilon_{sH}) \qquad (3.5)$$

$$\sigma_{sH} = \frac{E_s}{(1 - \nu_s^2)} \cdot (\varepsilon_{sH} + \nu_s\ \varepsilon_{sL}) \qquad (3.6)$$

3.2.3 Post-elastic biaxial stress-strain relationship

Once the stress-point has reached the yield surface, it keeps moving along the surface with increasing strains (Figure 3.2), and the relationship between stresses and strains is no longer governed by equations 3.5 and 3.6.

When the stress-point is on the yield surface let the stresses in steel be σ_{sL} and σ_{sH}. At this instant let there be a small increment of load for which the experimentally obtained strain increments are $\delta\varepsilon_{sL}$ and $\delta\varepsilon_{sH}$. The increments in stresses are then given by:

$$\delta\sigma_{sH} = \frac{E_s\,(\delta\varepsilon_{sL} - \gamma.\delta\varepsilon_{sH})}{\alpha - 2\nu_s - \gamma} \qquad (3.7)$$

$$\delta\sigma_{sL} = \alpha \circ \delta\sigma_{sH} \qquad (3.8)$$

$$\text{where } \gamma = \frac{2\sigma_{sL} - \sigma_{sH}}{2\sigma_{sH} - \sigma_{sL}} \qquad (3.9)$$

$$\text{and} \quad \alpha = -\frac{1}{\gamma} \qquad (3.10)$$

Equations 3.7 and 3.8 are derived from the generalised flow-law for perfectly plastic solids developed between 1950 and 1956 [3.6] (Appendix A). In the derivation of equations 3.7 and 3.8, it is assumed that the steel is elastic-perfectly plastic and obeys the Hencky-von Mise's yield criterion (Appendix B).

When $\delta\sigma_{sL}$ and $\delta\sigma_{sH}$ are added to the existing stresses, a new pair of values is obtained for σ_{sH} and σ_{sL}. This gives the new stress-point which should also lie on the yield surface providing $\delta\varepsilon_{sL}$ and $\delta\varepsilon_{sH}$ are sufficiently small.

3.2.4 Computer program

When the load-strain relationships for a stub column are known from experimental observations, the strains and stresses at first yield may be calculated, after some systematic trials, from the elastic equations 3.5 and 3.6 and the yield condition 3.4. The numerical process of finding the post-elastic stresses by using equations 3.7 and 3.8 may then be started and continued for small successive strain increments up to the failure of the column. The process is repetitive and is programed on a digital computer. Once the stresses in the steel are known, the stresses in the concrete are calculated from simple statics.

The program consists of the following steps:

(1) Read observed values of ε_{sL} and ε_{sH} for various values of P. Select the first value of ε_{sL} and of ε_{sH}.

(2) Substitute ε_{sL} and ε_{sH} in equations 3.5 and 3.6 to calculate σ_{sL} and σ_{sH}.

(3) Repeat step (2) for successive values of ε_{sL} and ε_{sH} until the left hand side of equation 3.4 is greater than the right hand side.

(4) Choose the last two pairs of strain values from step (3), i.e., one pair before yield and one after; use a process of successive bisection between these two pairs, repeat step (2) and find ε_{sL}, ε_{sH} and P for which σ_{sL} and σ_{sH} just satisfy equation 3.4. (This gives the loads, strains and stresses at first yield).

(5) Choose a small increment $\delta\varepsilon_{sL}$.

(6) Add $\delta\varepsilon_{sL}$ to the current value of ε_{sL}, find P corresponding to

the new value of ε_{sL} by linear interpolation, hence find $\delta\varepsilon_{sH}$.

(7) Calculate γ and α from equations 3.9 and 3.10. Substitute γ and α in equations 3.7 and 3.8 and obtain $\delta\sigma_{sH}$ and $\delta\sigma_{sL}$.

(8) Add $\delta\sigma_{sL}$ and $\delta\sigma_{sH}$ to the current values of σ_{sL} and σ_{sH} and get new values of σ_{sL} and σ_{sH}. Check that the new values of σ_{sL} and σ_{sH} satisfy equation 3.4, and proceed to step (9). Otherwise, take successively smaller values of $\delta\varepsilon_{sL}$ and repeat steps (6) and (7) until equation 3.4 is satisfied to a pre-assigned tolerance.

(9) Repeat steps (5) to (8) to obtain σ_{sL} and σ_{sH} for successively increasing values of ε_{sL}, ε_{sH} and P up to failure.

(10) List all values of P, ε_{sL}, ε_{sH}, σ_{sL} and σ_{sH} obtained in steps (2) to (9). For each set of values calculate $P_s = A_s\ \sigma_{sL}$, hence $\sigma_{cL} = \dfrac{P - P_s}{A_c}$; also calculate $\sigma_{cR} = -\sigma_{sH} \times \dfrac{2t}{d - 2t}$.

3.3 STUB COLUMN EXPERIMENTS

3.3.1 Description of tests

14 tests conducted at Imperial College [3.3] are chosen, because a complete record of strain readings for these tests is available.

Dimensions and material properties are given in table 3.1. Thickness was the variable parameter. The end cap consisted of a steel disc 2 1/2 in thick with a 1/4 in machined recess into which the end of the filled tube fitted closely. At each end of the tube the concrete surface was roughened by chipping. It was then capped with a thin

layer of cement mortar and made flush with the steel surface. It may therefore be assumed that the steel and concrete were loaded together. At the lower end a spherical bearing of large diameter was interposed between the end cap and machine platten, but the top end cap bore directly against the top platten.

The column was continuously strained until, and somewhat beyond the the maximum load. The strain rates were approximately: 30 $\mu\varepsilon$/min for 0 - 3000 $\mu\varepsilon$, 60 $\mu\varepsilon$/min for 3000 - 5400 $\mu\varepsilon$, 120 $\mu\varepsilon$/min for 5400 - 9000 $\mu\varepsilon$ and 300 $\mu\varepsilon$/min after 9000 $\mu\varepsilon$.

The longitudinal and hoop strain at the mid-height section, along two perpendicular diametral planes, were measured by 4 rosette gauges.

3.3.2 Experimental results

ε_{sL} and ε_{sH} are plotted against the total load in Figures 3.3 to 3.16. ε_{sL} and ε_{sH} are average values from four readings taken at two perpendicular diametral planes. At high loads there was a considerable difference between the maximum or minimum longitudinal strain and the average. This difference may have been caused by local weaknesses in the tube. The bending associated with non-uniform straining is ignored, and the arithmetic mean of the four readings is taken as the true axial strain (ε_{sL}). The same applies to ε_{sH}.

Only in column M17 did (Figure 3.9) ε_{sH} exceed ε_{sL}. It is shown later that M17 behaved differently from the other columns in so far as the calculated values of σ_{sL} and σ_{sH} are concerned. It may be inferred that strain readings for M17 are unreliable.

The maximum value of ε_{sL} in Figures 3.3 to 3.16 is 28000 $\mu\varepsilon$. Strain readings could not be taken up to failure for all the columns.

Table 3.2 gives the load P_T' up to which strain readings are available and the failure load P_T, the ratio between the two loads varies between 0.78 and 1.00.

The ratio between the test failure load P_T and the sum of the uniaxial compressive strengths of the steel and concrete P_L varies between 1.36 and 1.63. Thus the gain in failure load due to triaxial augmentation of the concrete strength is between 36 and 63 per cent of the uniaxial strength.

In column M12 a strain gauge was embedded in the concrete to measure the longitudinal strain ε_{cL}. ε_{cL} was compared with ε_{sL} and virtually no difference was observed. This means that there is no slip between the steel and concrete when the two are loaded together.

Overall bulging, i.e., bulging over the major part of the length was the basic mode of failure in all the columns.

3.4 DISCUSSION OF TEST RESULTS

3.4.1 Stresses calculated from strain readings

Longitudinal and lateral strains ε_{sL} and ε_{sH}, obtained experimentally (Figures 3.3 to 3.16), are fed into the computer program. The program prints out the values of longitudinal and lateral stresses in the steel and the concrete.

From no-load condition to failure the path followed by the steel stress-point (σ_{sL}, σ_{sH}) is shown in Figure 3.17 for column M24. The travel of the stress-point from O to A with increasing load is governed by the equations given in sub-section 3.2.2, and the movement along the

ellipse from A to B is determined by the equations given in sub-section 3.2.3. For column M24, the stress-point reaches the yield-surface (point A) at 64 per cent of the failure load, and at 98 per cent of the failure load $\sigma_{sL}/\sigma_y = 0.538$ and $\sigma_{sH}/\sigma_y = -0.616$ (point B).

The load and stresses at first yield are given in Table 3.3 for all the columns. The ratio between the first yield load P_y and the failure load P_T varies between 0.57 and 0.85 with an arithmetic mean of 0.66. At first yield, it may be seen from Table 3.3 that σ_{sH} is small, consequently σ_{cR} is less than 2 per cent of σ_m for the majority of columns. Thus it transpires that up to the first yield, i.e. approximately up to two-thirds of the failure load, triaxial effects are negligible.

At or near failure, however, σ_{cR} is appreciable; the ratio σ_{cR}/σ_m varies between 0.11 and 0.48 (Table 3.4).

Once the steel has yielded, the longitudinal stress in steel σ_{sL} drops to about 0.75 σ_y at failure, while the strength of the triaxially contained concrete reaches more than twice the uncontained strength, i.e. $\sigma_{cL} \simeq 2.0\ \sigma_m$. The arithmetic mean of σ_{sL}/σ_y at first yield for all the columns is 0.98 (Table 3.3) and the corresponding value near failure is 0.75 (Table 3.4). The arithmetic mean of σ_{cL}/σ_m at first yield is 0.92 (Table 3.3), and the corresponding value near failure is 2.08 (Table 3.4).

3.4.2 Equivalent stress-strain relationship

The relationships between the longitudinal stress and the longitudinal strain for the biaxially stressed steel and the triaxially stressed concrete may be looked upon as equivalent stress-strain relationships for the steel tube and the concrete core. The equivalent stress-strain

relationships derived in this sub-section are used in chapter 5 to incorporate triaxial effects in an approximate moment-curvature analysis.

Steel: The non-dimensional quantities σ_{sL}/σ_y and $\varepsilon_{sL}/\varepsilon_y$ are plotted for all the columns in Figure 3.18. The curves for M17 and M23 show wide scatter, probably because of errors in the strain readings. The remaining 12 curves form a well defined band which is represented by the smooth curve shown in Figure 3.19. The smooth curve is a lower bound fit to the band for values of $\varepsilon_{sL}/\varepsilon_y$ between 1.0 and 4.0, and then follows the mean path through the band. The smooth curve which may be regarded as the equivalent stress-strain relationship is expressed by the following equations:

$$\frac{\sigma_{sL}}{\sigma_y} = 0.95\ \frac{\varepsilon_{sL}}{\varepsilon_y}, \quad \text{when} \quad \frac{\varepsilon_{sL}}{\varepsilon_y} < 1.0$$

$$\frac{\sigma_{sL}}{\sigma_y} = \frac{1.063\ \frac{\varepsilon_{sL}}{\varepsilon_y} - 0.113}{1.417\ \frac{\varepsilon_{sL}}{\varepsilon_y} - 0.417}, \quad \text{when} \quad \frac{\varepsilon_{sL}}{\varepsilon_y} > 1.0 \qquad (3.11)$$

Equation 3.11 is asymptotic to $\sigma_{sL}/\sigma_y = 0.75$.

Concrete: σ_{cL}/σ_m is plotted against $\varepsilon_{cL}/\varepsilon_m$ for all the columns in Figure 3.20, where $\varepsilon_{cL} = \varepsilon_{sL}$, $\sigma_m = 0.8 f_{cu}$ and $\varepsilon_m = 0.0025$. Again the curves for M17 and M23 show wide scatter, while the remaining 12 curves show a definite band pattern, although the band width gets wider for high values of $\varepsilon_{cL}/\varepsilon_m$. A smooth mean curve is drawn to represent the band (Figure 3.21), and is expressed by the equation:

$$\frac{\sigma_{cL}}{\sigma_m} = \frac{2.41\ (\frac{\varepsilon_{cL}}{\varepsilon_m})}{1 + 1.105\ (\frac{\varepsilon_{cL}}{\varepsilon_m})} \qquad (3.12)$$

Equation 3.12, which is asymptotic to $\sigma_{cL}/\sigma_m = 2.18$, has the same initial slope as the uniaxial stress-strain curve for concrete (equation 2.5), and the two equations give the same stresses for strains less than $0.5\ \varepsilon_m$.

Thus equations 3.11 and 3.12 approximately represent the longitudinal stress-strain relationships for the biaxially stressed steel tube and the triaxially contained concrete core of a stub column under concentric loading. However, equations 3.11 and 3.12 are applicable only when d/t lies approximately between 17 and 37 (Table 3.1).

3.4.3 Effect of tube thickness

σ_{cR} is the containment stress for the concrete core. The relation between σ_{cR} and σ_{sH} is:

$$\sigma_{cR} = -\sigma_{sH} \frac{2t}{d - 2t} \qquad (3.1)$$

or $$\sigma_{cR} \simeq -\sigma_{sH} \frac{2t}{d} \qquad (3.13)$$

Thus σ_{sH} is a measure of the containment, and the relation between σ_{cR} and σ_{sH} is approximately linear for varying t/d.

Assuming that the steel has yielded biaxially and the stress-point $(\sigma_{sL}, \sigma_{sH})$ is progressing along the yield-ellipse (Figure 3.17), the value of the ratio σ_{sH}/σ_{sL} enables the individual values of σ_{sH} and σ_{sL} to be calculated. The higher the ratio σ_{sH}/σ_{sL} the higher is the containment. The relationship between σ_{sH}/σ_{sL} and d/t is studied in Figure 3.22 for values of σ_{sH}/σ_{sL} near failure (Table 3.4); there is no recognisable pattern, and in the absence of further data, a horizontal line through $\sigma_{sH}/\sigma_{sL} = -0.5$ is a fair approximation of the relationship.

The non-dimensional quantity σ_{cR}/σ_y is plotted against t/d in Figure 3.23; for $t/d = 0$, $\sigma_{cR}/\sigma_y = 0$. The relation between σ_{cR}/σ_y and

t/d may be approximated as:

$$\sigma_{cR} = \frac{2}{3} \frac{t}{d} \sigma_y \qquad (3.14)$$

It must be emphasized that equation 3.14 is tentative.

The effect of tube thickness on the strength of the filled tube is not established from Figures 3.18, 3.20, 3.22 and 3.23 and from Table 3.4, and it seems that further experiments are necessary.

3.4.4 Lateral/longitudinal strain

The ratio between the lateral and the longitudinal strain $\varepsilon_{cR}/\varepsilon_{cL}$ $(= \varepsilon_{sH}/\varepsilon_{sL})$ is plotted against P/P_T where P is the current load and P_T is the experimental failure load (Figures 3.24 and 3.25). The strain-ratio has an approximate value of 0.2 at low loads; it then increases slowly to 0.3 $(= \nu_s)$ when the load is between 55 per cent and 56 per cent of the failure load. M16 and M24 show different behaviours which may be attributed to experimental scatter. It may be mentioned here that the steel reaches the first yield at about two-thirds of the failure load. Thus the strain-ratio becomes equal to the Poisson's ratio of steel just before the steel yields. After this the strain-ratio increases rapidly up to a maximum of 0.8; this compares well with 0.75 observed by Richart [3.2] in spirally reinforced concrete columns.

3.4.5 Share of load carried by the concrete

Beyond the load at which the strain-ratio equals ν_s $(= 0.3)$, i.e. approximately after the steel has reached the first yield, concrete carries a progressively higher share of the total load. The ratio of the load carried by the concrete P_c to the yield load P_y has an arithmetic mean of 0.42 (Table 3.3), whilst the ratio of P_c to the load at

or near failure P_T' is 0.70 (Table 3.4).

The reduction in P_s, the load carried by the steel, beyond first yield is shown for columns M15 and M24 in Figures 3.26 and 3.27.

P_c/P is plotted against P in Figures 3.28 and 3.29 for all the columns. At low loads the ratio P_c/P varies between 0.28 and 0.73, it remains nearly constant until the steel yields, then it increases to 0.70 to 0.80.

3.4.6 Volume change

If a cylinder has a longitudinal strain ε_{cL} and a radial strain ε_{cR}, it may be shown that the change in unit volume or the volumetric strain ε_{cV} is given by:

$$\varepsilon_{cV} = \varepsilon_{cL} + (2\varepsilon_{cR} + \varepsilon_{cR}^2)(1 + \varepsilon_{cL}) \qquad (3.15)$$

Neglecting the higher order terms

$$\varepsilon_{cV} = \varepsilon_{cL} + 2\,\varepsilon_{cR} \qquad (3.16)$$

Even for strains of the order of 0.025, equation 3.16 gives values of ε_{cV} only up to 5 per cent smaller than the exact value given by equation 3.15. Equation 3.16 is used in all volumetric strain computation.

$\varepsilon_{cV}/\varepsilon_m$ is plotted against σ_{cV}/σ_m for all the columns in Figures 3.30 to 3.33; here $\varepsilon_m = 0.0025$, $\sigma_{cV} = \sigma_{cL} + 2\,\sigma_{cR}$, and $\sigma_m = 0.8\,f_{cu}$. It may be seen that volume decreases until σ_{cV}/σ_m is approximately unity, i.e. σ_{cV} is approximately equal to the peak stress of uncontained concrete. Then the volume starts increasing; the point at which the volume is equal to the original volume occurs when σ_{cV}/σ_m is approximately between 1.25 and 1.5. At failure up to 1.5 per cent volume increase is recorded (column M24, Figure 3.33).

3.4.7 Failure criterion for concrete

Available failure criteria for concrete under triaxial compression are discussed in Appendix C, and are compared in this sub-section with the stresses in the concrete core at or near failure.

The stresses in the concrete core σ_{cL} and σ_{cR} at or near failure (Table 3.4) are plotted in Figure 3.34 and Mohr's circles are drawn. The Mohr-envelope (equation C.5) derived from Richart's [3.5] failure criterion (equation C.1) is also drawn in Figure 3.34. The straight line envelope is a reasonable lower-bound fit to the circles, and may be regarded as a criterion for sliding failure of the concrete core. The angle between the envelope and the ordinate is 127° 52', therefore the inclination of the plane of sliding failure with the horizontal is expected to be $(127^{\circ} - 52' \div 2) \simeq 64^{\circ}$. Although columns M11 - M24 failed due to bulging, the comparison in Figure 3.34 indicates that if a shear failure should occur in the concrete core, the shear-plane would be approximately at 64° with the horizontal.

Values of σ_{cL} and σ_{cR} near failure (Table 3.4) are compared with Hannant and Frederick's [3.10] failure lines (equation C.6) in Figure 3.35. It may be seen that a better fit is obtained by:

$$\sigma_{cL} = f_{cy} + 5\,\sigma_{cR} \qquad (3.17)$$

Equation 3.17 is nearly the same as equation C.2 suggested by Richart[3.5] for relatively low values of the confining pressure σ_{cR} $(= \sigma_2 = \sigma_3)$. Thus equation 3.17 may be used as the failure criterion for the concrete core of a stub column.

3.5 PREDICTION OF FAILURE LOAD

3.5.1 General

The distinction between the squash load P_L and the stub column failure load P_H should be noted. P_L is the sum of the uniaxial compressive strengths of the steel and the concrete, i.e. $P_L = A_s\sigma_y + A_c\sigma_m$. Thus P_L is the failure load for a composite column in which there is no triaxial effect, for example, a cased stanchion. However, P_H is the failure load of a concentrically-loaded filled stub column for which triaxial effects must be taken into account. For a stub column P_H may be considerably greater than P_L. In this section equation 3.3 is discussed and a new equation is suggested for predicting P_H.

3.5.2 Derivation

The influence of d/t and other parameters on the ratio σ_{sH}/σ_{sL} $(= \beta)$ at failure is not recognisable from the test results of columns M11 - M24 (Figure 3.22), and it does not seem unreasonable to assume a constant value of β for all the columns. Substituting $\sigma_{sH} = \beta\sigma_{sL}$ in equation 3.4:

$$\sigma_{sL} = \frac{\sigma_y}{\sqrt{1 - \beta + \beta^2}} = \frac{\sigma_y}{\beta_1} \qquad (3.18)$$

where $\beta_1 = \sqrt{1 - \beta + \beta^2}$

σ_{sH} may then be found:

$$\sigma_{sH} = \beta\,\sigma_{sL} \qquad (3.19)$$

Substituting equations 3.19 and 3.18 in 3.1

$$\sigma_{cR} = -\sigma_{sH}\frac{2t}{d - 2t} = \frac{2t\beta\sigma_y}{d_i\,\beta_1} \qquad (3.20)$$

Equations C.1, C.2, C.3, C.6 and 3.17, which give various relationships between σ_{cL} and σ_{cR} at failure, are all of the form: $\sigma_{cL} = f_{cy} + \lambda\sigma_{cR}$, where λ is a constant. For uniformity with the rest of this work f_{cy} may be replaced by σ_m without any appreciable error; thus:

$$\sigma_{cL} = \sigma_m + \lambda \sigma_{cR} \qquad (3.21)$$

where λ is a constant.

Substituting σ_{cR} from equation 3.20 in 3.21:

$$\sigma_{cL} = \sigma_m + \frac{2t \lambda \beta \sigma_y}{d_i \beta_1} \qquad (3.22)$$

Substituting equations 3.18 and 3.22 in the relation $P_H = A_s\sigma_{sL} + A_c\sigma_{cL}$:

$$P_H = \frac{A_s \sigma_y}{\beta_1} + A_c \left(\sigma_m + \frac{2t \lambda \beta \sigma_y}{d_i \beta_1}\right) \qquad (3.23)$$

where $\beta = \sigma_{sH}/\sigma_{sL}$,

$\beta_1 = \sqrt{1 - \beta + \beta^2}$, and

λ = a constant (equation 3.21)

From Figure 3.22, - 0.5 may be taken as a reasonable value for β; and from equation 3.17 $\lambda = 5.0$. Substituting β and λ in equation 3.23:

$$P_H = 0.75 A_s \sigma_y + A_c \left(\sigma_m + \frac{3.8 t \sigma_y}{d_i}\right) \qquad (3.24)$$

3.5.3 Discussion

Failure load P_H is calculated by equation 3.24 and compared with test load P_T for columns M11 - M24 in Table 3.5. The agreement is satisfactory, P_H being always less than P_T. The ratio P_T/P_H varies between 1.02 and 1.14 with an arithmetic mean of 1.07.

Equation 3.3 was based on the arbitrary assumption that $\beta = \infty$,

i.e. $\sigma_{sH} = -\sigma_y$ and $\sigma_{sL} = 0$, and that $\lambda = 4.1$. Loads calculated by equation 3.3 are also given in Table 3.5. The ratio $(P_H)_{\text{equation 3.24}}/(P_H)_{\text{equation 3.3}}$ varies between 0.89 and 0.92.

Values of P_H are given for various values of β and λ in Table 3.6 for a thick and a thin tube. It may be seen that P_H based on $\beta = -0.5$ and $\lambda = 5.0$ is only 10 per cent smaller than P_H based on $\beta = \infty$ and $\lambda = 4.0$. This explains why equation 3.3 gave fair agreement with test results, in spite of being based on the limiting value of $\beta = \infty$.

Equation 3.24 is used to calculate the failure load P_H for 11 stub columns tested by Gardner [3.12]. The steel had a rounded stress-strain relationship, and for the purpose of equation 3.24 σ_y is taken as the 0.2 per cent proof stress. P_H is compared with the experimental failure load P_T in Table 3.7; the ratio P_T/P_H varies between 0.96 and 1.38 with an arithmetic mean of 1.18. The predicted load P_H for these columns is more conservative than for the Imperial College columns (M11 - M24). The reason for this may be ascribed to the fact that σ_y is taken as the 0.2 per cent proof stress.

It may be inferred that equation 3.24 can be safely used to predict the failure load of circular stub columns.

3.6 CONCLUSIONS

The following conclusions may be drawn regarding the behaviour of concentrically-loaded, concrete-filled, mild steel, circular stub columns:

(1) Longitudinal strains of the order of 20,000 $\mu\varepsilon$ may occur at only 80 per cent of the failure load. Strains greater than 28,000 $\mu\varepsilon$ have been observed at or near failure.

(2) The ratio of the lateral strain to the longitudinal strain is approximately 0.2 at low loads; the ratio gradually increases to 0.3 at about 60 per cent of the failure load, and then rapidly increases to a maximum of 0.8, at or near failure, associated with a volume increase of up to 1.5 per cent.

(3) A computer program has been written for calculating the elasto-plastic biaxial stresses in the steel from the measured values of the two strains.

(4) The steel yields under biaxial stresses approximately at two-thirds the failure load. At this stage the longitudinal stress is nearly equal to the uniaxial yield stress and the hoop stress is negligible. Therefore the restraining effect of the tube on the concrete core is not appreciable up to about two-thirds the failure load.

(5) At or near failure the longitudinal compression in the steel is approximately 0.75 x the uniaxial yield stress, and the hoop tension is half the longitudinal stress in magintude.

(6) The augmented strength of the concrete core, at or near failure, is nearly twice the strength of uncontained concrete.

(7) The relationship between the longitudinal stress and the longitudinal strain of the biaxially stressed steel is approximated by equation 3.11, and that of the triaxially stressed concrete by equation 3.12.

(8) Equation 3.17 may be used as the failure criterion for the concrete core.

(9) The failure load may be up to 1.6 times the sum of the uniaxial compressive strengths of the steel and the concrete, and can be predicted by equation 3.24.

CHAPTER 4

MOMENT-CURVATURE TESTS

4.1 PURPOSE OF THE TESTS

Under eccentric loading both the longitudinal and the hoop stress vary across the section, and no theory is available for the inelastic deformation of concrete under three unequal principal stresses. It is intended therefore to account for triaxial effects in eccentrically loaded columns by incorporating the results of experimentally determined moment-curvature relationships in the column analysis.

4.2 DESCRIPTION OF SPECIMENS

35 - 6 5/8 in diameter specimens were tested. These were divided into 7 groups, A to G, each consisting of five specimens, numbered 1 to 5. (Table 4.1). The variable parameter between groups was the tube thickness, and the variable between specimens within the same group was the axial load. Columns D1 - D5 were tested empty.

External dimensions of a typical specimen are shown in Figure 4.1. External diameter was measured at four points at 45^{o} around the mid-height section, and the arithmetic mean is given in Table 4.1. Thicknesses were measured at eight points at 45^{o} around the perimeter, and the mean value

is tabulated. The test specimen was 2 ft 3 in long. An 11 5/8 in long, 8 3/8 in diameter and 1 1/4 in thick tube was welded on to each end of the test specimen. The external surface of the end pieces was machined after being welded to the test specimen.

The total length of 4 ft 2 1/4 in was filled with concrete while the tube was held in a vertical position. Columns of the same group were filled with concrete on the same day; three columns were filled from one batch and the remaining two from a second batch of the same mix. A 1 1/4 in diameter poker vibrator was used.

Before pouring concrete the bottom of the tube was clamped tightly on to a steel plate so that the concrete was flush with the steel surface. The same result was achieved at the top by finishing the hardened surface of concrete with 'plycol'.

4.3 CONCRETE MIX

The concrete mix ratios by weight were:

water/cement	0.58
aggregate/cement	6.0
coarse/fine aggregate	1.5

Rapid hardening Portland cement was used. Maximum size of the aggregate was 3/4 in.

4.4 AUXILIARY TESTS

Two 6 in cubes were cast for each column, and cured under wet hessian for seven days. Then the cubes were stored in the ambient atmosphere of the laboratory until tested in accordance with BS 1881 (4.1) on the same

day as the column. Strengths of the two cubes were within 7 per cent of each other for all the columns, except for F4 when they were 10 per cent apart. The average value is given in Table 4.1.

Columns of the same group were cut from a single tube length from which three tensile coupons were also taken. The coupons were tested later, and the average values of the yield stress and Young's modulus are given in Table 4.1. The steel had a long yield plateau, the strain hardening strain being not less than 0.02.

4.5 INSTRUMENTATION

Figure 4.2 shows the positions of deflexion clocks and strain gauges. Deflexion measurements were taken on the convex side so that local wrinkling of the tube wall, if any, would have a minimum effect on the readings. The dial gauges were attached to a fixed vertical axis, therefore the readings do not represent deflexions relative to the column ends, but give the displacements of points 1, 2 and 3 (Figure 4.2) relative to one another. However, this has no effect on the value of the curvature calculated from the deflexions. It may be mentioned here that points 1 and 3 represent the centre of rotation of the top and bottom bearing respectively, therefore very small movements were anticipated at these two points.

The strain gauges were rosette type, each gauge being 10 mm long. The steel surface was cleaned with emery and the gauges were stuck with a commercial glue called "Devcon 101".

4.6 TEST RIG

The test rig is shown in Figure 4.3. It consisted of: (A) a 500 tonf lapped ram for applying a constant axial load, (B) two cylindrical oil-film bearings, (C) two moment arms into which the column ends were clamped, and, (D) two lapped rams, 10 tonf each, connected to the same pressure source but acting in opposite directions. The 10 tonf rams were connected to the moment arms through ball-seatings and were used to apply increasing moments, the distance between their centres being 4 ft 2 in.

Two smaller cylindrical bearings rotating in a plane at right angles to the plane of bending were interposed between the column ends and the oil-film bearings (B). The smaller bearings, which are not visible in Figure 4.3, were used to accommodate any initial out-of-straightness that the specimen may have had. However, the smaller bearings were locked immediately before the test had started.

The oil-film bearings (B) were practically frictionless; under a load of 300 tonf the bearings could be pushed sideways with one finger.

Three amsler cabinets were used - one for ram (A), one for ram (D) and the third for maintaining oil pressure in the oil-film bearings (B).

The structural frame of the rig consisted of 4 - 6 in diameter mild steel columns fixed at the bottom to the strong floor of the laboratory and at the top to a special box-girder. Friction clamps were used for all the eight connections.

4.7 EXPERIMENTAL PROCEDURE

Contact between the end faces of the specimen and the horizontal interior surface of clamps (C) was ensured by applying a small pressure

in ram (A). Pressure was next applied to the oil in the oil-film bearings (B), and then clamps (C) were tightly fixed. Initial gauge readings were taken at this stage. Oil pressure in ram (A) was then increased until the axial load reached a pre-assigned value P at which it was kept constant for the rest of the test.

After the constant axial load was reached, a continuously increasing moment was applied to the ends of the specimen by increasing the pressure in jacks (D). This was continued until the moment arms (C) were about to hit the 6 in diameter columns on one side of the structural frame. Then the pressure in rams (D) was released followed by release of pressure in ram (A). The test was complete. Strain and deflexion readings were taken throughout the test at fixed intervals of moment.

For 26 specimens strains were recorded by a digital data logger (SOLARTRON). For the remaining 9 specimens, i.e. all specimens in groups A and G except G2, a PEEKEL voltmeter was used. Deflexions were recorded manually for all the specimens.

4.8 EXPERIMENTAL RESULTS

The value of moment at which the test was terminated is given in Table 4.1. Since the centres of rotation of the top and bottom bearings (B) were only 7.5 in away from the mid-height of the test specimen, the deflexion at the mid-height of the specimen was small. Thus the additional moment (= axial load x deflexion) was small compared to the moment applied by the jacks (= load in jacks (D) x 4 ft 2 in), and is neglected.

Columns A1, B1, C1, D1, E1, F1 and G1 were tested under low axial loads, 3.9, 5.0, 6.0, 5.0, 5.0, 5.0 and 12.0 tonf. These were intended

to be tested under P = 0, however, a low value of P had to be maintained in order to secure the specimen in the top and bottom clamps. Successive columns in the same group were tested under increasing axial loads. (Table 4.1).

Strains of the order of 22,000 $\mu\varepsilon$ were measured. Strains ε_1, and ε_2 in gauges 1 and 2 (Figure 4.2B) give the curvature

$$\rho_s = \frac{\varepsilon_1 - \varepsilon_2}{d}$$

Within the elastic limit ε_3 and ε_4 are found to be nearly equal. However, they differ significantly in the post-elastic range, probably due to local weaknesses in the steel.

The deflexion readings also give a value of curvature. From the first order difference formula (Figure 4.2A)

$$\rho_d = \frac{\delta_1 - 2\delta_2 + \delta_3}{7.5^2}$$

For small values, ρ_s and ρ_d show close agreement, but for higher values they differ appreciably in some tests. ρ_s values are not available at high curvature because strain gauges 1 and 2 had failed by then. ρ_d is used in all the moment-curvature plots in Figures 4.4 to 4.10, except for A2 when ρ_s is plotted.

Maximum curvature in Figures 4.4 to 4.10 is 10,000 $\mu\varepsilon$/in. For the empty tube tests, group D, the moment-curvature curves show flat plateaus indicating that the stress-strain relationship for steel is trapezoidal. The falling part of the curve for D4 is ascribed to local wrinkling of the tube wall. Curves for the filled tubes, particularly those with high axial load, do not show a flat plateau because of the augmentation of the strength of concrete due to lateral containment.

Tests were terminated when the moment arm (C) (Figure 4.3) was about to touch the structural frame of the rig. At this stage the specimens were appreciably bent.

CHAPTER 5

COMPARISON OF EXPERIMENTAL MOMENT-CURVATURE CHARACTERISTICS WITH CALCULATIONS BASED ON EQUIVALENT STRESS-STRAIN CURVES

5.1 INTRODUCTION

Moment-load-curvature characteristics (referred to as M-P-ρ characteristics) have been experimentally determined for 35 circular sections of 6 5/8 in nominal diameter, comprising 7 thicknesses with 5 levels of axial load for each thickness. Five of the columns, (D1 - D5), were tested empty, and the remainder were filled. For the filled columns, when the axial load is low the triaxial effects are insignificant. The effect of triaxial augmentation increases with increasing axial load, approaching the maximum augmentation in the limiting case of a concentrically-loaded stub column.

In this chapter, a semi-rational method is presented for numerically simulating the experimental M-P-ρ characteritics on a digital computer, because a rigorous analysis is impracticable when triaxial effects are significant. Once the computer program is developed for simulating all the 35 experimental M-P-ρ curves, it may then be used for generating similar characteristics for any other section.

The process of numerical simulation consists primarily of developing a computer program which may calculate the M-P-ρ characteristics of any tubular section, either filled or empty, for any given set of stress-strain

relationships for the steel and concrete. The computer program is then used in three stages with pre-assumed sets of stress-strain relationships for the materials, and the calculated M-P-ρ curves are compared with the experimental ones. The three stages are:

Stage 1 - Empty tubes (D1 - D5): The uniaxial stress-strain relationship determined for the steel from tensile coupon tests, is used in the computer program. The computed M-P-ρ curves are then compared with the experimental ones.

Stage 2 - Uniaxial M-P-ρ curves: The stress-strain relationships for the steel and concrete, which have been used to determine the uniaxial column failure loads, are fed into the computer program to generate uniaxial M-P-ρ curves. These are then compared with the experimental curves to ascertain the level of the axial load above which triaxial effects must be included.

Stage 3 - Triaxial M-P-ρ curves: An approximate calculation is carried out by using a set of equivalent stress-strain relationships, augmented for the concrete and reduced for the steel, and based on the results of axially-loaded stub column tests. The calculated M-P-ρ characteristics are compared with the experimental curves.

5.2 STRESS-STRAIN RELATIONSHIPS

The available information on the relationships between the longitudinal stress and the longitudinal strain for the steel and the concrete is as follows:

Steel: The tensile coupon tests showed a long yield plateau, the strain hardening strain being not less than 0.02. Therefore it is

reasonable to assume the uniaxial stress-strain relationship for the steel as trapezoidal (Relationship 1 in Figure 5.1).

When the axial load is high the steel is stressed biaxially and it cannot sustain the uniaxial yield stress in the presence of a hoop tension. In the limiting case of a concentrically-loaded stub column, it has been shown that the relationship between the longitudinal stress and the longitudinal strain in the biaxially stressed steel may be approximated as:

$$\frac{\sigma}{\sigma_y} = 0.95\left(\frac{\varepsilon}{\varepsilon_y}\right) \qquad \text{when } \frac{\varepsilon}{\varepsilon_y} < 1.0$$

$$\frac{\sigma}{\sigma_y} = \frac{1.063\,(\varepsilon/\varepsilon_y) - 0.113}{1.417\,(\varepsilon/\varepsilon_y) - 0.417} \qquad \text{when } \frac{\varepsilon}{\varepsilon_y} > 1.0 \qquad (5.1)$$

Equation 5.1 has been derived from experimental results of stub columns having d/t ratios between 17 and 37; it may be mentioned here that the 35 M-P-ρ specimens have the same range of d/t. Equation 5.1 is plotted in Figure 5.1 and marked as relationship 2.

Concrete: The uniaxial stress-strain relationship for concrete has already been defined in Chapter 2:

$$\frac{\sigma}{\sigma_m} = 2.41(\varepsilon/\varepsilon_m) - 1.865(\varepsilon/\varepsilon_m)^2 + 0.5(\varepsilon/\varepsilon_m)^3 - 0.045(\varepsilon/\varepsilon_m)^4$$

$$\text{when } \frac{\varepsilon}{\varepsilon_m} < 4.0 \qquad (5.2)$$

$$\frac{\sigma}{\sigma_m} = 0 \qquad \text{when } \frac{\varepsilon}{\varepsilon_m} > 4.0$$

Equation 5.2 is plotted in Figure 5.2 and is marked as relationship 1.

Relationship 1 for concrete, when used with a trapezoidal stress-strain relationship for steel, would lead to M-P-ρ curves with a drooping part beyond the peak. However, the experimental M-P-ρ (Figures 4.4 to 4.10) do not have any falling part even when the axial load is small.

When the axial load is small the experimental M-P-ρ curves show a nearly flat plateau. This suggests that the stress-strain relationship for the concrete should also have a flat plateau instead of a falling branch beyond the peak. Thus a modified uniaxial stress-strain relationship identical to equation 5.2 for $\varepsilon/\varepsilon_m \leq 1.0$ and then having a flat plateau may be assumed. The modified stress-strain curve is shown as relationship 2 in Figure 5.2.

Whereas the peak stress in concrete under uniaxial compression is σ_m, it may be twice as strong when the radial stress is significant. It has been shown that the relationship between the longitudinal stress and the longitudinal strain in the concrete core of a stub column under increasing axial load may be approximated as:

$$\frac{\sigma}{\sigma_m} = \frac{2.41 \left(\frac{\varepsilon}{\varepsilon_m}\right)}{1 + 1.105 \left(\frac{\varepsilon}{\varepsilon_m}\right)} \qquad (5.3)$$

Equation 5.3 is plotted in Figure 5.2, and is marked as relationship 3.

5.3 COMPUTER PROGRAM

A computer program has been written for calculating the M-P-ρ characteristics for circular or rectangular concrete filled sections. An empty tube is analysed by specifying a zero stress for all strains in concrete. The same program can generate M-P-ρ curves for reinforced concrete sections.

The program is so written that it may take any stress-strain relationships for the steel and concrete (different relationships in tension and compression) into account. Various stress-strain relationships are used in the program, and they are stated as and when they occur. For the time

being it may be assumed that the stresses in the steel and concrete for a given strain are known.

The assumptions on which the computation is based are:

(1) There is no slip between the steel and concrete, and plane sections remain plane after bending;

(2) Stress-strain relationships are reversible and are identical in bending and compression;

(3) For any strain distribution the steel and concrete in the section may be replaced by a sufficient number of strips parallel to the neutral axis, so that the error involved in assuming a uniform stress distribution across the strip is negligible.

The computation of M-P-ρ characteristics consists basically of calculating the internal force and moment for a given strain distribution defined by the curvature ρ and the distance Y of the neutral axis from the centroidal axis. For given values of ρ and Y the strains at the centres of the strips are known, and the stresses may be calculated from known strain values by using the relevant stress-strain relationships. The stress at the centre of a strip is assumed to be uniform over the strip, whence the force in the strip and the moment of this force about the centroidal axis are calculated. The sum of the strip forces and moments gives the force and moment over the section for the given values of ρ and Y.

The process of dividing the steel and the concrete into a number of strips, makes it possible to incorporate any stress-strain relationship in the relevant sub-routine of the computer program without involving

the main program. In the computation the steel is divided into 30 strips and the concrete in 20; for the simple case of a square tube with trapezoidal stress-strain curves, this gives values of force and moment close to those obtained by rigorous integration.

The computation consists of the following steps:

(1) Select suitable values of the curvature ρ (40 - 10,000 $\mu\varepsilon$/in in increments of 40 $\mu\varepsilon$/in is used);

(2) Choose the value of the axial load P for which the moment-curvature relationship is required;

(3) Take the smallest value of ρ;

(4) Select a trial value of the distance Y of the neutral axis from the centroidal axis;

(5) Using the values of ρ and Y calculate the axial force P and the moment M;

(6) If the calculated P is equal to the required P, proceed to step (7). Otherwise modify the value of Y and repeat step (5) until the calculated and required values of P are within a pre-assigned tolerance;

(7) Take successively increasing values of ρ and repeat steps (4) to (6) for each value of ρ.

Steps (1) to (7) give the M-ρ relationship for one value of P; the process may be repeated for other values of P.

The program is used in three stages to calculate M-P-ρ characteristics for: (1) empty tubes, (2) filled tubes with uniaxial stress-strain relationships and (3) filled tubes with triaxial augmentation.

5.4 EMPTY TUBE

Five sections, D1 - D5, were tested empty under axial loads of 5, 20, 40, 80 and 100 tonf. Measured dimensions and material properties are given in Table 4.1, and the squash load P_L ($= A_s\sigma_y$) is given in Table 5.1. It may be seen that the ratio P/P_L varies between 0.05 and 0.95. Column D5 failed under 95 per cent of the calculated squash load before any moment was applied.

The experimental M-P-ρ curves for the remaining 4 sections are compared in Figures 5.3 to 5.6 with the curves computed from a trapezoidal stress-strain realtionship for the steel; it may be seen that there is satisfactory agreement. The experimental curve of column D4 shows a falling part because of local wrinkling of the tube walls under high strain.

The comparison in Figures 5.3 to 5.6 confirms the trapezoidal stress-strain relationship for the steel.

5.5 UNIAXIAL M-P-ρ RELATIONSHIP

M-P-ρ characteristics calculated from uniaxial stress-strain relationships for the steel and concrete are compared with the experimental characteristics in order to ascertain the level of axial load below which triaxial effects are insignificant.

The stress-strain relationships fed into the computer program are marked relationship 1 for the steel in Figure 5.1 and relationship 1 for the concrete in Figure 5.2.

In Table 5.1 the calculated uniaxial moments are compared with the test moments, and the axial load is given in the non-dimensional form

P/P_L where P_L is the nominal squash load ($= A_s\sigma_y + A_c\sigma_m$). It may be seen that P/P_L varies between 0.02 and 1.10, and that the agreement between the uniaxial moment and the test moment is satisfactory for low values of P/P_L. As the axial load increases, the triaxial effects become progressively higher.

The experimental M-P-ρ curves are compared with the calculated uniaxial curves for the first two columns of each series, i.e. for A1, A2, B1, B2, ..., G1 and G2 which were tested under low axial loads (Figures 5.7 to 5.18). There is excellent agreement between the experimental and the calculated curve up to the peak of the calculated curve. Beyond the peak the calculated curve has a falling part whereas the experimental curve has either a flat plateau or a gentle upward slope after the initial steep rise.

The above comparison suggests that even at low values of the axial load the stress-strain relationship of the concrete core does not have a falling part. The uniaxial stress-strain curve for concrete is, therefore, modified by adding a flat plateau at the peak instead of a falling part (called relationship 2 in Figure 5.2). This modified uniaxial stress-strain curve for the concrete is then used together with the trapezoidal curve for the steel, and M-P-ρ characteristics are calculated; these are called the modified uniaxial M-P-ρ characteristics.

The modified uniaxial M-P-ρ characteristics are plotted in Figures 5.7 to 5.18 for columns A1, A2, B1, B2, ..., G1 and G2. It may be seen that these curves are in satisfactory agreement with the experimental curves for all values of curvature. For these 12 columns the uniaxial M-P-ρ curves have nearly the same peak value of the moment as the modified uniaxial M-P-ρ curves, this means that column failure loads calculated from these two M-P-ρ curves will be nearly equal while P has a low value.

For the 12 columns, A1, A2, B1, B2, ..., G1 and G2, the ratio P/P_L varies between 0.02 and 0.32, and the modified uniaxial M-P-ρ curves are in satisfactory agreement with the experimental curves. As the ratio P/P_L becomes greater the difference between the experimental and modified uniaxial M-P-ρ curves becomes larger; this may be seen from Figures 5.19 to 5.21 where M-P-ρ curves are plotted for columns E3, E4 and E5 for which P/P_L varies between 0.47 and 0.87.

It is necessary to find the value of P/P_L up to which the modified uniaxial M-P-ρ curves are acceptable. This is done by comparing the maximum values of the moment for the experimental and the calculated M-P-ρ curves. Figure 5.23 shows a plot of the ratio (maximum experimental moment/maximum uniaxial moment) against P/P_L, and Figure 5.24 shows a similar plot using the modified uniaxial moments. It may be inferred that the modified uniaxial M-P-ρ curves can be used for all values of P/P_L up to 0.4.

In conclusion, M-P-ρ characteristics calculated from a trapezoidal stress-strain relationship for the steel, and a modified uniaxial stress-strain relationship for the concrete (shown as relationship 2 in Figure 5.2) show close agreement with experimental M-P-ρ characteristics for all values of P/P_L up to 0.4. As the value of P/P_L increases the difference between the calculated and the experimental M-P-ρ curves becomes greater because of increasing triaxial effects. Therefore, a different set of stress-strain relationships is necessary for simulating the experimental M-P-ρ curves when P/P_L is greater than 0.4; this is done in the next section.

Furlong [5.1, 5.2 and 5.3] tested 22 circular and 17 square sections under various amounts of axial loads, which were held constant while moments were increased until the columns ceased to sustain the axial loads.

The M-P-ρ curves are not given, instead the axial load and the moment at failure are tabulated. The ratio P/P_L varies between 0.0 and 0.86, 25 tests having P/P_L less than 0.50. The experimental failure moments are compared in Table 5.2 with calculated uniaxial moments. The pattern of increasing triaxial effects with increasing P/P_L is not as consistent as in the Imperial College tests, but the general conclusions drawn from the Imperial College tests are sustained.

5.6 TRIAXIAL M-P-ρ RELATIONSHIP

A set of stress-strain relationships for the steel and the concrete have to be assumed for generating M-P-ρ curves when P/P_L is greater than 0.4, i.e. triaxial effects are significant.

The available information on the stress-strain relationships for the steel and the concrete has been discussed in Section 5.2. It has also been shown that for $P/P_L \leq 0.4$ stress-strain relationship 1 for the steel (Figure 5.1) and relationship 2 for the concrete (Figure 5.2) are applicable. As P/P_L increases the triaxial effects become progressively higher, attaining the maximum triaxial effects in a concentrically-loaded stub column. For a concentrically-loaded stub column the equivalent stress-strain relationship for the steel is given by equation 5.1 (relationship 2, Figure 5.1) and for the concrete by equation 5.3 (relationship 3, Figure 5.2). Using these two stress-strain relationships the failure load of a stub column under pure compression may be calculated as:

$$P_u = 0.75\, A_s \sigma_y + 2.18\, A_c \sigma_m \qquad (5.4)$$

Equation 5.4 gives an approximate estimate of the failure load; a more exact estimate is given by equation 3.24.

The stress-strain relationships for the steel and concrete are known for the two limiting cases, namely, (i) when $P = 0.4\ P_L$ and an increasing moment is applied, and (ii) when there is no moment and P is increased until the column fails under a load P_u. For all intermediate cases, as P varies between $0.4\ P_L$ and P_u a linear interpolation for stress between the two limiting stress-strain curves may be adopted in the calculation of M-P-ρ relationships. This assumption is conjectural, but it is seen later that it leads to M-P-ρ curves in good agreement with the experimental curves.

The stress-strain relationships fed into the computer program for simulating experimental M-P-ρ curves when P is greater than $0.4\ P_L$, are summarised below:

(1) For the steel

(a) in compression -

A linear interpolation for stress between relationships 1 and 2 (Figure 5.1) as P varies between $0.4\ P_L$ and P_u

(b) in tension -

Relationship 1, i.e. a trapezoidal stress-strain curve, for all values of P. (When the steel is under a state of biaxial yield, the presence of hoop tension ($\leqslant \sigma_y$) can only increase the longitudinal tension beyond the yield stress. Therefore, it is safe to assume the full uniaxial stress-strain curve for the steel in tension, even when the axial load is high and triaxial effects are significant)

(2) For the concrete

(a) in compression -

A linear interpolation for stress between relationships 2 and 3 (Figure 5.2) as P varies between 0.4 P_L and P_u

(b) in tension -

Zero stress for all strains.

The above set of stress-strain relationships are fed into the computer and the 'triaxial' M-P-ρ characteristics are generated for the last three columns of each series, i.e. A3, A4, A5, B3, B4, B5, .., G3, G4 and G5 which have P/P_L varying between 0.4 and 1.10. The calculated triaxial curves are compared with the experimental M-P-ρ curves in Figures 5.25 to 5.41. The uniaxial M-P-ρ curves are also plotted on the same Figures to show the extent of triaxial augmentation. No comparison can be made for column B5 which failed under an axial load of 170 tonf before any moment was applied. For B5 the approximate stub column failure load P_u is 215 tonf; the reason for its premature failure cannot be traced.

From the comparison for the 17 columns in Figures 5.25 to 5.41 it may be inferred that the simulated triaxial M-P-ρ curves are in good agreement with the experimental curves.

5.7 CONCLUDING REMARKS AND SUGGESTIONS FOR FUTURE WORK

A method is now available for simulating the experimental M-P-ρ characteristics on a digital computer. The method may be used for all circular sections with the d/t ratios varying between 17 and 37.

The reported tests cover a range of d/t between 17 and 37, whereas the manufactured tubes have a d/t range of 15 to 52. Therefore some

further tests with thin tubes are necessary.

Although the method is applicable to all values of the axial load up to P_u, test data are not available for axial loads greater than the nominal squash load, i.e. $P_L \leq P \leq P_u$. When further tests are done the complete set of M-P-ρ curves will be available and failure loads may then be predicted for all eccentrically-loaded circular columns taking triaxial effects into account; in the meantime, it will be safe to analyse those eccentrically-loaded columns which have maximum loads less than P_L. The method of predicting the failure load for a given length and eccentricity from pre-determined M-P-ρ curves for the section is well known [5.4], however the analysis is not included in this thesis.

A similar set of tests on square and rectangular tubes seems to be necessary.

BIBLIOGRAPHY

CHAPTER 1

1.1 CHATEAU S. du

Tubular structures for the roofing of sports buildings.

Paper presented at the third International Conference on Building with Hollow Sections, organised by CIDECT at Essen, 6 May 1969.

1.2 MAKOWSKI Z. S.

The Boeing 747 hangar at London Airport - analysis and design.

Paper presented at the third International Conference on Building with Hollow Sections, organised by CIDECT at Essen, 6 May 1969.

1.3 QUATTORDIO G.

Selected applications in the field of tubular structures in Italy, port installations, domes, bridges.

Paper presented at the third International Conference on Building with Hollow Sections, organised by CIDECT at Essen, 6 May 1969.

1.4 EGA R.

Selected applications in the field of tubular structures in Belgium, masts, towers, road signal gantries.

Paper presented at the third International Conference on Building with Hollow Sections, organised by CIDECT at Essen, 6 May 1969.

1.5 GOFFAUX R.

Composite construction in the tour madou, Brussels.

Tubular Structures 4, September 1965.

1.6 KERENSKY O. A. and DALLARD N. J.

The four-level interchange between M4 and M5 motorways at Almondsbury.

Proc., I.C.E., July 1968.

1.7 CLIFT A.

The protection of tubular structures against corrosion.

Tubular Structures 7, February 1967.

1.8 BETTZIECHE P.

The structural design of joints in rectangular hollow sections.

Paper presented at the third International Conference on Tubular Structures, organised by CIDECT, Essen, 6 May 1969.

1.9 BONDALE D. S. and CLARK P. J.

Composite construction in the Almondsbury interchange.

B.C.S.A. Conference, September 1966.

1.10 CODE OF PRACTICE

Composite Columns - CP 117 (Part 3) Under preparation.

1.11 BLEICH F.

Buckling strength of metal structures.

McGraw Hill Book Co., Inc., 1952.

1.12 NEOGI P. K.

Concrete-filled tubular columns.

Ph.D. thesis, University of London, 1967.

1.13 NEOGI P. K., SEN H. K. and CHAPMAN J. C.

Concrete-filled tubular steel columns under eccentric loading.

Journ., Inst. of Struct. Engrs., May 1969.

1.14 KLOPPEL K. and GODER W.

Collapse load tests on concrete-filled steel tubes and derivation of a design formula.

Der Stahlbau, Vol. 26, January and February, 1957.

1.15 JANSS J.

Composite steel-concrete construction. Part 3. Tests on concrete-filled tubular columns.

Report published by the Centre of Scientific Research and Industrial Techniques of Metal Fabrication (CRIF), Brussels.

1.16 KATO B. and KANATANI H.

Experimental studies on concrete-filled steel tubular columns.

Steel Structures Laboratory Report, Department of Architecture, Faculty of Engineering, Tokio University, October 1966.

1.17 GARDNER N. J. and JACOBSON E. R.

Structural behaviour of concrete-filled steel tubes.

AC I, Journal, July 1967, pp 404.

1.18 GARDNER N. J.

Use of spiral welded steel tubes in pipe columns.

AC I, Journal, November 1968.

1.19 GUIAUX P. and DEHOUSSE N. M.

Tests on 22 eccentrically loaded square and rectangular concrete-filled tubular columns.

Test Report No. R 766, Laboratoires D'essais des Constructions du Genie Civil et D'Hydraulique Fluviale, University of Liege, Belgium, September 1968.

1.20 BASU A. K.

Computation of failure loads of composite columns.

Journal, Inst. of Civil Engineers, Proc. Vol. 36, March, 1967.

CHAPTER 2

2.1 NEOGI P. K., SEN H. K. and CHAPMAN J.C.
Concrete-filled tubular steel columns under eccentric loading.
Journal, Institution of Structural Engineers, May 1969.

2.2 GUIAUX P. and DEHOUSSE N. M.
Tests on 22 eccentrically-loaded square and rectangular concrete-filled tubular columns.
Test Report No. R766, Laboratoires D'essais des Constructions du Genie Civil et D'Hydraulique Fluviale, Universite de Liege, September 1968.

2.3 KERENSKY O. A. and DALLARD N. J.
The four-level interchange between M4 and M5 motorways at Almondsbury.
Proc., Institution of Civil Engineers, March 1967.

2.4 BASU A. K.
Computation of failure loads of composite columns.
Proc., Institution of Civil Engineers, March 1967.

2.5 HOGNESTAD E.
A study of combined bending and axial load in reinforced concrete members.
Univ. of Illinois, Bulletin No. 399, Nov 1951.

2.6 BARNARD P. R.
On the collapse load of composite beams.
Ph. D. thesis, Univ. of Cambridge, Sept 1963.

2.7 SCARBOROUGH J. B.
Numerical Mathematical Analysis.
The John Hopkins Press, Baltimore, Sixth edition, 1966.

2.8 FURLONG R. W.

Strength of steel-encased concrete beam-columns.

ASCE, Journ. of the Struct. Div., Oct 1967.

2.9 COLUMN RESEARCH COUNCIL

Guide to design criteria for metal compression members.

Edited by B. G. Johnston. Second Edition. John Wiley and Sons, Inc., 1966.

2.10 BRESLER B.

Design criteria for reinforced columns under axial load and biaxial bending.

ACI, Journal, Nov 1960.

2.11 RUSSIAN SPECIFICATION

Standards and specifications for the design of concrete and reinforced concrete structures.

Moscow 1955.

2.12 BASU A. K. and SOMMERVILLE W.

Derivation of formulae for the design of rectangular composite columns.

Institution of Civil Engrs., Paper No. 7206S, to be published.

2.13 BRITISH STANDARD

Specification for structural steel sections. Part 2 - Hot rolled hollow sections.

BS 4 (Part 2) - 1965 - pp 7.

2.14 BRITISH STANDARD

Specification for the use of structural steel in building.

BS 449, 1959 (reset and reprinted 1965).

2.15 MAUCH S. P.

Effect of creep and shrinkage on the capacity of concrete columns.
Symposium on R. C. Columns, SP-13, ACI, Detroit, 1966.

2.16 MANUEL R. F. and MACGREGOR J. G.

Analysis of restrained reinforced concrete columns under sustained load.
ACI, Journ. 1967, Proc. Vol. 64, No. 1.

2.17 BROMS B. and VIEST I. M.

Long reinforced concrete columns.
Trans., ASCE, Vol. 126, Part III.

2.18 RUSCH H.

Researches toward a general flexural theory for structural concrete.
ACI, Journ. 1960, Proc. Vol. 57, No. 1.

2.19 SEN H. K. and CHAPMAN J. C.

Ultimate load tables for concrete-filled tubular steel columns (circular, square and rectangular columns).
To be published by the Construction Industry Research and Information Association (CIRIA), Technical Note 9.

2.20 BRITISH STANDARD

Specification for weldable steel.
BS 4360, 1968.

2.21 CODE OF PRACTICE

CP 117 (Part 3): Composite construction in structural steel and concrete - columns in building and in bridges.

2.22 BRITISH STANDARD

New specification for bridges (under preparation) which will replace BS 153.

2.23 CODE OF PRACTICE

Draft Unified Code of Practice

2.24 CODE OF PRACTICE

The structural use of reinforced concrete in buildings.

CP 114, 1957.

2.25 CIRIA STUDY COMMITTEE ON STRUCTURAL SAFETY

Guidance for the drafting of Codes of Practice for structural safety.

Construction Industry Research and Information Association (CIRIA), Technical Note 2, August 1968.

2.26 TIMOSHENKO S. P. and GERE J. M.

Theory of elastic stability.

Second International Student Edition - pp 15. McGraw Hill Book Company, Inc.

2.27 BONDALE D.S. and CLARK P. J.

Composite construction in the Almondsbury Interchange.

B.C.S.A. Conference, September 1966.

CHAPTER 3

3.1 NEVILLE A. M.

Properties of concrete.

Sir Isaac Pitman and Sons Ltd, 1963.

3.2 RICHART R. E., BRANDTZAEG A. and BROWN R. L.

The failure of plain and spirally reinforced concrete in compression.

Illinois Univ., Bull. No. 190, April 2, 1929.

3.3 NEOGI P. K.

Concrete-filled tubular columns.

Ph. D. thesis, Univ. of London, 1967.

3.4 GARDNER N. J. and JACOBSON E. R.

Structural behaviour of concrete-filled steel tubes.

Journal, ACI, July 1967.

3.5 RICHART F. E., BRANDTZAEG A. and BROWN R. L.

A study of the failure of concrete under combined compressive stresses.

Illinois Univ., Bull. No. 185, November 20, 1928.

3.6 GOODIER J. N. and HODGE P. G. (JR).

Elasticity and Plasticity.

Written as the first report on Surveys in Applied Mathematics.

John Wiley and Sons, Inc., 1958.

3.7 MURPHY G.

Advanced mechanics of materials.

McGraw Hill Book Company, Inc., 1946. Chapter IV, articles 39 and 40.

3.8 SWAMY N.

The strength of plain, reinforced and prestressed concrete under combined stresses.

The Indian Concrete Journal, Vol. 35, No. 10, October 1961, pp 368 - 374.

3.9 NEWMAN K.

The structure and engineering properties of concrete.

International Symposium on the Theory of Arch Dams held at Southampton University, April 1964, pp 683 - 712.

3.10 HANNANT D. J. and FREDERICK C. O.

Failure criteria for concrete in compression.

Magazine of Concrete Research, Vol. 20, No. 64, September 1968.

3.11 GARDNER N. J.

Triaxial behaviour of concrete.

ACI, Journ., No. 2, Proc. Vol. 66, February 1969.

3.12 GARDNER N. J.

Use of spiral welded steel tubes in pipe columns.

ACI, Journ., No. 11, Proc. Vol. 65, November 1968.

CHAPTER 4

4.1 BRITISH STANDARD

Method for testing concrete.

BS 1881 - 1952.

CHAPTER 5

5.1 FURLONG R. W.

Strength of steel-encased concrete beam columns.

Journ. of the Struct. Div., A.S.C.E., Proc., Jan. 1968.

5.2 FURLONG R. W.

Design of steel-encased concrete beam columns.

Journ. of the Struct. Div., A.S.C.E., Proc., Jan. 1968.

5.3 FURLONG R. W.

Personal communication.

5.4 BASU A. K.

Computation of failure loads of composite columns.

Proc., Institution of Civil Engineers, March 1967.

APPENDIX A

YIELD CONDITION AND FLOW LAW FOR PLASTIC SOLIDS

The generalised yield condition and flow law for perfectly plastic solids were established between 1950 and 1956, and have been summarised by Hodge [3.6]. This appendix follows Hodge's summary.

When two or more independent stress components exist at a point, the elastic range cannot be represented by any finite number of values of the stress components; a functional representation is needed. Therefore it is assumed that there exists some function f which depends generally upon the stress components and the previous stress history, such that when f is less than some pre-assigned number the material is elastic. For a perfectly plastic solid, this yield function is, by definition, independent of the stress history and depends only upon the stress. Therefore, defining f in a suitably normalized fashion, the condition for elastic behaviour may be written as:

$$f(Q_1, Q_2, \ldots\ldots, Q_n) < 1$$

where $Q_1, Q_2, \ldots\ldots, Q_n$ are the generalised stress components.

Further it follows from the definition of perfect plasticity that f can never be greater than 1. Since f does not change with stress history, it is evident that plastic flow can take place only when f is and remains at unity. This may be presented as follows:

$$\begin{aligned} &\text{Plastic:} \quad f = 1 \quad \text{and} \quad \dot{f} = 0 \\ &\text{Elastic:} \quad f < 1 \quad \text{or} \quad \dot{f} < 0 \end{aligned} \tag{A.1}$$

where dots indicate differentiation with respect to time.

These conditions may be conveniently visualized in a stress space whose co-ordinates are the variables Q_i. The equation $f = 1$ then represents the yield surface and $f < 1$ is that side of the surface toward the origin.

Before proceeding further to establish a relation between plastic strain components and stress components, it is necessary to state Drucker's [3.6] postulate of plastic irreversibility: Let a perfectly plastic solid be in equilibrium under an arbitrary set of body forces and surface tractions. Now, let some external agency apply an additional load to the body and then remove it. Then the work done by the external agency during the loading is positive, and the work done by the external agency during the complete cycle of loading and unloading is non-negative. This requirement was first formulated by Drucker (1950 - 52) and is essentially a statement of plastic irreversibility. In other words, energy put into a plastic deformation can never be recovered.

The consequences of this postulate may now be discussed in the geometrical terminology of Figure 3.2. Let the equilibrium stress point under a set of body forces and surface tractions be at Q^* (inside or on the yield surface) at a time $t = 0$. Let the external agency be such as to move it first to point Q at a time t and then along the yield surface to point $Q + \delta Q$ at time $t + \delta t$. Removal of this agency then returns the point to Q^* at a time t^*. Denoting the components of Q^* by Q_i^* and the corresponding strains by q_i^*, etc., the total work done during the cycle may be written as

$$\delta W_T = \int_0^t Q_i \, q_i \, dt + \int_t^{t+\delta t} Q_i \, q_i \, dt + \int_{t+\delta t}^{t^{**}} Q_i \, q_i \, dt \tag{A.2}$$

Now, quite generally the total strain rates may be written as the sum of an elastic and a plastic part

$$\dot{q}_i = \dot{e}_i + \dot{p}_i \tag{A.3}$$

Then, since plastic straining can occur only from t to $t + \delta t$, equation A.2 becomes:

$$\delta W_T = \int_0^t Q_i \, \dot{e}_i \, dt + \int_t^{t+\delta t} Q_i \, (\dot{e}_i + \dot{p}_i) dt + \int_{t+\delta t}^{t^{**}} Q_i \, \dot{e}_i \, dt \tag{A.4}$$

$$\text{or} \quad \delta W_T = \oint Q_i \, \dot{e}_i \, dt + \int_t^{t+\delta t} Q_i \, \dot{p}_i \, dt \tag{A.5}$$

Here, the symbol $\oint$ refers to integration about the complete path, returning to the point Q . However, since by definition this integral is elastic, the net work done in a closed cycle is zero, and equation A.5 reduces to

$$\delta W_T = \int_t^{t+\delta t} Q_i \, \dot{p}_i \, dt \tag{A.6}$$

Therefore, work done by the external agency alone is

$$\delta W_e = \int_t^{t+\delta t} (Q_i - Q_i^{**}) \, \dot{p}_i \, dt \tag{A.7}$$

whence

$$\lim_{\delta t \to 0} \frac{\delta W_e}{\delta t} = (Q_i - Q_i^{**}) \, \dot{p}_i \tag{A.8}$$

Therefore the postulate that work done by an external agency during a complete cycle of loading and unloading be non-negative amounts to:

$$(Q_i - Q_i^*)\ \dot{P}_i \geq 0 \qquad \text{(A.9)}$$

Equation A.9 imposes a very severe restriction on the allowable shapes of the yield surface $f = 1$. Since the left hand side is a vector product, condition A.9 can be satisfied only if $\text{Cos}\theta \geq 0$ or $\theta \leq \pi/2$, where θ is the angle between vector $(Q_i - Q_i^*)$ and vector $\dot{p}_i$. That is $\dot{p}_i$ must make a non-obtuse angle with every vector $(Q_i - Q_i^*)$, and this must be true for any Q^* in or on the yield surface. Therefore, if a plane is drawn through Q perpendicular to $\dot{p}_i$, then all admissible points Q^* must lie on or to one side of this plane. This means that the yield surface $f = 1$ must be convex.

Reversing the above argument, $\dot{p}_i$ must make a non-obtuse angle with every vector $(Q_i - Q_i^*)$. At a point on the surface with a uniquely defined normal, this can only be satisfied if $\dot{p}_i$ is in the direction of the normal. Thus

$$\dot{P}_i = \dot{\lambda} \frac{\partial f}{\partial Q_i} \qquad \text{(A.10)}$$

where $\dot{\lambda}$ is an undetermined but non-negative scalar quantity.

In conclusion, given the convex function f, the behaviour of the perfectly plastic material is governed by equation A.3 relating elastic and plastic strains, A.1 stating the condition for elastic or plastic behaviour, and A.10 giving the plastic flow law.

APPENDIX B

POST-ELASTIC BIAXIAL STRESS-STRAIN RELATIONSHIP

The generalised yield condition and flow law, stated in Appendix A, are applied here to the particular case of a tubular column. An element of steel in the tube is subjected to a longitudinal compression σ_{sL}, a hoop stress σ_{sH} and a radial pressure σ_{sR} (Figure 3.1). σ_{sR} is small compared to the first two stresses, and is neglected; consequently, the problem is reduced to a biaxial stress condition.

When the steel stress-point is on the yield-ellipse defined by equation 3.4, let the stresses be σ_{sL} and σ_{sH}. At this instant let there be a small increment of load on the filled tube for which the experimentally determined strain increments are $\delta\varepsilon_{sL}$ and $\delta\varepsilon_{sH}$. With the small increment of load the individual values of the stresses change while the stress-point moves to a new position on the yield ellipse. The problem is to calculate the stress increments $\delta\sigma_{sL}$ and $\delta\sigma_{sH}$ from the known strain increments $\delta\varepsilon_{sL}$ and $\delta\varepsilon_{sH}$.

From equation A.3 it follows that the two strain increments may be written as the sum of an elastic and a plastic component:

$$\delta\varepsilon_{sL} = \delta\varepsilon^{e}_{sL} + \delta\varepsilon^{p}_{sL} \qquad (B.1)$$

$$\delta\varepsilon_{sH} = \delta\varepsilon^{e}_{sH} + \delta\varepsilon^{p}_{sH} \qquad (B.2)$$

From flow law A.10 it follows that

$$\frac{\delta\varepsilon^p_{sL}}{\delta\varepsilon^p_{sH}} = \frac{\partial f/\partial \sigma_{sL}}{\partial f/\partial \sigma_{sH}}$$

where f is the yield surface given by equation 3.4 in our case. Hence

$$\frac{\delta\varepsilon^p_{sL}}{\delta\varepsilon^p_{sH}} = \frac{2\,\sigma_{sL} - \sigma_{sH}}{2\,\sigma_{sH} - \sigma_{sL}} = \gamma \quad \text{(say)} \qquad \text{(B.3)}$$

Taking the partial derivatives of equation 3.4 with respect to σ_{sL} and σ_{sH} and adding them together

$$2\sigma_{sL}\,\partial\sigma_{sL} - \sigma_{sH}\,\partial\sigma_{sL} - \sigma_{sL}\,\partial\sigma_{sH} + 2\sigma_{sH}\,\partial\sigma_{sH} = 0$$

or

$$\frac{\partial\sigma_{sL}}{\partial\sigma_{sH}} = \frac{\sigma_{sL} - 2\,\sigma_{sH}}{2\,\sigma_{sL} - \sigma_{sH}} = -\frac{1}{\gamma} = \alpha \quad \text{(say)} \qquad \text{(B.4)}$$

Since σ_{sL} and σ_{sH} are known, γ and α may be calculated from equations B.3 and B.4.

For the elastic components $\delta\varepsilon^e_{sL}$ and $\delta\varepsilon^e_{sH}$ the following relations are applicable

$$E_s\,\delta\varepsilon^e_{sL} = \delta\,\sigma_{sL} - \nu_s\,\delta\sigma_{sH}$$

or

$$E_s\,\frac{\partial\varepsilon^e_{sL}}{\partial\sigma_{sH}} = \frac{\partial\sigma_{sL}}{\partial\sigma_{sH}} - \nu_s \qquad \text{(B.5)}$$

Substituting equation B.4 in B.5 and rearranging

$$\frac{\partial\varepsilon_{sL}}{\partial\sigma_{sH}} = \frac{\alpha - \nu_s}{E_s} \qquad \text{(B.6)}$$

Similarly,

$$\frac{\partial \varepsilon^{e}_{sH}}{\partial \sigma_{sH}} = \frac{1 - \nu_s \alpha}{E_s} \tag{B.7}$$

It follows from equation B.1 that

$$\delta\varepsilon^{p}_{sL} = \delta\varepsilon_{sL} - \delta\varepsilon^{e}_{sL}$$

or

$$\frac{\partial \varepsilon^{p}_{sL}}{\partial \sigma_{sH}} = \frac{\partial \varepsilon_{sL}}{\partial \sigma_{sH}} - \frac{\partial \varepsilon^{e}_{sL}}{\partial \sigma_{sH}} \tag{B.8}$$

Substituting equation B.6 in B.8

$$\frac{\partial \varepsilon^{p}_{sL}}{\partial \sigma_{sH}} = \frac{\partial \varepsilon_{sL}}{\partial \sigma_{sH}} - \frac{\alpha - \nu_s}{E_s} \tag{B.9}$$

Similarly,

$$\frac{\partial \varepsilon^{p}_{sH}}{\partial \sigma_{sH}} = \frac{\partial \varepsilon_{sH}}{\partial \sigma_{sH}} - \frac{1 - \nu_s \alpha}{E_s} \tag{B.10}$$

Dividing B.9 by B.10

$$\frac{\partial \varepsilon^{p}_{sL}}{\partial \varepsilon^{p}_{sH}} = \frac{\delta\varepsilon_{sL} - \frac{\delta\sigma_{sH}}{E_s}(\alpha - \nu_s)}{\delta\varepsilon_{sH} - \frac{\delta\sigma_{sH}}{E_s}(1 - \nu_s \alpha)} \tag{B.11}$$

Substituting equation B.3 in B.11, noting $\alpha = -\frac{1}{\gamma}$, and rearranging

$$\delta\sigma_{sH} = \frac{E_s (\delta\varepsilon_{sL} - \gamma\, \delta\varepsilon_{sH})}{\alpha - 2\nu_s - \gamma} \tag{B.12}$$

From equation B.4 it follows that

$$\delta\sigma_{sL} = \alpha\, \delta\sigma_{sH} \tag{B.13}$$

Equations B.12 and B.13 give the increments in stresses for small increments of strain when the steel is in a state of yield under stresses σ_{sL} and σ_{sH}. When $\delta\sigma_{sL}$ and $\delta\sigma_{sH}$ are added respectively to σ_{sL} and σ_{sH},

a new pair of values is obtained for σ_{sL} and σ_{sH}. This pair of values also lies on the yield-ellipse providing $\delta\varepsilon_{sL}$ and $\delta\varepsilon_{sH}$ are sufficiently small.

APPENDIX C

FAILURE CRITERIA FOR CONCRETE

Surveys of failure criteria for concrete under multiaxial stresses have been compiled by several authors (3.5, 3.8 and 3.9) who have pointed out the limitations of various theories.

The concrete core in a filled tube is stressed by triaxial compression where $\sigma_1 > \sigma_2 = \sigma_3$ ($\sigma_1 = \sigma_{cL}$ and $\sigma_2 = \sigma_3 = \sigma_{cR}$). Fortunately, reliable experimental evidence is available for this state of stress in concrete; the most comprehensive set of results was published by Richart et al. (3.5), who tested 208 concrete cylinders under various combinations of axial and radial compression. Series 3A consisted of 64 - 4 in x 8 in cylinders tested under a state of stress similar to that acting on the core of filled tubes, i.e. $\sigma_1 > \sigma_2 = \sigma_3$. There is, however, one difference in the stress-history of these tests and a filled tube. In a filled tube $\sigma_2 = \sigma_3$ ($= \sigma_{cR}$) develops simultaneously with σ_1 ($= \sigma_{cL}$), whereas in series 3A, $\sigma_2 = \sigma_3$ was first raised to the pre-determined value and then σ_1 was applied in increments to failure.

In series 3A $\sigma_2 = \sigma_3$ varied between 180 and 4090 lbf/in^2 and σ_1 between 2840 and 19000 lbf/in^2. 64 cylinders were made of three different mixes with f_{cy} = 1050, 2575 and 3660 lbf/in^2. The following conclusions were reached:

(i) The presence of lateral pressure adds to the strength of the specimen an amount, in general 4.1 times the magnitude of the lateral pressure, i.e., at failure

$$\sigma_1 = f_{cy} + 4.1\ \sigma_2 \qquad (C.1)$$

At low lateral pressure the overall expression C.1 is conservative. For $\sigma_2 = \sigma_3 < 1000$ lbf/in^2, the following expression is more accurate:

$$\sigma_1 = f_{cy} + 5.1\ \sigma_2 \qquad (C.2)$$

However, at high values of $\sigma_2 = \sigma_3$ a better fit is given by

$$\sigma_1 = f_{cy} + 3.5\ \sigma_2 \qquad (C.3)$$

(ii) Laterally contained concrete has high ductility. The longitudinal strain at maximum load ranged from 5000 to 70,000 $\mu\varepsilon$.

It may be noted here that equations C.1, C.2 and C.3 can be related to Coulomb's "internal friction theory", i.e., for each individual element the resistance to sliding τ is taken to be made up of two parts, one term τ_o, representing the shear strength of the material, and the second, $C\sigma$, a constant times the normal stress, representing the frictional resistance:

$$\tau = \tau_o + C\sigma \qquad (C.4)$$

If Mohr's circles are plotted for equation C.1, the resulting Mohr-envelope is a straight line of the form of equation C.4:

$$\tau = \tau_o + 0.78\ \sigma \qquad (C.5)$$

where $\tau_o = 0.25\ f_{cy}$

Equation C.5 may be regarded as a criterion for sliding failure.

Richart et al. [3.2] tested concrete columns with spiral reinforcement under axial loading and got a confirmation of equation C.1; in this case, $\sigma_2 = \sigma_3$ developed simultaneously with σ_1 as in the case of a stub column.

Hannant and Frederick [3.10] have recently compiled most available data for concrete under triaxial compression and recommended a two stage minimum strength line of the form of equations C.1 to C.3:

$$\begin{aligned} \sigma_1 &= f_{cy} + 4\sigma_2 , \quad \text{for} \quad \sigma_1 < 4f_{cy} \\ \sigma_1 &= 1.75f_{cy} + 3\sigma_2 , \quad \text{for} \quad 4f_{cy} < \sigma_1 < 8f_{cy} \end{aligned} \tag{C.6}$$

Gardner [3.11] tested 28 cylinders under triaxial compression and found agreement with equation C.1 given by Richart.

Section (Axis of bending)	Specimen	d Depth cm	b Breadth cm	t Thickness cm	l Length (hinge to hinge) cm	l/d	e eccentricity cm	y_{oc} Initial central deflection cm	$e+0.9y_{oc}$ cm	σ_y yield stress tonnes/cm^2	f_{cu} 20 cm cube strength Tonnes/cm^2	P_T Experimental failure load Tonnes	P_m Calculated failure load Tonnes	P_T/P_m	Mode of failure
Rectangular Major-axis (Filled)	A1	20.14	10.16	0.575	366.5	18.2	0.0	0.36	0.324	4.4815	0.435	108.0	176.2 (102.8)*	1.050	A
	A2	20.44	10.24	0.585	366.5	17.9	2.03	0.25	2.255		0.435	100.7	126.1 (107.2)	0.939	A
	A3	20.39	10.15	0.565	367.7	18.0	4.06	0.15	4.195		0.435	97.7	97.8 (102.1)	0.999	A
	A4	20.44	10.22	0.530	367.7	18.0	8.12	0.18	8.282		0.435	72.7	68.8 (99.6)	1.057	A
	A5	20.46	10.25	0.570	367.7	18.0	12.18	0.17	12.333		0.535	>49.0	60.8 (109.4)		B
Rectangular Minor-axis (Empty)	BE1	20.38	10.25	0.575	72.0	7.0	6.10	0.0	6.100	4.4815	0.0	56.7	62.4	0.909	C
	BE2	20.39	10.06	0.545	122.7	12.2		0.05	6.145		0.0	47.7	54.1	0.882	C
	BE3	20.49	10.23	0.550	183.6	17.9		0.04	6.136		0.0	45.2	50.6	0.893	C
	BE4	20.34	10.25	0.580	244.6	23.9		0.10	6.190		0.0	47.2	47.4	0.996	A
	BE5	20.42	10.18	0.560	305.6	30.0		0.27	6.343		0.0	40.7	40.3	1.010	A
	BE6	20.48	10.27	0.560	366.6	35.7		0.06	6.154		0.0	38.2	36.8	1.038	A
Rectangular Minor-axis (Filled)	BF1	20.44	10.19	0.520	72.0	7.1	6.10	0.0	6.100	4.4815	0.439	76.7	76.0	1.009	A
	BF2	20.48	10.24	0.540	122.6	12.0		0.04	6.136		0.443	76.7	73.1	1.049	A
	BF3	20.40	10.17	0.505	183.7	18.1		0.06	6.154		0.443	65.2	61.5	1.060	A
	BF4	20.36	10.22	0.570	244.5	23.9		0.10	6.190		0.439	60.7	58.6	1.036	A
	BF5	20.41	10.13	0.540	305.6	30.2		0.10	6.190		0.443	49.5	48.7	1.016	A
	BF6	20.37	10.23	0.560	366.6	35.8		0.13	6.217		0.443	45.4	43.9	1.034	A
Square (Filled)	C1	20.34	20.25	0.630	122.7	6.1	8.12	0.06	8.174	4.2288	0.484	163.7	160.6	1.019	C
	C2	20.29	20.30	0.635	244.0	12.0		0.15	8.255		0.484	149.7	145.2	1.031	A
	C3	20.26	20.34	0.635	305.5	15.1		0.31	8.399		0.484	143.7	134.6	1.068	A
	C4	20.36	20.40	0.635	366.6	18.0		0.19	8.291		0.484	127.7	127.2	1.004	A
	C5	20.40	20.37	0.655	488.3	23.9		0.28	8.372		0.484	119.2	110.1	1.083	A

(E_s = 2000 tonnes/cm^2)

* Figures within parenthesis are minor axis buckling loads

Mode of failure: A = overall bending
B = test incomplete
C = local wrinkling or bulging

Table 2.1 Comparison between calculated and experimental loads for square and rectangular columns

Specimen	Test load P_T	Computed loads					P_T/P_c	P_T/P_{xy}
		P_x	P_{ay}	P_{ax}	P_c = smaller of P_x and P_{ay}	P_{xy} calculated from Equation 2.14a		
A1	108.0	176.2	102.8	176.2	102.8	102.8	1.05	1.05
A2	100.7	126.1	107.2	189.3	107.2	83.5	0.94	1.20
A3	97.7	97.8	102.1	190.8	97.8	67.7	1.00	1.44
A4	72.7	68.8	99.6	181.9	68.8	52.4	1.06	1.39
A5	> 49.0	60.8	109.4	202.7	60.8	48.4	-	-

(all loads are in metric tons)

P_{ay} and P_{ax} take measured initial out-of-straightness into account.

Table 2.2 Comparison between experimental loads and loads calculated from equation 2.14a - Series A

(Liege tests)

Cube strength lbf/in^2	Yield stress tonf/in^2	Length ft	Thickness = 0.144 in: Failure load tonf P_1	P_2	P_3	P_4	Thickness = 0.25 in: Failure load tonf P_1	P_2	P_3	P_4
3000	16	6	36.1	35.9	36.1	36.5	55.7	55.4	55.8	56.6
		8	32.4	31.8	32.3	32.8	50.0	49.2	49.9	50.7
		10	26.9	26.2	26.7	27.3	41.7	40.5	41.4	42.3
		12	21.4	20.6	21.1	21.7	33.1	31.9	32.7	33.6
		14	16.8	16.2	16.6	17.0	26.0	25.0	25.6	26.3
	23	6	50.0	49.5	49.9	50.4	77.8	77.0	77.7	78.4
		8	42.5	41.5	42.2	43.0	66.2	64.6	65.7	67.0
		10	32.8	31.8	32.4	33.1	51.1	49.4	50.4	51.5
		12	24.7	23.8	24.3	24.8	38.2	36.9	37.7	38.5
		14	18.6	18.0	18.4	18.7	29.0	28.0	28.6	29.1
9000	16	6	51.2	50.6	50.9	51.3	67.8	67.2	67.7	68.2
		8	43.0	42.0	42.7	43.4	59.4	58.2	59.1	60.2
		10	34.4	33.4	34.1	34.8	48.3	46.7	47.8	48.9
		12	26.7	25.7	26.3	27.0	37.7	36.3	37.2	38.1
		14	20.4	19.5	20.1	20.6	29.2	28.0	28.7	29.4
	23	6	66.2	65.3	66.0	66.7	92.3	91.2	92.1	93.1
		8	53.8	52.4	53.4	54.4	76.3	74.2	75.6	77.0
		10	40.4	39.1	39.8	40.7	57.5	55.6	56.7	57.9
		12	29.6	28.5	29.1	29.7	42.5	41.0	41.9	42.7
		14	21.7	21.0	21.4	21.8	31.8	30.7	31.3	35.0

d = diameter = 4.5 in

e = eccentricity = 0.0

y_{oc} = initial central deflection = $0.00006\ l^2/d$

ρ_{oc} = initial central curvature = $0.0006/d$

e_o = Fictitious eccentricity (to replace initial out-of-straightness)
= $r.y_{oc}$, where r is taken as 1.0, 0.9 and 0.8 for loads P_2, P_3 and P_4 respectively

P_1 = failure load for the column with an initial central curvature ρ_{oc}

P_2, P_3 and P_4 = see the definition of e_o

Table 2.3 Influence of r (where $e_o = r.y_{oc}$) on the failure load

σ_y/γ_m = 16 tonf/in^2																						
f_{cu}/γ_m		3000 lbf/in^2							6000 lbf/in^2							9000 lbf/in^2						
P_L		365 tonf							516 tonf							666 tonf						
e/d		0	0.1	0.2	0.4	0.6	0.8	1.0	0	0.1	0.2	0.4	0.6	0.8	1.0	0	0.1	0.2	0.4	0.6	0.8	1.0
Effective length - 1 ft	6	345	273	226	162	120	94.0	76.4	492	377	308	206	146	110	87.6	637	480	383	244	166	122	95.2
	8	335	263	218	156	116	91.0	74.3	468	362	294	196	140	106	84.6	602	458	364	230	157	116	91.6
	10	322	252	208	149	112	87.8	71.9	448	343	278	186	133	101	81.5	575	433	342	216	149	111	87.9
	12	309	239	198	142	107	84.5	69.5	425	324	261	175	126	97.1	78.4	543	406	319	202	140	106	84.4
	14	295	227	187	135	102	81.3	67.2	401	303	245	165	120	92.9	75.4	509	378	296	189	133	101	80.9
	16	282	214	177	128	97.9	78.2	64.9	377	283	229	156	114	89.0	72.6	474	350	274	177	126	96.4	77.8
	18	272	203	167	122	93.7	75.4	62.7	354	264	213	146	109	85.2	69.9	440	323	253	166	119	92.2	74.9
	20	263	191	157	116	89.6	72.4	60.6	334	245	199	138	103	81.7	67.3	409	298	234	156	113	88.2	72.0
	22	254	181	148	110	85.8	69.7	58.6	316	228	185	130	98.4	78.3	64.9	381	274	217	146	108	84.4	69.3
	24	244	172	140	105	82.2	67.1	56.6	299	213	173	123	93.7	75.1	62.6	355	253	202	138	102	80.9	66.7
	26	231	162	132	99.5	78.6	64.6	54.7	282	198	162	116	89.4	72.1	60.3	331	233	187	130	97.3	77.4	64.2
	28	218	153	125	94.7	75.3	62.2	52.9	263	185	151	110	85.2	69.2	58.1	307	216	174	122	92.6	74.3	61.9
	30	204	145	118	90.0	72.1	59.9	51.0	244	173	141	104	81.3	66.4	56.1	284	200	162	115	88.2	71.2	59.6
	35	169	124	103	79.5	64.7	54.4	46.9	200	146	120	91.0	72.5	60.0	51.2	230	165	136	99.7	78.1	64.1	54.3
	40	139	106	89.2	70.3	58.2	49.5	43.0	162	122	103	79.8	64.6	54.3	46.8	183	137	115	86.8	69.4	57.8	49.5

Area: Steel 13.4 in^2 Concrete 140.5 in^2

Moment of inertia: Steel 315 in^4 Concrete 1571 in^4

Table 2.4 Ultimate loads for 14 in diameter x 5/16 in thick column (when γ_m = 1.0 for steel and concrete)

σ_y/γ_m = 23 tonf/in^2																							
f_{cu}/γ_m		3000 lbf/in^2							6000 lbf/in^2							9000 lbf/in^2						
P_L		459 tonf							609 tonf							760 tonf						
e/d		0	0.1	0.2	0.4	0.6	0.8	1.0	0	0.1	0.2	0.4	0.6	0.8	1.0	0	0.1	0.2	0.4	0.6	0.8	1.0
Effective length - 1 ft	6	439	346	285	208	158	125	103	579	450	367	257	187	144	116	725	553	446	299	211	159	127
	8	428	333	274	200	152	121	99.8	563	431	351	246	180	139	113	699	528	425	284	202	153	122
	10	415	319	262	192	147	117	96.6	542	410	333	233	172	134	109	670	500	401	268	191	146	117
	12	402	304	248	184	140	112	93.3	519	387	314	220	163	128	104	637	469	376	252	181	139	112
	14	391	289	235	174	134	108	90.0	495	364	295	208	155	122	100	603	438	350	236	171	133	108
	16	383	274	222	164	128	104	86.8	474	340	275	196	147	117	96.3	569	406	324	221	162	126	103
	18	372	259	209	156	122	99.4	83.5	456	318	257	184	140	112	92.4	540	376	300	207	153	120	98.8
	20	357	245	197	147	116	95.3	80.4	434	297	239	173	132	106	88.7	509	348	277	193	145	115	94.7
	22	340	231	186	139	111	91.3	77.5	408	277	223	163	126	102	85.2	475	321	256	181	137	109	90.7
	24	319	217	175	132	106	87.5	74.4	379	258	207	153	119	97.0	81.8	438	296	237	169	129	104	87.0
	26	295	203	164	125	101	83.7	71.6	348	239	193	144	113	92.7	78.5	400	273	219	159	122	99.3	83.4
	28	272	190	155	118	95.8	80.2	68.9	318	222	180	135	107	88.5	75.3	364	252	203	149	116	94.6	80.0
	30	248	178	145	112	91.2	76.8	66.2	289	206	168	127	102	84.5	72.3	330	231	188	139	110	90.3	76.6
	35	197	148	124	97.1	80.7	68.9	60.1	227	169	141	110	89.4	75.5	65.2	255	187	156	119	95.9	80.2	68.9
	40	156	124	106	84.7	71.5	61.9	54.4	176	139	119	94.7	78.7	67.3	58.9	194	152	130	102	84.0	71.4	62.1
Area: Steel 13.4 in^2									Moment of inertia: Steel 315 in^4														
Concrete 140.5 in^2									Concrete 1571 in^4														

Table 2.5 Ultimate loads for 14 in diameter x 5/16 in thick column (when γ_m= 1.0 for steel and concrete)

σ_y/γ_m = 16 tonf/in^2																						
f_{cu}/γ_m		3000 lbf/in^2							6000 lbf/in^2							9000 lbf/in^2						
P_L		405 tonf							553 tonf							701 tonf						
e/d		0	0.1	0.2	0.4	0.6	0.8	1.0	0	0.1	0.2	0.4	0.6	0.8	1.0	0	0.1	0.2	0.4	0.6	0.8	1.0
Effective length - l ft	6	384	305	253	183	137	108	88.1	526	407	333	228	164	125	100	669	508	410	267	185	138	109
	8	373	294	244	176	133	105	85.7	503	390	319	218	157	121	96.9	635	486	390	253	176	132	105
	10	359	281	233	169	128	101	83.1	482	371	303	207	150	116	93.4	606	460	367	238	167	126	101
	12	345	268	222	161	122	97.4	80.4	459	351	286	196	143	111	90.0	573	432	344	224	158	121	96.8
	14	331	254	211	153	117	93.9	77.7	434	330	268	185	136	106	86.7	539	403	320	210	150	115	93.0
	16	319	241	199	146	112	90.4	75.3	410	309	251	175	130	102	83.6	504	375	298	197	142	110	89.5
	18	310	229	188	139	108	87.1	72.7	387	289	235	165	123	97.8	80.5	470	347	277	186	135	106	86.0
	20	301	217	178	133	103	83.9	70.3	367	270	220	156	118	93.7	77.6	439	321	257	174	129	101	82.8
	22	291	207	169	126	99.0	80.7	68.1	351	252	206	147	112	90.0	74.9	412	297	239	164	122	96.7	79.7
	24	279	196	160	120	94.8	77.8	65.8	334	236	193	139	107	86.4	72.2	388	275	222	155	116	92.7	76.8
	26	266	186	151	114	90.9	75.0	63.7	315	221	181	132	102	82.9	69.7	363	255	207	146	111	88.9	74.0
	28	251	176	143	109	87.1	72.3	61.5	295	207	169	125	97.6	79.7	67.3	338	237	193	138	106	85.2	71.3
	30	235	166	136	104	83.5	69.6	59.5	274	194	159	119	93.3	76.6	64.8	312	220	180	130	101	81.8	68.7
	35	195	143	118	91.8	75.2	63.3	54.7	225	164	136	104	83.2	69.3	59.3	254	184	152	113	89.4	73.7	62.7
	40	161	123	103	81.3	67.6	57.6	50.2	183	139	117	91.1	74.4	62.8	54.3	204	154	129	98.8	79.6	66.6	57.3

Area: Steel 16.0 in^2
Concrete 137.9 in^2

Moment of inertia: Steel 373 in^4
Concrete 1513 in^4

Table 2.6 Ultimate loads for 14 in diameter x 3/8 in thick column (when γ_m = 1.0 for steel and concrete)

σ_y/γ_m = 23 tonf/in^2																						
f_{cu}/γ_m		3000 lbf/in^2							6000 lbf/in^2							9000 lbf/in^2						
P_L		518 tonf							666 tonf							814 tonf						
e/d		0	0.1	0.2	0.4	0.6	0.8	1.0	0	0.1	0.2	0.4	0.6	0.8	1.0	0	0.1	0.2	0.4	0.6	0.8	1.0
Effective length - 1 ft	6	497	392	323	237	181	144	119	634	494	404	287	212	165	134	774	595	483	330	237	181	144
	8	484	378	311	229	175	140	116	616	474	387	275	204	159	129	749	570	461	315	227	174	140
	10	471	362	297	219	169	135	112	594	452	368	261	195	153	125	719	540	436	298	216	166	134
	12	458	346	283	209	162	130	108	570	427	348	248	186	147	120	686	508	409	280	205	159	129
	14	449	329	268	199	155	125	105	547	402	327	234	177	140	116	651	475	382	263	194	152	124
	16	440	313	254	189	148	120	101	528	378	306	221	168	134	111	619	443	355	247	184	144	119
	18	427	297	240	179	141	115	97.3	510	355	286	208	159	128	107	591	411	330	232	174	138	114
	20	411	281	227	170	135	111	93.7	487	332	267	196	151	123	103	560	382	306	217	165	132	109
	22	391	266	214	161	129	106	90.2	459	311	250	185	144	117	98.5	524	354	284	204	156	125	105
	24	367	250	202	152	122	102	86.8	427	290	233	174	137	112	94.6	484	328	263	191	148	120	100
	26	341	235	190	144	117	97.5	83.6	393	270	218	164	130	107	90.9	443	304	244	180	140	114	96.2
	28	314	220	179	136	111	93.5	80.4	359	251	204	154	123	102	87.3	404	281	227	169	133	109	92.3
	30	287	206	168	129	106	89.5	77.5	327	233	190	145	117	97.8	83.8	366	259	211	159	126	104	88.5
	35	228	172	144	113	93.9	80.5	70.2	257	192	161	126	103	87.3	75.6	285	211	176	136	110	92.5	79.8
	40	181	144	123	98.5	83.4	72.2	63.7	201	159	136	109	91.0	78.0	68.4	219	173	147	117	96.8	82.5	71.9
Area: Steel 16.0 in^2 Concrete 137.9 in^2									Moment of inertia: Steel 373 in^4 Concrete 1513 in^4													

Table 2.7 Ultimate loads for 14 in diameter x 3/8 in thick column (when $\gamma_m = 1.0$ for steel and concrete)

σ_y/γ_m = 16 tonf/in^2																							
f_{cu}/γ_m		3000 lbf/in^2							6000 lbf/in^2							9000 lbf/in^2							
P_L		443 tonf							588 tonf							732 tonf							
e/d		0	0.1	0.2	0.4	0.6	0.8	1.0	0	0.1	0.2	0.4	0.6	0.8	1.0	0	0.1	0.2	0.4	0.6	0.8	1.0
Effective length - 1 ft	6	420	334	277	202	152	120	98.7	556	434	357	248	180	139	112	697	533	433	288	203	152	121
	8	408	322	267	194	147	117	96.1	535	417	342	237	173	134	108	664	511	413	274	193	146	117
	10	394	309	256	186	142	113	93.2	514	397	325	226	166	129	104	634	484	390	259	184	140	112
	12	379	294	244	178	136	109	90.4	489	375	308	214	158	123	101	601	456	366	243	175	134	108
	14	365	380	232	170	131	105	87.4	464	354	290	203	151	118	97.0	566	426	342	229	166	128	104
	16	354	267	220	163	126	102	84.7	440	332	272	192	144	114	93.6	531	397	319	216	158	123	100
	18	346	254	208	155	121	97.9	82.0	418	311	255	181	137	109	90.2	498	369	297	203	150	118	96.3
	20	337	242	198	148	116	94.4	79.3	400	292	239	172	131	105	87.0	468	343	277	191	143	113	92.7
	22	326	230	187	141	111	91.0	76.7	384	274	224	163	125	101	84.0	443	318	258	180	136	108	89.3
	24	313	219	178	134	106	87.6	74.3	366	257	211	154	119	96.7	81.1	419	296	240	170	129	104	86.1
	26	298	208	169	128	102	84.5	71.9	346	242	198	146	114	92.9	78.3	393	276	224	161	123	99.3	83.0
	28	281	197	160	122	98.0	81.5	69.5	324	228	186	139	109	89.4	75.5	366	257	210	152	117	95.3	80.0
	30	263	187	152	116	94.0	78.5	67.2	302	214	175	132	104	85.9	72.9	340	240	196	144	112	91.4	77.2
	35	219	161	133	103	84.7	71.6	61.9	249	182	150	115	93.1	77.8	66.8	277	201	166	125	99.8	82.6	70.4
	40	181	138	116	91.5	76.3	64.2	56.9	203	154	130	102	83.4	70.6	61.2	223	169	142	110	88.9	74.7	64.4
Area: Steel 18.6 in^2									Moment of inertia: Steel 429 in^4														
Concrete 135.3 in^2									Concrete 1457 in^4														

Table 2.8 Ultimate loads for 14 in diameter x 7/16 in thick column (when γ_m = 1.0 for steel and concrete)

σ_y/γ_m = 23 tonf/in^2																						
f_{cu}/γ_m		3000 lbf/in^2							6000 lbf/in^2							9000 lbf/in^2						
P_L		573 tonf							718 tonf							863 tonf						
e/d		0	0.1	0.2	0.4	0.6	0.8	1.0	0	0.1	0.2	0.4	0.6	0.8	1.0	0	0.1	0.2	0.4	0.6	0.8	1.0
Effective length - 1 ft	6	550	434	359	264	203	162	134	685	535	438	314	234	183	149	818	634	516	359	260	200	161
	8	537	419	345	255	196	157	130	665	513	420	301	225	177	145	795	607	493	342	250	193	156
	10	523	402	330	244	189	152	126	643	490	400	287	216	170	140	765	577	467	324	238	185	150
	12	511	384	314	233	181	146	122	618	464	378	272	206	163	135	731	543	440	306	226	176	144
	14	502	367	299	222	173	141	118	596	438	356	258	196	156	129	697	510	412	288	214	169	138
	16	492	350	283	211	166	135	114	579	413	334	244	187	150	125	666	476	384	271	203	161	133
	18	479	333	268	200	159	130	110	560	388	313	230	178	143	120	640	444	357	255	193	154	127
	20	462	315	254	190	151	125	106	536	365	294	217	169	137	115	608	413	332	239	183	147	122
	22	439	298	240	180	145	120	102	506	342	275	205	161	131	111	570	385	309	225	173	140	117
	24	413	281	226	171	138	115	98.3	472	320	257	193	153	125	106	528	358	287	211	164	134	113
	26	384	264	213	162	131	110	94.5	435	298	241	182	145	120	102	484	332	267	199	156	128	108
	28	353	247	201	153	125	106	91.1	398	278	225	171	138	115	98.1	441	307	249	187	148	122	104
	30	323	231	189	145	119	101	87.7	362	259	211	162	131	110	94.3	401	284	232	175	140	116	99.5
	35	257	194	162	127	106	91.0	79.6	285	214	179	140	116	98.1	85.2	312	233	194	151	123	104	89.7
	40	204	162	139	111	94.3	81.8	72.2	223	177	152	122	102	87.9	77.2	242	191	163	130	108	92.5	80.9
Area: Steel 18.6 in^2									Moment of inertia: Steel 429 in^4													
Concrete 135.3 in^2									Concrete 1457 in^4													

Table 2.9 Ultimate loads for 14 in diameter x 7/16 in thick column (when γ_m = 1.0 for steel and concrete)

E_s $\frac{tonf}{in^2}$ / 1 ft	12000	12500	13000	13500	14000
10	321.8	321.9	322.0	322.1	322.2
15	318.1	318.4	318.7	318.8	319.1
20	311.4	312.2	312.9	313.4	314.0
30	255.2	261.3	266.7	271.7	276.6
45	127.1	132.3	137.0	142.3	147.2
60	72.6	75.5	78.5	81.4	84.5

(all loads are given in tonf)

(10 in x 10 in x 0.375 in, σ_y = 23 tonf/in^2, f_{cu} = 0.0, e/d = 0.01, initially straight)

Table 2.10 $P_m - E_s$ relationship

1 ft (1)	BS 449 load x 1.7 Tonf (2)	Failure load calculated by the computer. Tonf (3)	(2)/(3) (4)
e = 0.0			
6	299	288	1.04
10	293	286	1.02
14	282	284	0.99
18	265	268	0.99
22	240	243	0.99
26	210	212	0.99
30	178	177	1.01
e = 6 in			
6	107	128	0.84
10	107	121	0.88
14	105	110	0.95
18	102	100	1.02
22	99	92	1.08
26	94	83	1.13
30	87	76	1.14

(10 in x 10 in x 0.5 in, σ_y = 16 tonf/in^2, f_{cu} = 0.0, BS 449 initial imperfection)

Table 2.11 Comparison between loads calculated according to BS 449 and by the computer program

Column	Thickness in	Length ft	Eccentricity in	Design load (Dead + live) P_w tonf	Computed failure load tonf		Load Factor	
					Short-term P_{ms}	Long-term P_{ml}	P_{ms}/P_w	P_{ml}/P_w
A7	0.375	17.8	0.609	253	2045	1930	8.08	7.63
B6	0.375	28.6	0.609	360	1934	1710	5.37	4.75
D5A	0.375	9.0	0.609	321	2099	2049	6.54	6.38
F4A	0.375	7.8	0.609	320	2103	2061	6.57	6.44
H1	0.375	8.2	0.609	373	2102	2058	5.64	5.52
A9	0.375	13.6	0.609	312	2076	1996	6.65	6.40
C7	0.375	23.4	0.609	282	1994	1821	7.07	6.46
D6A	0.375	10.1	0.844	764	2046	1995	2.68	2.61
F5A	0.500	8.9	0.999	957	2243	2200	2.34	2.30
H4A	0.375	9.6	0.845	764	2048	1999	2.68	2.62
J3	0.375	19.6	0.609	305	2031	1896	6.66	6.22
C8	0.375	20.4	0.609	335	2023	1881	6.04	5.61
K3	0.375	19.6	0.609	347	2032	1897	5.86	5.47
L1	0.375	9.1	0.609	351	2099	2048	5.98	5.83
D9	0.375	10.1	0.609	387	2094	2038	5.41	5.27
F6A	0.375	9.1	0.609	332	2099	2048	6.32	6.17
H5A	0.375	9.7	0.609	332	2095	2043	6.31	6.15
K4	0.375	33.6	0.609	394	1866	1602	4.74	4.06
L3	0.375	15.8	0.609	355	2062	1963	5.81	5.53
D6B	0.625	7.6	0.997	1102	2470	2432	2.24	2.21
D5B	0.375	6.8	0.750	633	2079	2044	3.28	3.23
D4B	0.375	8.3	0.609	404	2102	2056	5.20	5.09
D1	0.375	31.2	0.75	536	1858	1623	3.47	3.03
F2	0.438	17.0	0.843	849	2111	2004	2.49	2.36
F4B	0.625	8.1	0.997	1138	2467	2426	2.17	2.13
F5B	1.500	6.6	1.312	1780	3993	3955	2.24	2.22
F6B	0.625	7.0	0.997	1149	2473	2438	2.15	2.12
F8	0.438	17.1	0.843	750	2110	2001	2.81	2.67
H9	0.375	33.0	0.75	533	1832	1583	3.44	2.97
H6B	0.375	8.8	0.609	404	2099	2053	5.20	5.08
H5B	0.375	8.3	0.75	645	2072	2031	3.21	3.15
H4B	0.625	10.3	0.997	1102	2456	2399	2.23	2.18
D4C	0.688	11.9	0.997	1150	2524	2455	2.19	2.13
F5C	1.750	11.4	1.714	3200	7129	7031	2.23	2.20
H6C	0.625	12.0	0.997	1150	2444	2375	2.12	2.06

Diameter - 42 in for F5C; 30 in for the others
Yield stress - 22 tonf/in^2 for F5B and F5C; 22.5 tonf/in^2 for D4C; 23 tonf/in^2 for the others
Cube strength - 7500 lbf/in^2 for F5B and F5C; 6000 lbf/in^2 for the others
(The strain corresponding to the peak stress in concrete is taken as 0.0025 and 0.0050 in the computation of short- and long-term load respectively)

Table 2.12 Comparison between the design load and the computed failure load of the concrete-filled columns at the Almondsbury Interchange (2.3)

Specimen	Length (in)		Measured (in)		$\frac{d}{t}$	Steel properties					Cube strength f_{cu} lbf/in^2
	Tube	Overall l	Diameter d	Thickness t		Yield stress σ_y tonf/in^2	0.1 % Proof stress tonf/in^2	0.5 % Proof stress tonf/in^2	Ultimate stress tonf/in^2	Young's modulus E_s tonf/in^2	
M11	27	31	6.62	0.179	37.0	19.2	19.2	19.8	30.6	13400	5530
M12	27	31	6.63	0.179	37.0	19.2	19.2	19.8	30.6	13400	7950
M13	27	31	6.62	0.179	37.0	19.2	19.2	19.8	30.6	13400	4170
M14	27	31	6.63	0.178	37.2	19.2	19.2	19.8	30.6	13400	7840
M15	27	31	6.67	0.201	33.2	20.0	19.9	20.0	31.9	13400	8915
M16	27	31	6.66	0.222	30.0	19.1	19.1	19.2	29.8	13400	8915
M17	27	31	6.65	0.260	25.6	19.3	19.2	19.6	31.6	13400	8915
M18	27	31	6.63	0.257	25.8	19.3	19.2	19.6	31.6	13400	5910
M19	27	31	6.63	0.256	25.9	19.3	19.2	19.6	31.6	13400	9270
M20	27	31	6.67	0.292	22.8	20.2	20.2	20.5	30.9	13400	8265
M21	27	31	6.65	0.357	18.6	20.9	20.9	21.2	32.4	13400	8265
M22	27	31	6.66	0.390	17.1	19.7	19.7	19.7	29.6	13400	8265
M23	27	31	6.66	0.389	17.1	19.7	19.7	19.7	29.6	13400	5910
M24	27	31	6.67	0.389	17.1	19.7	19.7	19.7	29.6	13400	9270

Table 3.1 Dimensions and material properties of stub columns M11 - M24 - Imperial College tests[3.3]

Specimen	Load up to which strain readings are available P'_T tonf	Experimental failure load P_T tonf	Nominal squash load = $A_s\sigma_y + A_c\sigma_m$ P_L tonf	$\frac{P'_T}{P_T}$	$\frac{P_T}{P_L}$
M11	187	201	131	0.93	1.53
M12	211	224	156	0.94	1.44
M13	157	175	115	0.90	1.52
M14	192	212	156	0.91	1.36
M15	261	261	180	1.00	1.45
M16	249	253	182	0.99	1.39
M17	268	280	195	0.95	1.44
M18	200	241	161	0.83	1.50
M19	250	268	196	0.93	1.37
M20	281	294	203	0.95	1.45
M21	314	340	229	0.92	1.48
M22	280	349	231	0.80	1.51
M23	266	340	208	0.78	1.63
M24	355	361	241	0.98	1.50

Table 3.2 Failure loads for stub columns M11 - M24

Specimen	P_y tonf	$\frac{P_y}{P_T}$	$\frac{\sigma_{sL}}{\sigma_y}$	$\frac{\sigma_{sH}}{\sigma_y}$	$\frac{\sigma_{cL}}{\sigma_m}$	$\frac{\sigma_{cR}}{\sigma_m}$	$P_s = A_s \sigma_{sL}$ tonf	$\frac{P_s}{P_y}$	$P_c = A_c \sigma_{cL}$ tonf	$\frac{P_c}{P_y}$
M11	117.6	0.58	0.98	-0.03	0.81	+0.02	68.4	0.58	49.2	0.42
M12	156.0	0.70	0.95	-0.09	1.02	+0.04	66.2	0.42	89.8	0.58
M13	108.1	0.62	0.98	-0.04	0.88	+0.03	67.9	0.63	40.2	0.37
M14	181.0	0.85	1.01	+0.01	1.28	-0.01	69.8	0.38	111.2	0.62
M15	189.2	0.72	0.98	-0.03	1.11	+0.01	80.5	0.42	108.7	0.58
M16	175.5	0.69	1.02	+0.05	0.91	-0.02	87.8	0.50	87.7	0.50
M17	192.4	0.69	0.90	-0.18	1.08	+0.09	90.7	0.47	101.7	0.53
M18	141.9	0.59	1.00	-0.00	0.69	+0.00	98.9	0.70	43.0	0.30
M19	176.3	0.66	1.00	-0.00	0.80	+0.00	98.9	0.56	77.4	0.44
M20	191.2	0.65	0.97	-0.06	0.90	+0.04	114.1	0.60	77.1	0.40
M21	215.6	0.63	0.99	-0.02	0.86	+0.02	145.6	0.68	70.0	0.32
M22	224.6	0.64	1.00	+0.00	0.91	-0.00	151.6	0.67	73.0	0.33
M23	194.5	0.57	1.00	+0.00	0.75	-0.00	151.5	0.78	43.0	0.22
M24	231.5	0.64	1.01	+0.01	0.88	-0.01	152.3	0.66	79.2	0.34

(Compression + ve)

Table 3.3 Loads and stresses at the first yield of steel - stub columns M11 - M24

Column	$\frac{t}{d}$x100	Load near failure P'_T tonf	$\frac{P'_T}{P_T}$	$\frac{\sigma_{sL}}{\sigma_y}$	$\frac{\sigma_{sH}}{\sigma_y}$	$\frac{\sigma_{cL}}{\sigma_m}$	$\frac{\sigma_{cR}}{\sigma_m}$	P_s tonf	$\frac{P_s}{P'_T}$	P_c tonf	$\frac{P_c}{P'_T}$
M11	2.7	187.1	0.93	0.87	-0.22	2.08	+0.12	60.8	0.32	126.3	0.68
M12	2.7	211.2	0.94	0.71	-0.43	1.84	+0.17	49.5	0.23	161.7	0.77
M13	2.7	156.8	0.90	-	-	-	-	-	-	-	-
M14	2.7	192.2	0.91	0.83	-0.28	1.55	+0.11	57.8	0.30	134.4	0.70
M15	3.0	261.0	1.00	0.70	-0.44	2.07	+0.18	57.4	0.22	203.6	0.78
M16	3.3	249.4	0.99	0.67	-0.48	1.99	+0.20	57.5	0.23	191.9	0.77
M17	3.9	267.8	0.95	0.74	-0.42	2.06	+0.21	74.4	0.28	193.4	0.72
M18	3.9	199.8	0.83	0.80	-0.32	1.94	+0.25	79.2	0.40	120.6	0.60
M19	3.9	249.6	0.93	0.82	-0.30	1.73	+0.15	81.3	0.32	168.3	0.68
M20	4.4	281.0	0.95	0.70	-0.44	2.31	+0.29	82.6	0.29	198.4	0.71
M21	5.4	313.7	0.92	0.77	-0.36	2.45	+0.31	113.8	0.36	199.9	0.64
M22	5.8	280.5	0.80	0.82	-0.29	1.95	+0.26	124.2	0.44	156.3	0.56
M23	5.8	265.9	0.78	-	-	-	-	-	-	-	-
M24	5.8	354.8	0.98	0.54	-0.62	3.03	+0.48	81.3	0.23	273.5	0.77

(Compression + ve)

Table 3.4 Stresses near failure at load P'_T - stub columns M11 - M24

Specimen	Failure load tonf			$\frac{P_T}{(P_H)_{\text{equation 3.24}}}$	$\frac{(P_H)_{\text{equation 3.24}}}{(P_H)_{\text{equation 3.3}}}$
	Test P_T	Calculated P_H			
		Equation 3.24	Equation 3.3		
M11	201	177	196	1.14	0.90
M12	224	204	222	1.10	0.92
M13	175	162	181	1.08	0.90
M14	212	203	221	1.04	0.92
M15	261	235	257	1.11	0.91
M16	253	240	262	1.05	0.92
M17	280	261	287	1.07	0.91
M18	241	227	253	1.06	0.90
M19	268	262	287	1.02	0.91
M20	294	281	310	1.05	0.91
M21	340	324	359	1.05	0.90
M22	349	328	364	1.06	0.90
M23	340	305	341	1.11	0.89
M24	361	338	374	1.07	0.90

Table 3.5 Comparison between calculated and experimental failure loads - stub columns M11 - M24

β	P_H (tonf) from equation 3.23							
	λ = 3		λ = 4		λ = 5		λ = 6	
	Tube 1	Tube 2	Tube 1	Tube 2	Tube 1	Tube 2	Tube 1	Tube 2
0.0	123	176	123	176	123	176	123	176
-0.2	132	194	137	204	142	214	147	224
-0.4	139	205	148	223	157	240	166	258
-0.5	141	209	151	230	162	250	172	271
-0.6	143	214	155	237	167	261	179	285
-0.8	145	218	159	247	173	275	187	304
-1.0	147	223	163	255	179	287	195	320
-1.2	148	224	165	259	182	294	200	329
-1.5	150	226	169	264	188	302	207	339
∞	149	224	177	279	205	335	233	390

Description:

Item	Tube 1	Tube 2
d in	6.625	6.625
t in	0.176	0.375
σ_y tonf/in^2	16.0	16.0
f_{cu} lbf/in^2	6000	6000

β and λ are defined in subsection 3.5.2.

Table 3.6 Influence of β and λ on the stub column failure load P_H

Specimen	Diameter in	Thickness in	0.2 °/o proof-stress Kips/in^2	Cube strength lbf/in^2	Failure load tonf		$\frac{P_T}{P_H}$
					Test P_T	Equation 3.24 P_H	
1a	6.64	0.104	43.2	2600	133	100	1.33
2a	6.64	0.104	43.2	4950	122	127	0.96
3a	6.66	0.103	46.0	5300	131	135	0.97
4a	6.66	0.103	46.0	4870	133	130	1.02
5a	6.62	0.142	32.1	3860	156	113	1.38
6a	6.62	0.142	32.1	4750	144	123	1.17
6b	6.62	0.142	32.1	4750	147	123	1.20
7a	6.64	0.197	37.8	4770	197	165	1.19
7b	6.64	0.197	37.8	4770	198	165	1.20
8a	6.64	0.197	37.8	3980	199	156	1.28
8b	6.64	0.197	37.8	3980	199	156	1.28

Table 3.7 Comparison between experimental and calculated failure loads for 11 stub columns tested by Gardner (3.12)

Specimen	Diameter in	Thickness in	Cube strength lbf/in^2	Yield stress $tonf/in^2$	Young's modulus $tonf/in^2$	Axial load tonf	Maximum moment tonf.in
A1	6.647	0.181	8450	23.7	13650	3.9	240.0
A2	6.660	0.184	7880			38.0	244.0
A3	6.661	0.177	8660			100.0	219.0
A4	6.655	0.176	8570			100.0	140.0
A5	6.661	0.185	7880			170.0	140.5
B1	6.661	0.188	6640	23.9	13310	5.0	240.0
B2	6.672	0.179	6400			50.0	234.0
B3	6.667	0.194	6890			100.0	214.0
B4	6.655	0.189	6600			150.0	170.0
B5	6.650	0.191	6070			170.0	0.0
C1	6.615	0.206	7900	23.1	13070	6.0	248.0
C2	6.616	0.211	7590			50.0	270.0
C3	6.613	0.208	7340			100.0	260.0
C4	6.614	0.208	7840			150.0	215.0
C5	6.620	0.217	7580			200.0	90.0
D1	6.675	0.228	0.0	22.9	13420	5.0	202.5
D2	6.676	0.212	0.0			20.0	186.0
D3	6.608	0.218	0.0			40.0	174.0
D4	6.677	0.227	0.0			80.0	79.5
D5	6.674	0.228	0.0			100.0	0.0
E1	6.622	0.268	7460	25.8	13490	5.0	312.5
E2	6.611	0.275	7430			50.0	312.5
E3	6.622	0.269	7310			100.0	298.0
E4	6.621	0.276	7760			155.0	255.0
E5	6.609	0.279	7240			190.0	165.0
F1	6.637	0.331	6770	23.9	13530	5.0	390.0
F2	6.621	0.323	7160			50.0	367.5
F3	6.624	0.328	6630			100.0	360.0
F4	6.619	0.326	6670			150.0	330.0
F5	6.632	0.331	6820			200.0	280.0
G1	6.672	0.396	8380	21.0	13610	12.0	374.0
G2	6.672	0.397	7960			60.0	430.0
G3	6.665	0.399	8870			100.0	372.0
G4	6.664	0.398	7960			150.0	372.0
G5	6.671	0.399	8340			200.0	240.0

(Specimens B5 and D5 failed under the axial load)

Table 4.1 Experimental data for the moment-load-curvature tests - Imperial College

Specimen	Experimental		Calculated		$\frac{P}{P_L}$	$\frac{M_T}{M_c}$
	Axial load P tonf	Maximum moment M_T tonf.in	Nominal squash load P_L tonf	Maximum moment M_c tonf.in		
A1	3.9	240.0	180.8	211.6	0.02	1.13
A2	38.0	244.0	176.2	230.1	0.22	1.06
A3	100.0	219.0	182.0	171.4	0.55	1.28
A4	100.0	140.0	180.4	168.3	0.55	0.83
A5	170.0	140.5	176.6	-	0.96	-
B1	5.0	240.0	164.9	216.6	0.03	1.11
B2	50.0	234.0	158.8	210.0	0.32	1.11
B3	100.0	214.0	170.5	154.4	0.59	1.39
B4	150.0	170.0	164.7	35.7	0.91	4.76
B5	170.0	0.0	159.6	0.0	1.06	-
C1	6.0	248.0	181.1	227.8	0.03	1.09
C2	50.0	270.0	179.8	238.0	0.28	1.13
C3	100.0	260.0	175.8	163.5	0.57	1.59
C4	150.0	215.0	181.2	71.9	0.83	2.99
C5	200.0	90.0	182.2	0.0	1.10	-
D1	5.0	202.5	105.8	214.6	0.05	0.94
D2	20.0	186.0	98.6	190.3	0.20	0.98
D3	40.0	174.0	100.2	161.3	0.40	1.08
D4	80.0	79.5	105.3	74.6	0.76	1.07
D5	100.0	0.0	105.7	17.9	0.95	-
E1	5.0	312.5	215.5	308.2	0.02	1.01
E2	50.0	312.0	217.8	314.9	0.23	0.99
E3	100.0	298.0	214.4	247.9	0.47	1.20
E4	155.0	255.0	222.2	152.7	0.70	1.67
E5	190.0	165.0	217.5	66.5	0.87	2.48
F1	5.0	390.0	224.5	340.8	0.02	1.14
F2	50.0	367.5	224.4	333.2	0.22	1.10
F3	100.0	360.0	221.3	270.5	0.45	1.33
F4	150.0	330.0	220.6	164.4	0.68	2.01
F5	200.0	280.0	224.8	61.6	0.89	4.54
G1	12.0	374.0	245.2	362.6	0.05	1.03
G2	60.0	430.0	241.5	355.8	0.25	1.21
G3	100.0	372.0	250.6	324.9	0.40	1.14
G4	150.0	372.0	241.4	212.0	0.62	1.76
G5	200.0	240.0	245.8	110.7	0.81	2.17

(Dimensions and material properties are given in Table 4.1);

(Columns D1 - D5 were tested empty)

Table 5.1 Comparison between experimental and uniaxial maximum moments - Imperial College tests

Shape	Size in	Thickness in	Yield stress $\frac{tonf}{in^2}$	Cylinder strength $\frac{lbf}{in^2}$	Experimental: Axial load P tonf	Experimental: Maximum moment M_T tonf.in	Calculated: Nominal squash load P_L tonf	Calculated: Maximum moment M_c tonf.in	$\frac{P}{P_L}$	$\frac{M_T}{M_c}$
Square	5.00	0.189	31.38	6500	111.6	138.4	172.5	114.4	0.65	1.21
					67.0	162.9		189.6	0.39	0.86
					67.0	192.0		189.6	0.39	1.01
					44.6	200.9		220.7	0.26	0.91
Round	4.50	0.125	26.78	4200	44.6	44.6	71.0	40.3	0.63	1.11
					40.2	47.3		46.3	0.57	1.02
					33.5	58.5		55.2	0.47	1.06
					22.3	62.9		67.3	0.31	0.94
					11.2	64.3		71.9	0.16	0.89
Square	4.00	0.084	21.43	3400	37.5	19.8	49.2	18.7	0.76	1.06
					37.5	19.9		18.7	0.76	1.06
					24.3	40.9		37.7	0.49	1.08
					9.0	46.8		49.7	0.18	0.94
					9.0	50.9		49.7	0.18	1.02
Round	6.00	0.061	21.43	3750	57.0	39.3	67.1	20.3	0.85	1.94
				3750	42.3	70.4	67.1	46.5	0.63	1.51
				3750	28.7	68.2	67.1	64.7	0.43	1.05
				3050	13.7	64.0	59.2	64.2	0.23	1.00
				3050	13.6	59.4	59.2	64.2	0.23	0.92
Square	4.00	0.125	21.43	4180	43.9	53.1	66.2	35.4	0.66	1.50
					30.7	72.3		54.3	0.46	1.33
					30.3	72.3		54.9	0.46	1.32
					26.2	84.8		60.6	0.40	1.40
					12.9	93.3		69.5	0.20	1.34
					12.9	86.2		69.5	0.20	1.24
					4.0	73.7		68.6	0.06	1.07
					0.0	91.1		66.6	0.00	1.37
Round	5.00	0.095	18.75	5100	57.0	34.8	66.4	16.0	0.86	2.18
					53.6	50.0		21.6	0.81	2.32
					40.2	62.9		41.9	0.61	1.50
					35.3	62.5		48.6	0.53	1.29
					35.0	56.4		48.9	0.53	1.15
					34.6	62.7		49.4	0.52	1.27
					30.7	67.2		53.7	0.46	1.25
					26.8	69.6		56.7	0.40	1.23
					26.2	69.4		57.1	0.40	1.22
					17.5	65.0		59.8	0.26	1.09
					8.9	62.8		57.9	0.13	1.08
					4.4	58.0		55.0	0.07	1.05

Table 5.2 Comparison between experimental and uniaxial maximum moments - Furlong's tests (5.1 and 5.2)

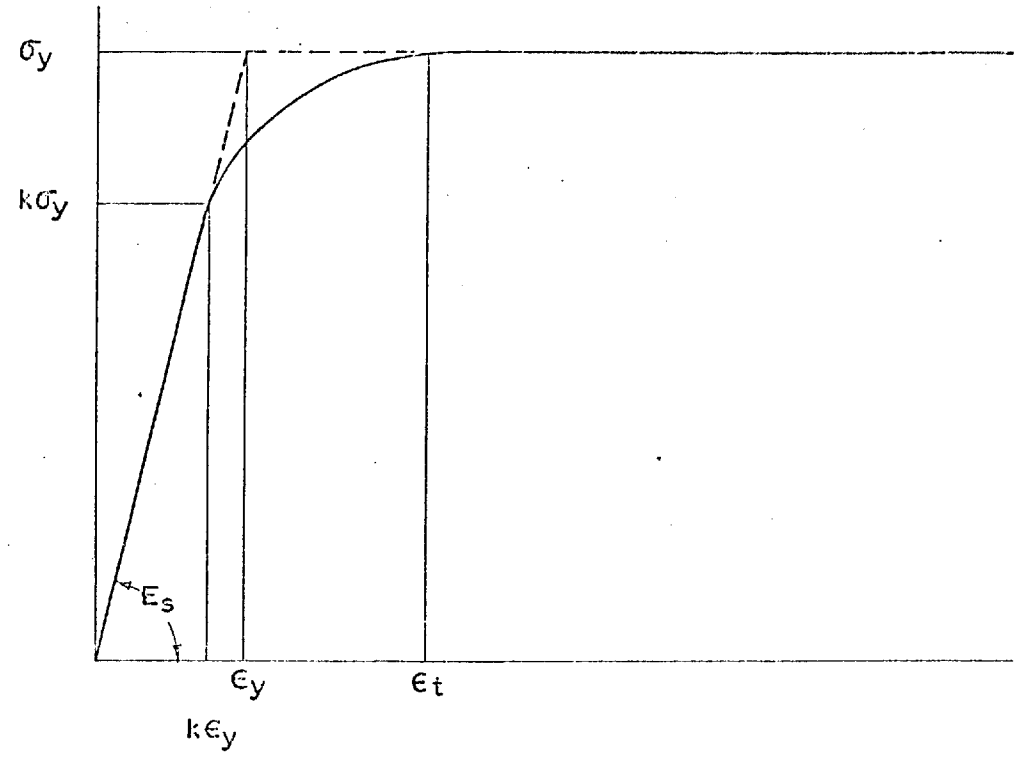

FIG. 2·1 UNIAXIAL STRESS-STRAIN RELATIONSHIP FOR STEEL.

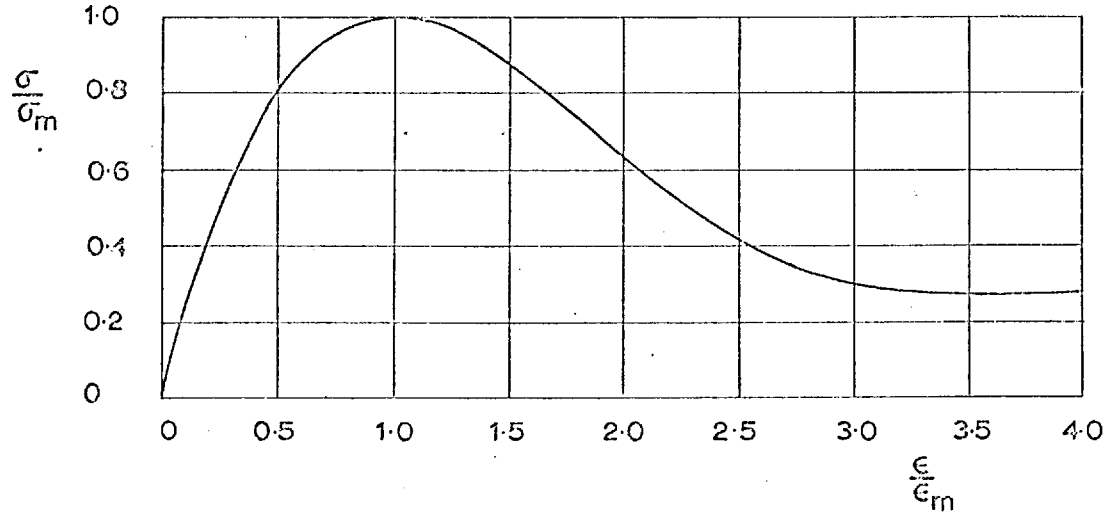

FIG. 2·2 UNIAXIAL STRESS-STRAIN RELATIONSHIP FOR CONCRETE.

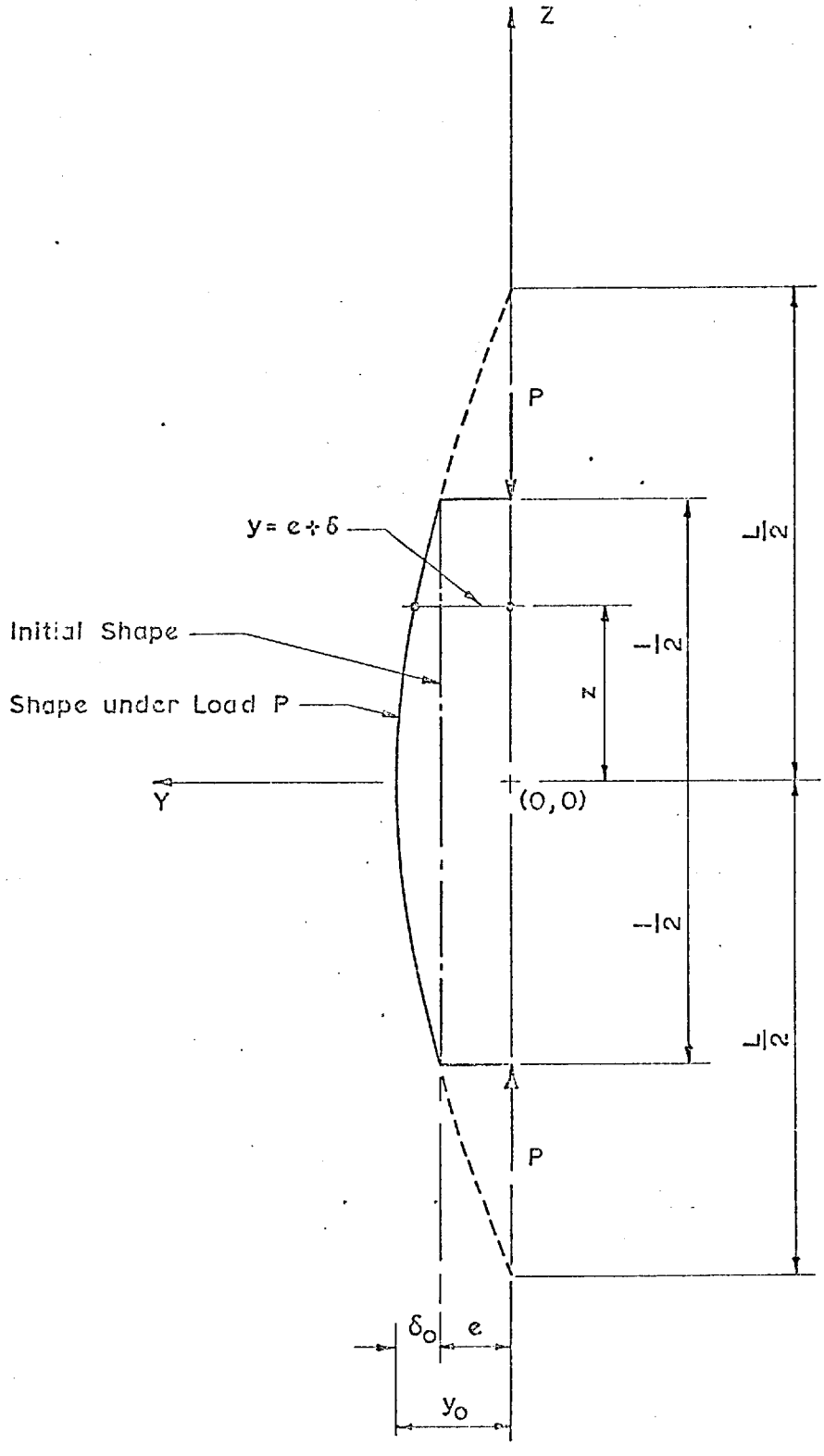

FIG. 2·3 DEFLECTED SHAPE.

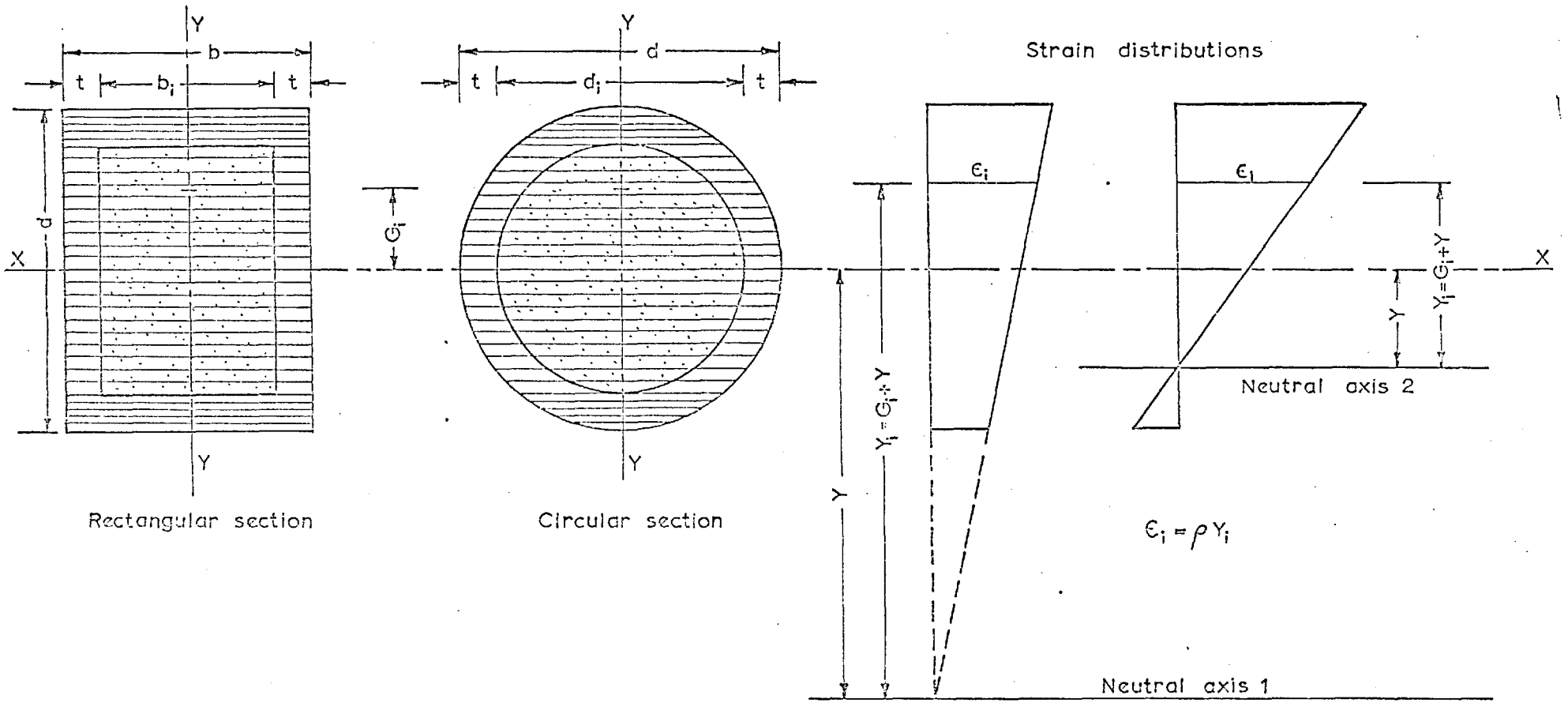

FIG. 2.4 CROSS-SECTIONAL PARAMETERS AND STRAIN DISTRIBUTION

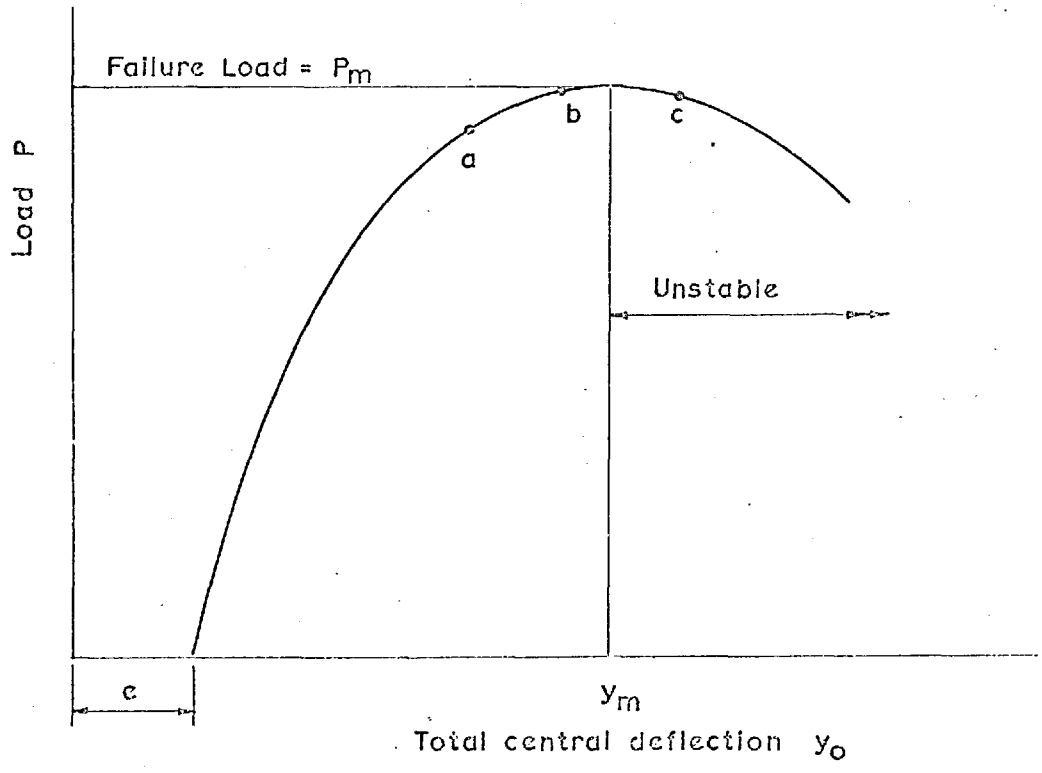

FIG. 2·5 TYPICAL LOAD-DEFLECTION CURVE

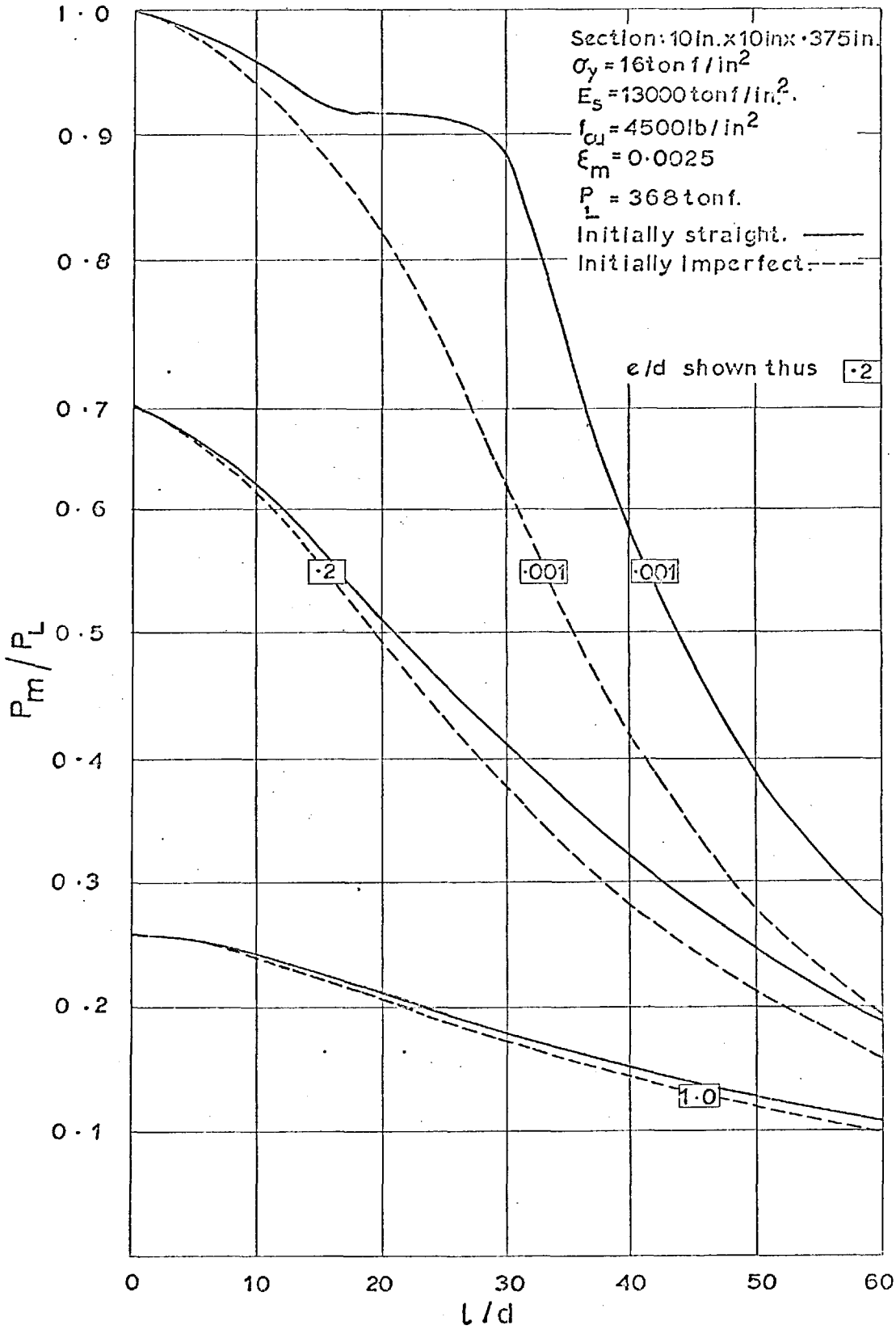

FIG. 2·6 COMPARISON BETWEEN THE FAILURE LOADS OF INITIALLY STRAIGHT & IMPERFECT COLUMNS.

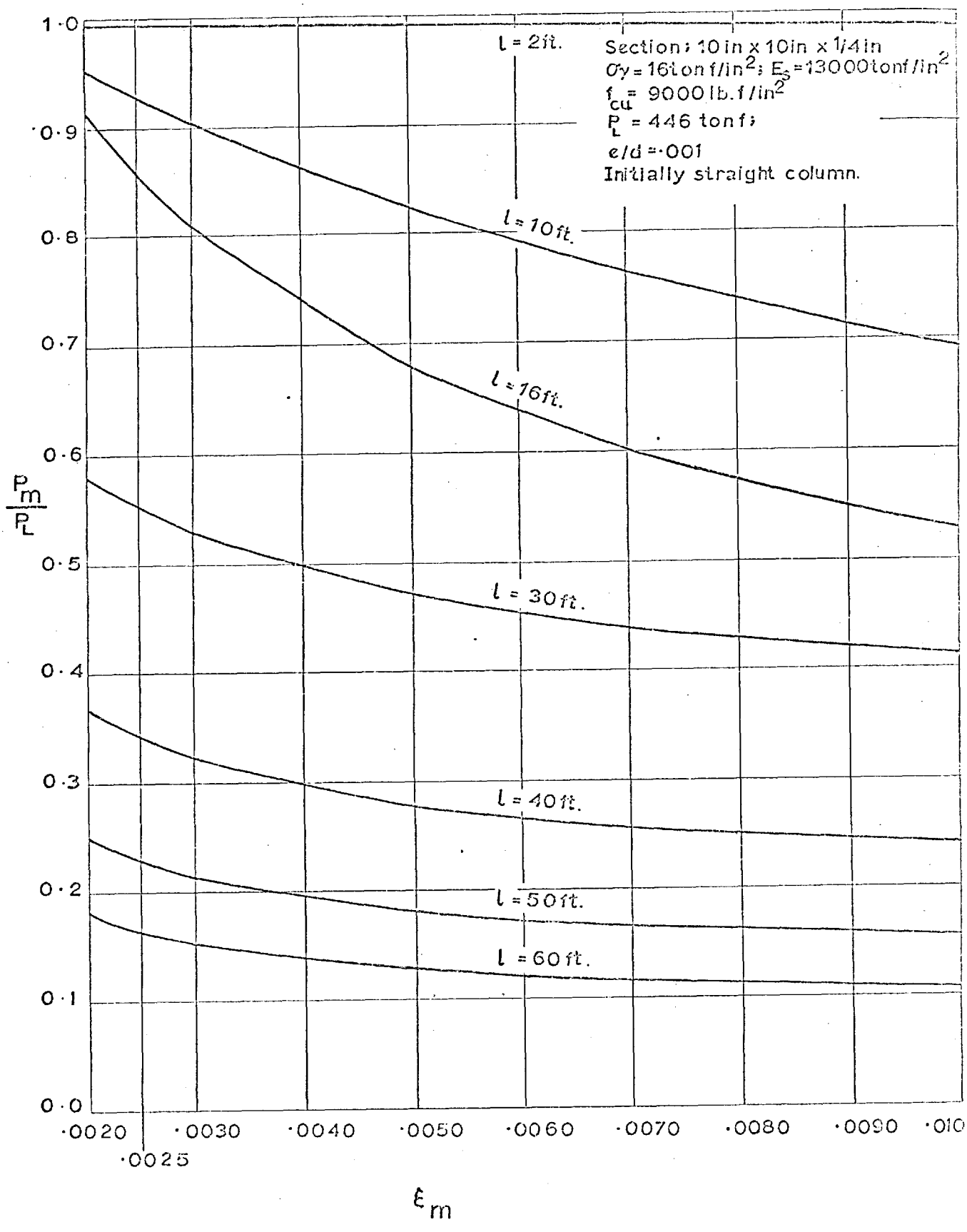

FIG. 2·7 $P_m - \varepsilon_m l$ RELATIONSHIP

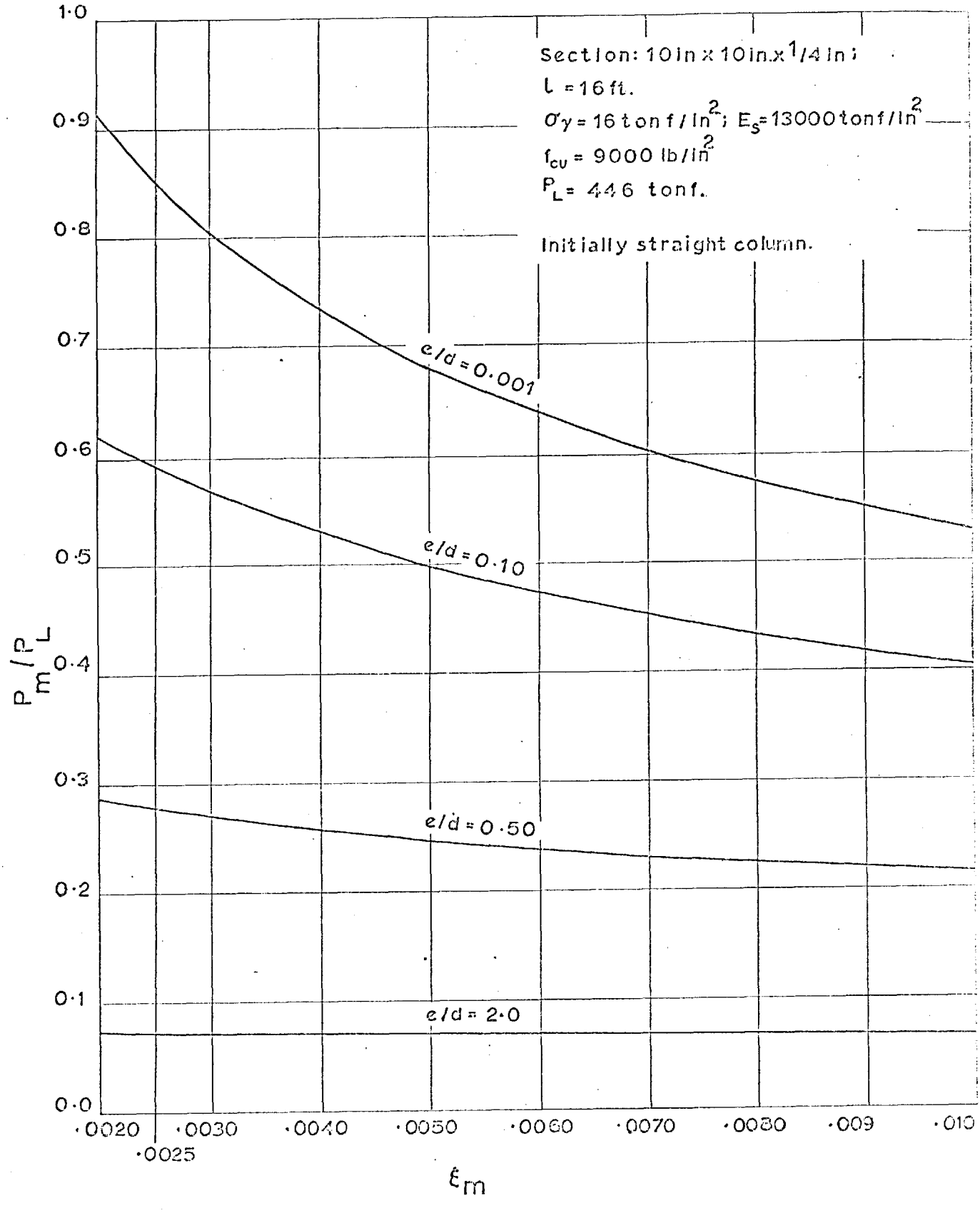

FIG. 2·8 $P_m - \varepsilon_m - e/d$ RELATIONSHIP

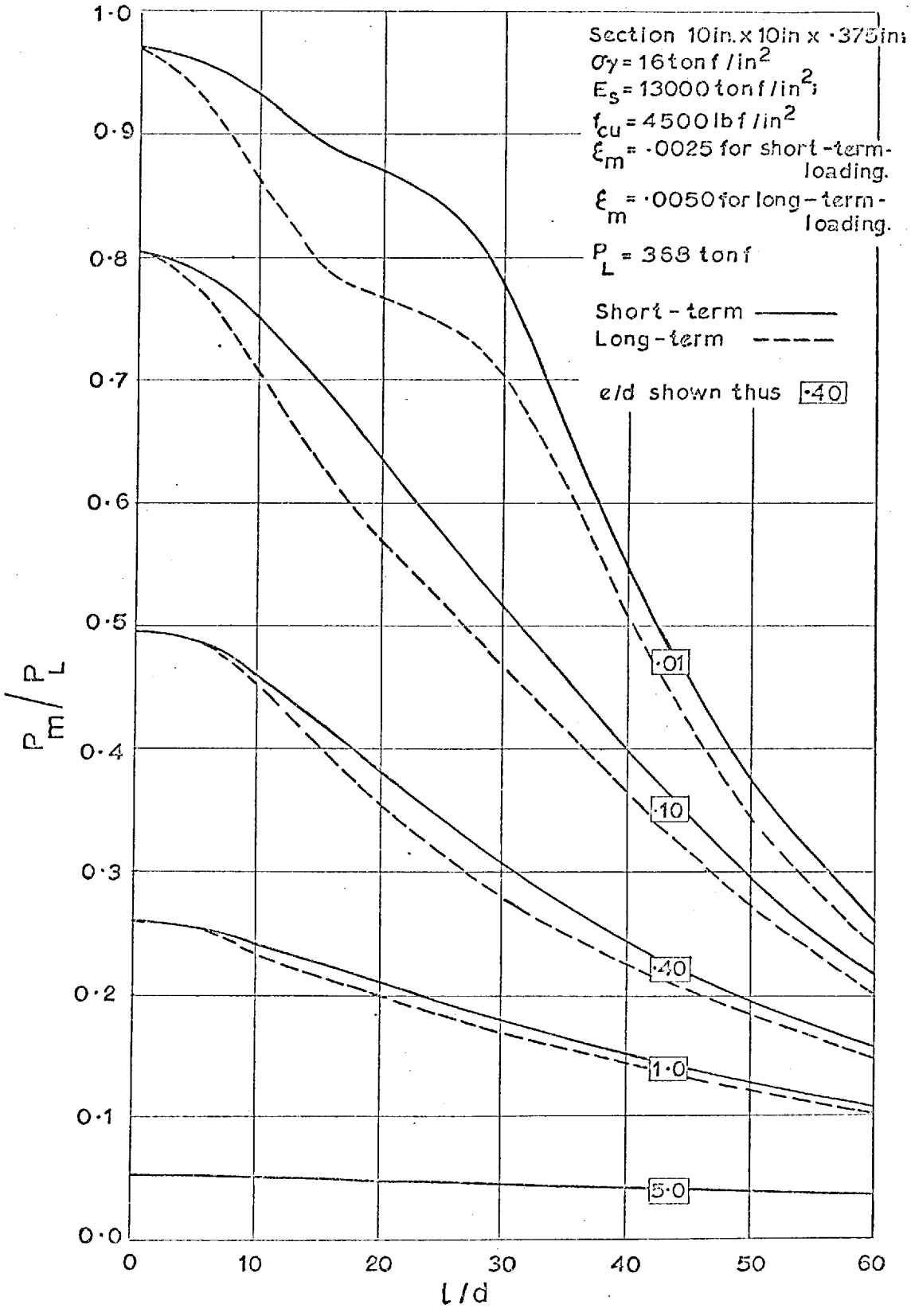

FIG. 2·9 COMPARISON BETWEEN SHORT-TERM & LONG-TERM FAILURE LOADS

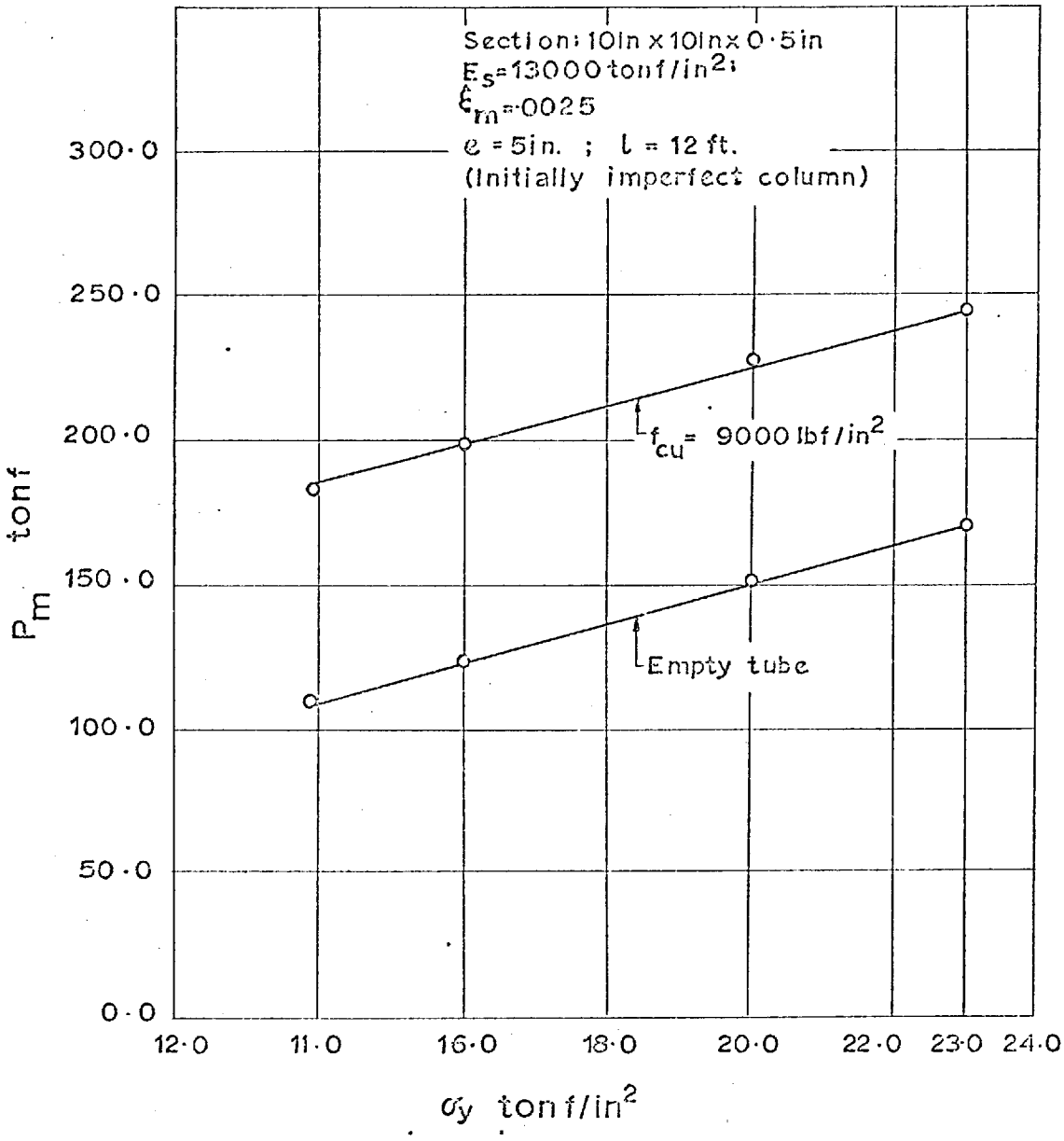

FIG. 2·10 P_m — σ_y RELATIONSHIP

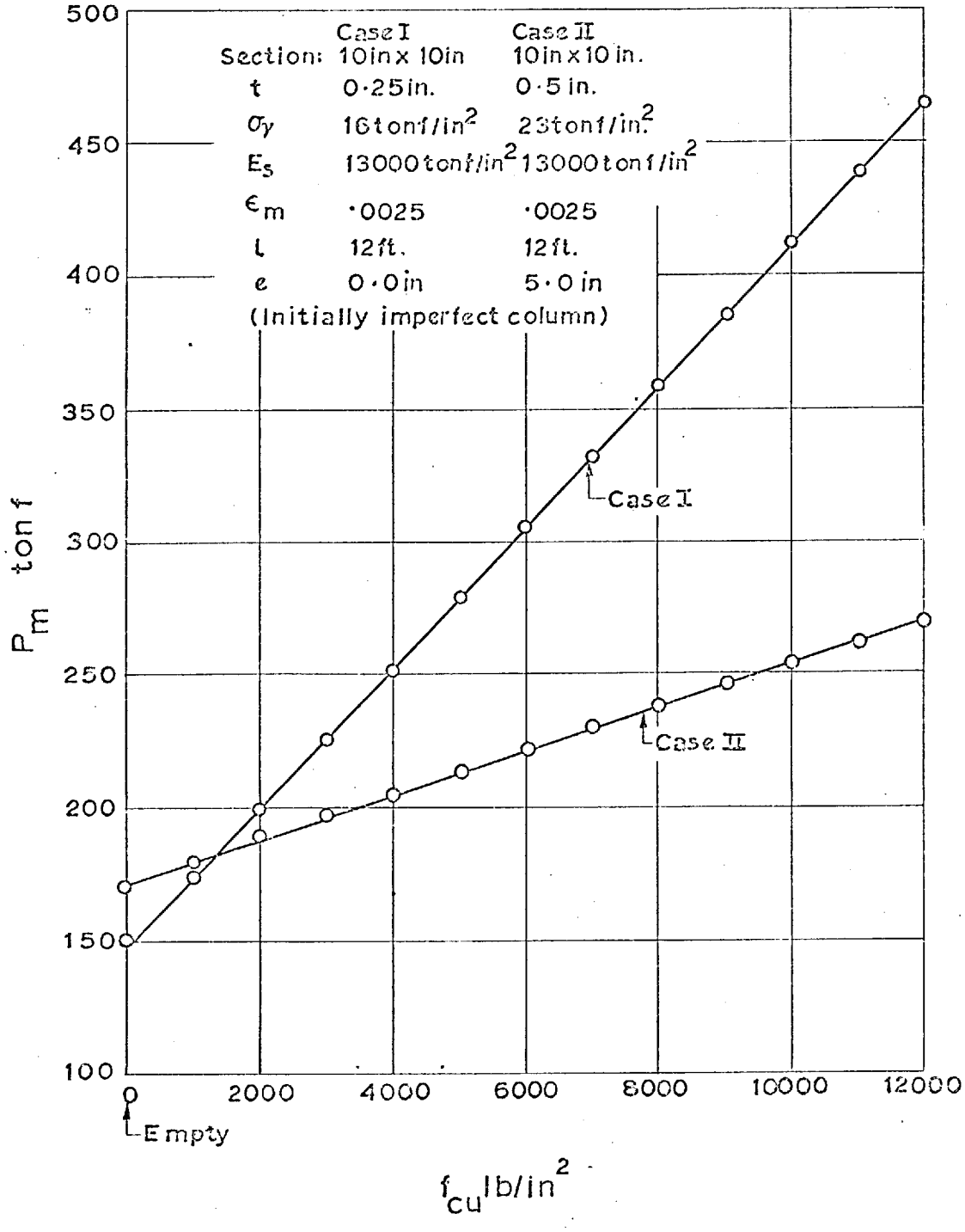

FIG. 2·11 P_m — f_{cu} RELATIONSHIP

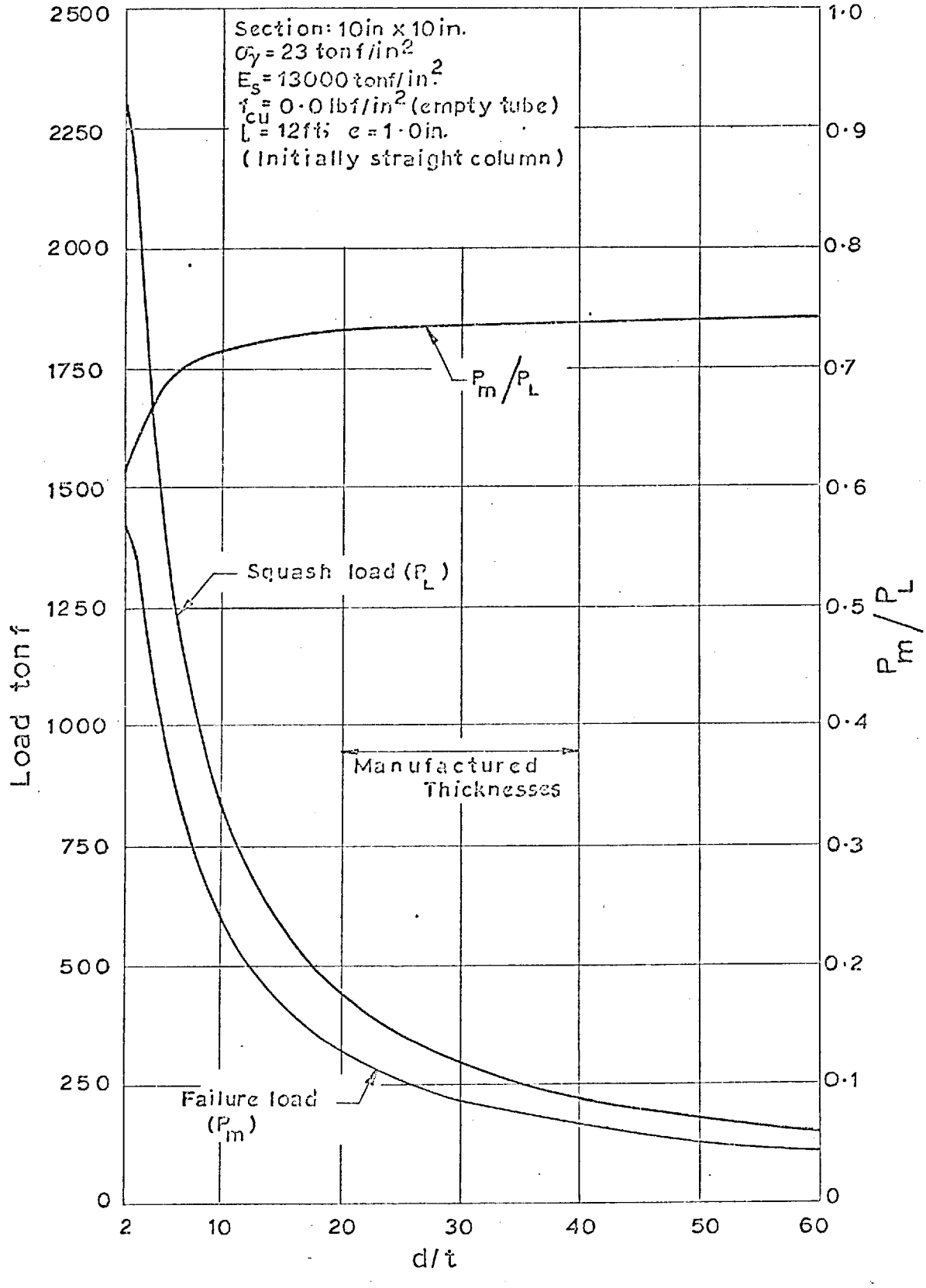

FIG. 2·12 P_m - d/t RELATIONSHIP.

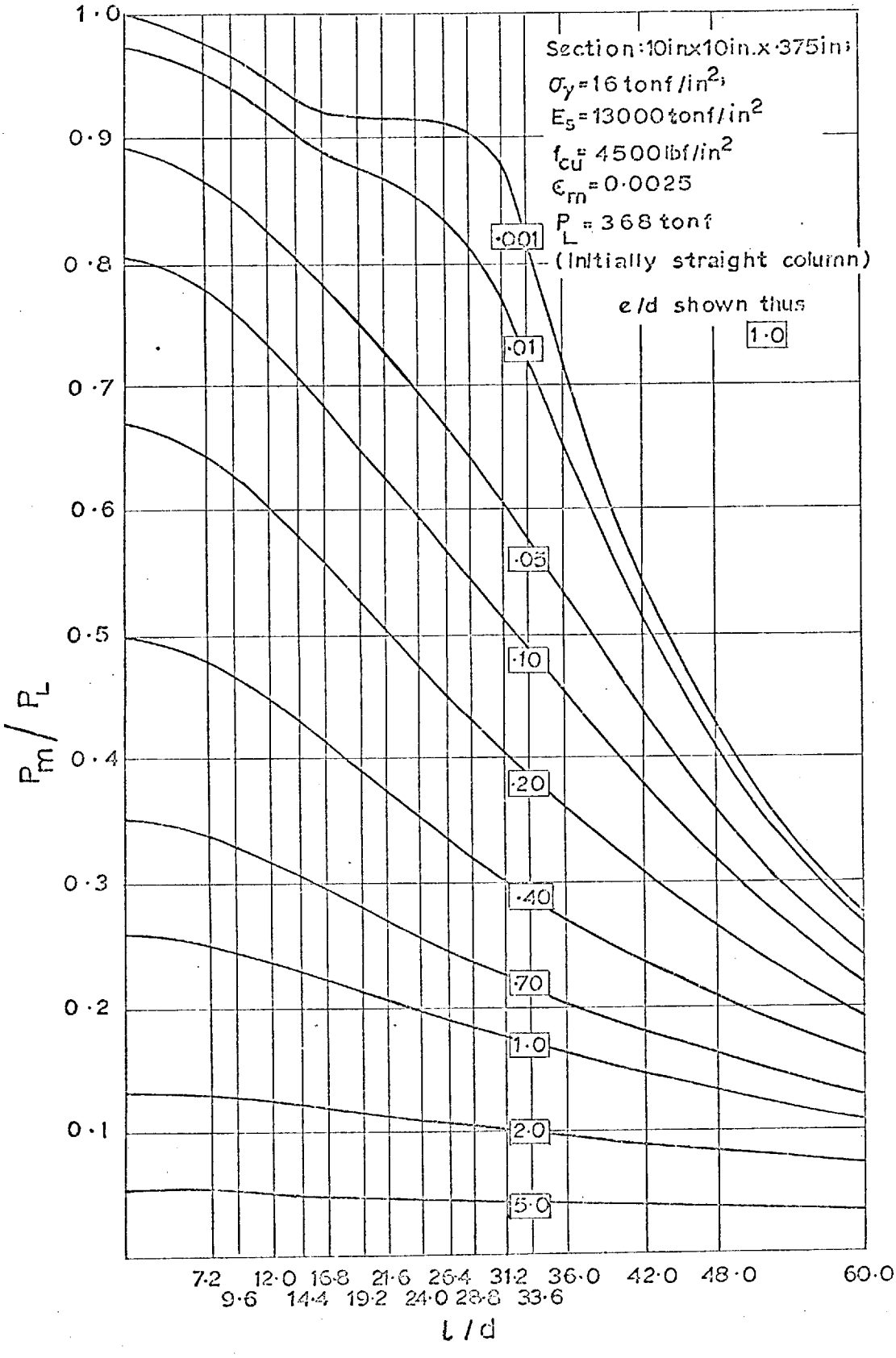

FIG. 2·13 P_m — l/d RELATIONSHIP

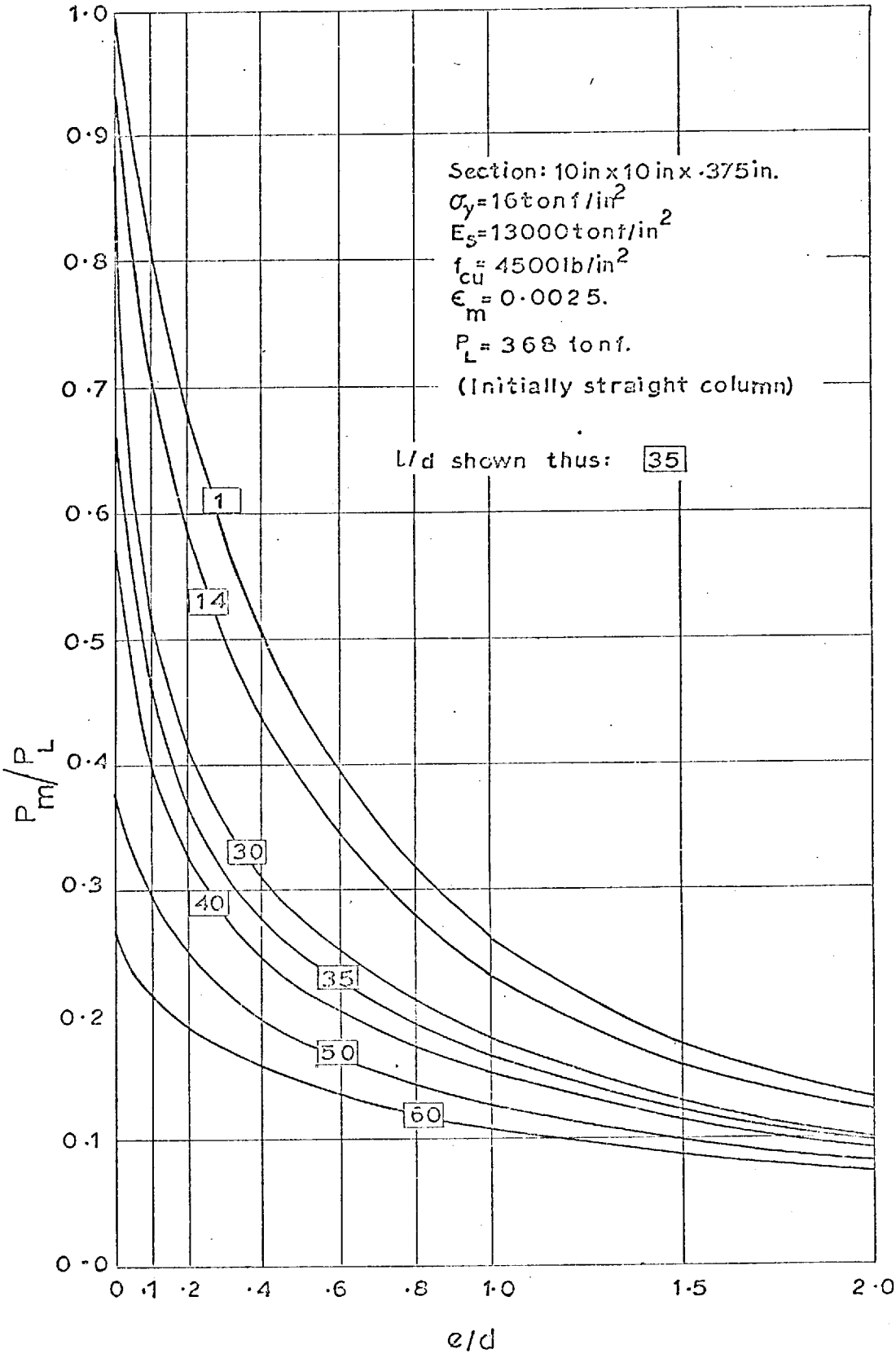

FIG.2.14 P_m — e/d RELATIONSHIP

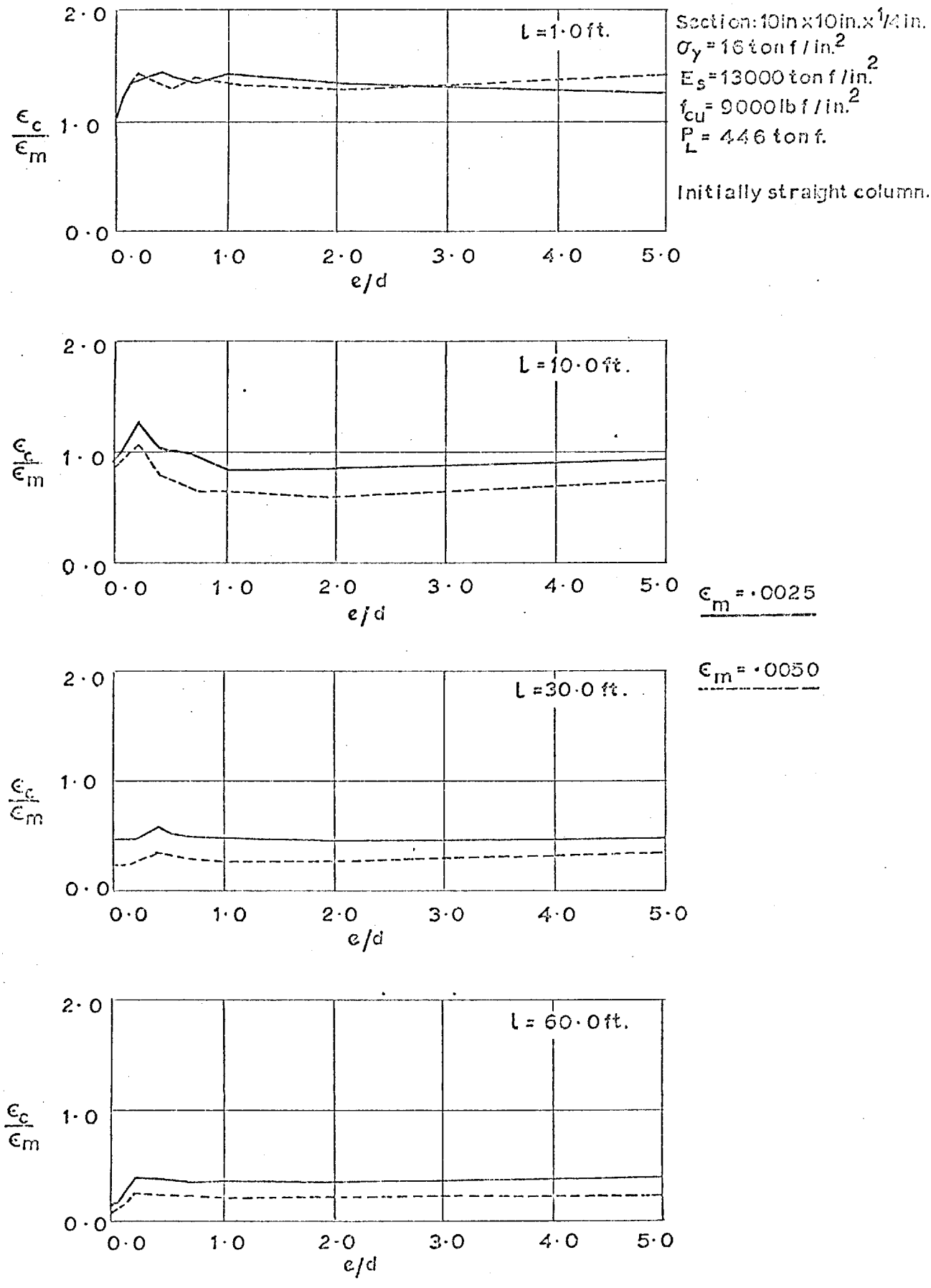

FIG. 2·15 $\frac{\epsilon_c}{\epsilon_m} - \frac{e}{d} - L$ RELATIONSHIP

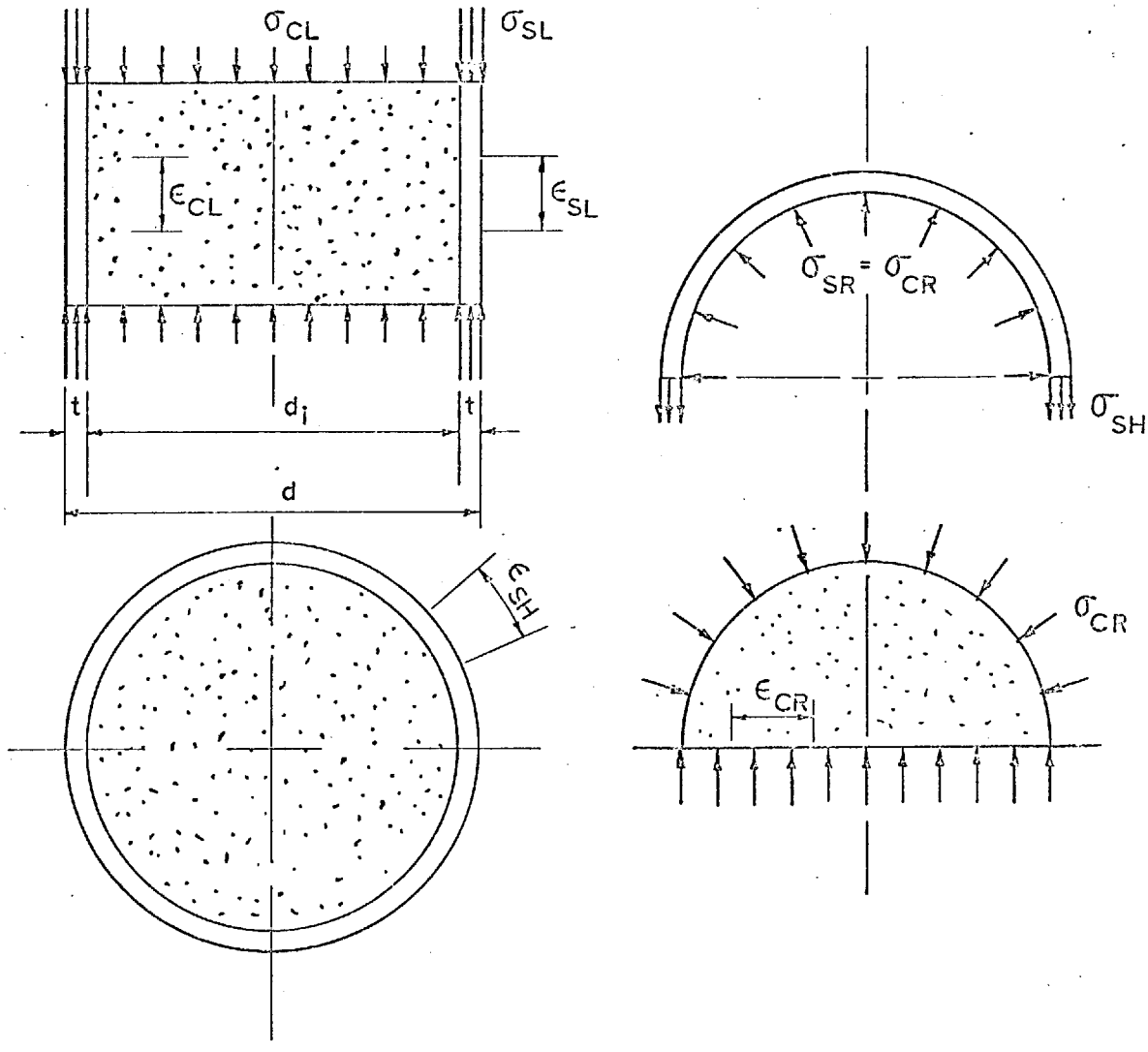

FIG. 3·1 STRESSES AND STRAINS IN A STUB COLUMN.

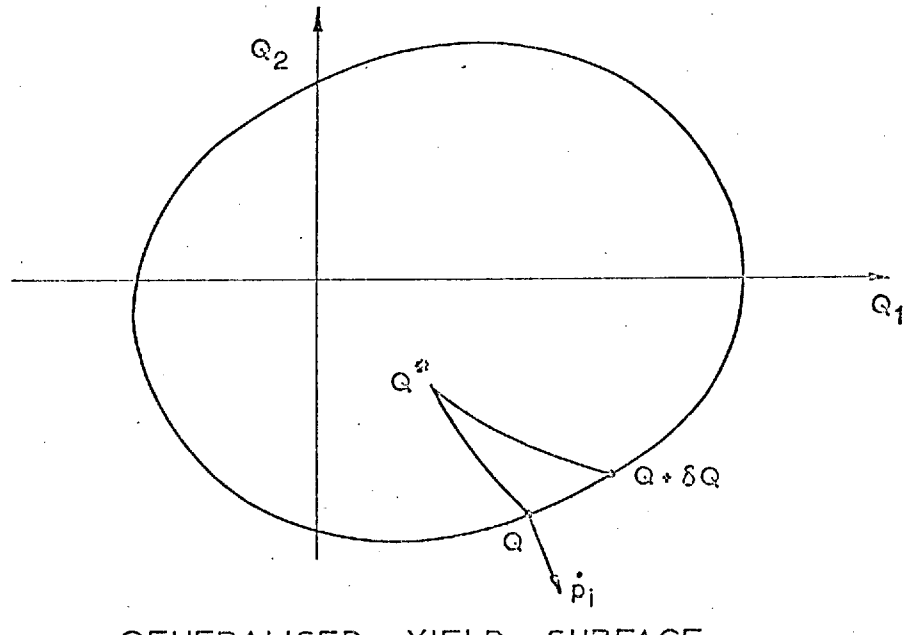

FIG. 3·2 GENERALISED YIELD SURFACE.

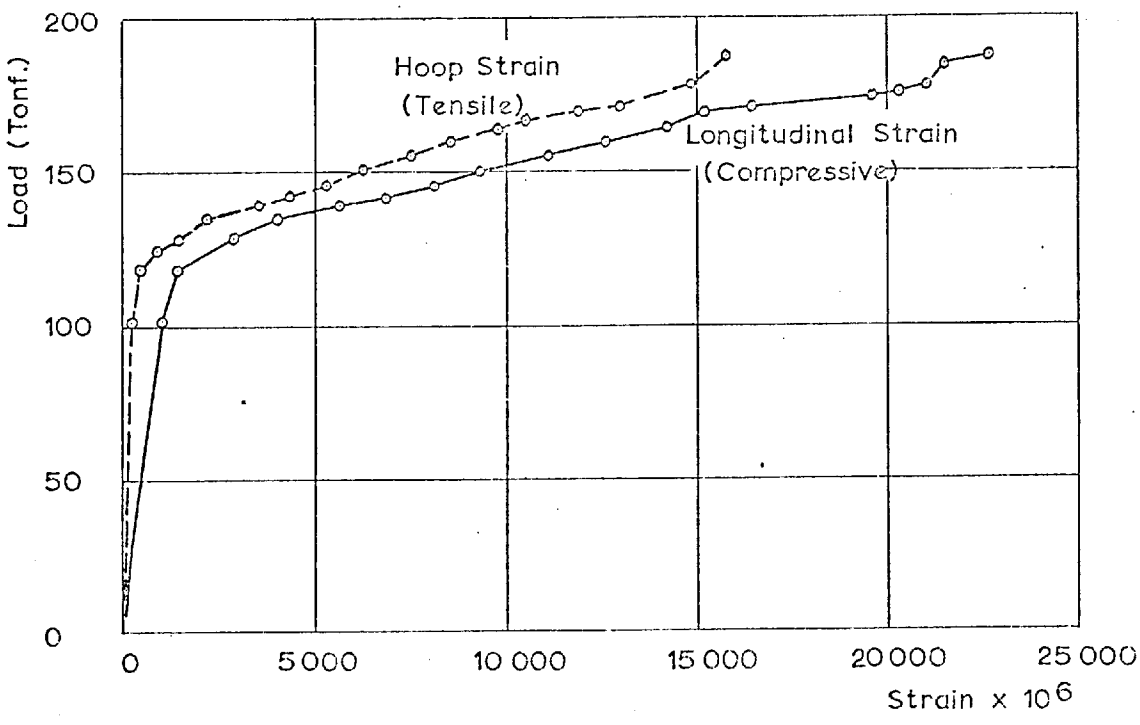

FIG. 3·3 EXPERIMENTAL LOAD-STRAIN RELATIONSHIP FOR COLUMN M11 – IMPERIAL COLLEGE TESTS

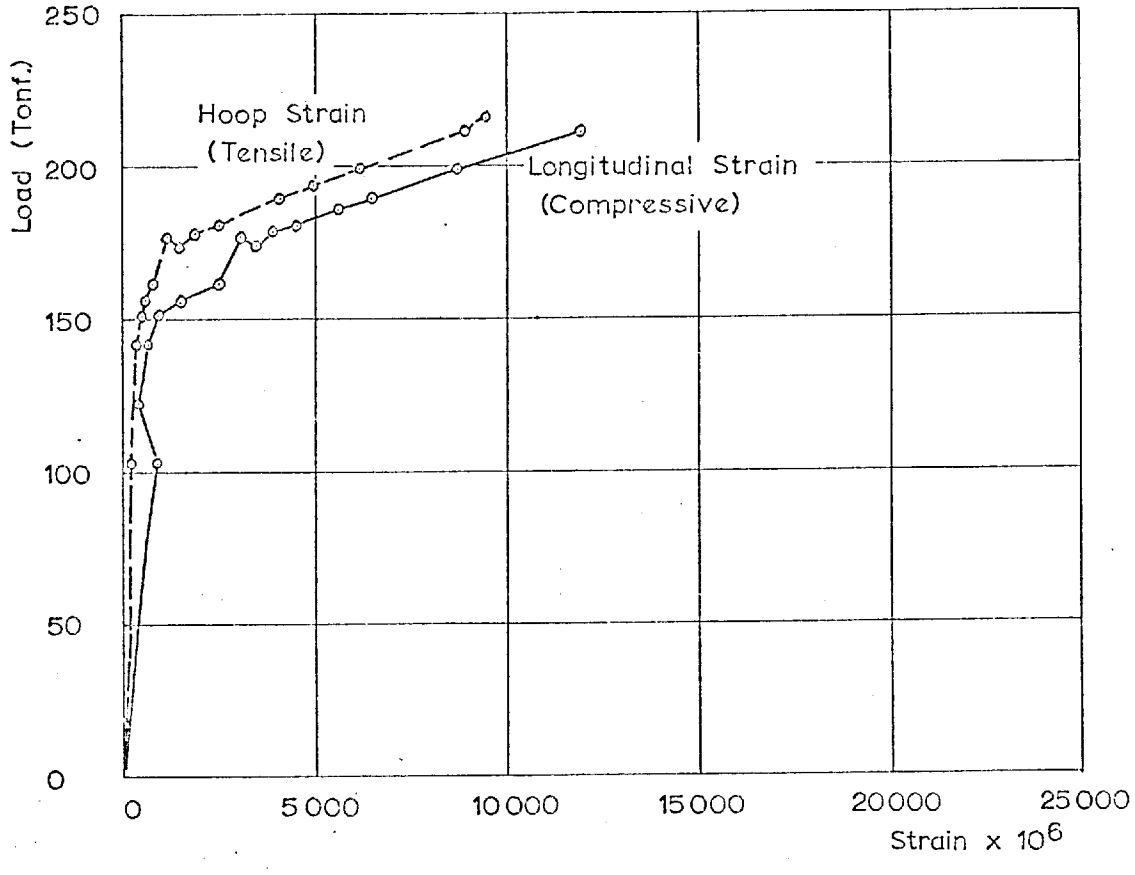

FIG. 3·4 EXPERIMENTAL LOAD-STRAIN RELATIONSHIP FOR COLUMN M12 – IMPERIAL COLLEGE TESTS

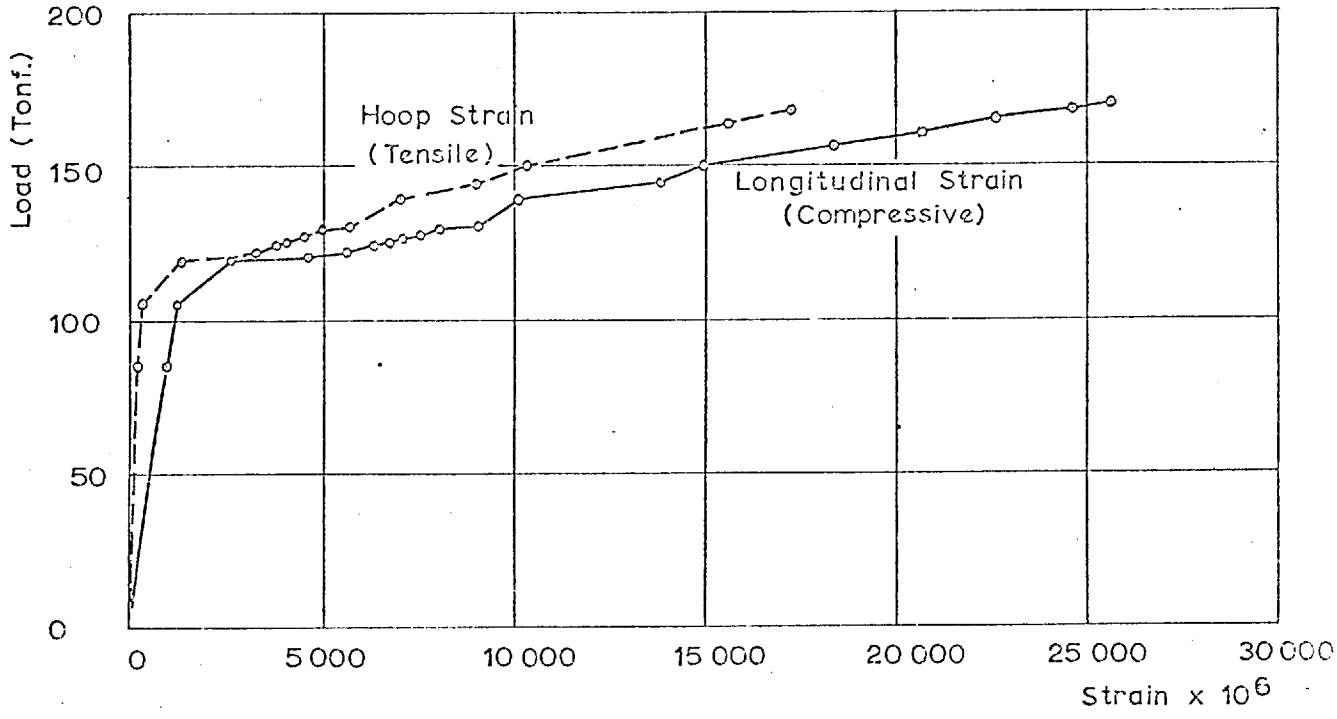

FIG.3.5 EXPERIMENTAL LOAD-STRAIN RELATIONSHIP FOR COLUMN M13 - IMPERIAL COLLEGE TESTS

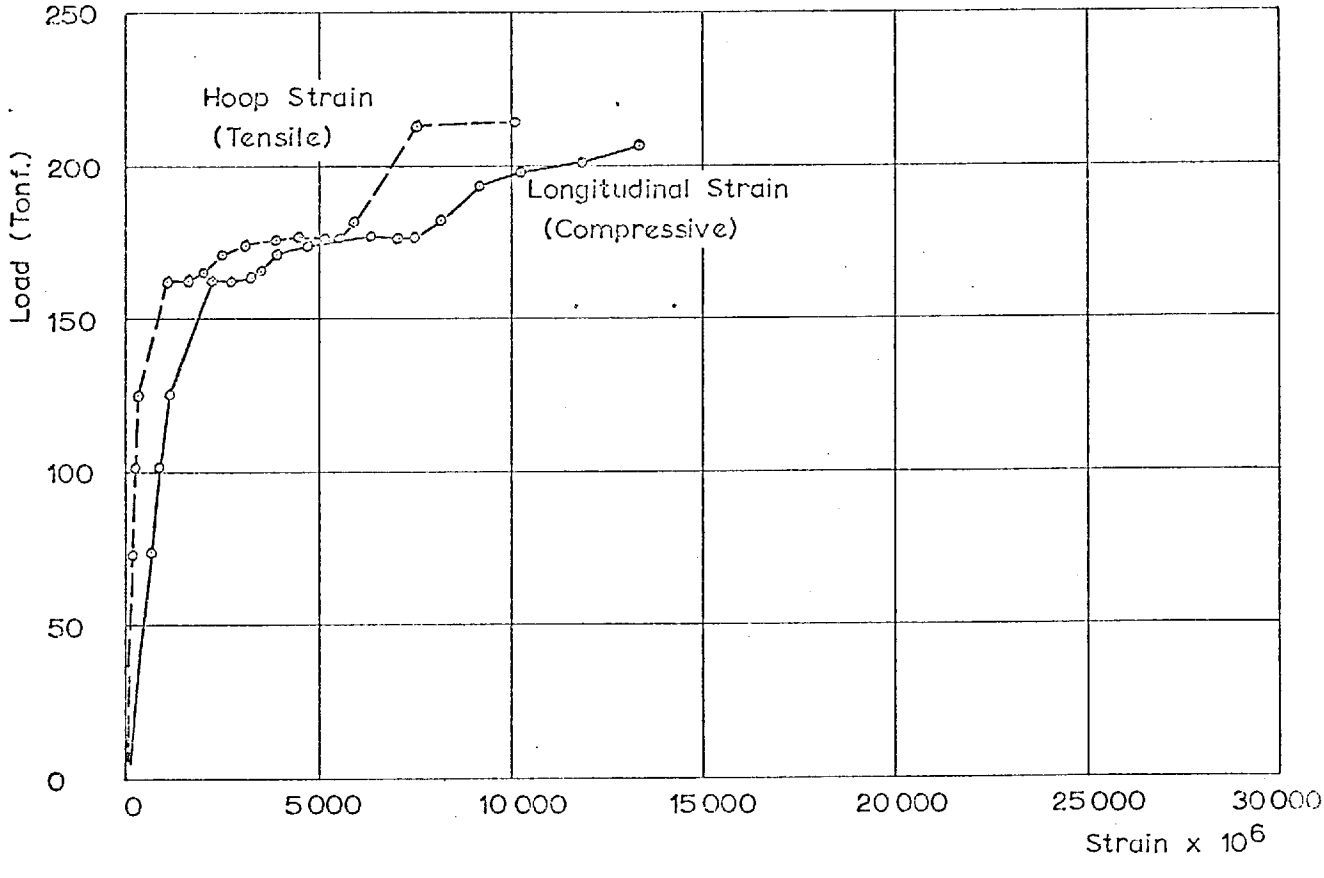

FIG.3.6 EXPERIMENTAL LOAD-STRAIN RELATIONSHIP FOR COLUMN M14 - IMPERIAL COLLEGE TESTS

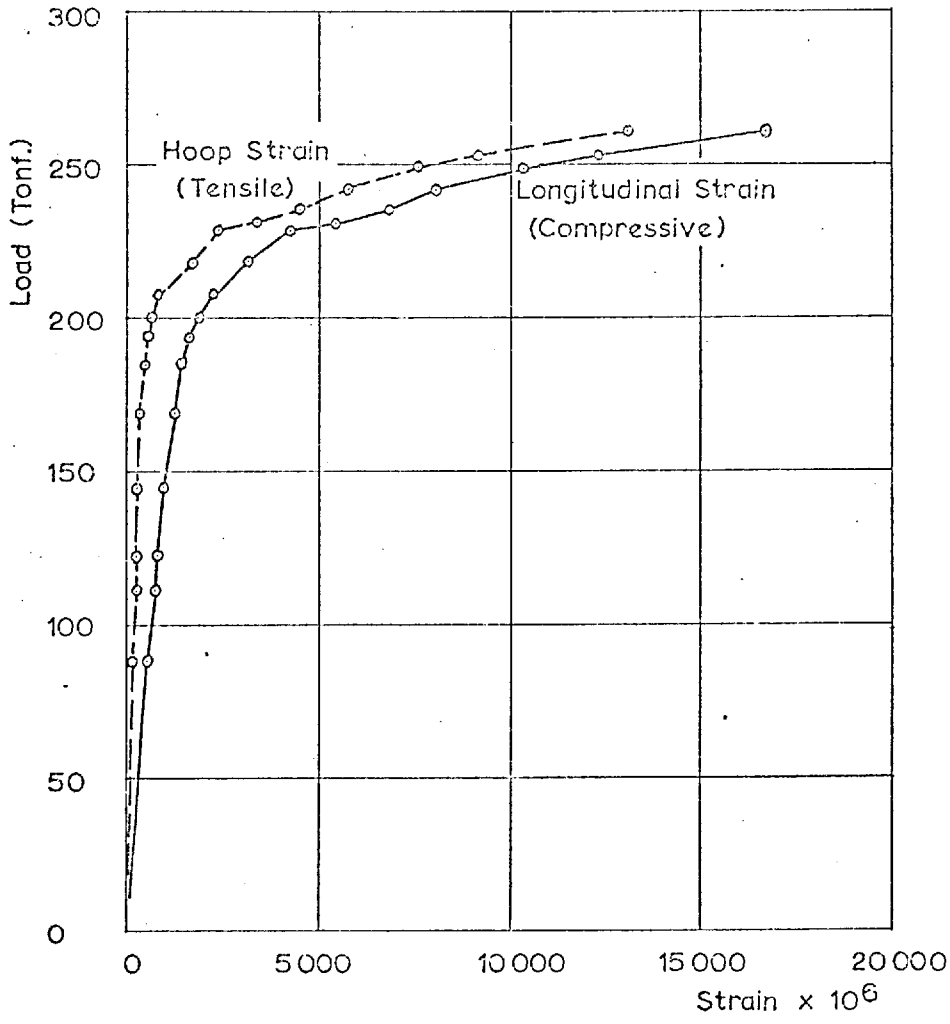

FIG. 3·7 EXPERIMENTAL LOAD-STRAIN RELATIONSHIP FOR COLUMN M15 – IMPERIAL COLLEGE TESTS

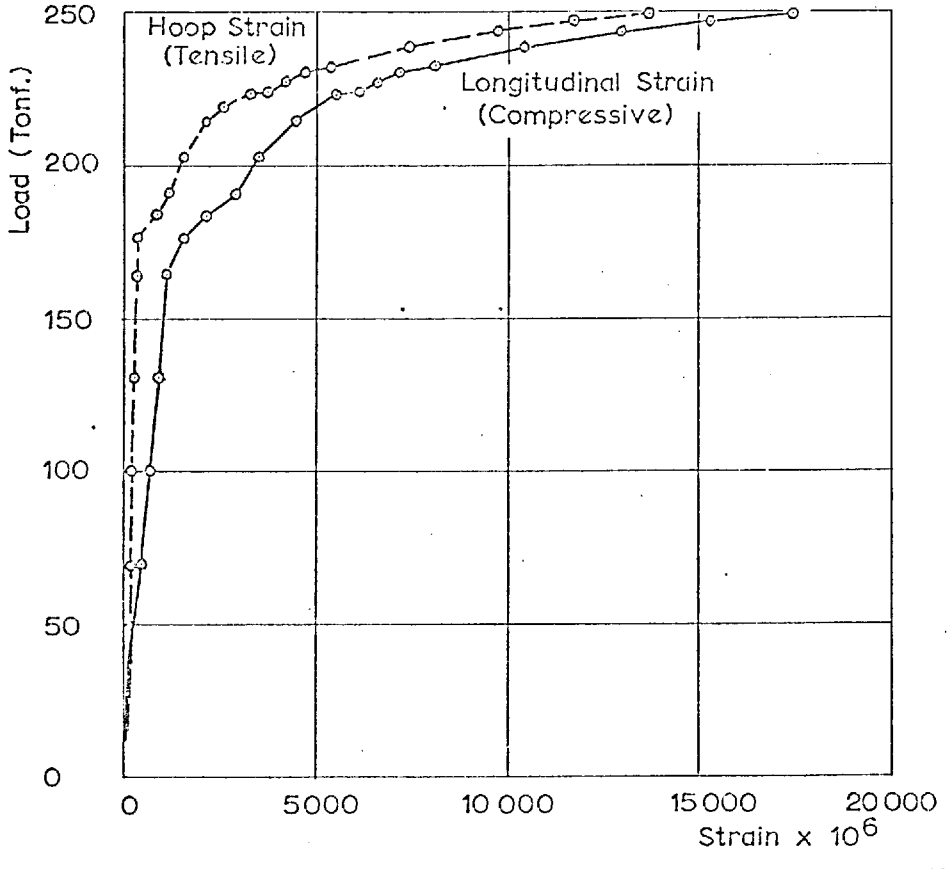

FIG. 3·8 EXPERIMENTAL LOAD-STRAIN RELATIONSHIP FOR COLUMN M16 – IMPERIAL COLLEGE TESTS

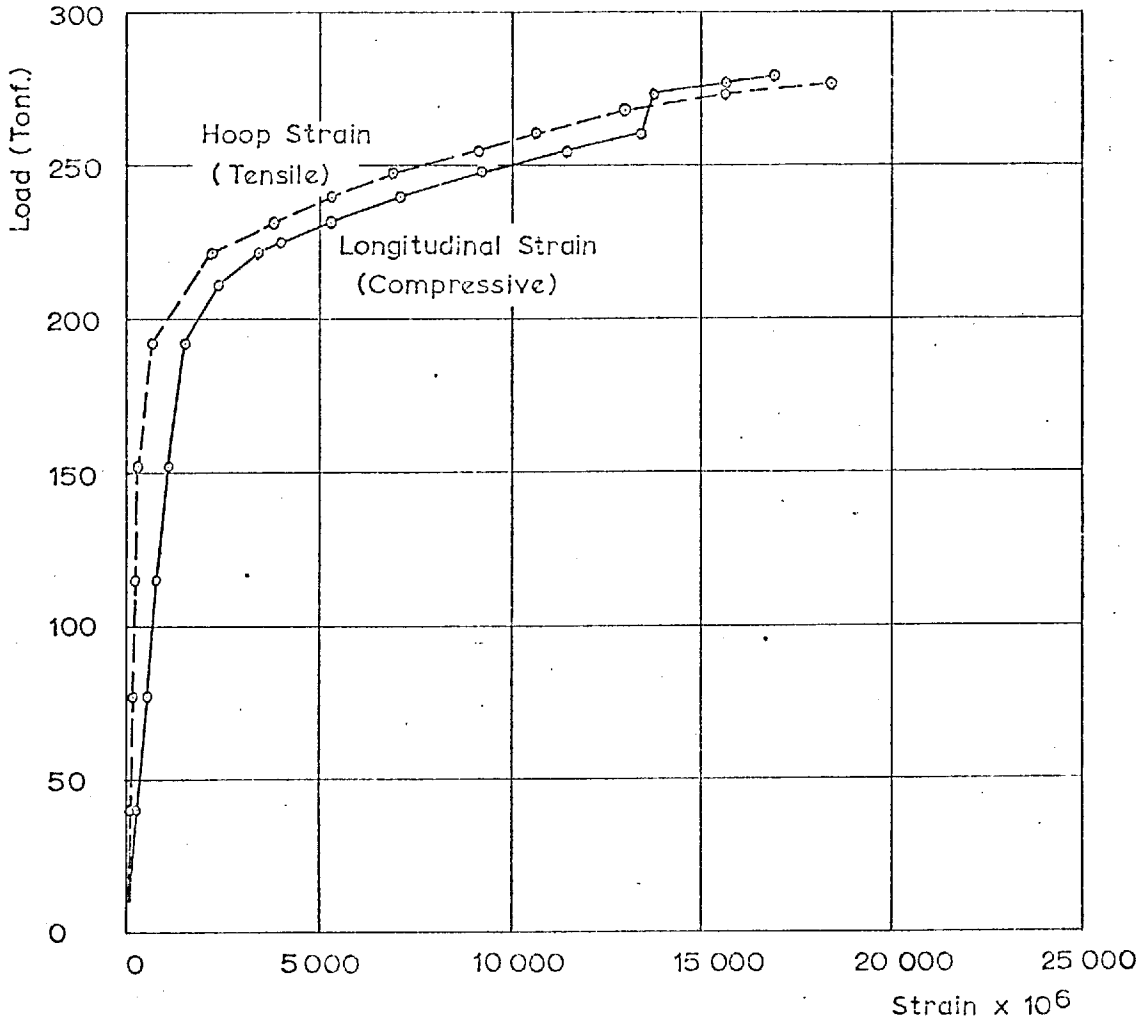

FIG. 3·9 EXPERIMENTAL LOAD - STRAIN RELATIONSHIP FOR COLUMN M17 – IMPERIAL COLLEGE TESTS

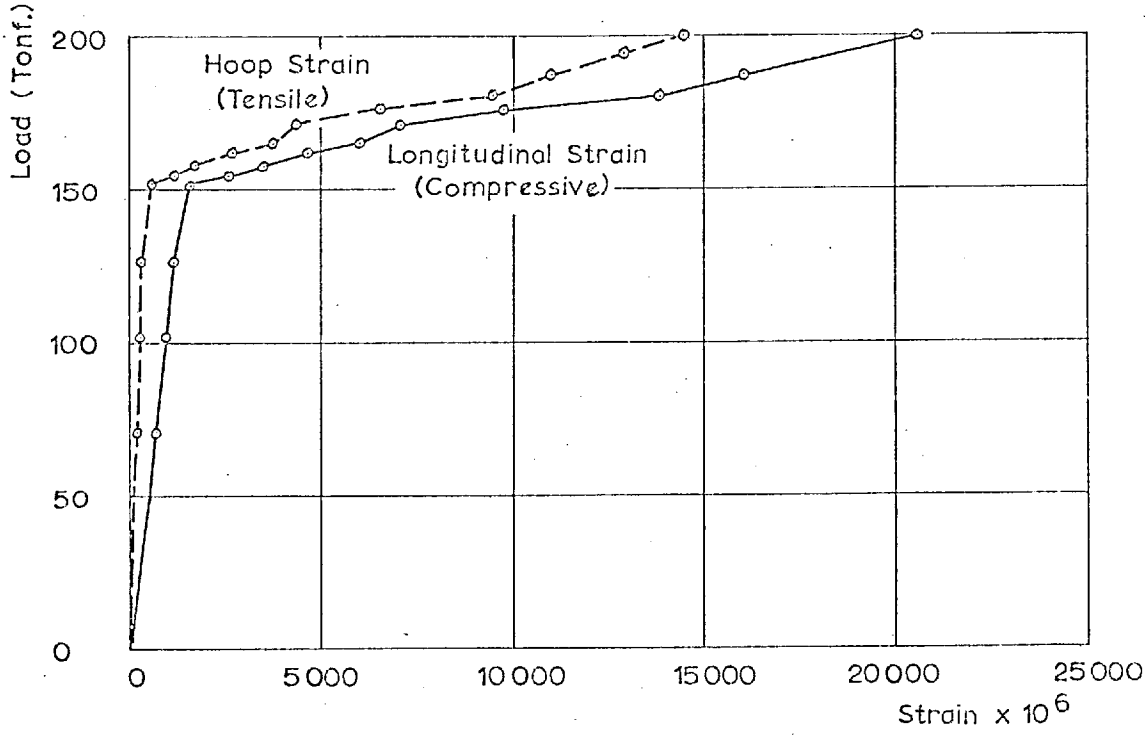

FIG. 3·10 EXPERIMENTAL LOAD - STRAIN RELATIONSHIP FOR COLUMN M18 – IMPERIAL COLLEGE TESTS

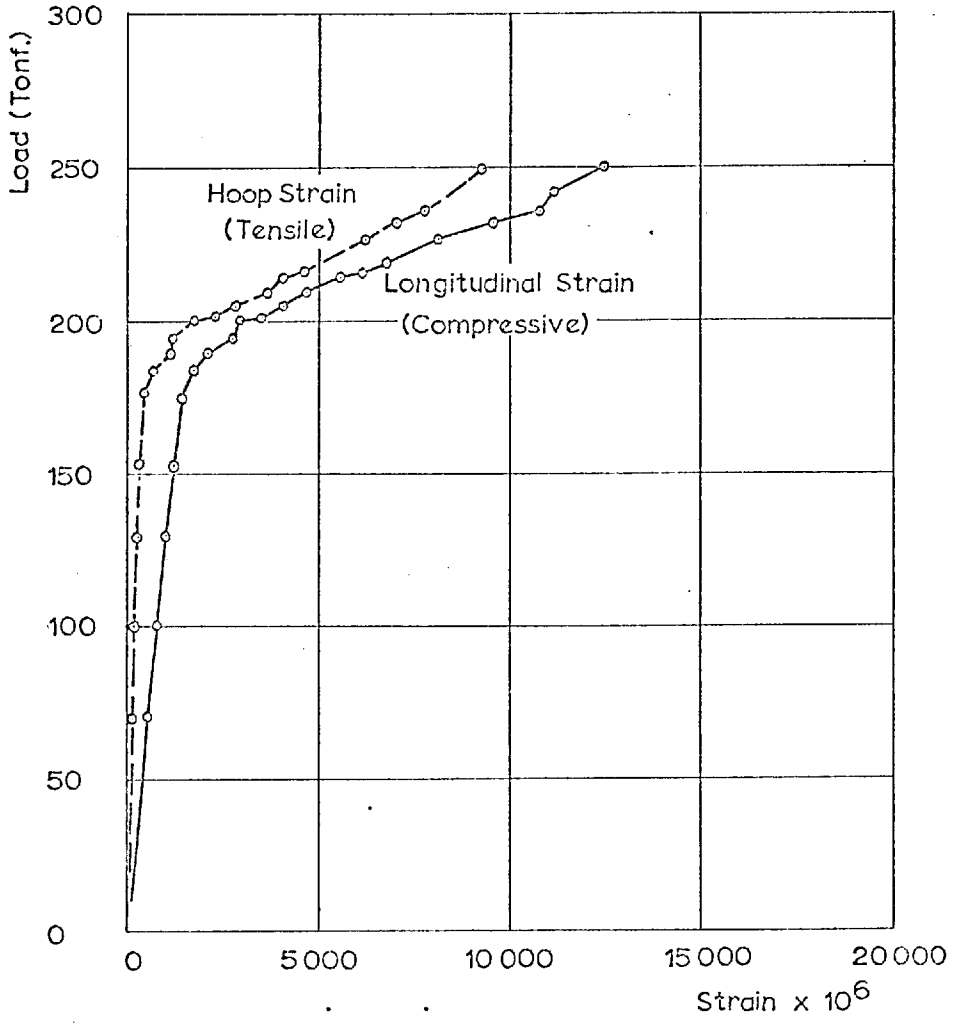

FIG. 3·11 EXPERIMENTAL LOAD-STRAIN RELATIONSHIP FOR COLUMN M19 - IMPERIAL COLLEGE TESTS

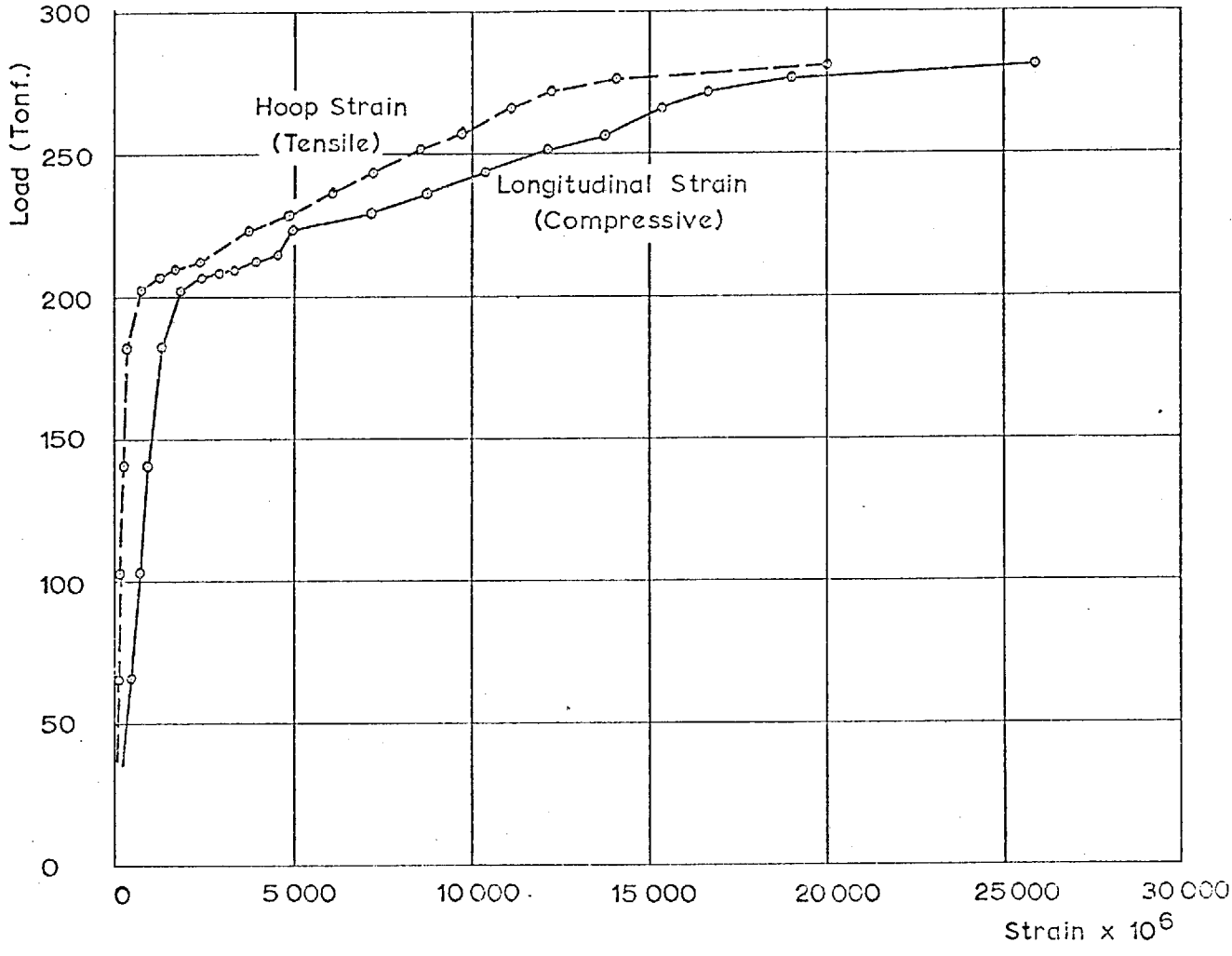

FIG.3.12 EXPERIMENTAL LOAD-STRAIN RELATIONSHIP FOR COLUMN M20 - IMPERIAL COLLEGE TESTS

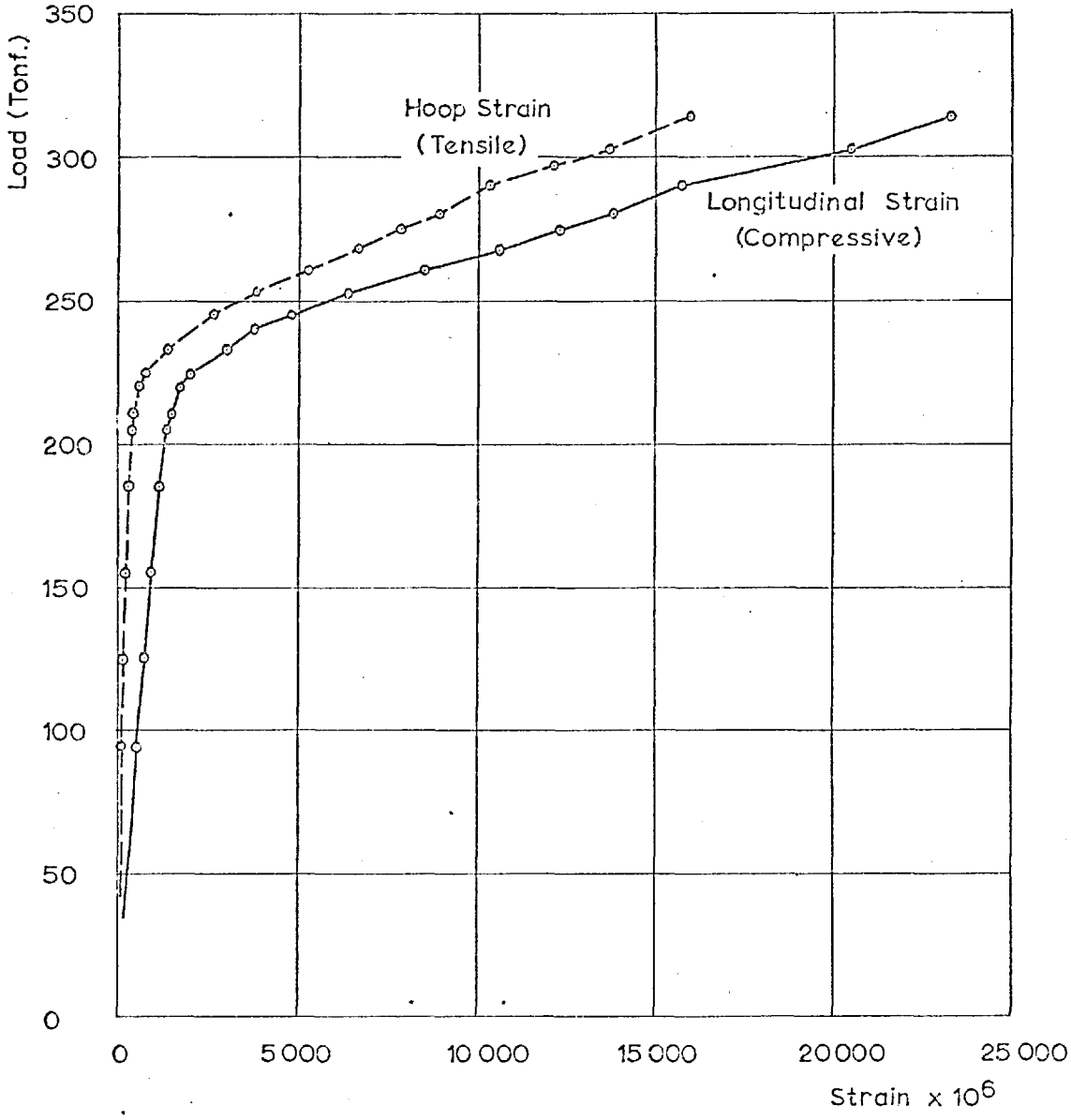

FIG. 3.13 EXPERIMENTAL LOAD-STRAIN RELATIONSHIP FOR COLUMN M 21 – IMPERIAL COLLEGE TESTS

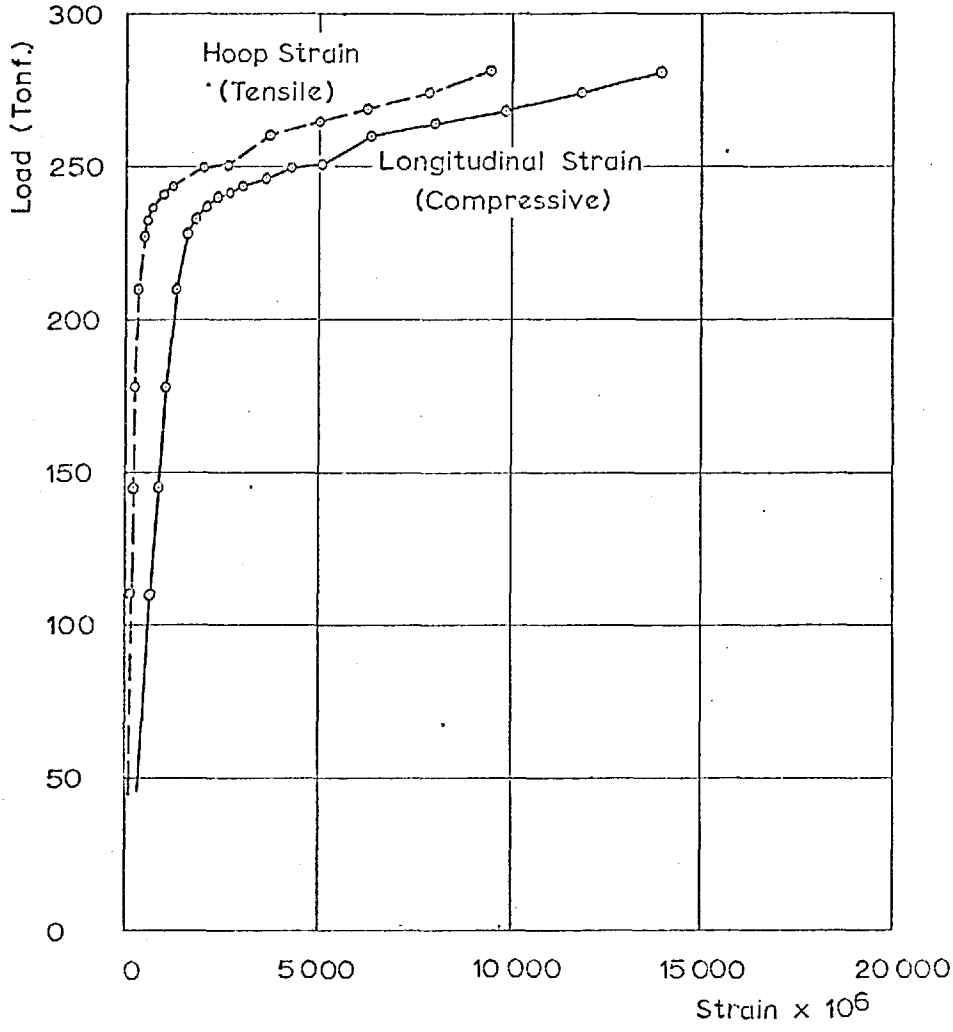

FIG. 3.14 EXPERIMENTAL LOAD-STRAIN RELATIONSHIP FOR COLUMN M22 – IMPERIAL COLLEGE TESTS

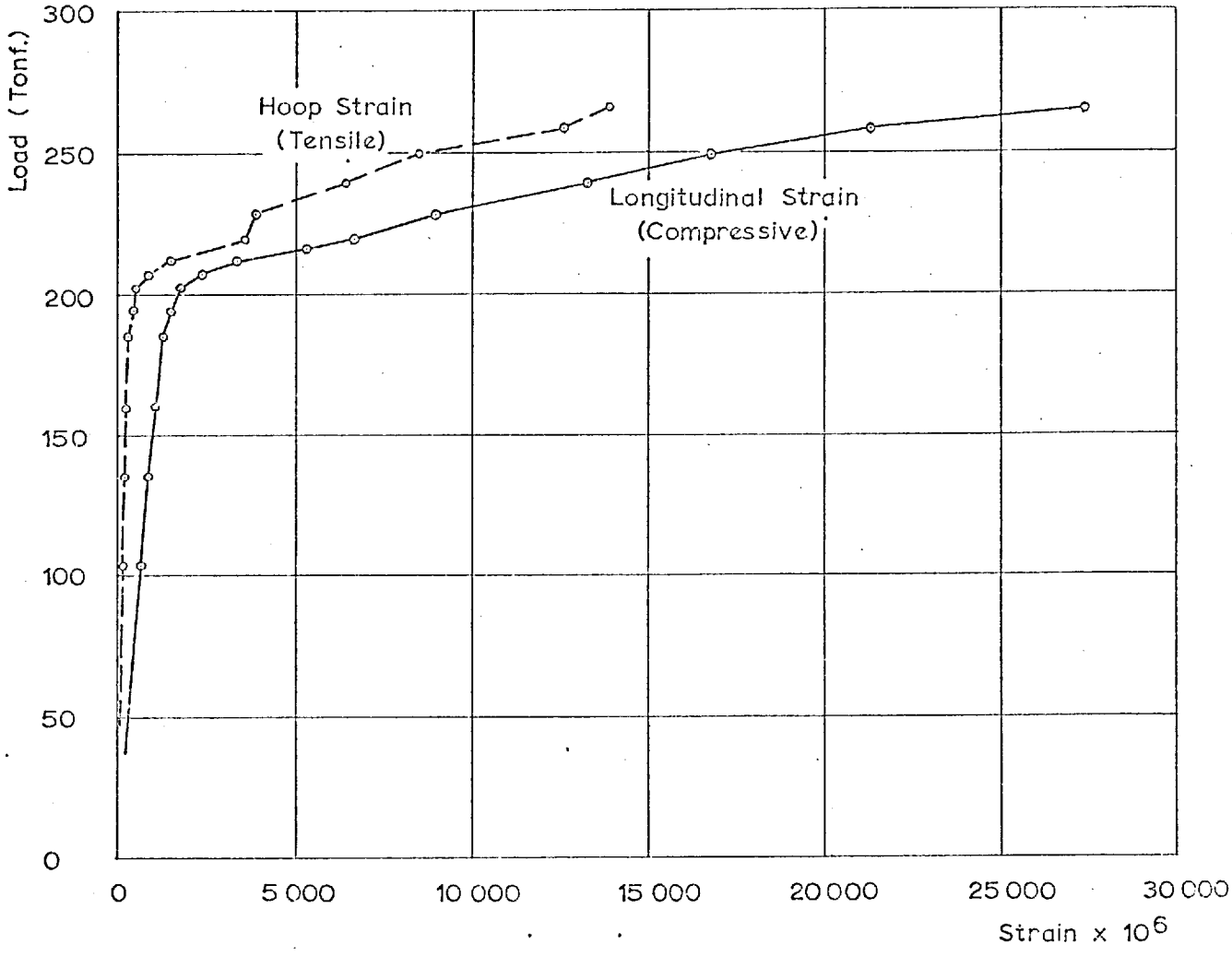

FIG.3.15 EXPERIMENTAL LOAD-STRAIN RELATIONSHIP FOR COLUMN M 23 – IMPERIAL COLLEGE TESTS

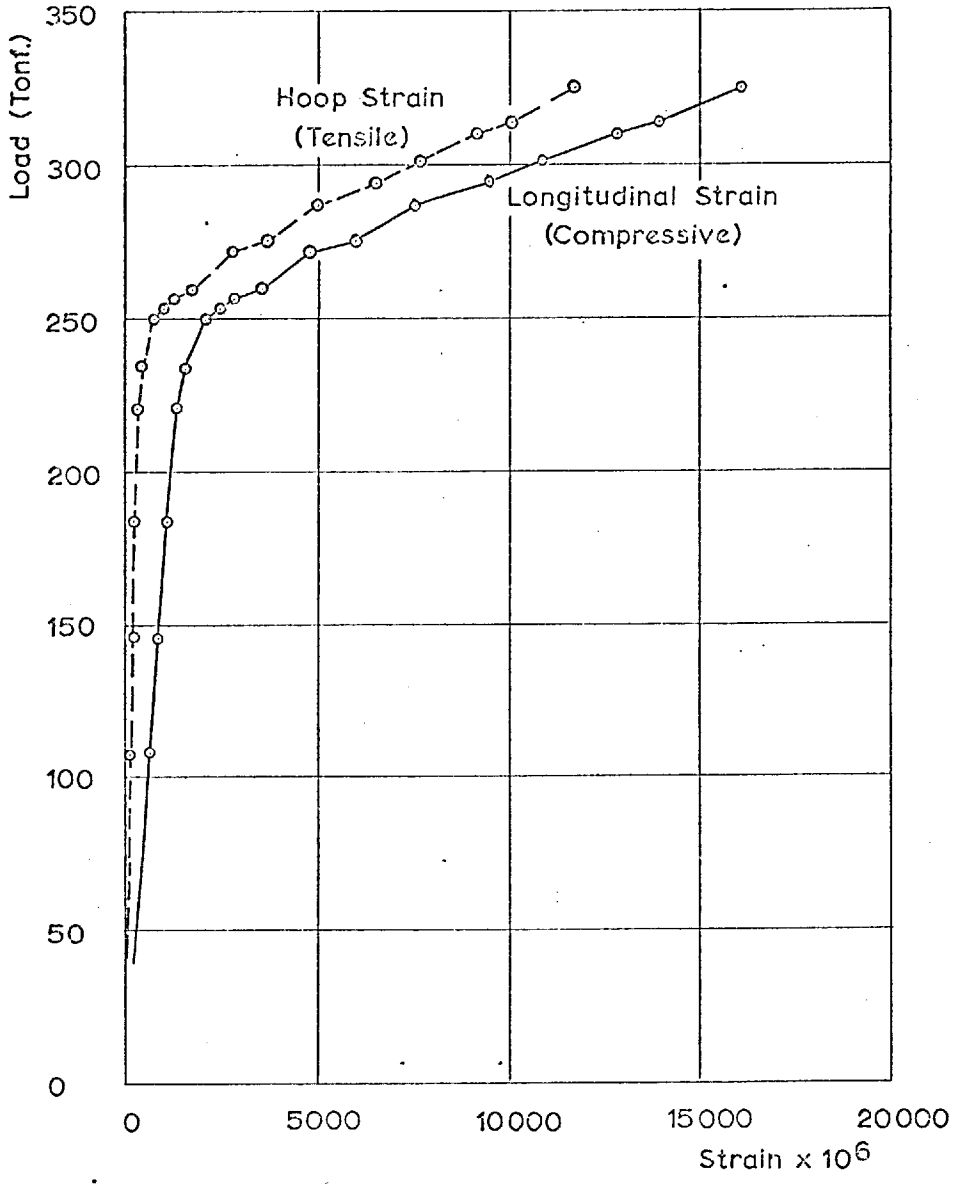

FIG.3.16 EXPERIMENTAL LOAD-STRAIN RELATIONSHIP FOR COLUMN M24 – IMPERIAL COLLEGE TESTS

σ_y = 19.7 tonf./in^2
P_T = Failure load = 361 tonf.
P_L = $A_s\sigma_y + A_c\sigma_m$ = 242 tonf.
P_L/P_T = 0.67

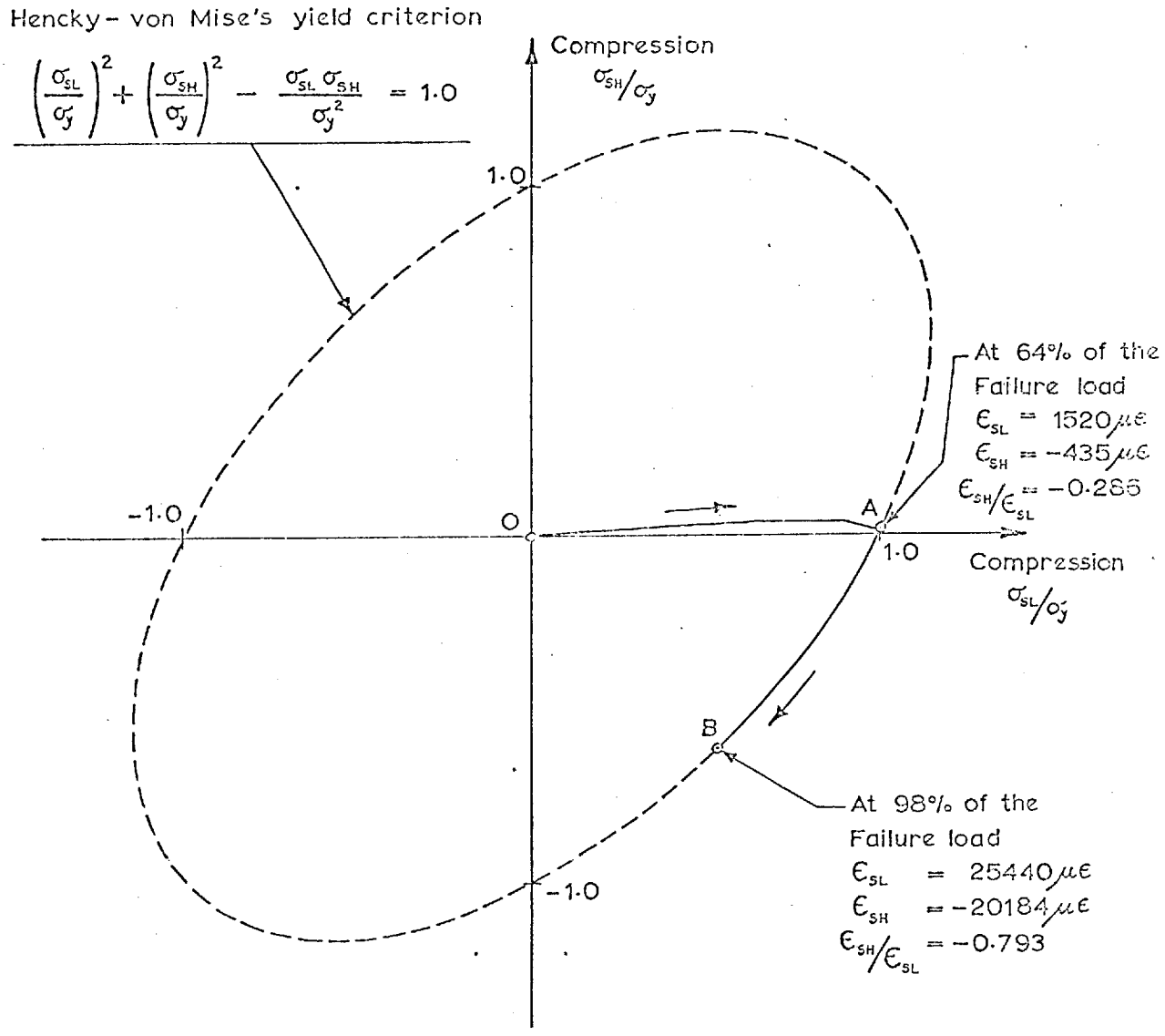

FIG. 3.17 BIAXIAL STRESSES IN THE STEEL - STUB COLUMN M24

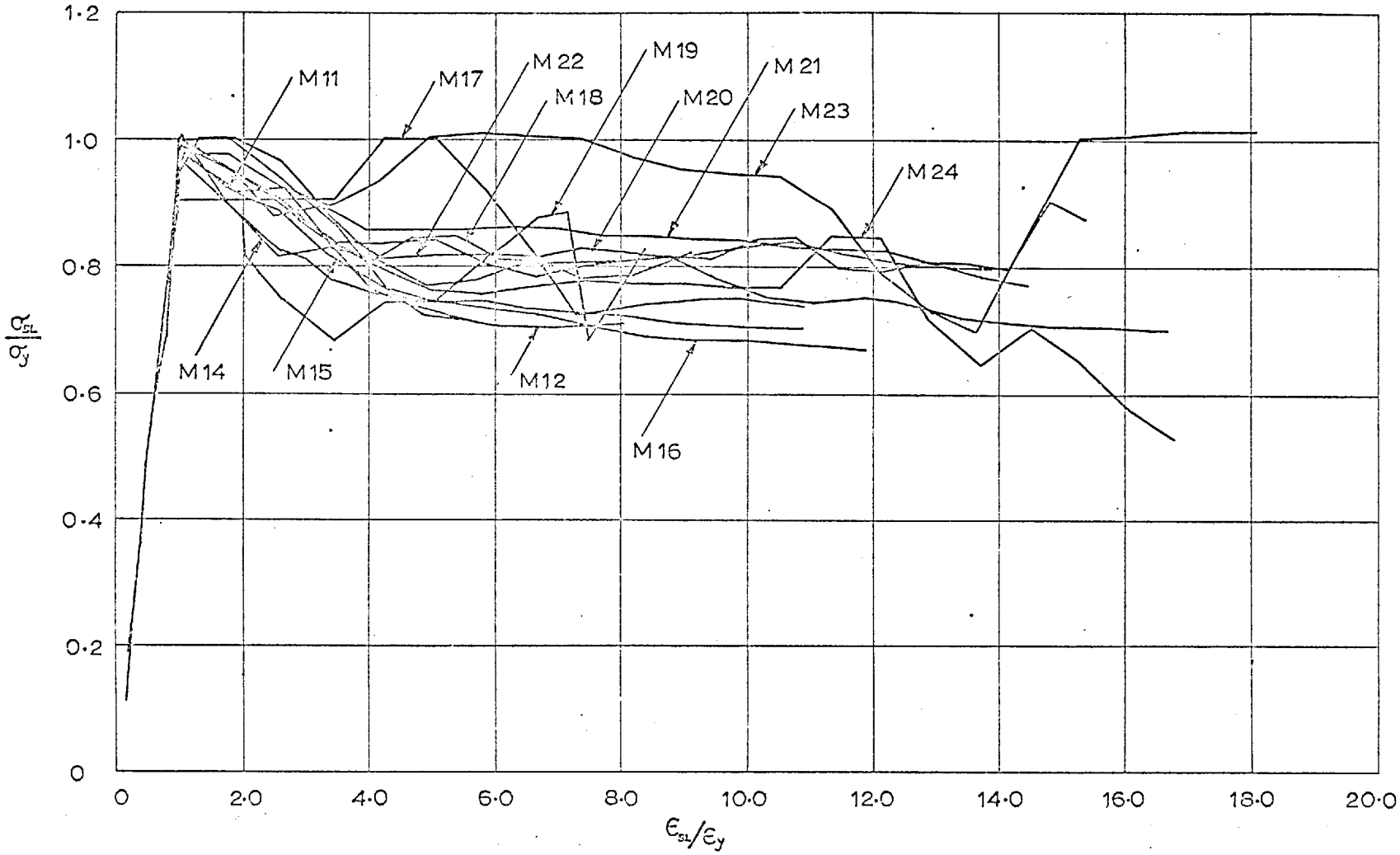

FIG. 3.18 LONGITUDINAL STRESS-STRAIN RELATIONSHIP FOR THE BIAXIALLY STRESSED STEEL — STUB COLUMNS M11-M24

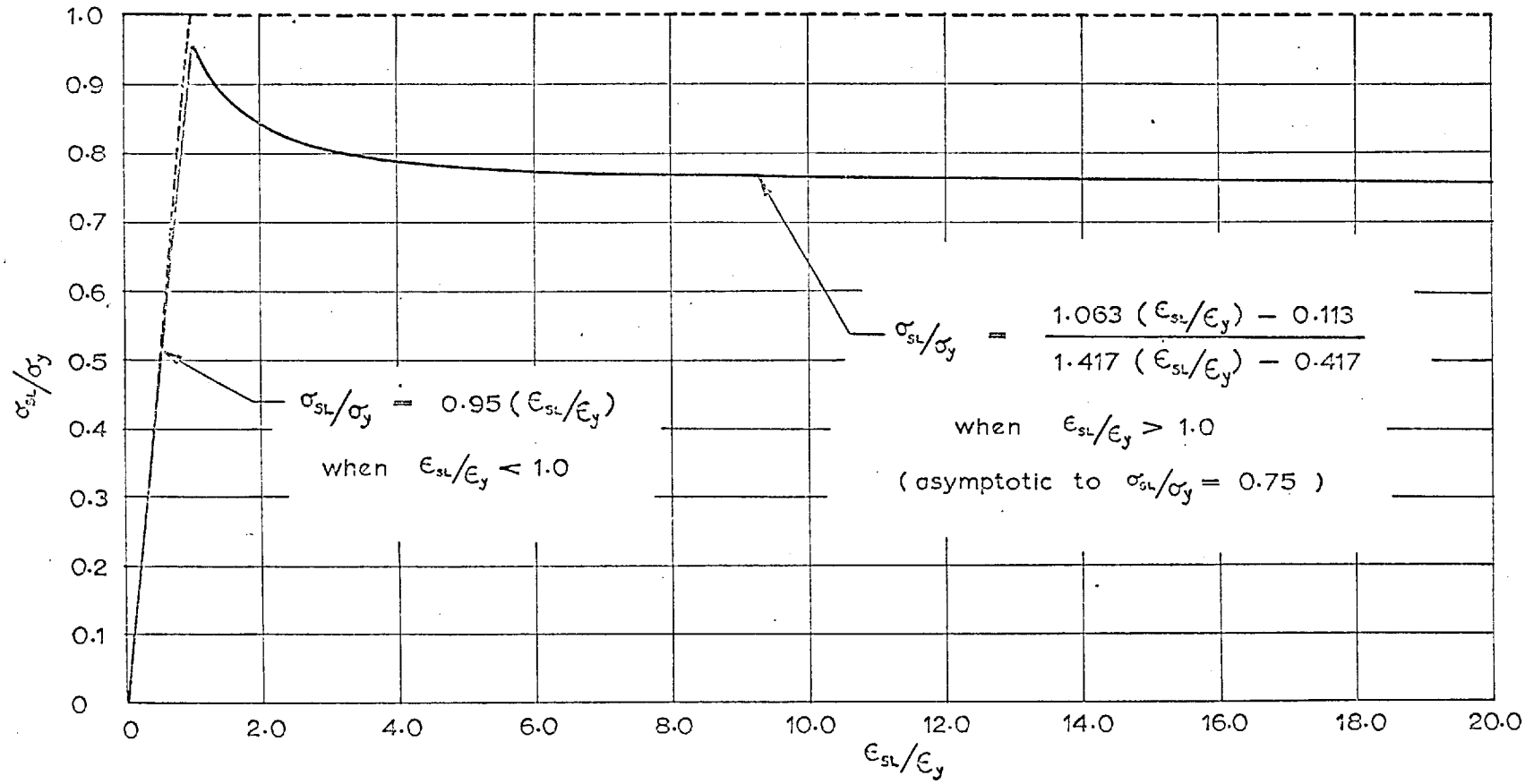

FIG. 3.19 EQUIVALENT STRESS-STRAIN RELATIONSHIP FOR THE STEEL IN CONCENTRICALLY-LOADED CIRCULAR STUB COLUMNS

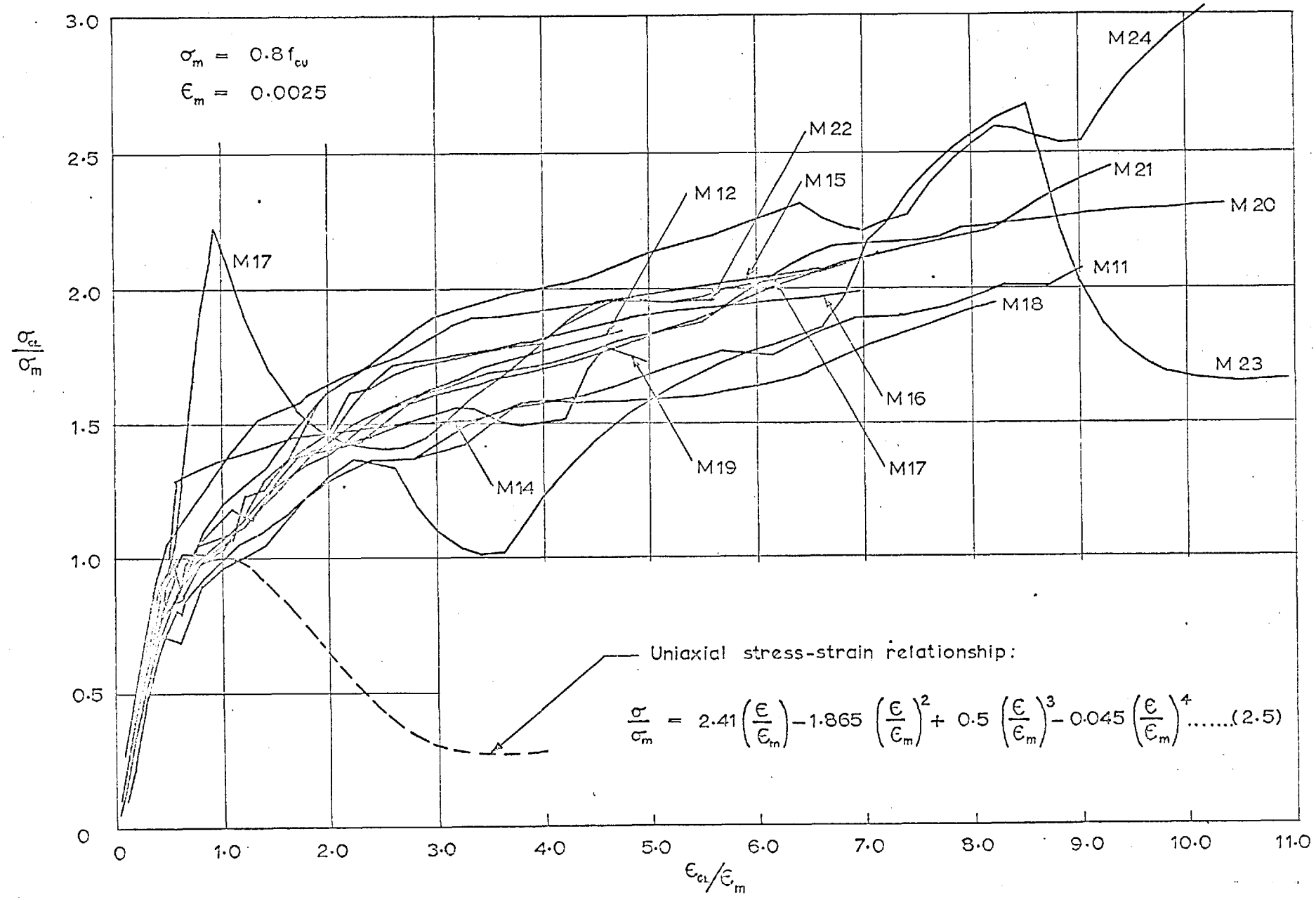

FIG. 3.20 LONGITUDINAL STRESS STRAIN RELATIONSHIP FOR THE TRIAXIALLY STRESSED CONCRETE — STUB COLUMNS M11-M24.

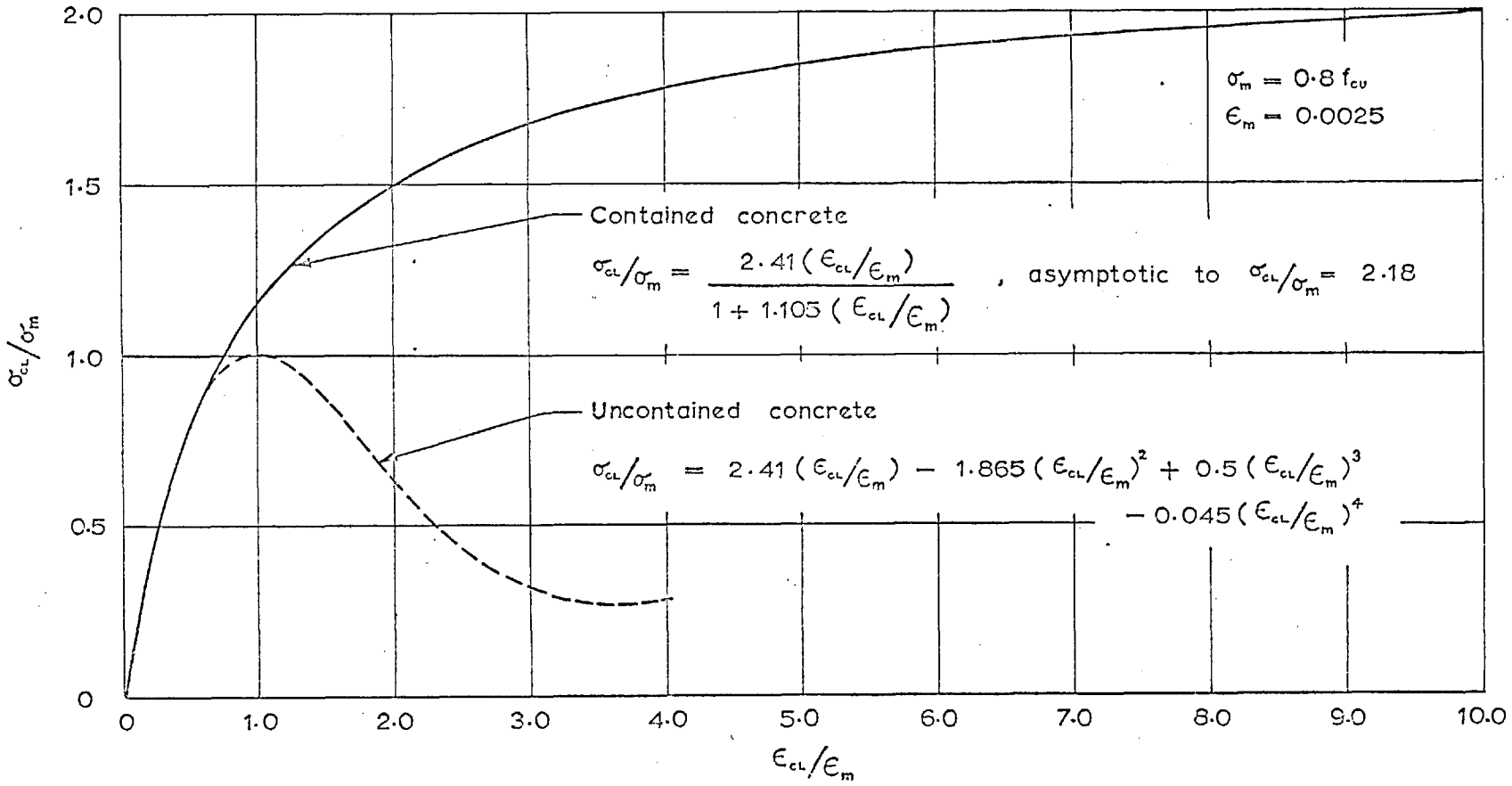

FIG. 3·21 EQUIVALENT STRESS-STRAIN RELATIONSHIP FOR THE CONCRETE IN CONCENTRICALLY-LOADED CIRCULAR STUB COLUMNS

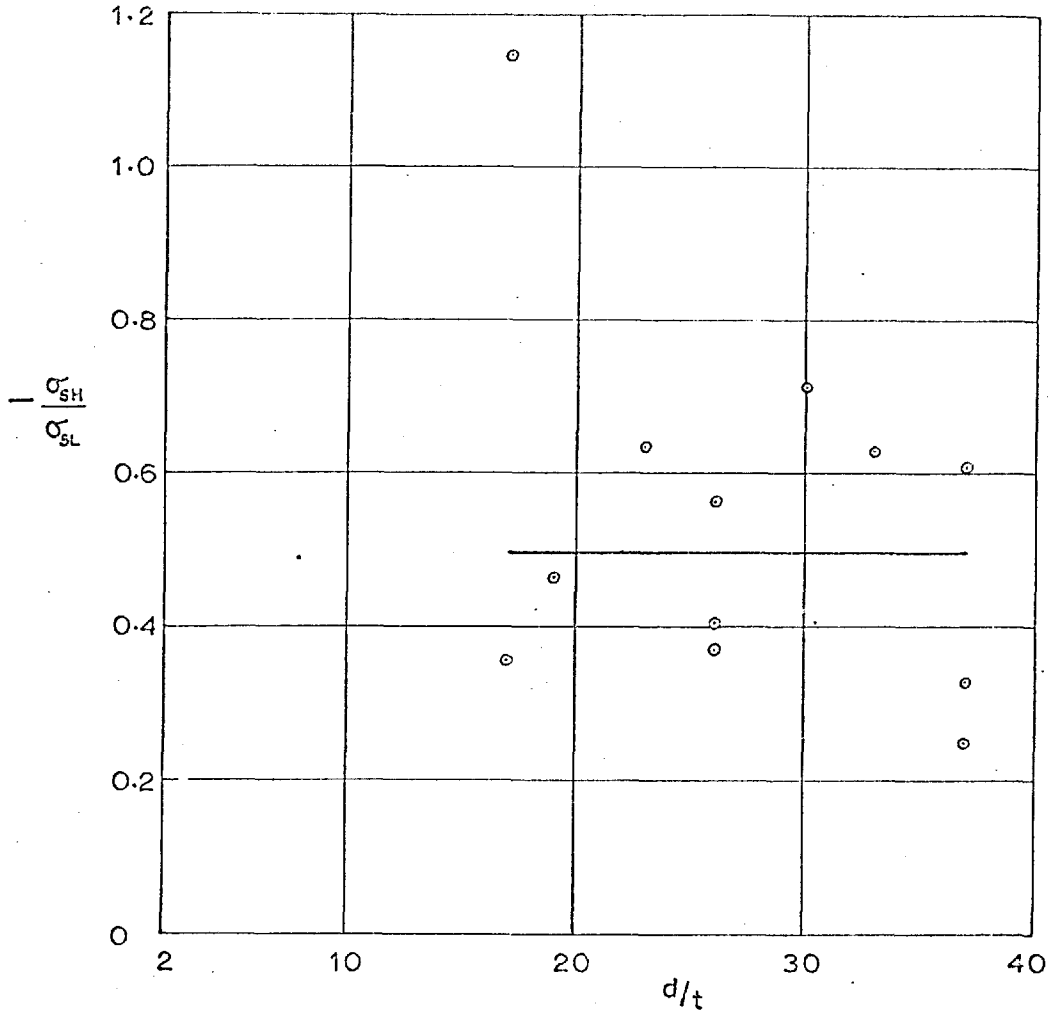

FIG. 3.22 σ_{SH}/σ_{SL} -- d/t RELATIONSHIPS NEAR FAILURE

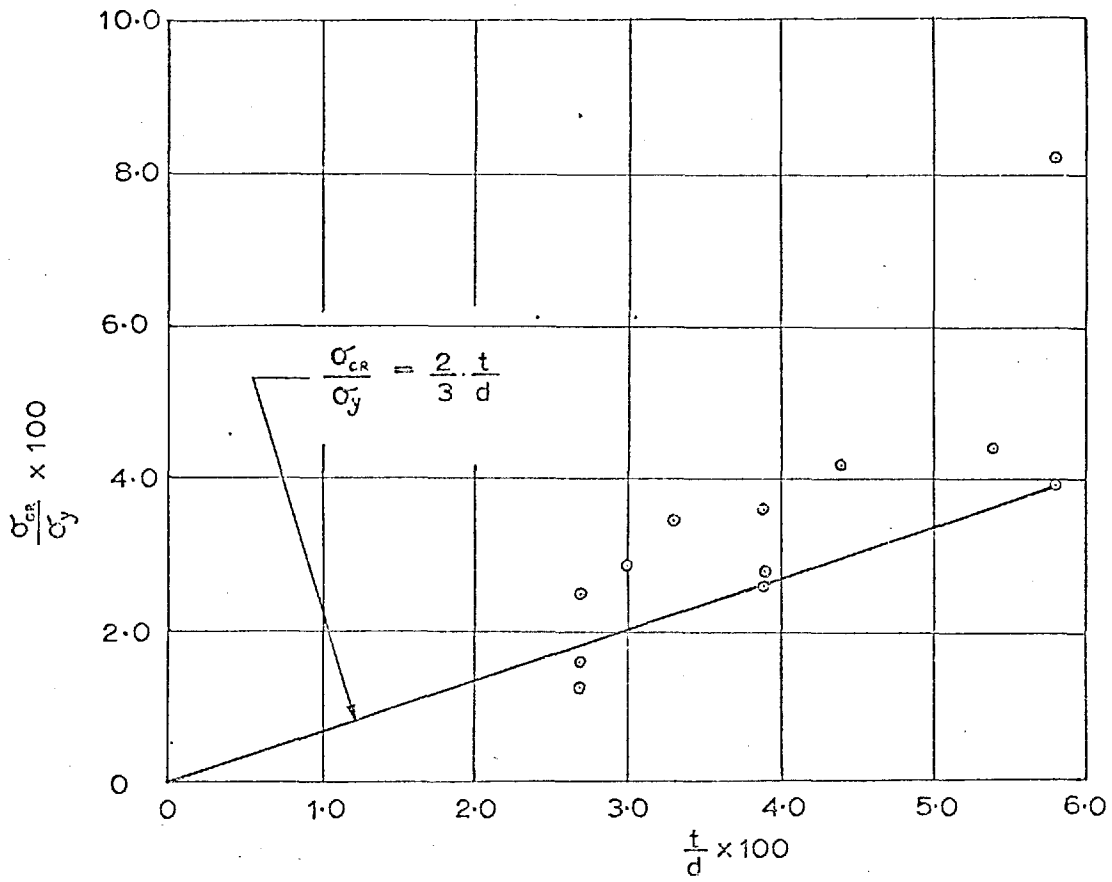

FIG. 3.23 σ_{CR}/σ_y -- t/d RELATIONSHIPS NEAR FAILURE

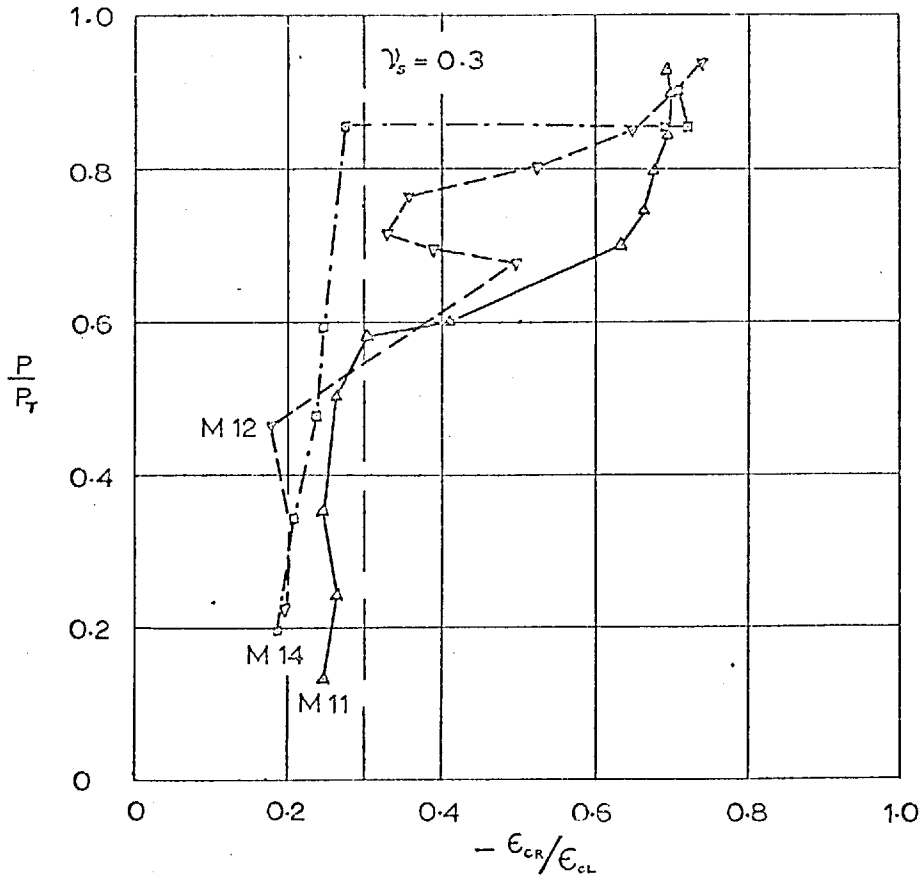

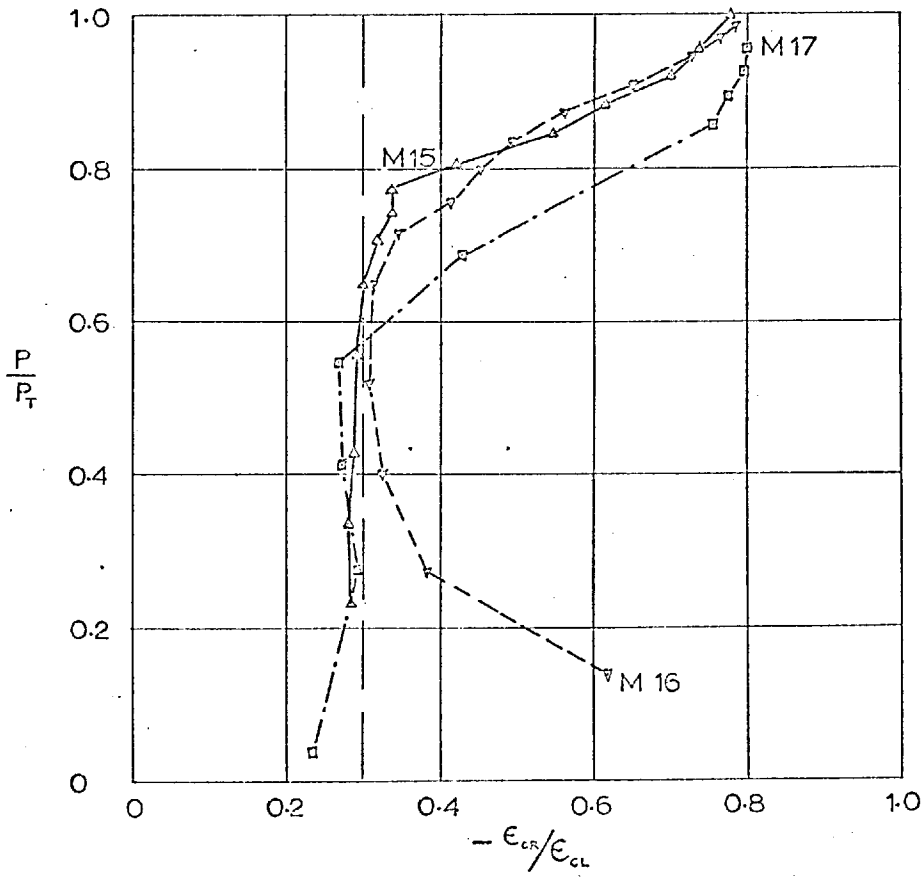

FIG. 3·24 RATIO OF LATERAL TO LONGITUDINAL STRAINS IN CONCRETE— COLUMNS M11 - M17

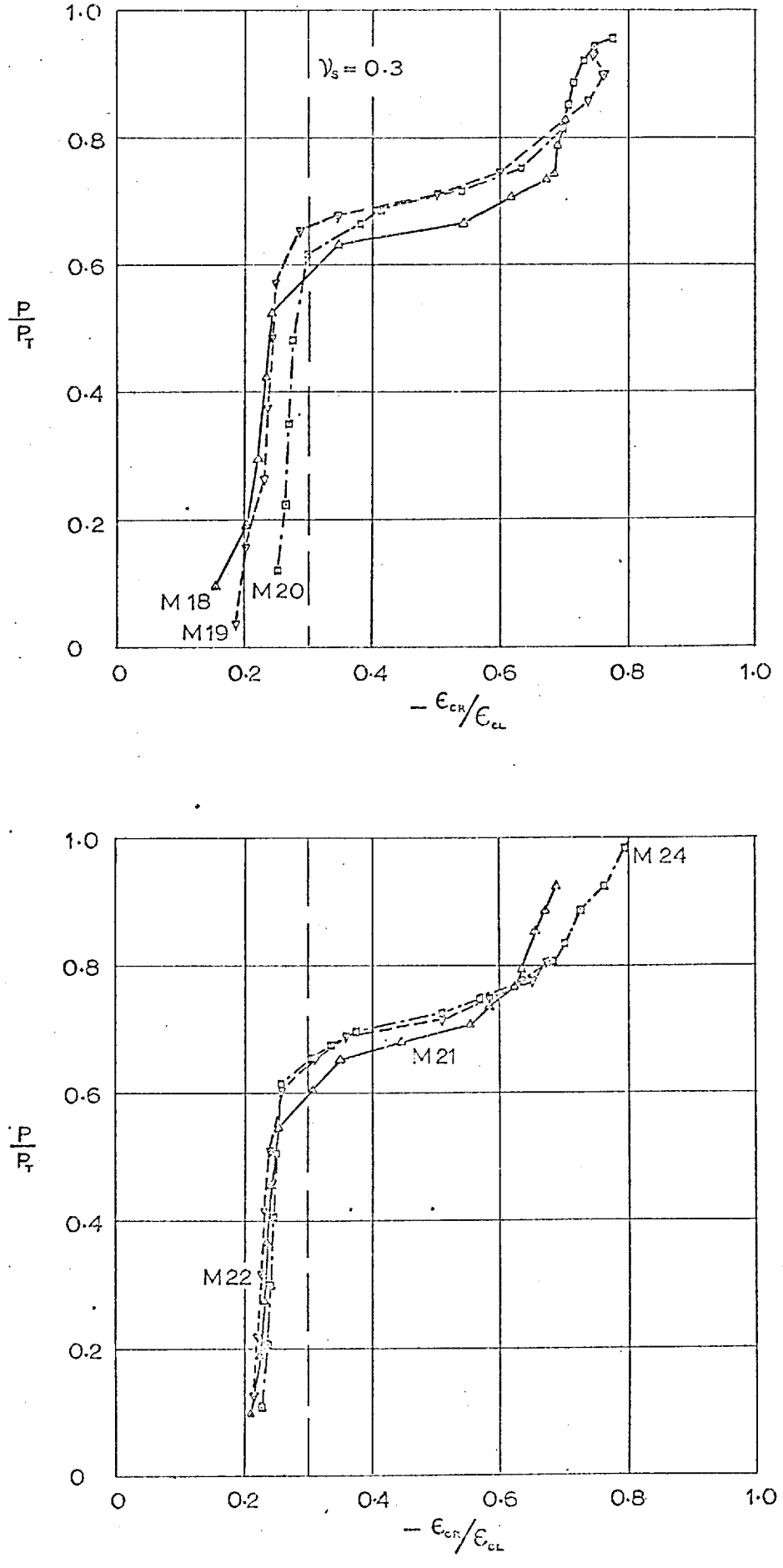

FIG. 3.25 RATIO OF LATERAL TO LONGITUDINAL STRAINS IN CONCRETE — COLUMNS M18 - M24

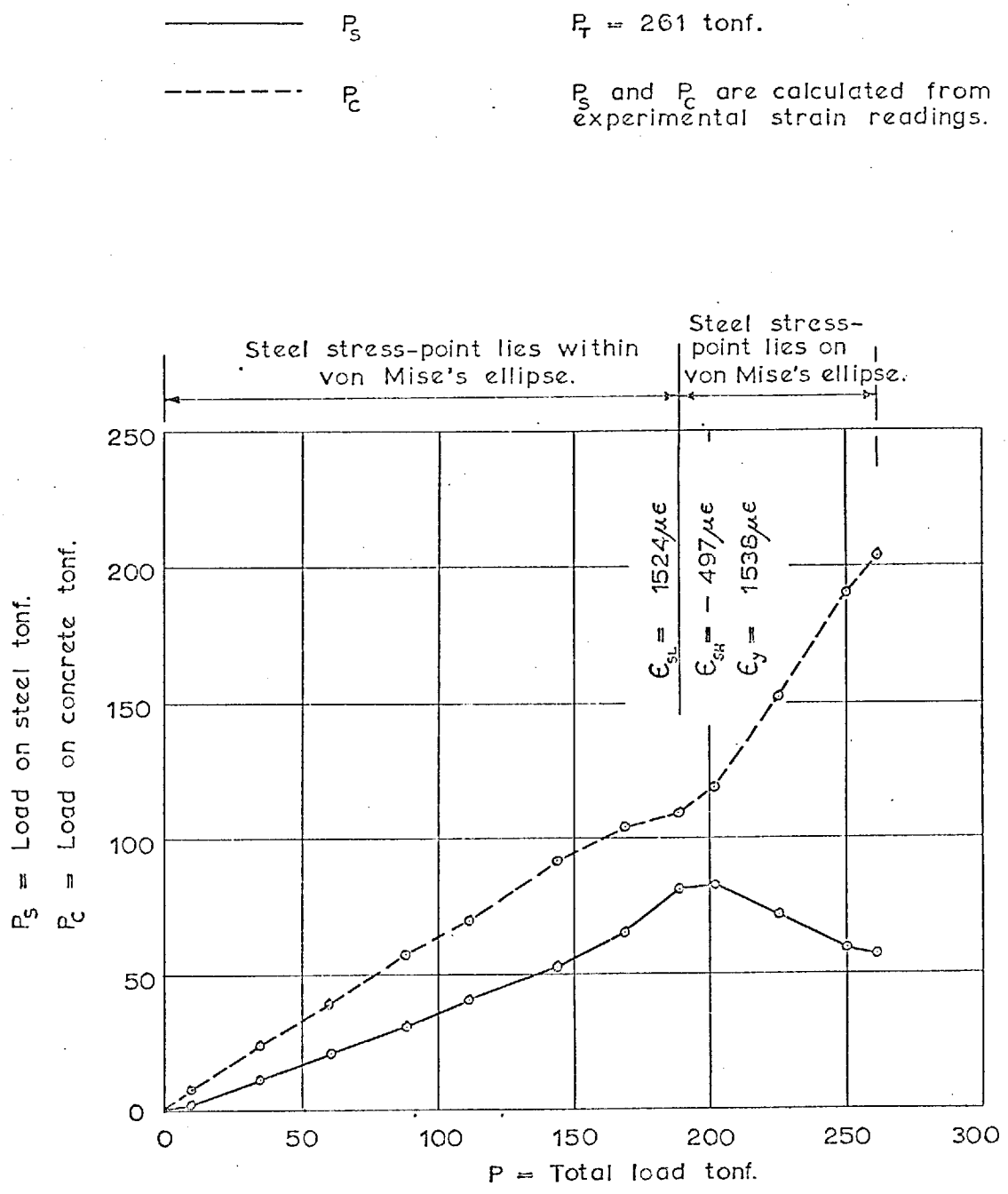

FIG. 3.26 $P_S - P$ AND $P_C - P$ RELATIONSHIPS FOR COLUMN M15

——————— P_S P_T = 361 tonf.

- - - - - - - - P_C P_S and P_C are calculated from experimental strain readings.

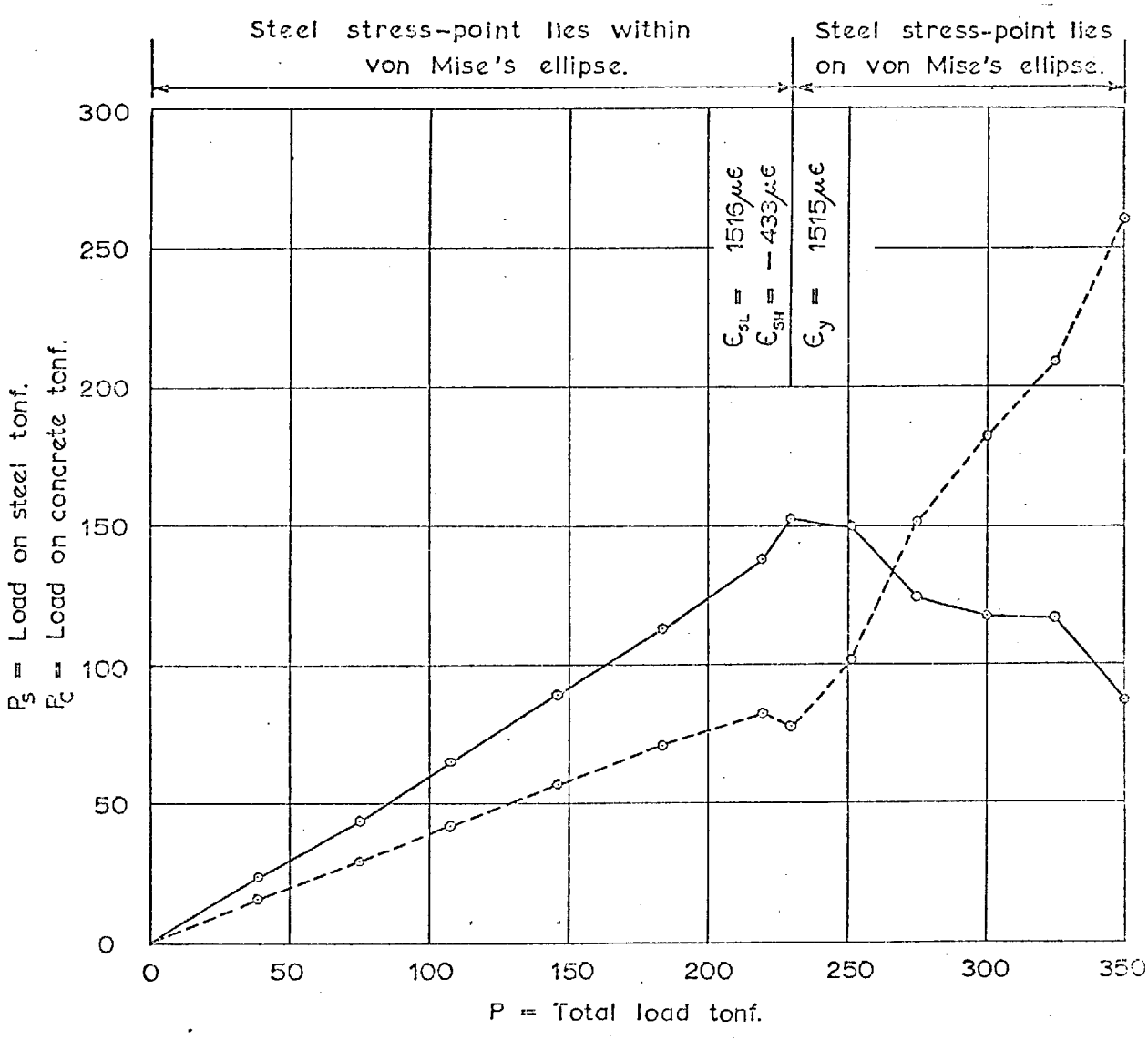

FIG. 3.27 P_S – P AND P_C – P RELATIONSHIPS FOR COLUMN M 24

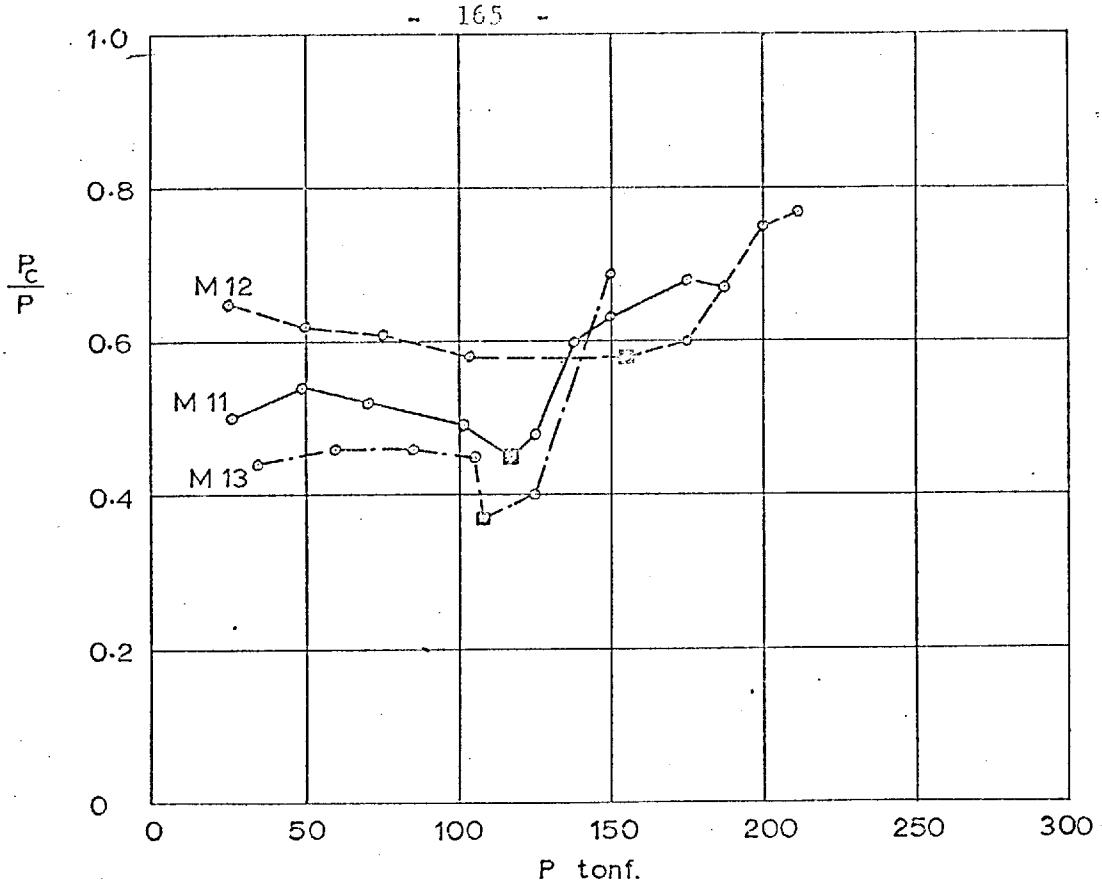

First yield of steel shown thus : ⊠

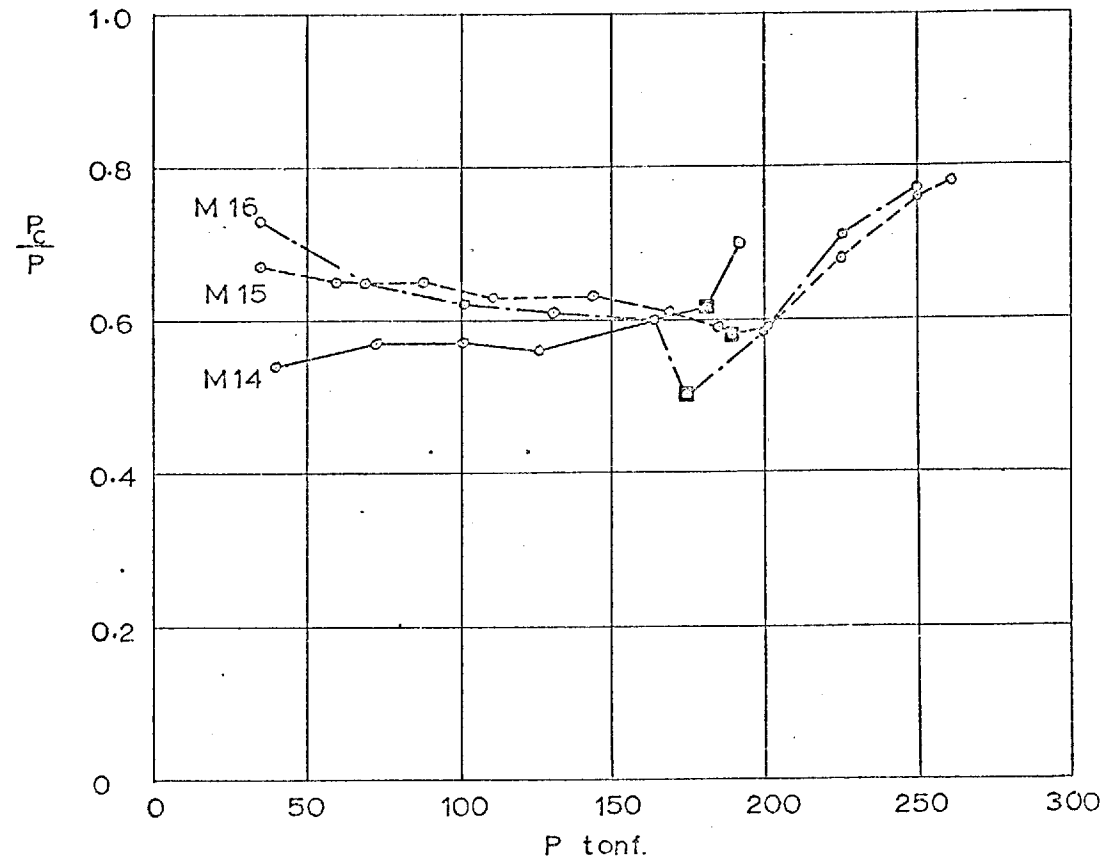

FIG. 3.28 RATIO OF LOAD CARRIED BY THE CONCRETE TO TOTAL LOAD — COLUMNS M11-M16

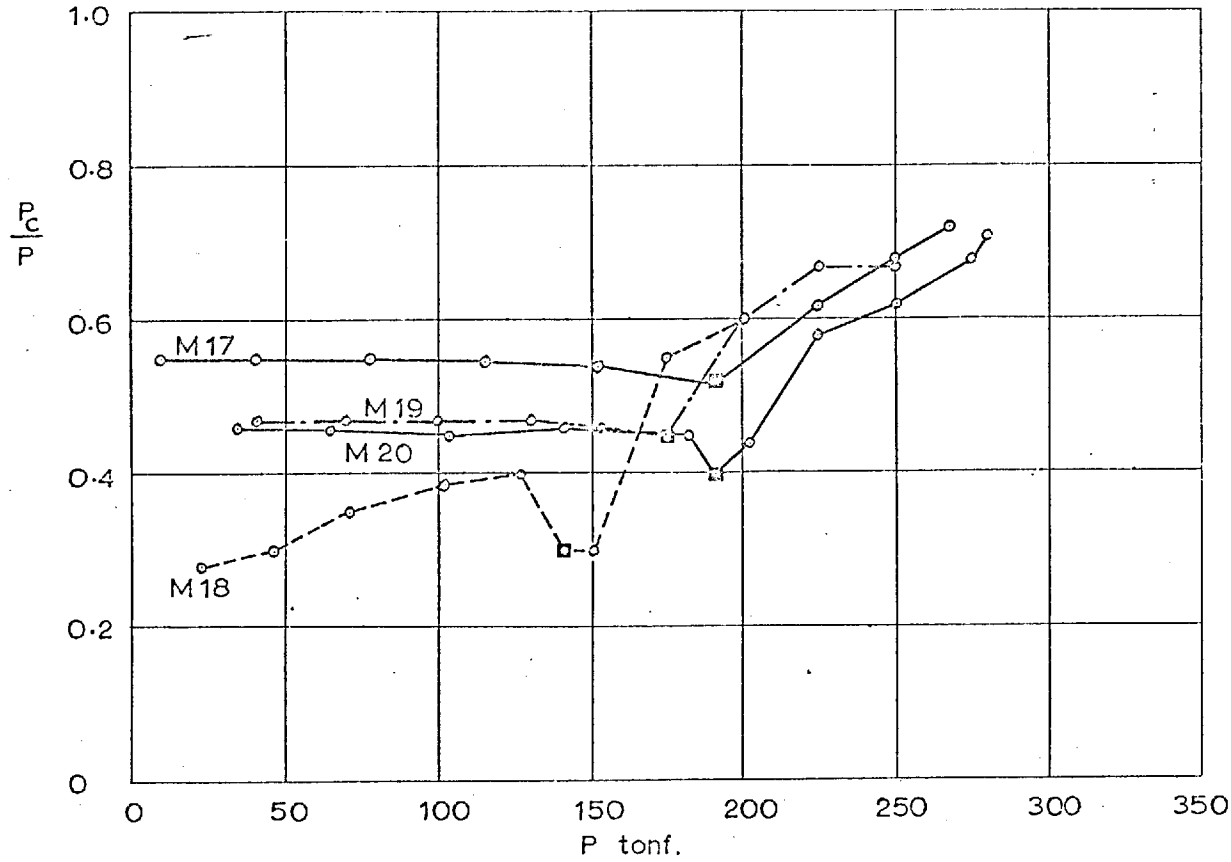

First yield of steel shown thus : ◘

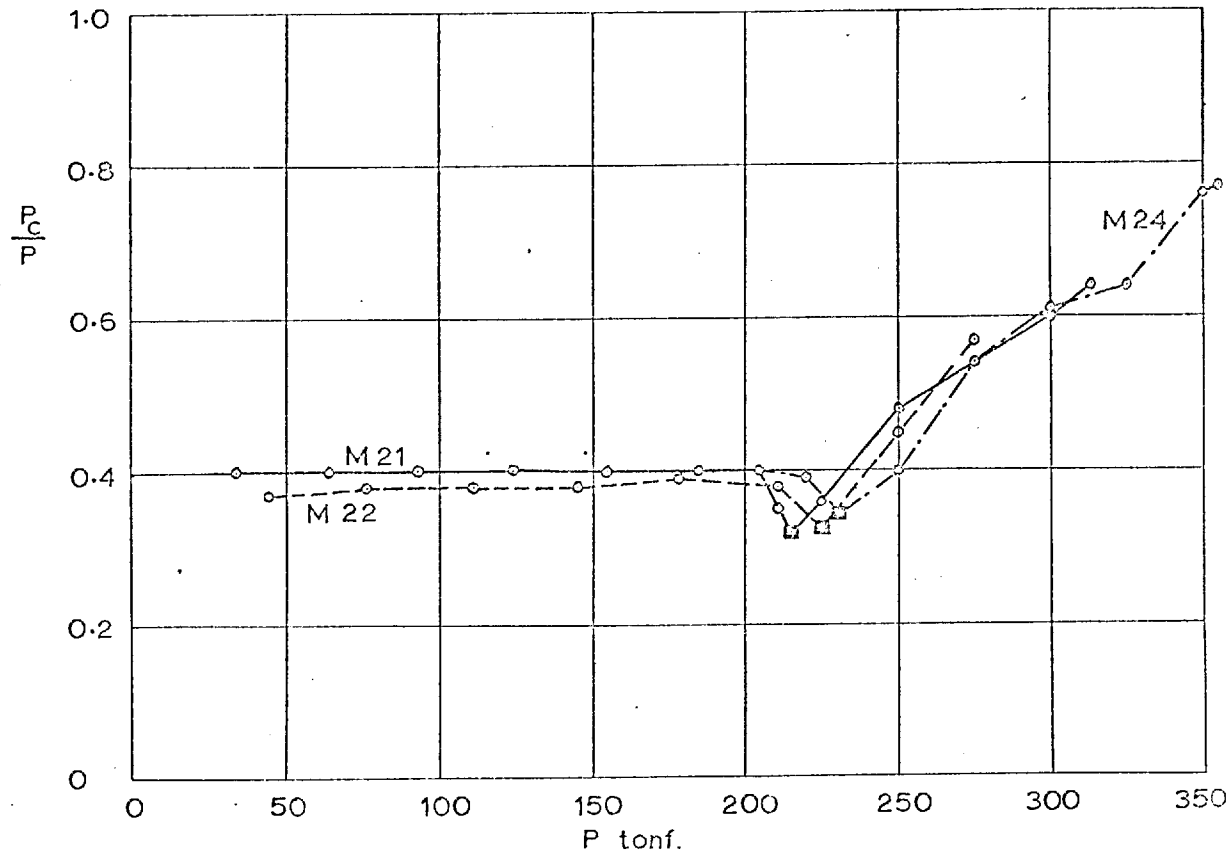

FIG. 3·29 RATIO OF LOAD CARRIED BY THE CONCRETE TO TOTAL LOAD – COLUMNS M 17 – M 24.

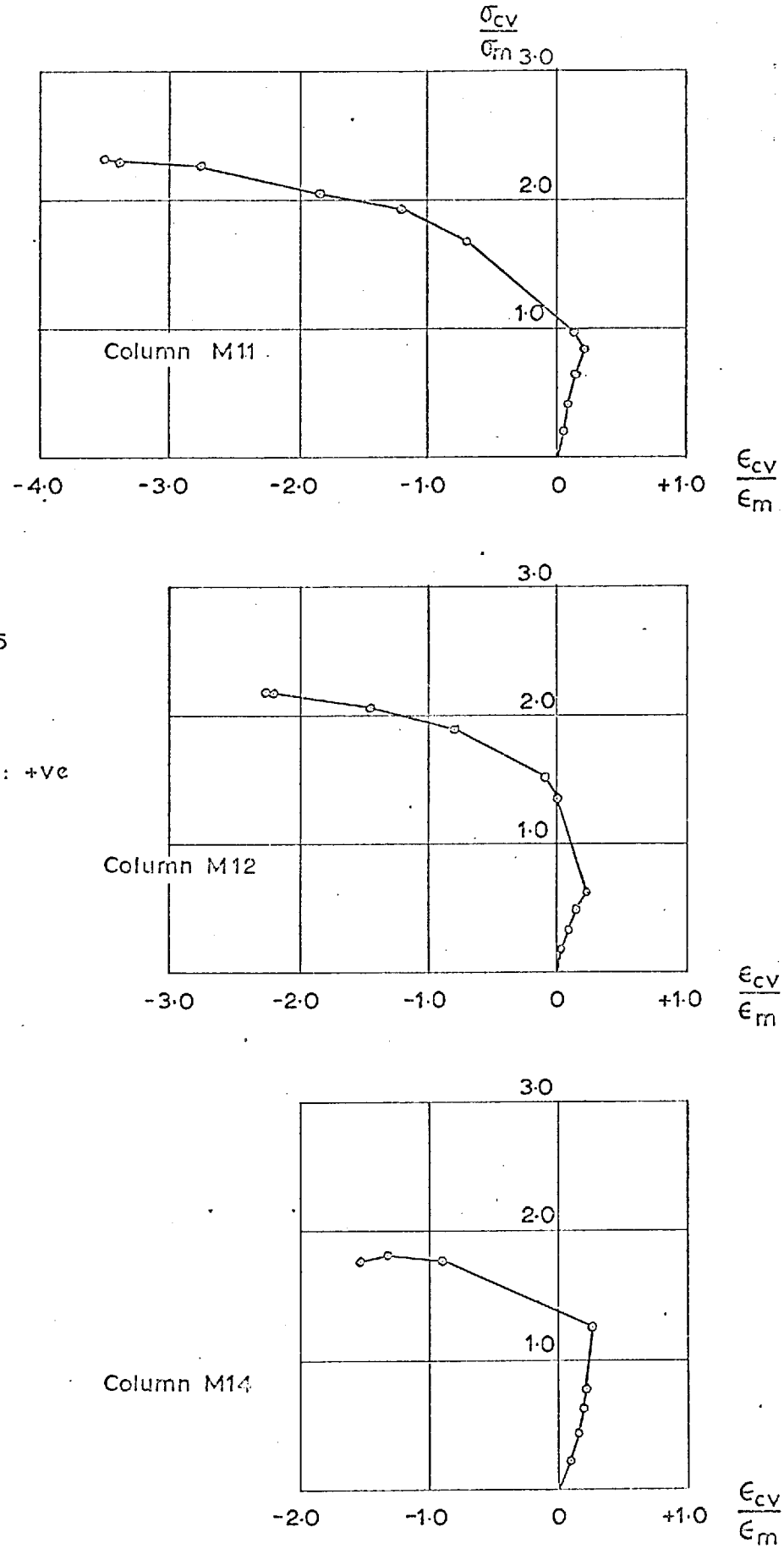

ϵ_m = 0·0025

σ_m = 0·8 f_{cu}

Compression : +ve

FIG. 3·30 VOLUME CHANGES IN COLUMNS M11, M12 & M14

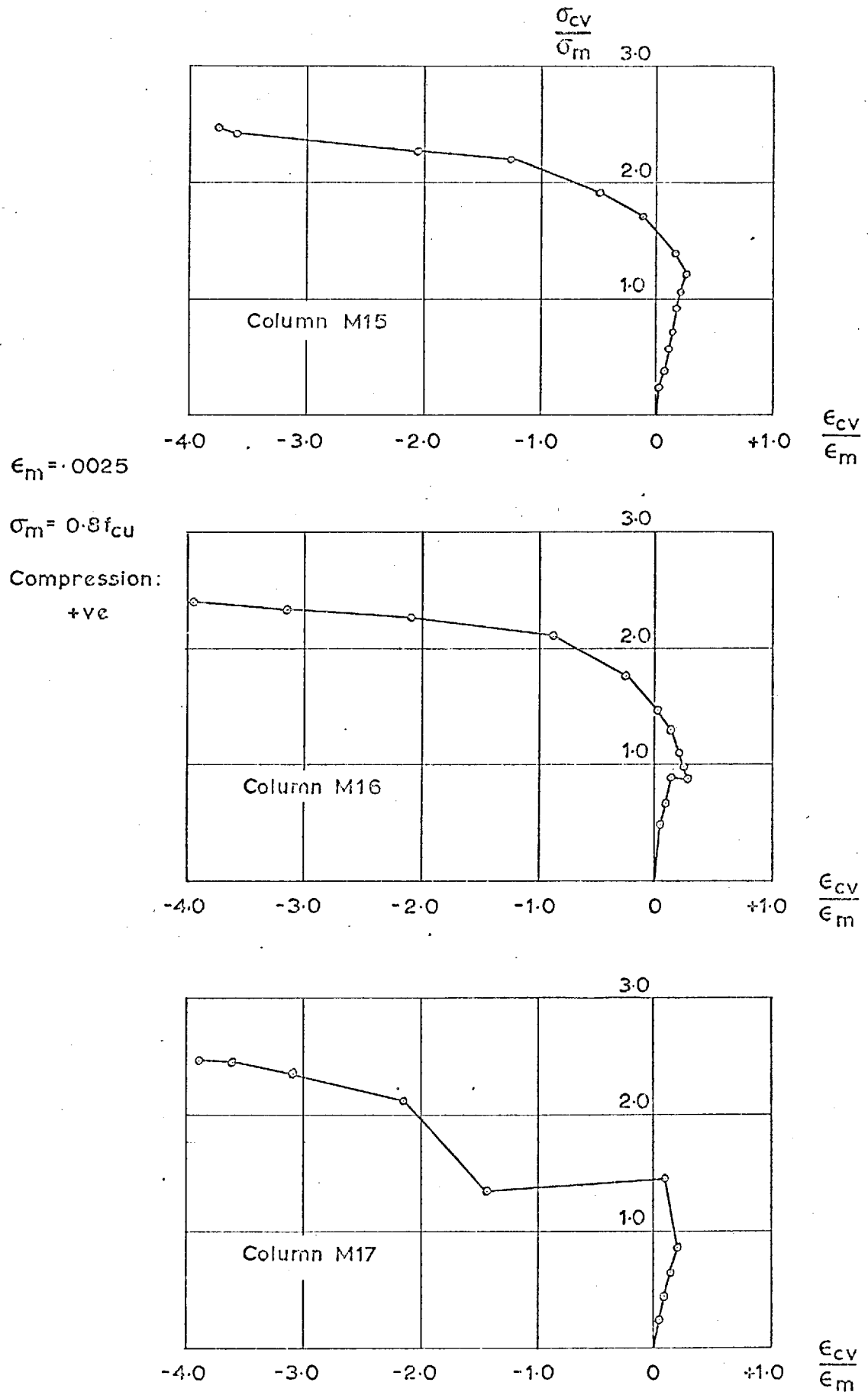

FIG.3.31 VOLUME CHANGES IN COLUMNS M15, M16 & M17

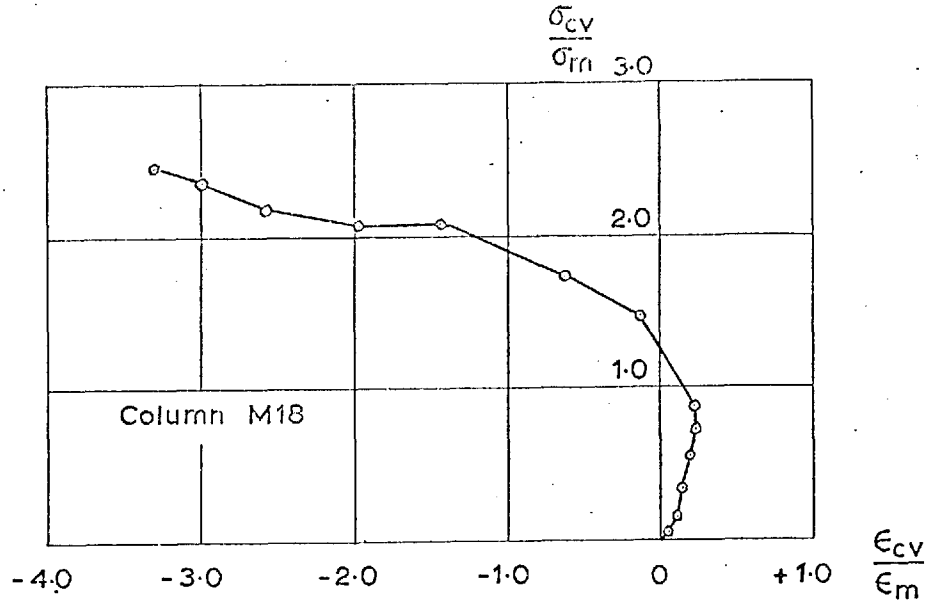

ϵ_m = 0·0025

σ_m = 0·8 f_{cu}

Compression: +vc

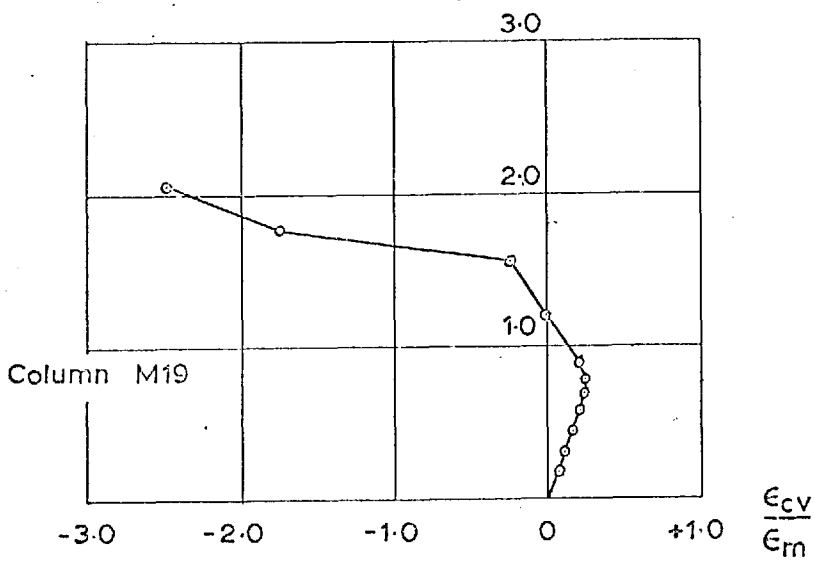

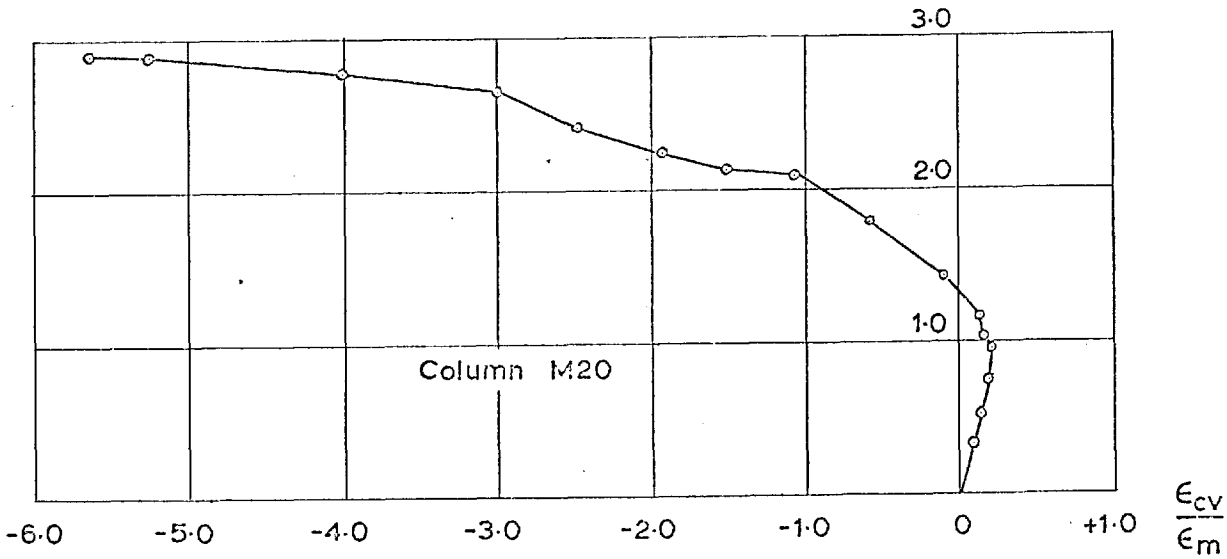

FIG.3.32 VOLUME CHANGES IN COLUMNS M18, M19 & M20

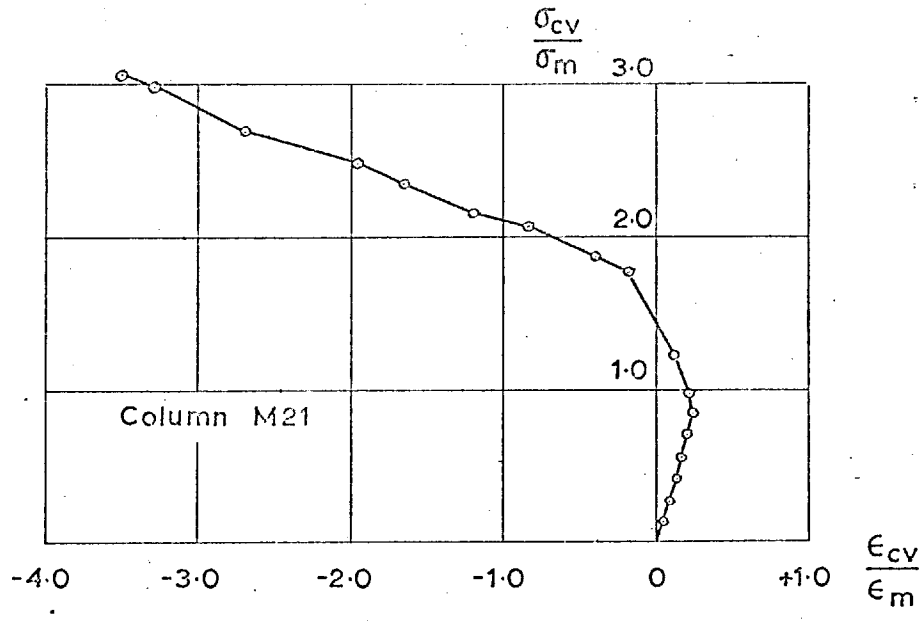

$\epsilon_m = 0.0025$

$\sigma_m = 0.8 f_{cu}$

Compressive : +ve

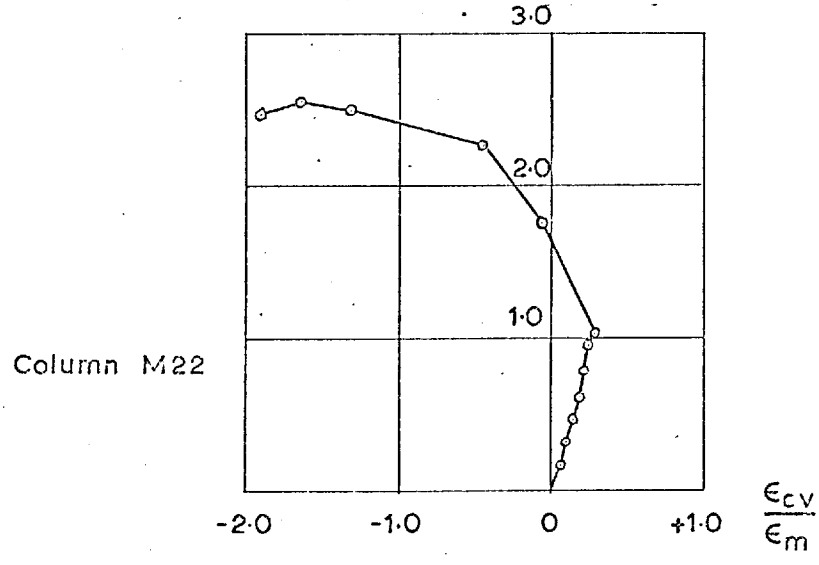

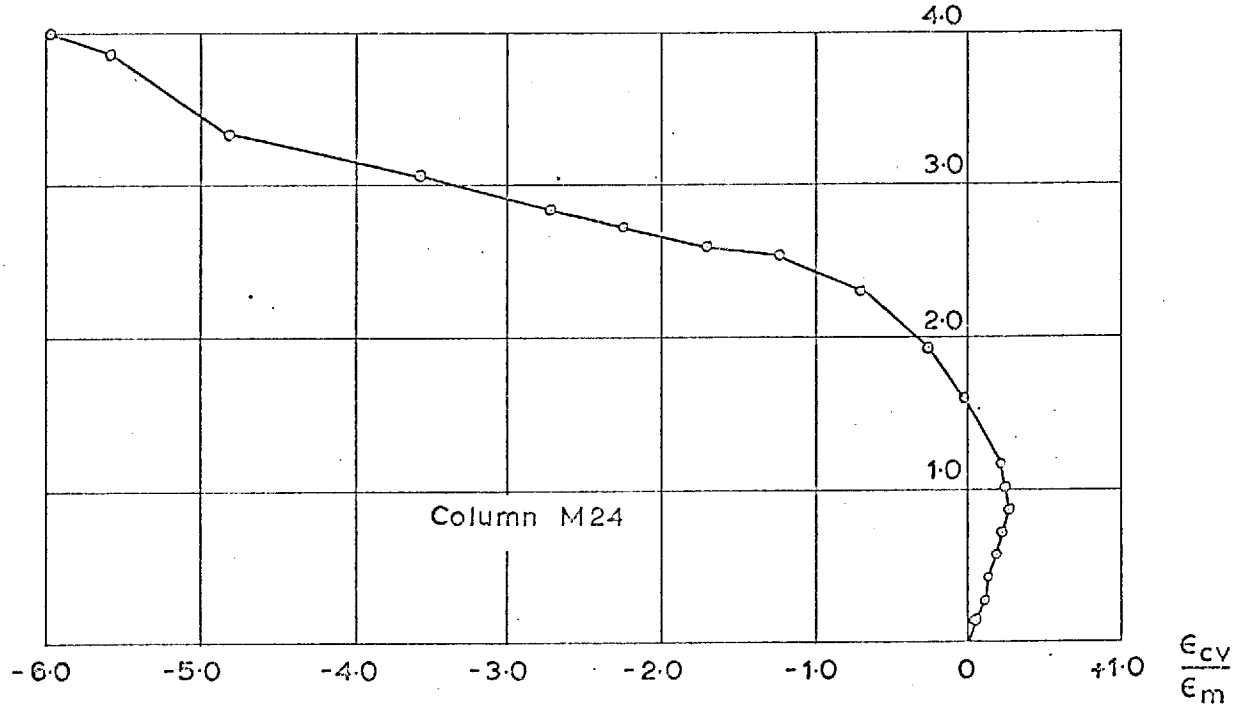

FIG.3.33 VOLUME CHANGES IN COLUMNS M21, M22 & M24

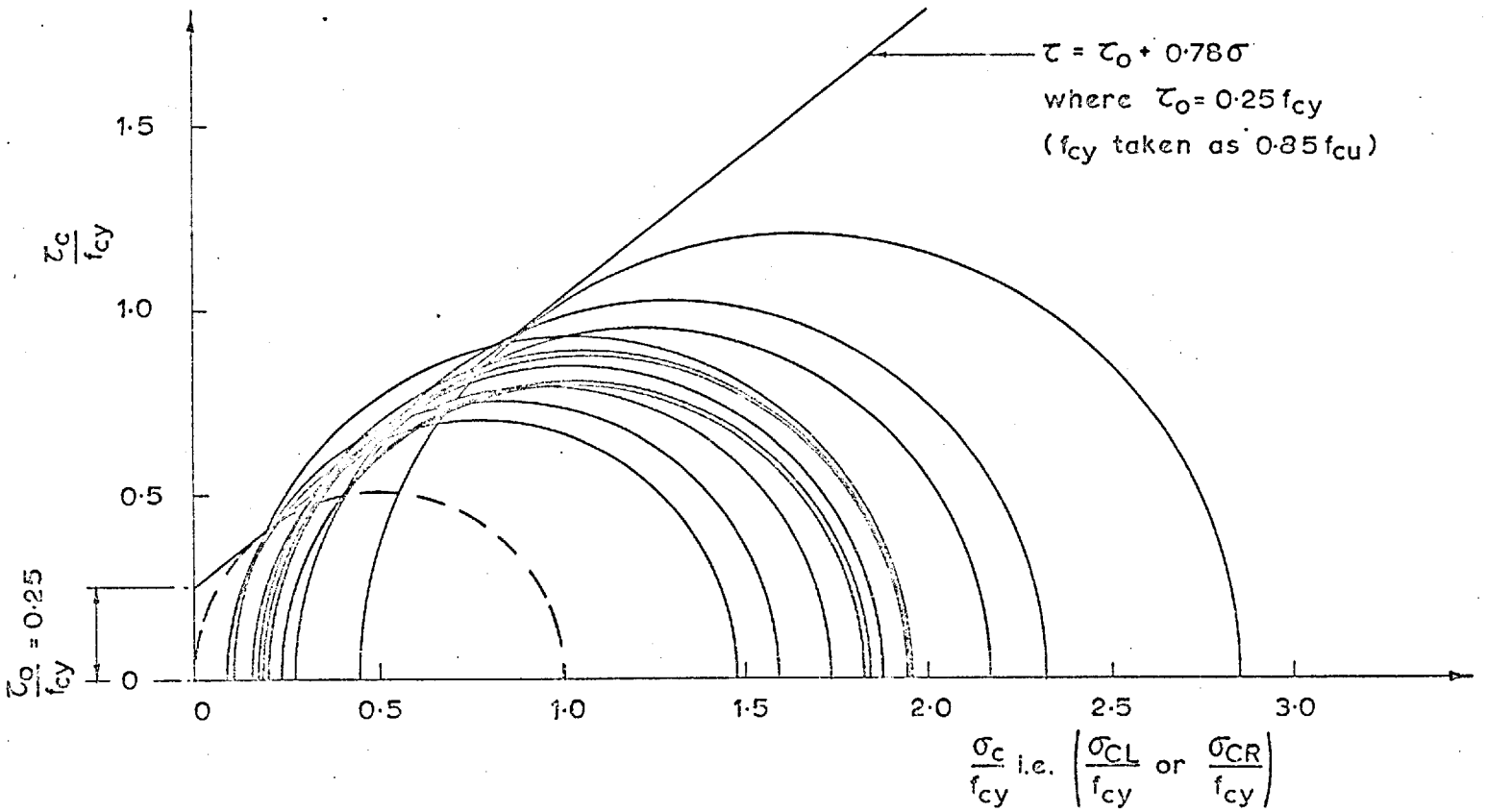

Note: For loads and stresses see table 3·4

FIG. 3·34 MOHR CIRCLES FOR CONCRETE NEAR FAILURE – COLUMNS M11–M24.

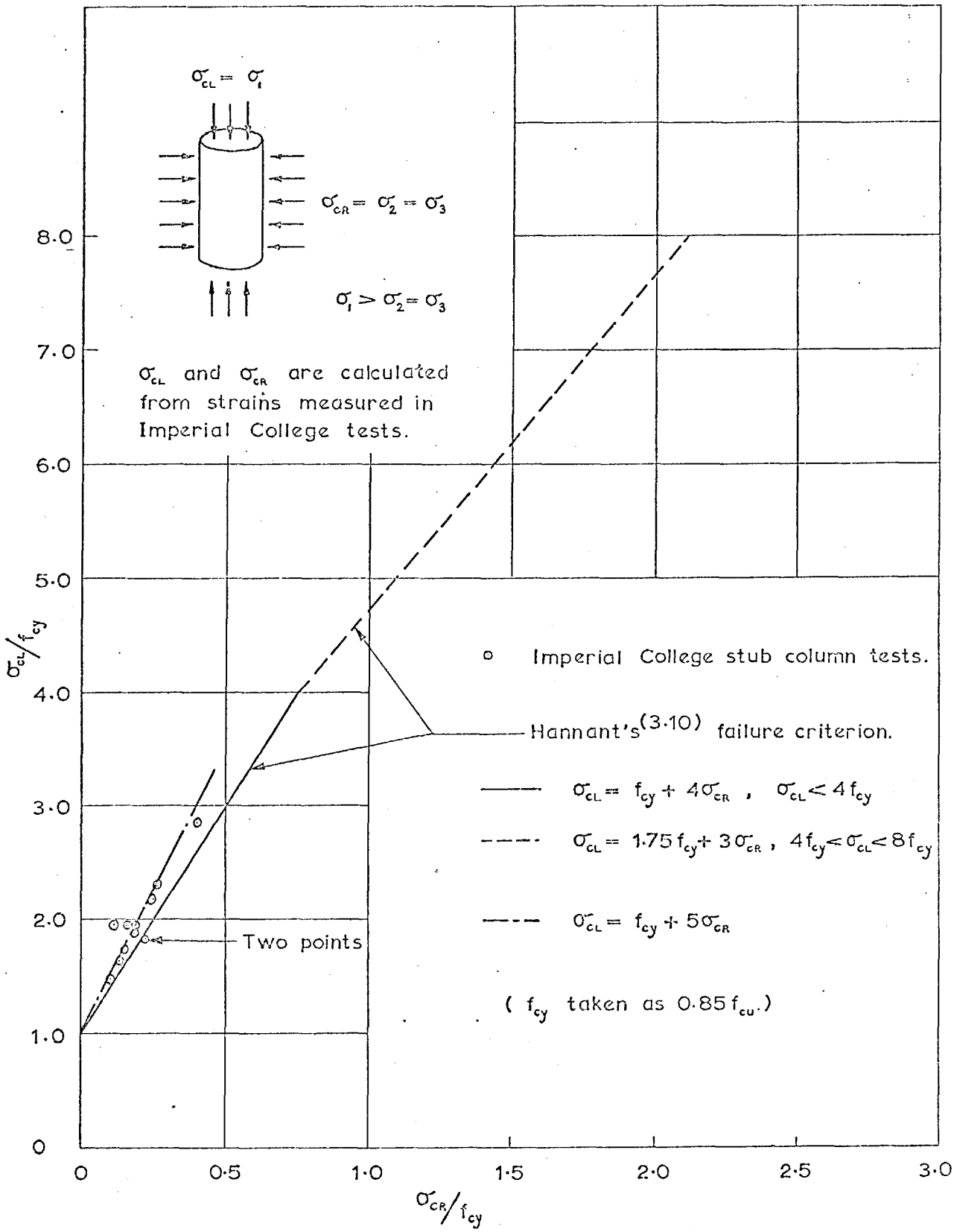

FIG.3.35 COMPARISON BETWEEN STRESSES IN CONCRETE CORE OF STUB COLUMNS NEAR FAILURE AND AVAILABLE FAILURE CRITERIA OF CONCRETE UNDER TRIAXIAL COMPRESSION — IMPERIAL COLLEGE TESTS.

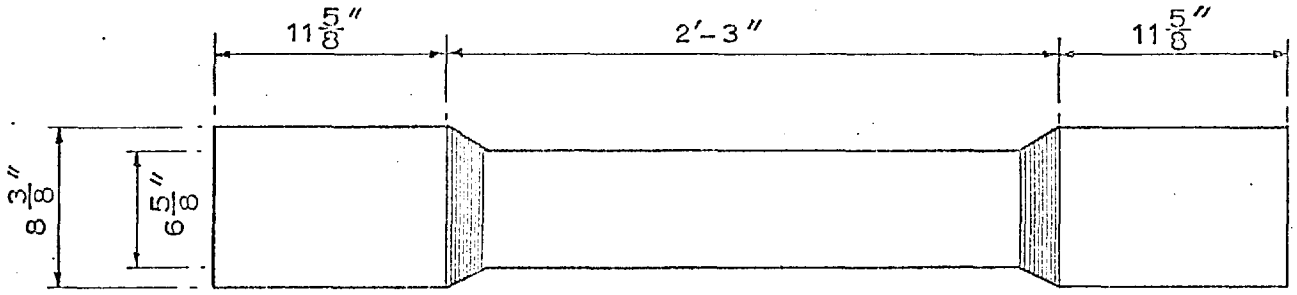

FIG. 4.1 EXTERNAL DIMENSIONS OF A MOMENT-CURVATURE SPECIMEN

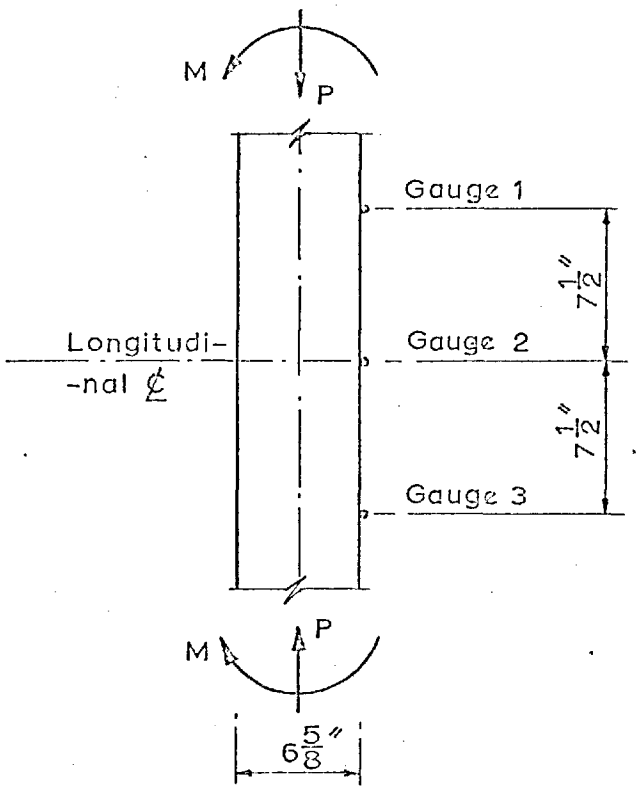

A. Deflection gauges.

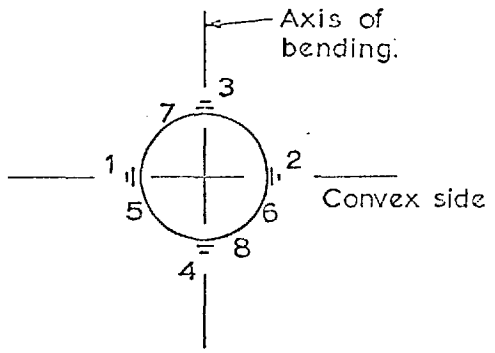

Longitudinal gauges - 1, 2, 3, 4.
Hoop gauges - 5, 6, 7, 8.

B. Strain gauges.

FIG. 4.2 INSTRUMENTATION OF THE MOMENT-CURVATURE SPECIMEN

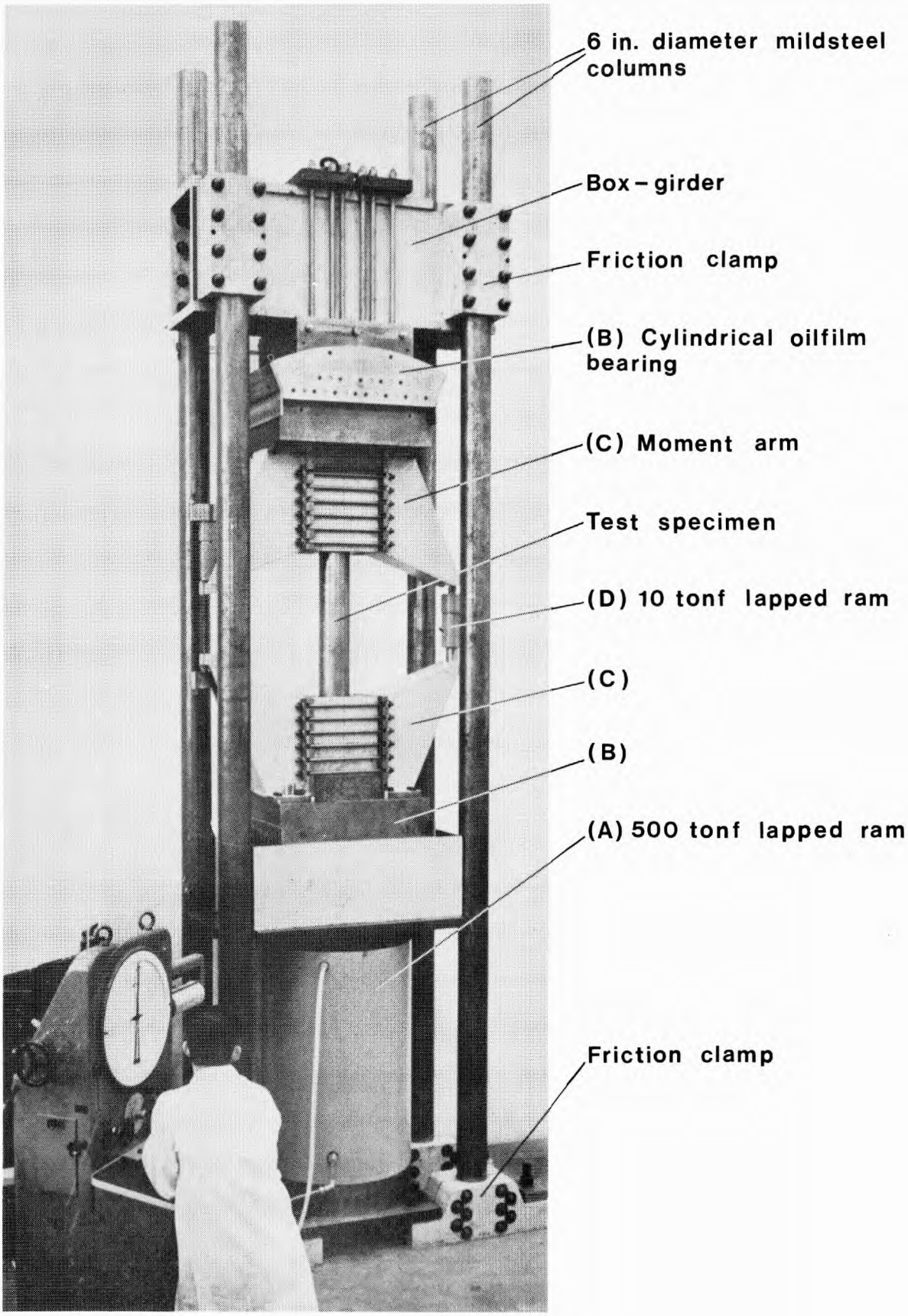

FIG 4.3. MOMENT AND AXIAL COMPRESSION RIG

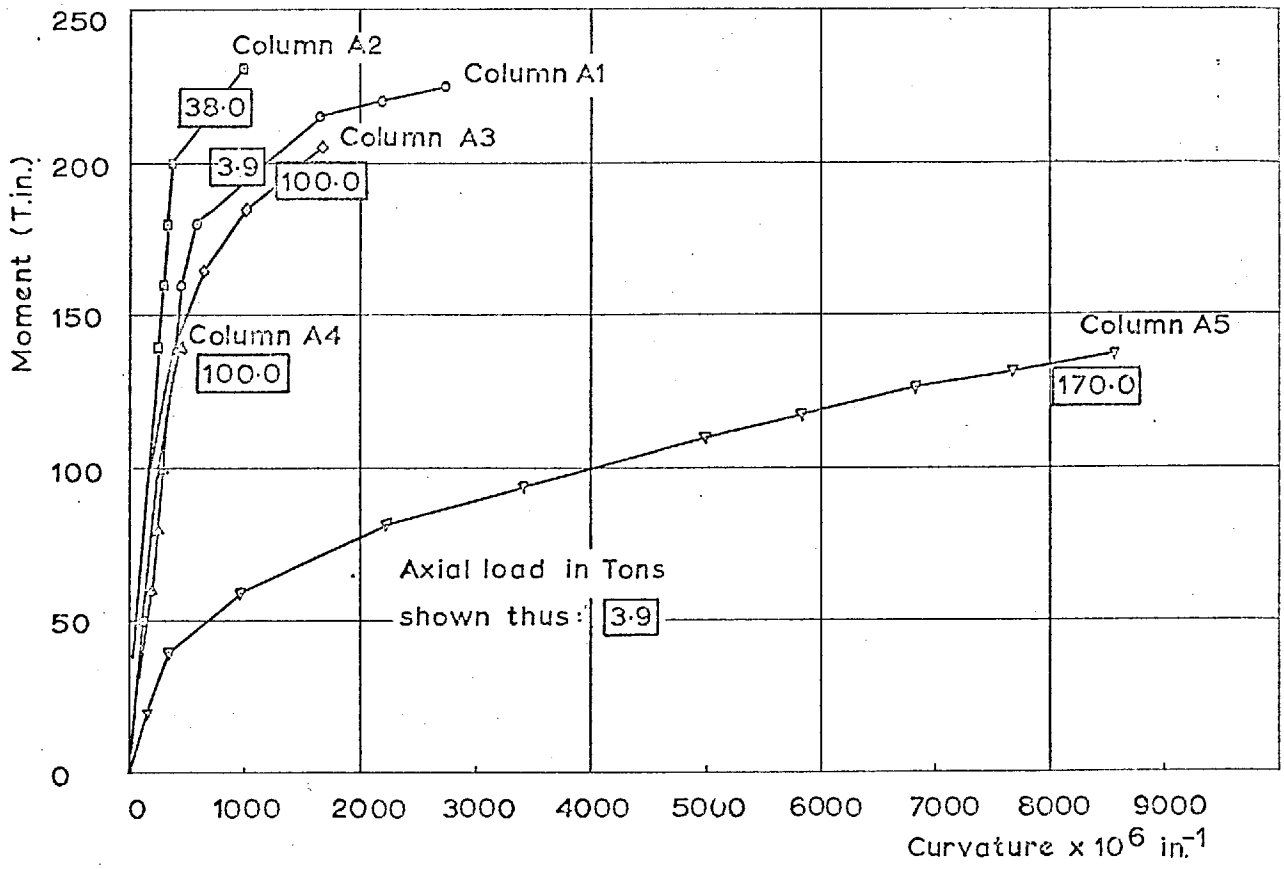

FIG. 4·4 EXPERIMENTAL MOMENT-CURVATURE RELATIONSHIP FOR SERIES A – IMPERIAL COLLEGE TESTS

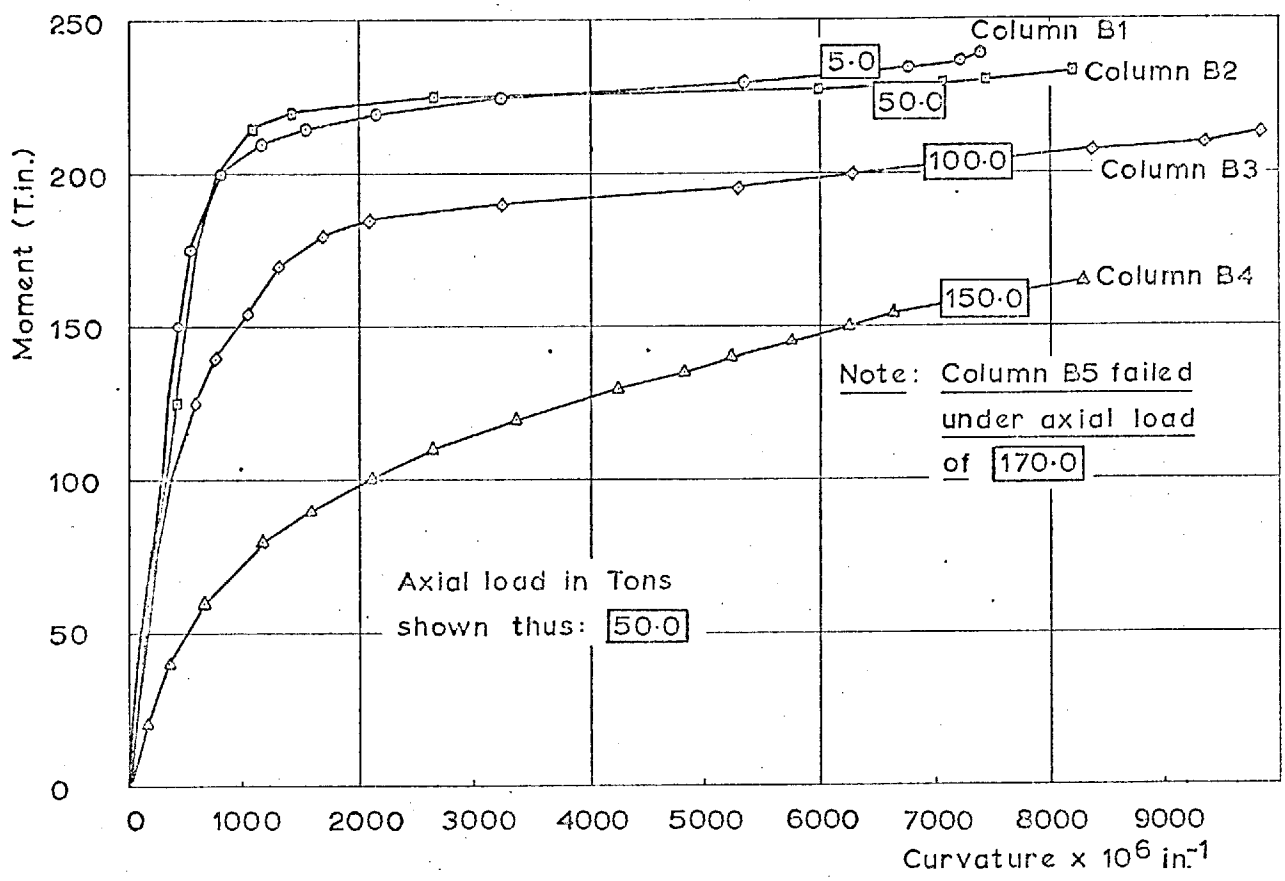

FIG. 4·5 EXPERIMENTAL MOMENT-CURVATURE RELATIONSHIP FOR SERIES B – IMPERIAL COLLEGE TESTS

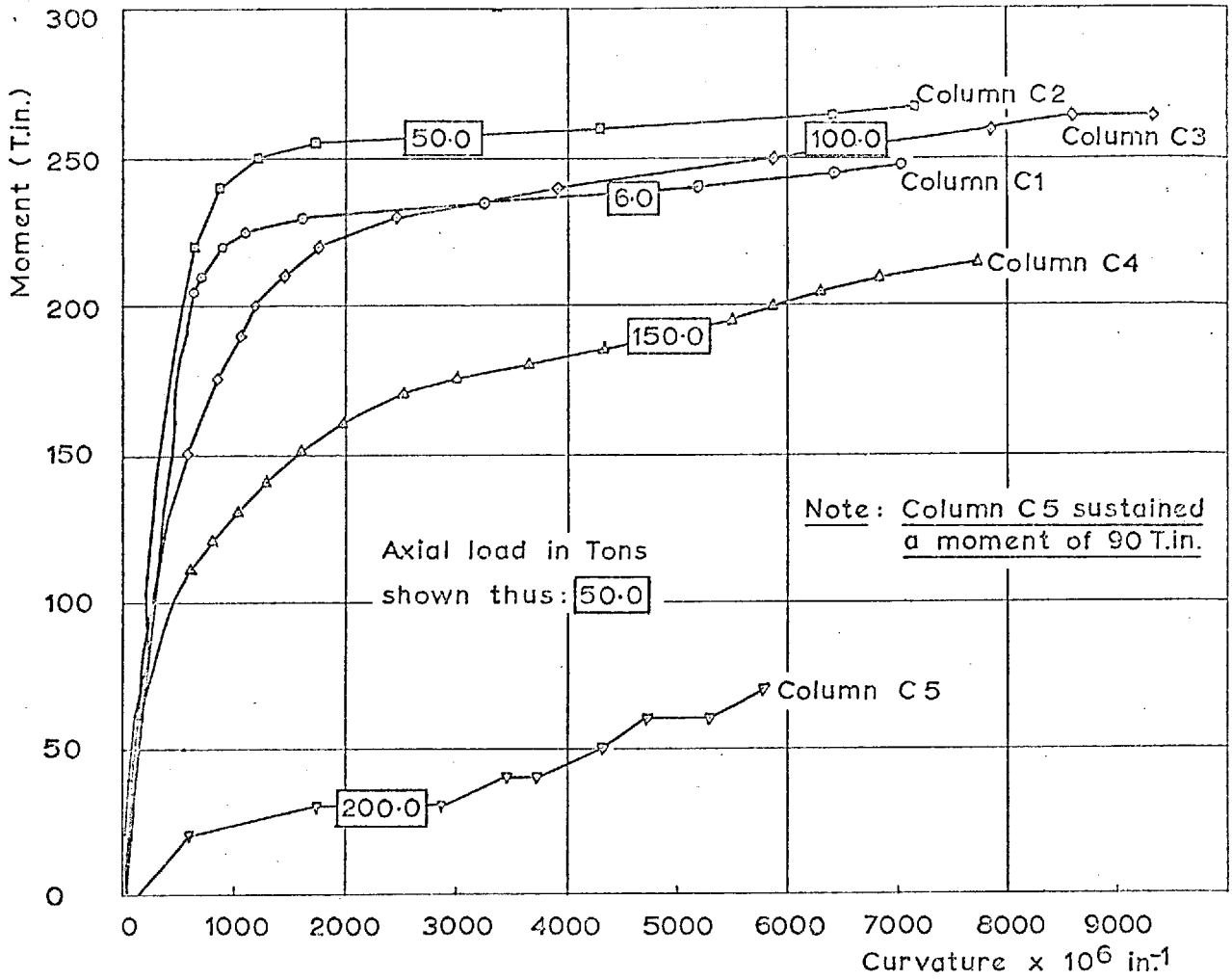

FIG. 4·6 EXPERIMENTAL MOMENT-CURVATURE RELATIONSHIP FOR SERIES C – IMPERIAL COLLEGE TESTS

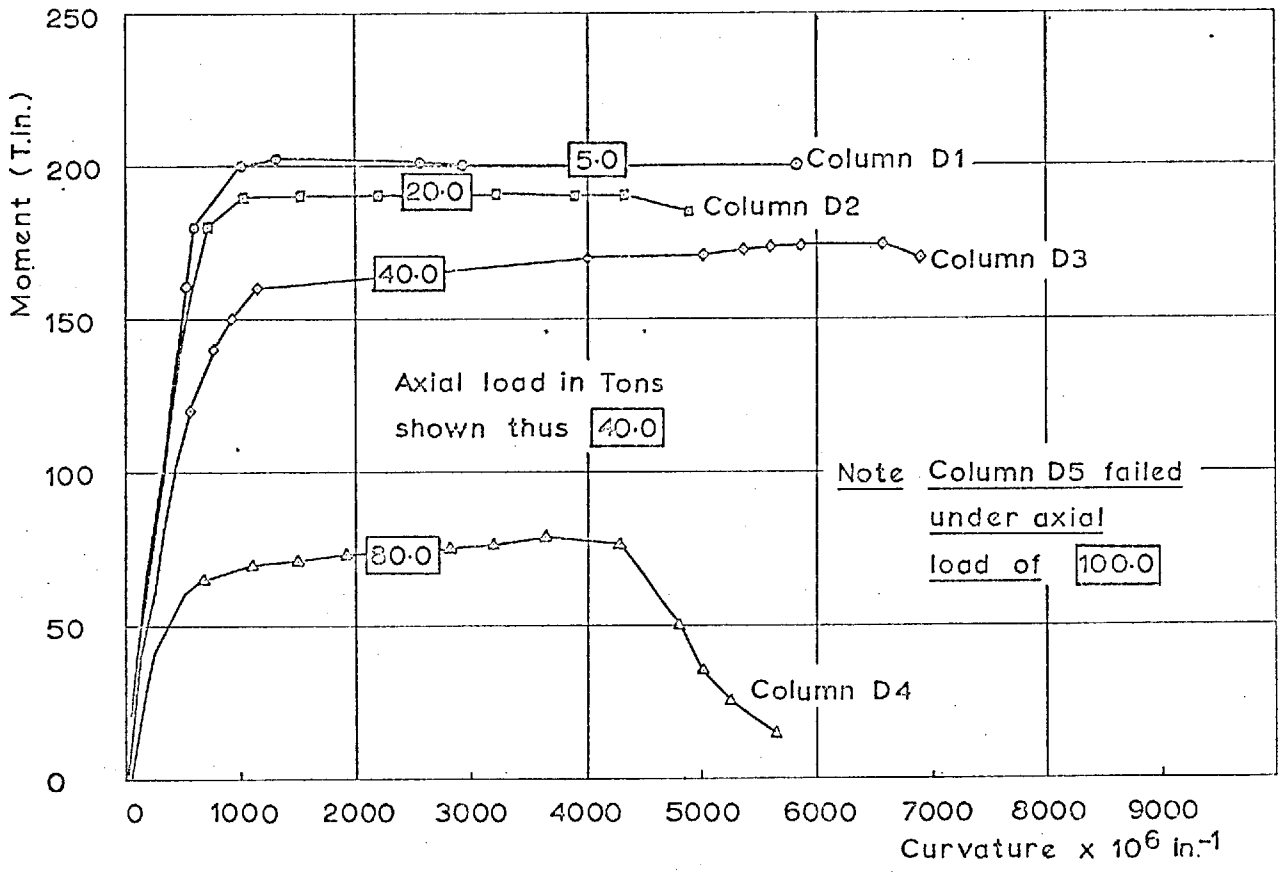

FIG. 4·7 EXPERIMENTAL MOMENT-CURVATURE RELATIONSHIP FOR SERIES D – IMPERIAL COLLEGE TESTS

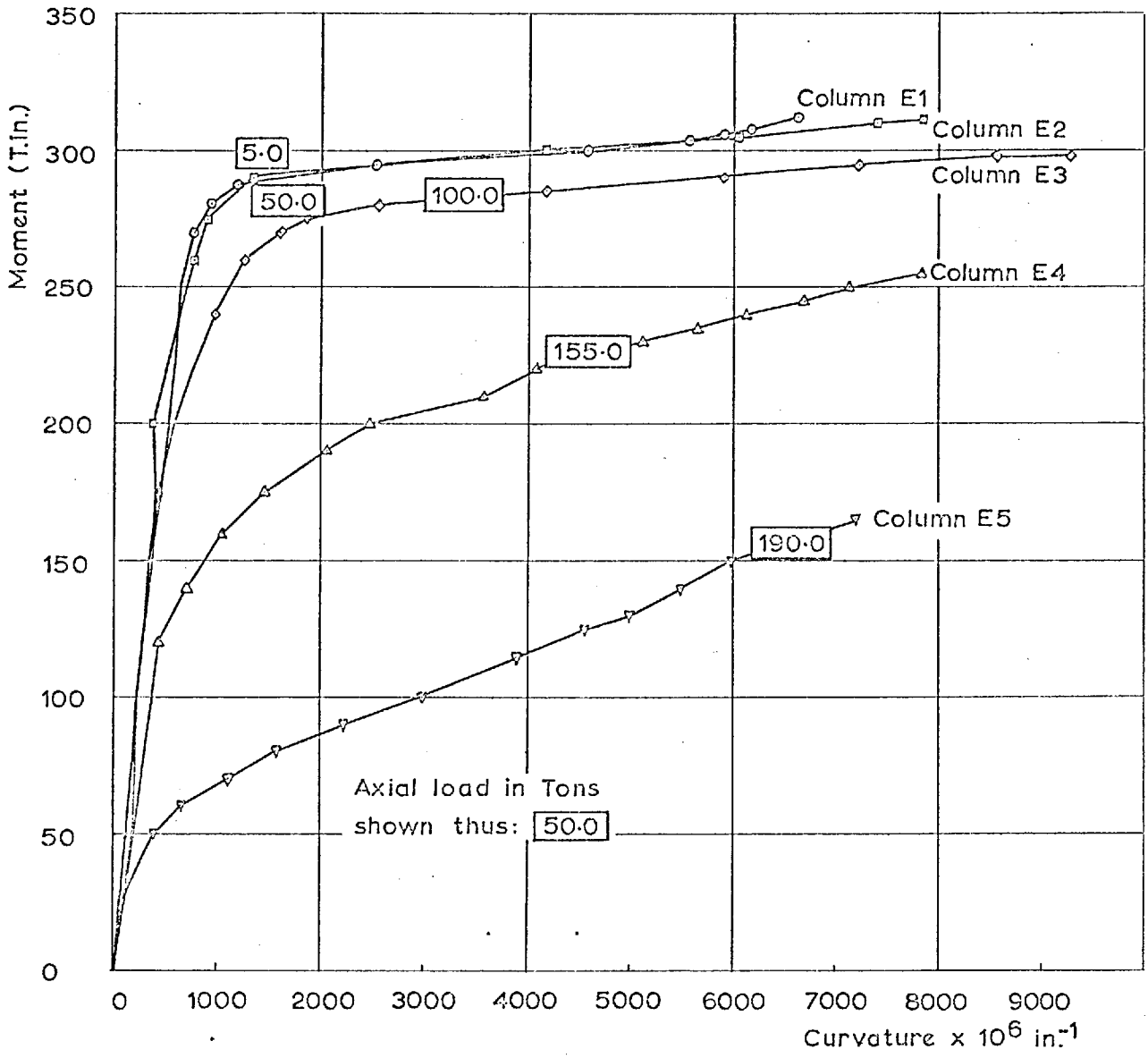

FIG .4·8 EXPERIMENTAL MOMENT-CURVATURE RELATIONSHIP FOR SERIES E — IMPERIAL COLLEGE TESTS

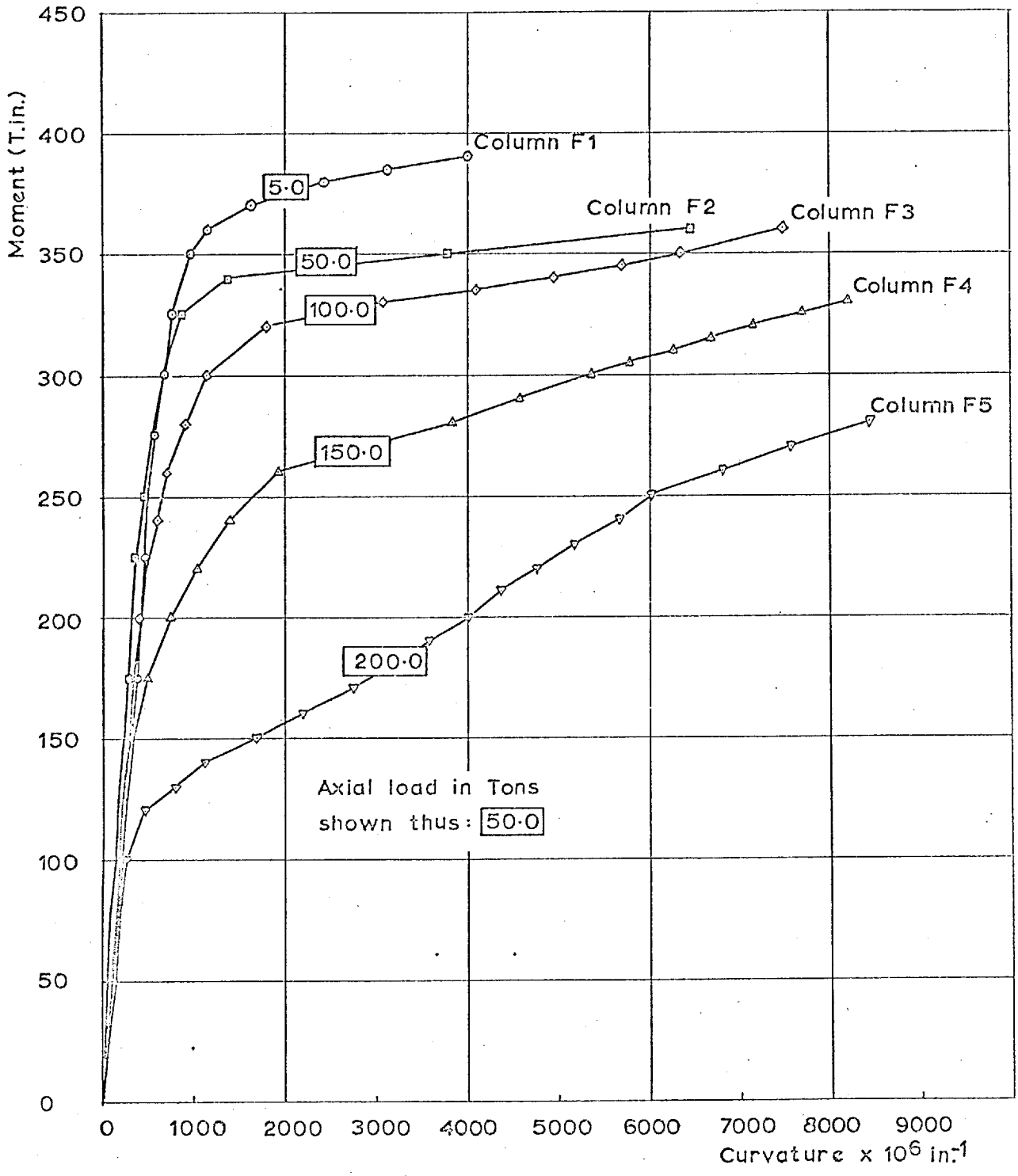

FIG. 4·9 EXPERIMENTAL MOMENT-CURVATURE RELATIONSHIP FOR SERIES F – IMPERIAL COLLEGE TESTS

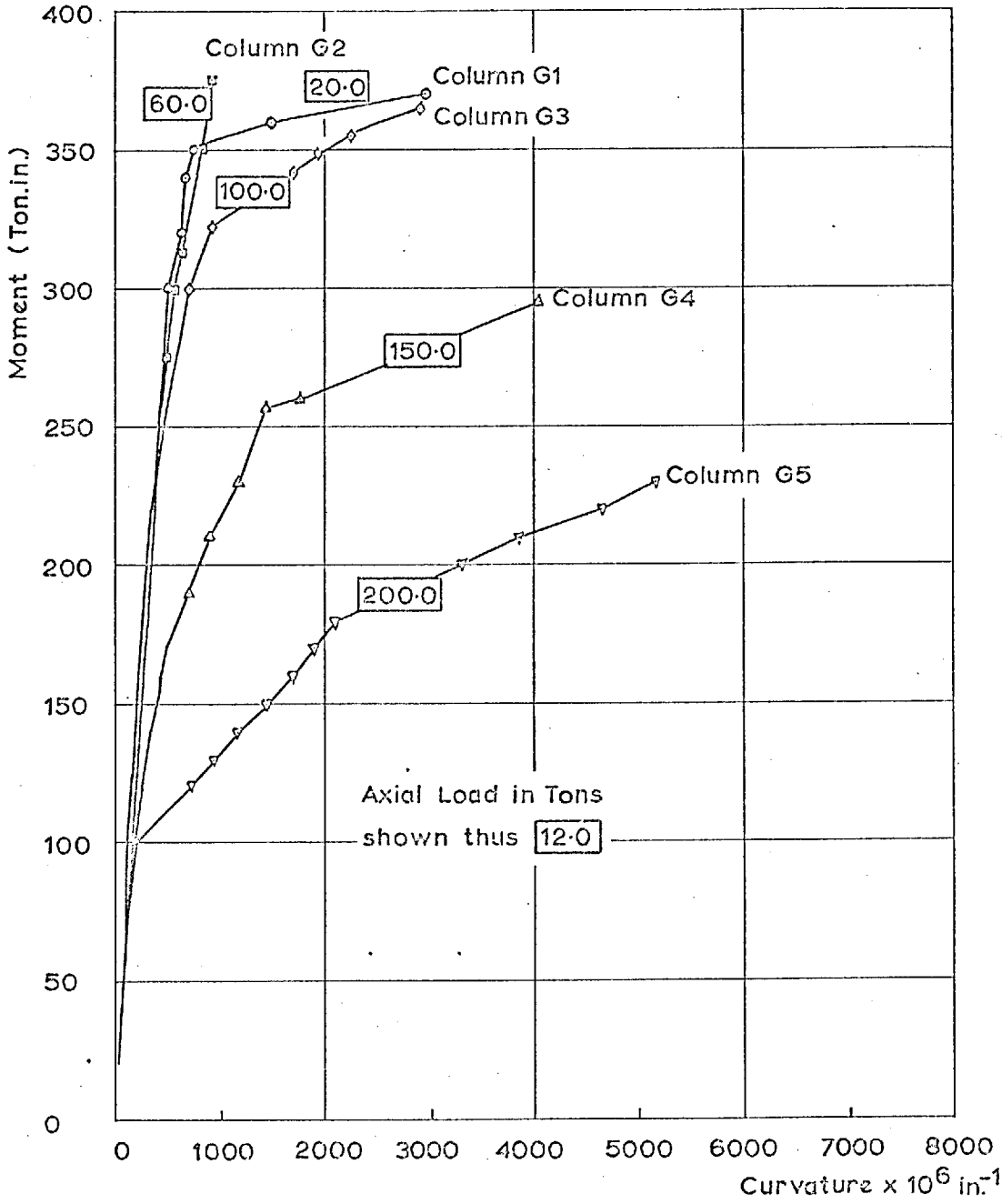

FIG. 4·10 EXPERIMENTAL MOMENT–CURVATURE RELATIONSHIP FOR SERIES G – IMPERIAL COLLEGE TESTS.

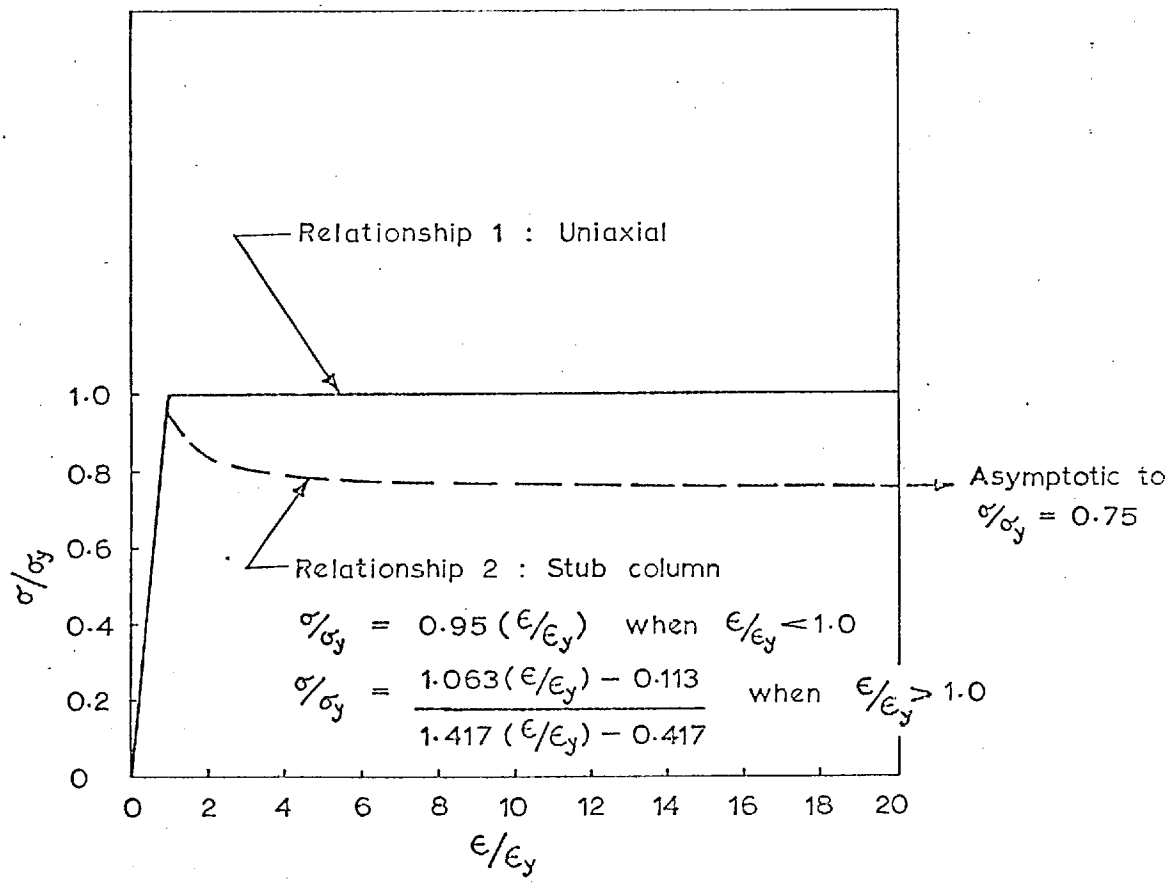

FIG. 5.1 STRESS-STRAIN RELATIONSHIPS FOR THE STEEL

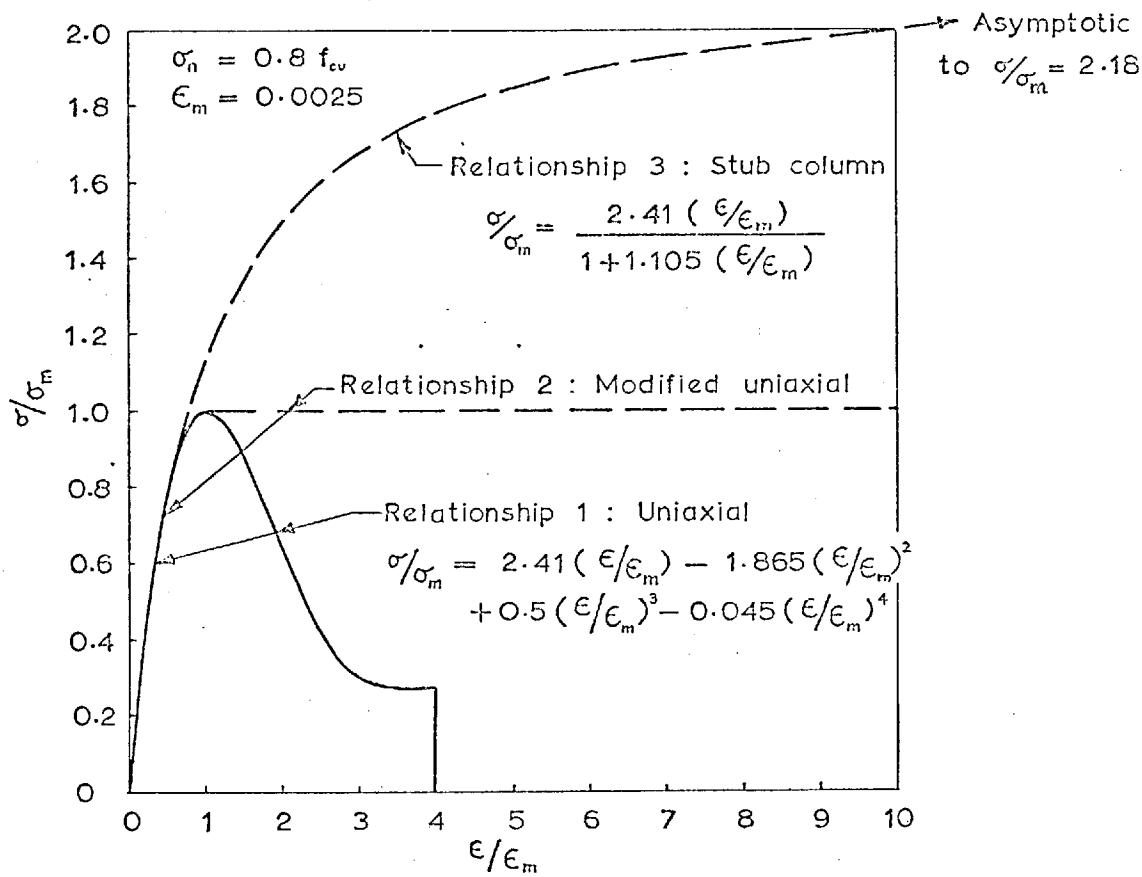

FIG. 5.2 STRESS-STRAIN RELATIONSHIPS FOR THE CONCRETE

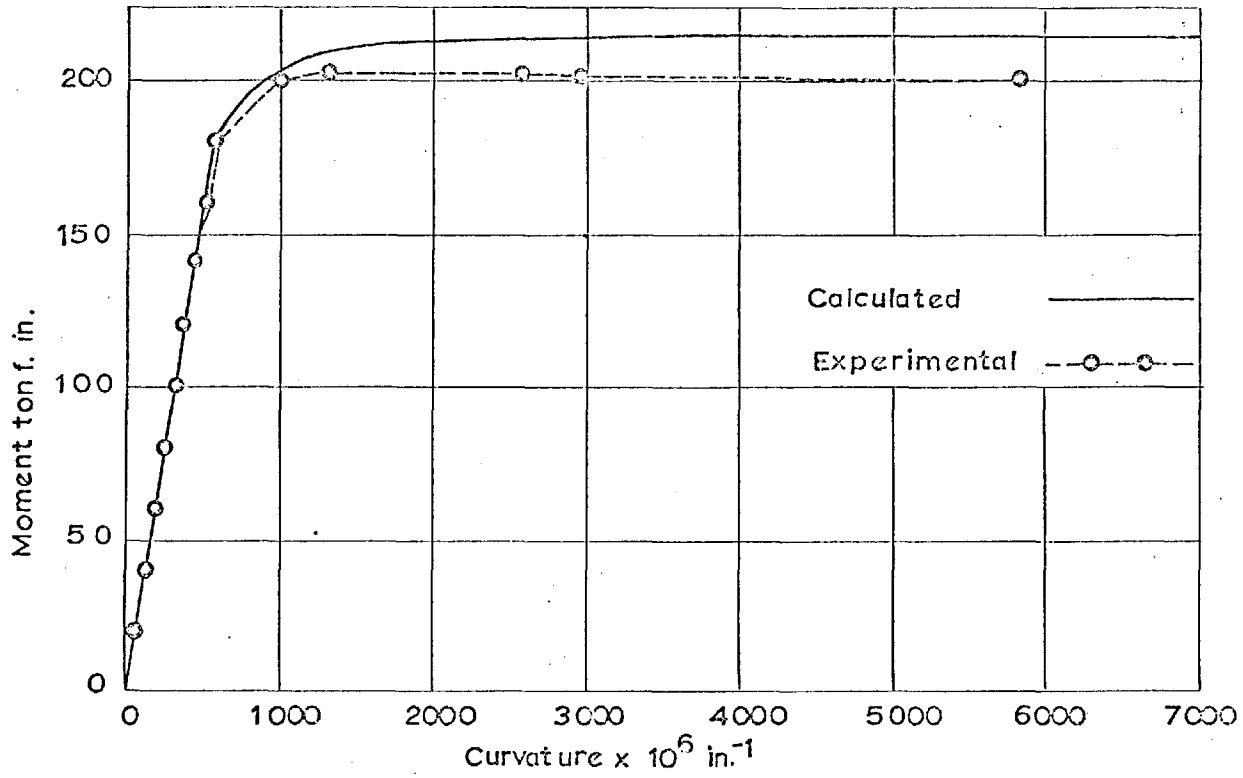

FIG. 5.3 COMPARISON BETWEEN EXPERIMENTAL AND CALCULATED MOMENT-CURVATURE RELATIONSHIP FOR COLUMN D1. (Empty tube)

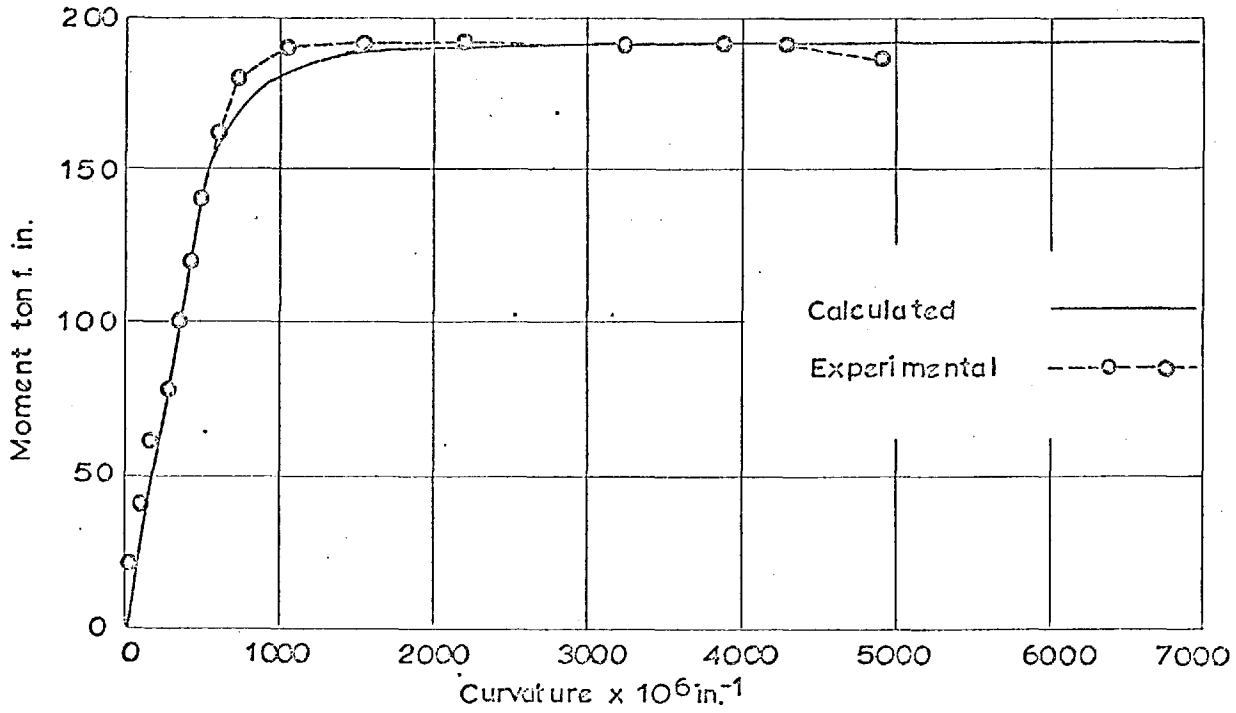

FIG. 5.4 COMPARISON BETWEEN EXPERIMENTAL AND CALCULATED MOMENT-CURVATURE RELATIONSHIP FOR COLUMN D2. (Empty tube)

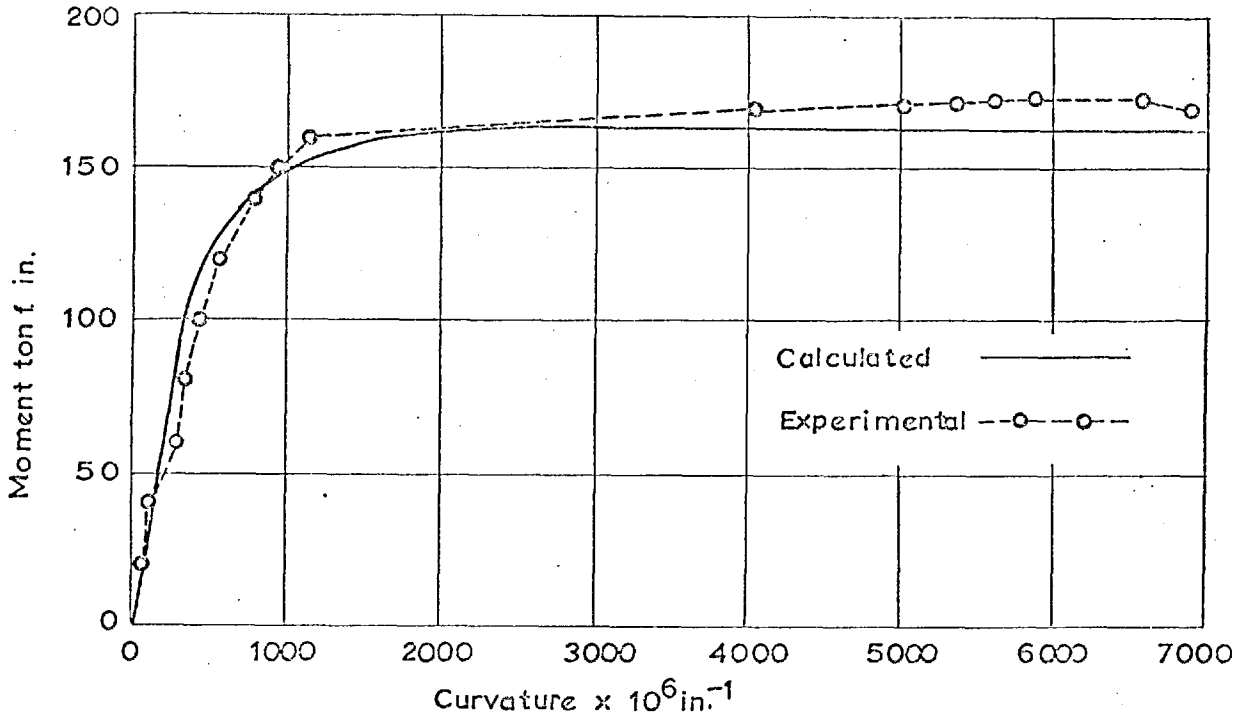

FIG. 5.5 COMPARISON BETWEEN EXPERIMENTAL AND CALCULATED MOMENT-CURVATURE RELATIONSHIP FOR COLUMN D3. (Empty tube.)

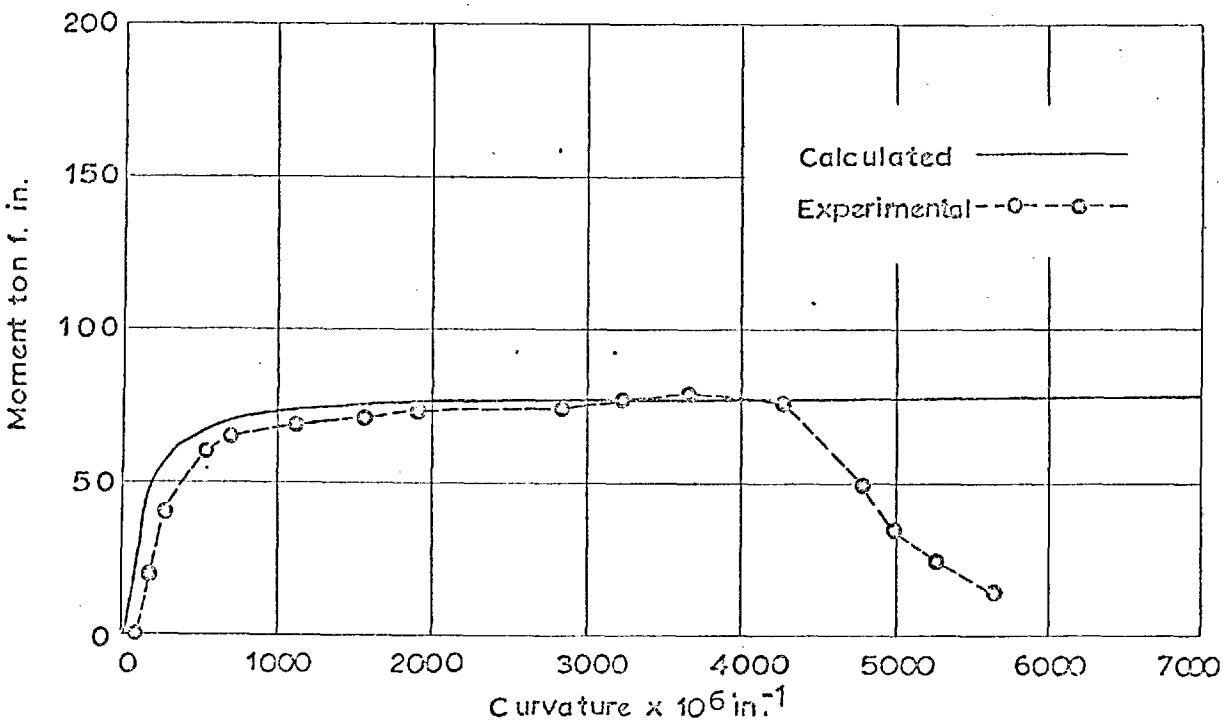

FIG. 5.6 COMPARISON BETWEEN EXPERIMENTAL AND CALCULATED MOMENT-CURVATURE RELATIONSHIP FOR COLUMN D4 (Empty tube)

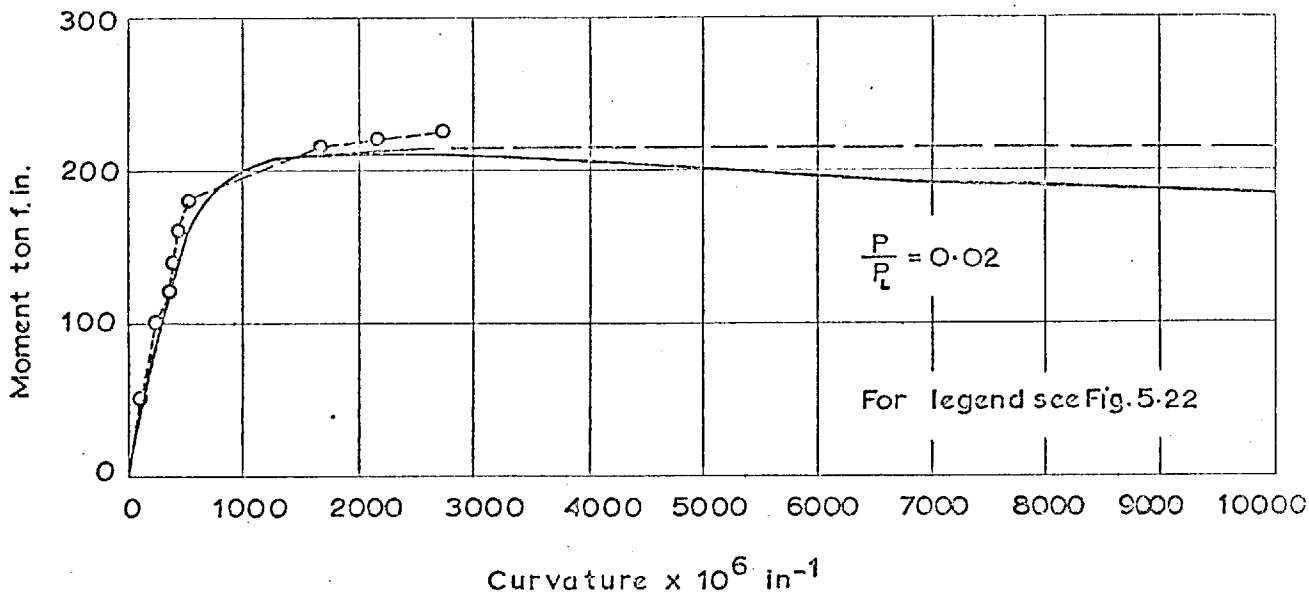

FIG. 5·7 COMPARISON BETWEEN EXPERIMENTAL AND CALCULATED MOMENT-CURVATURE RELATIONSHIPS FOR COLUMN A1.

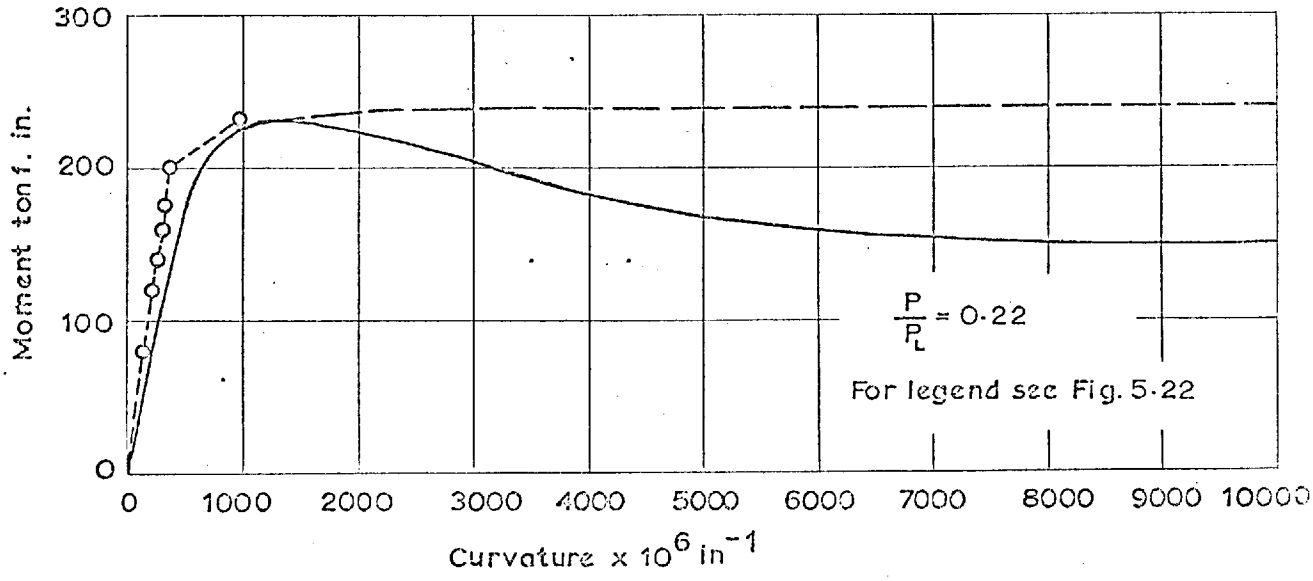

FIG. 5·8 COMPARISON BETWEEN EXPERIMENTAL AND CALCULATED MOMENT-CURVATURE RELATIONSHIPS FOR COLUMN A2.

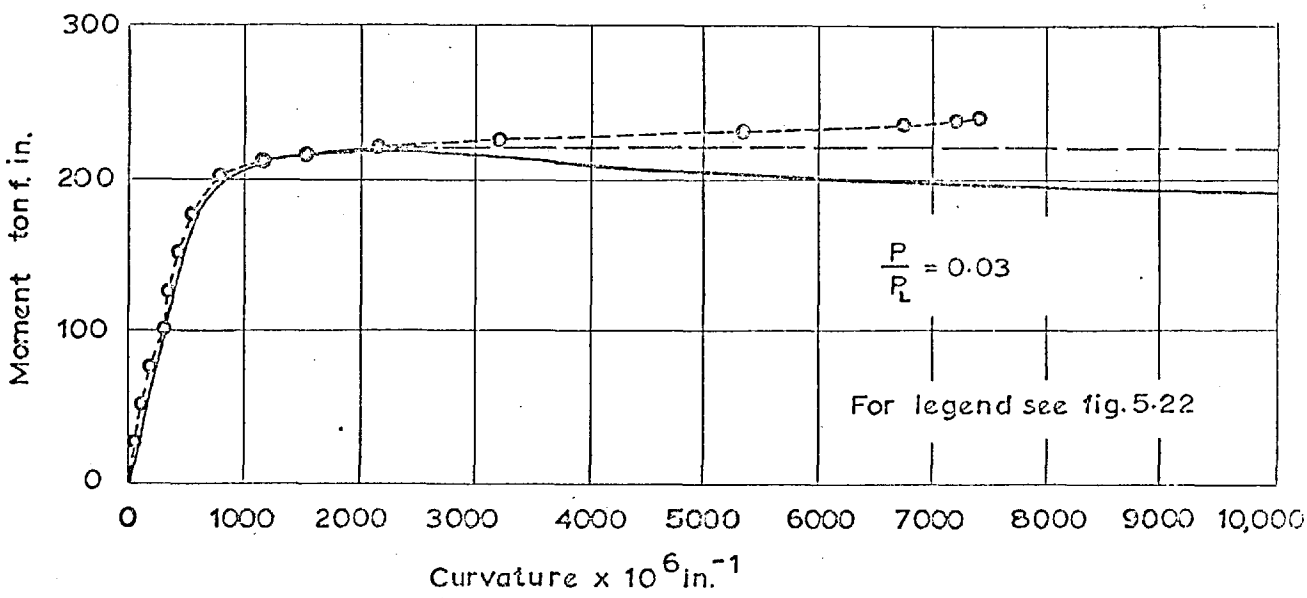

FIG. 5.9 COMPARISON BETWEEN EXPERIMENTAL AND CALCULATED MOMENT-CURVATURE RELATIONSHIPS FOR COLUMN B1.

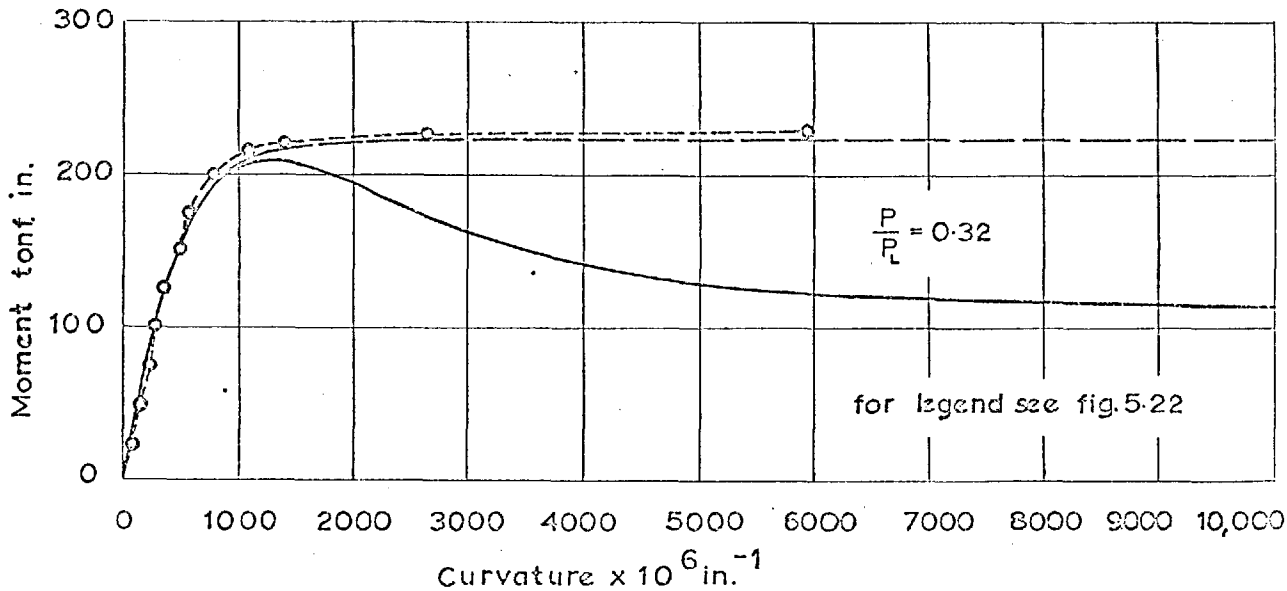

FIG. 5.10 COMPARISON BETWEEN EXPERIMENTAL AND CALCULATED MOMENT-CURVATURE RELATIONSHIPS FOR COLUMN B2.

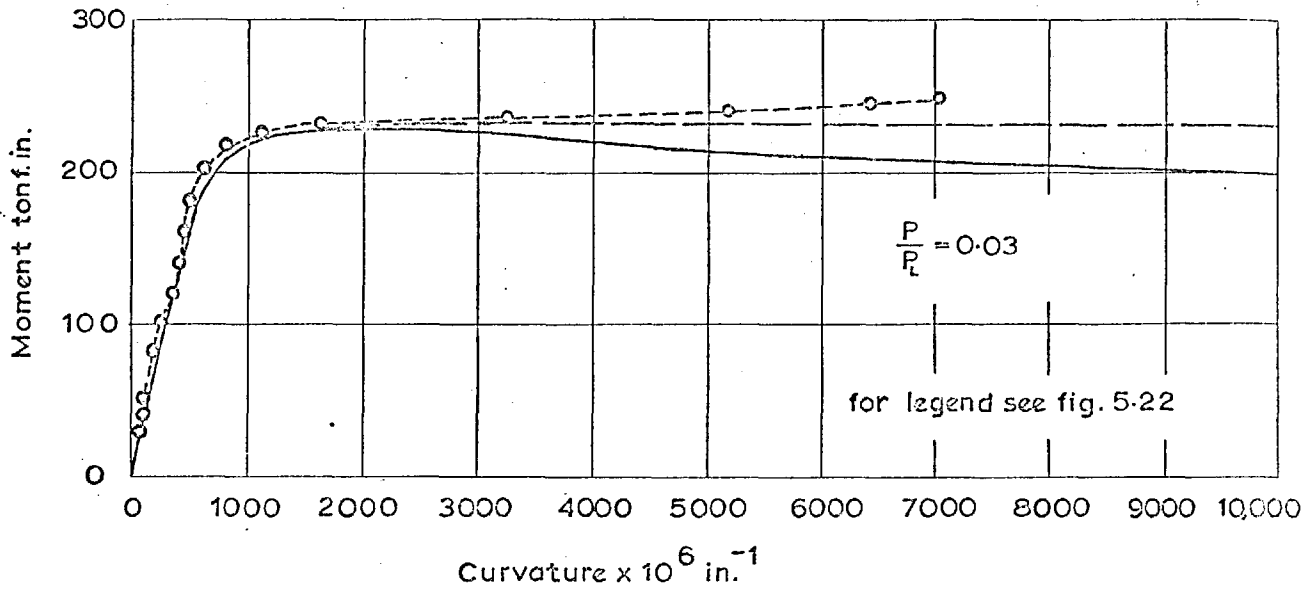

FIG. 5·11 COMPARISON BETWEEN EXPERIMENTAL AND CALCULATED MOMENT-CURVATURE RELATIONSHIPS FOR COLUMN C1.

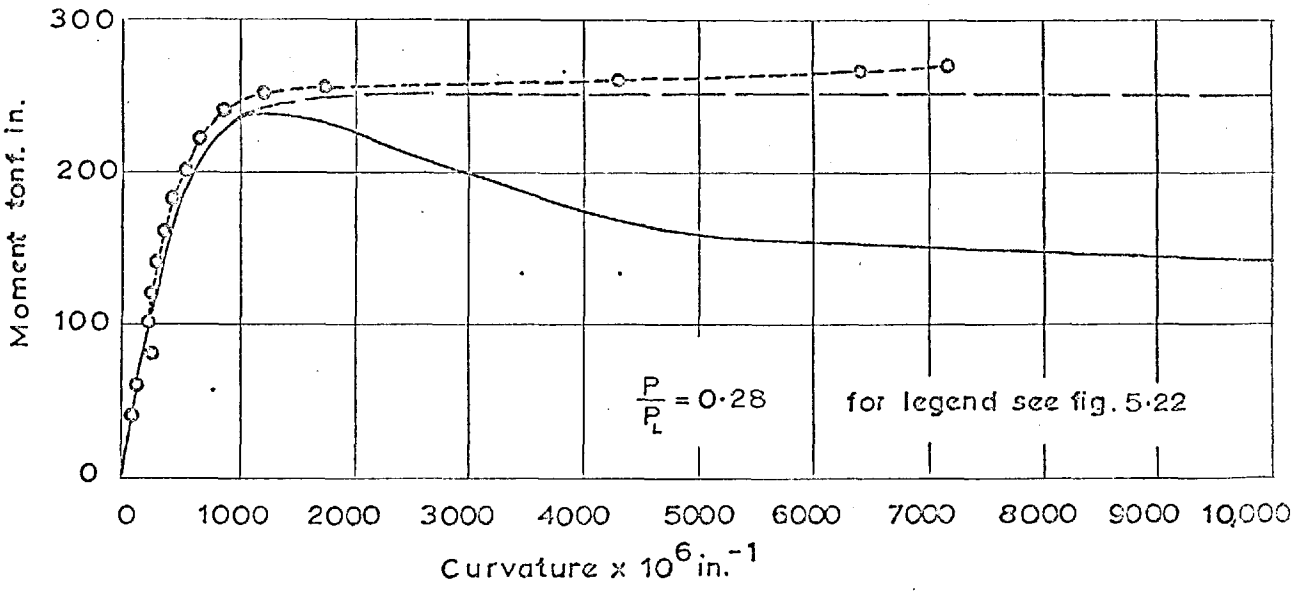

FIG. 5·12 COMPARISON BETWEEN EXPERIMENTAL AND CALCULATED MOMENT-CURVATURE RELATIONSHIPS FOR COLUMN C2.

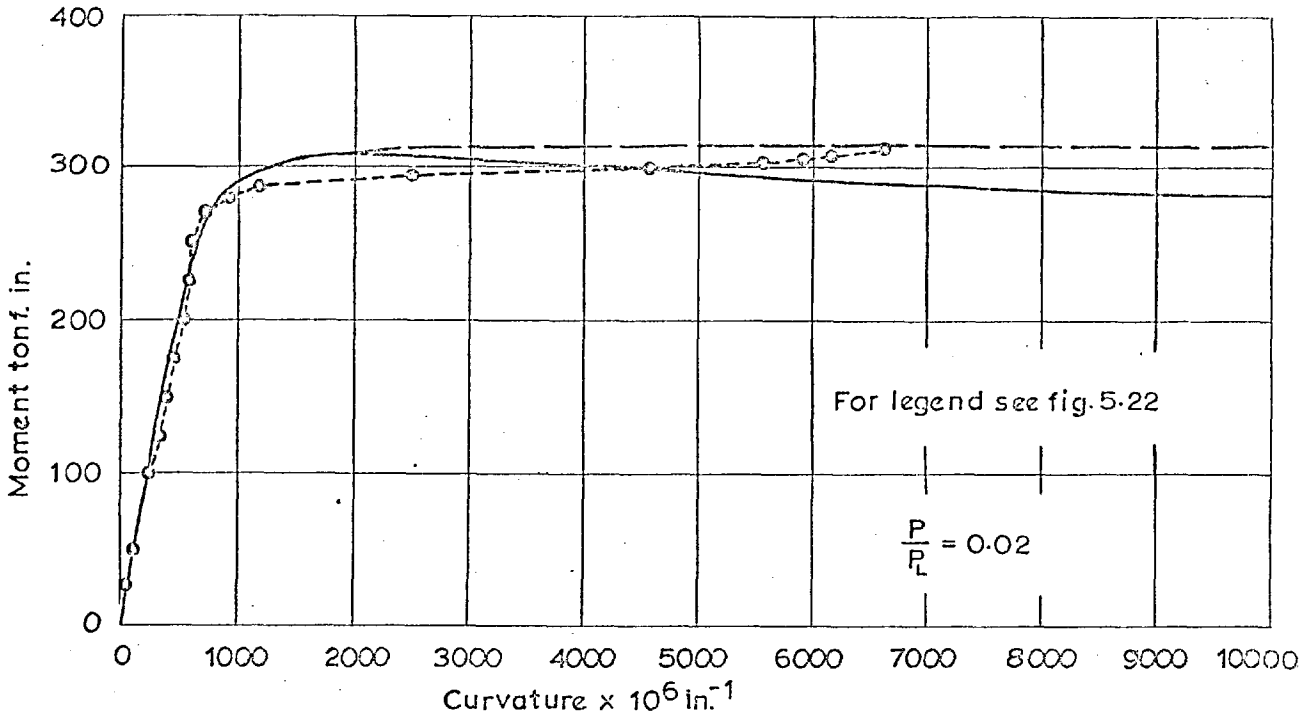

FIG. 5·13 COMPARISON BETWEEN EXPERIMENTAL AND CALCULATED MOMENT-CURVATURE RELATIONSHIPS FOR COLUMN E1.

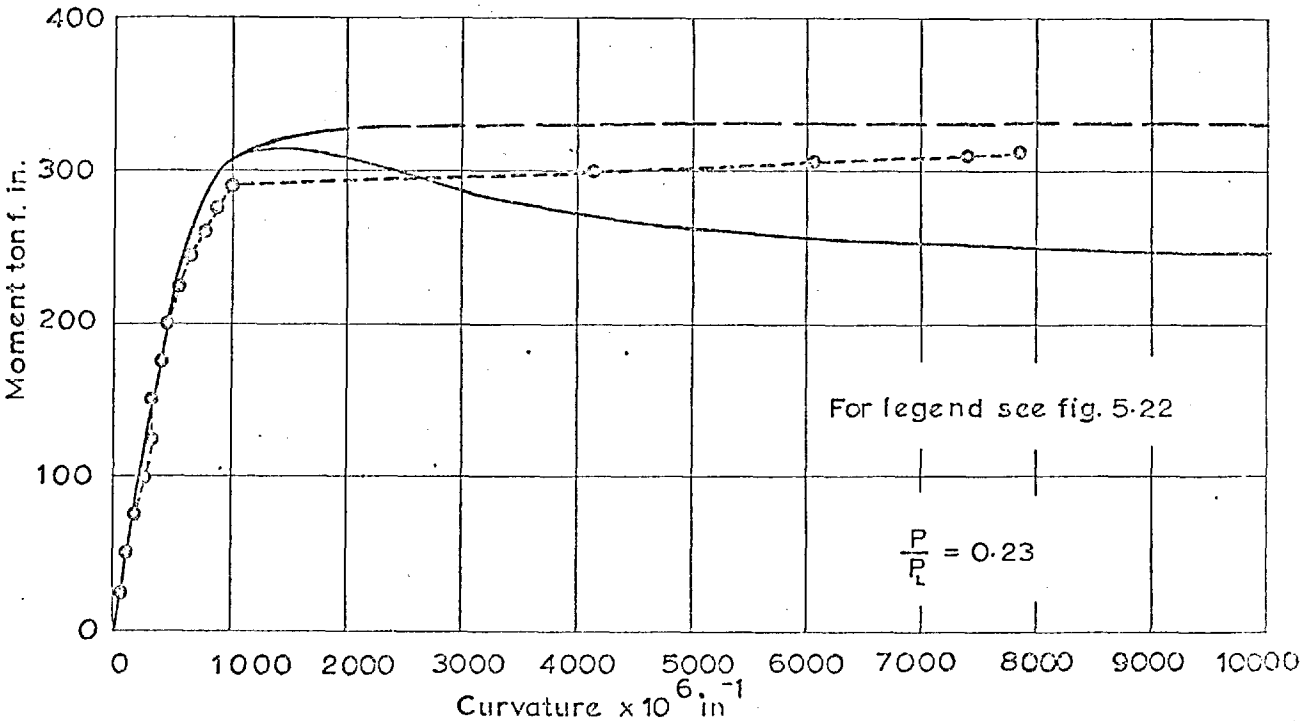

FIG. 5·14 COMPARISON BETWEEN EXPERIMENTAL AND CALCULATED MOMENT-CURVATURE RELATIONSHIP FOR COLUMN E2

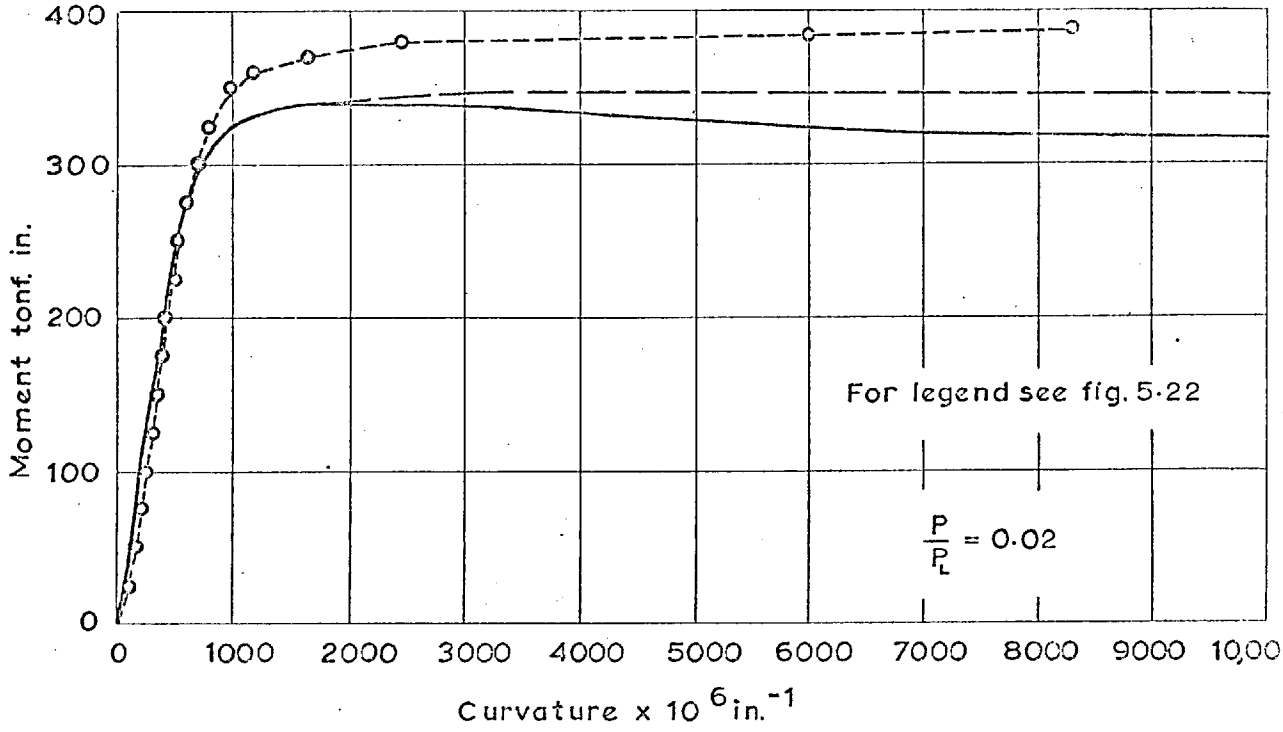

FIG. 5·15 COMPARISON BETWEEN EXPERIMENTAL AND CALCULATED MOMENT-CURVATURE RELATIONSHIPS FOR COLUMN F1.

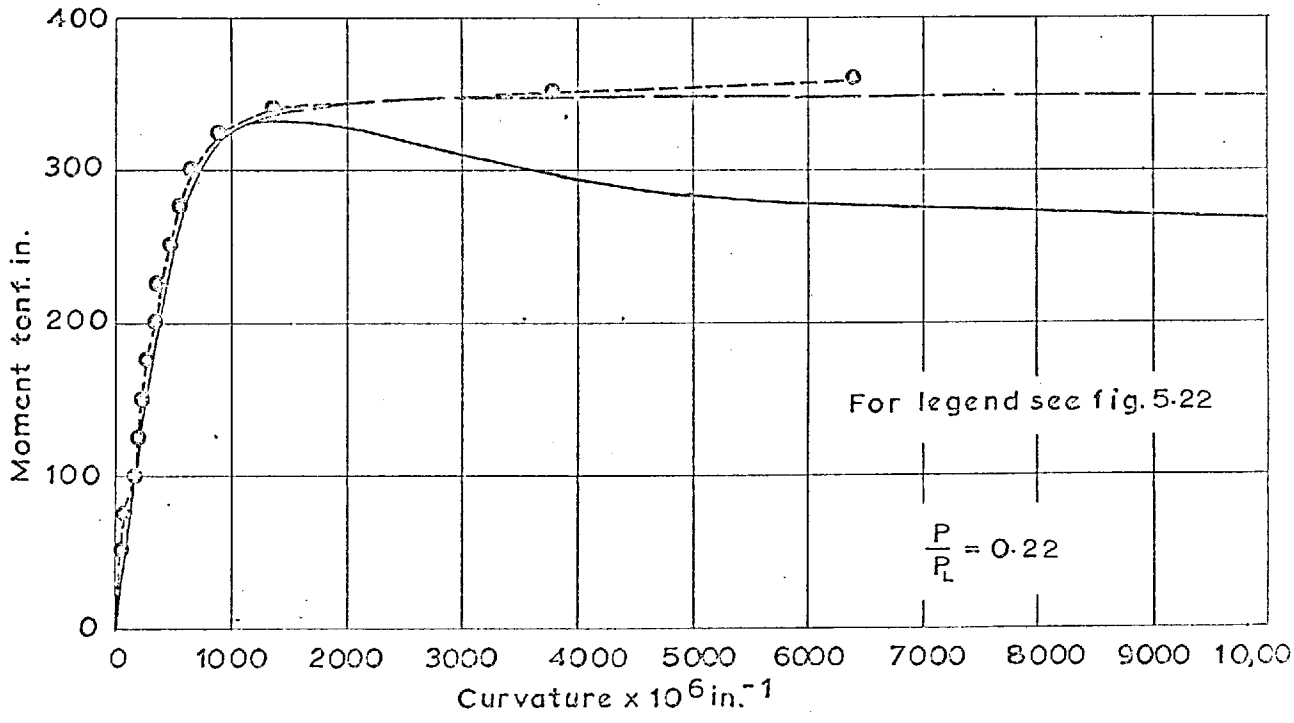

FIG. 5·16 COMPARISON BETWEEN EXPERIMENTAL AND CALCULATED MOMENT-CURVATURE RELATIONSHIPS FOR COLUMN F2.

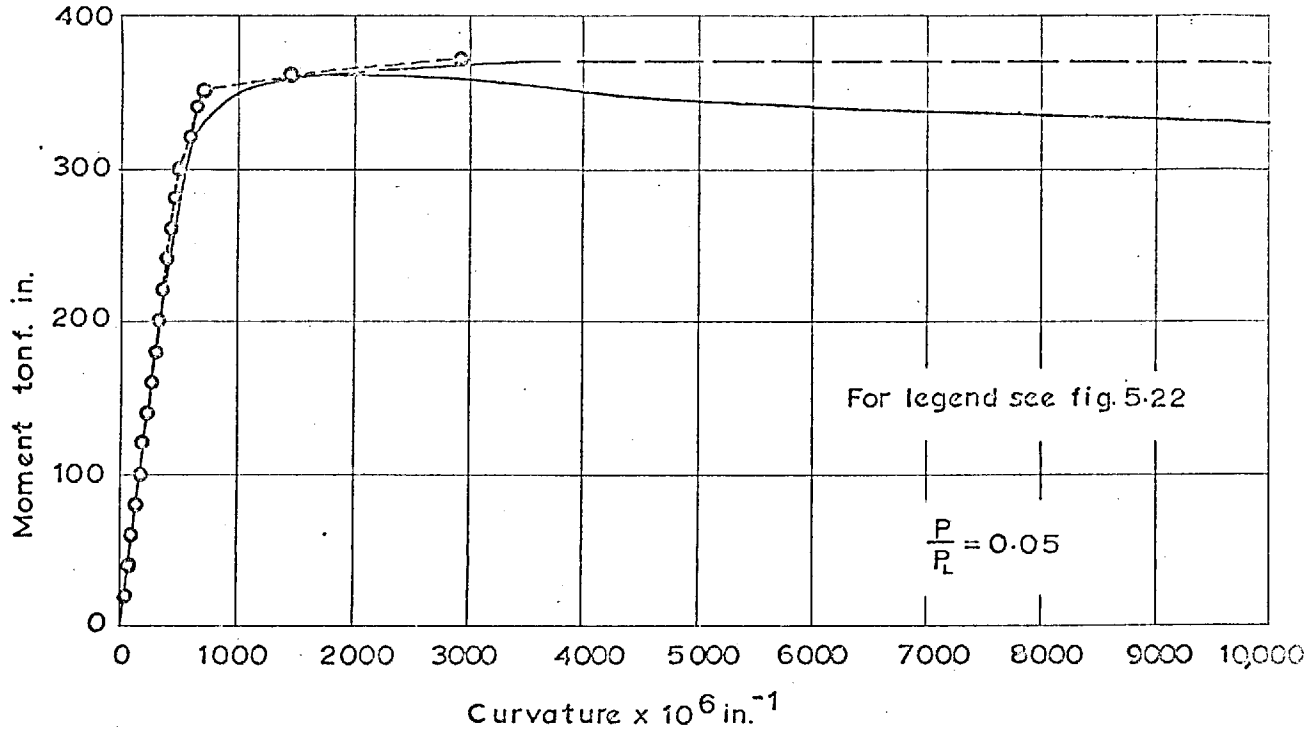

FIG. 5.17 COMPARISON BETWEEN EXPERIMENTAL AND CALCULATED MOMENT - CURVATURE RELATIONSHIPS FOR COLUMN G1.

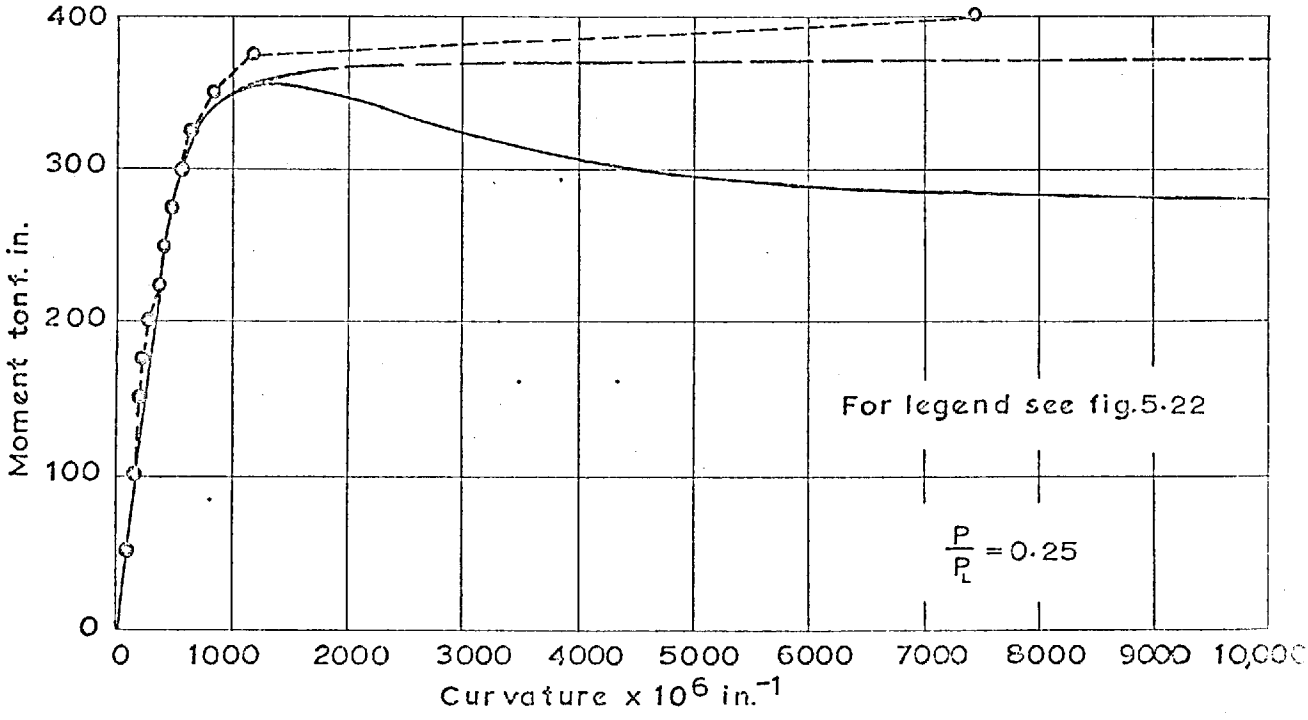

FIG. 5.18 COMPARISON BETWEEN EXPERIMENTAL AND CALCULATED MOMENT-CURVATURE RELATIONSHIPS FOR COLUMN G2.

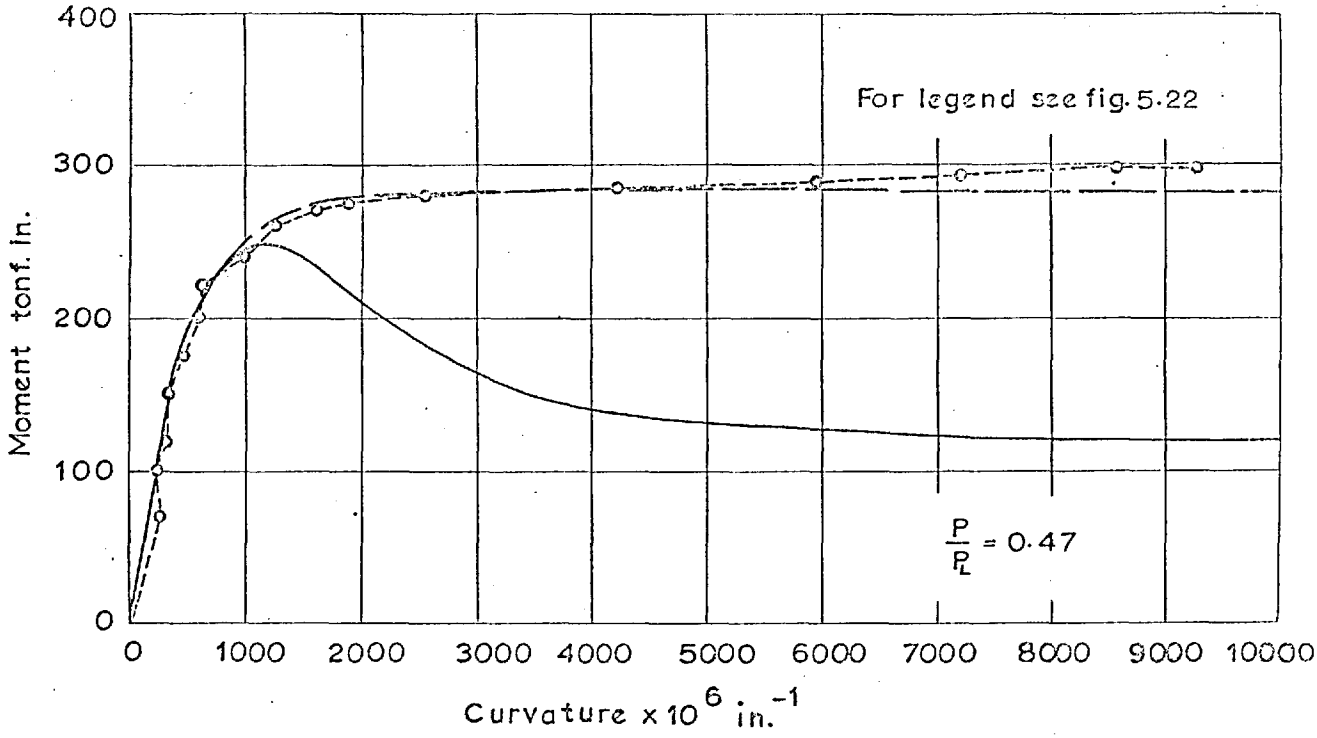

FIG. 5-19 COMPARISON BETWEEN EXPERIMENTAL AND CALCULATED MOMENT-CURVATURE RELATIONSHIPS FOR COLUMN E3

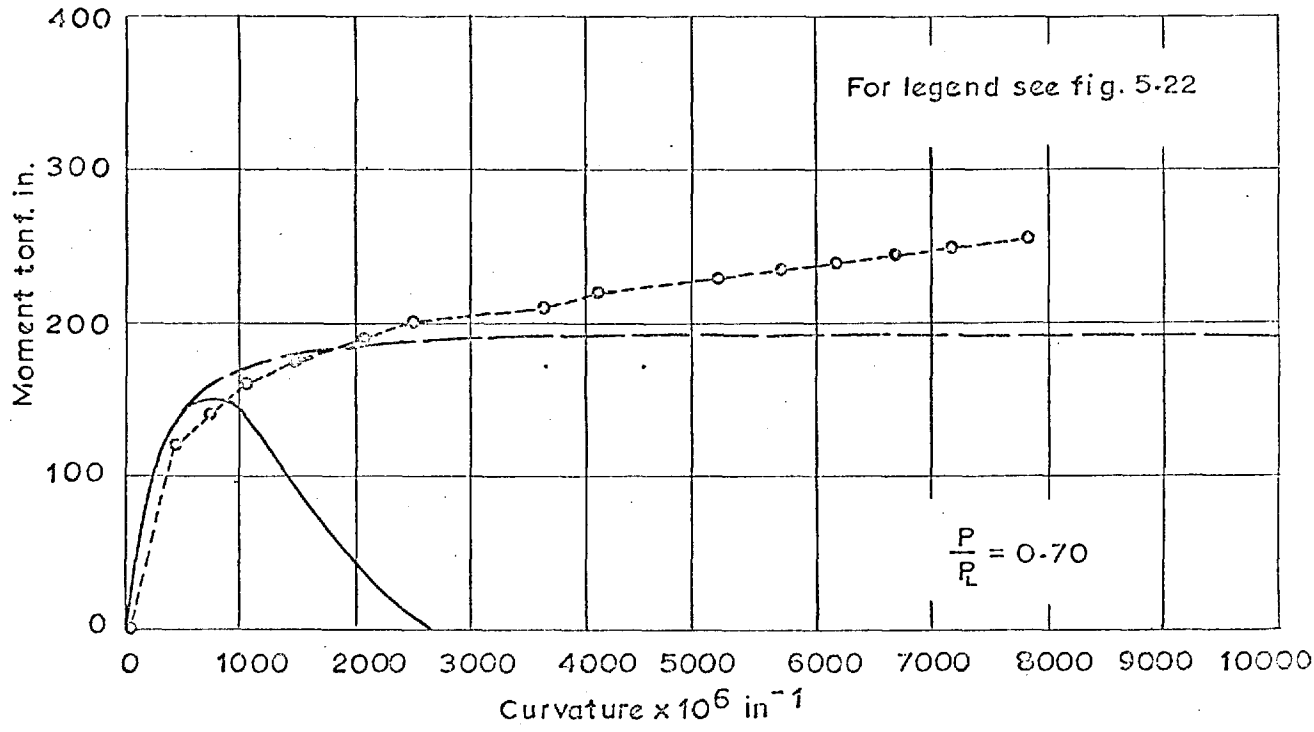

FIG. 5-20 COMPARISON BETWEEN EXPERIMENTAL AND CALCULATED MOMENT-CURVATURE RELATIONSHIPS FOR COLUMN E4.

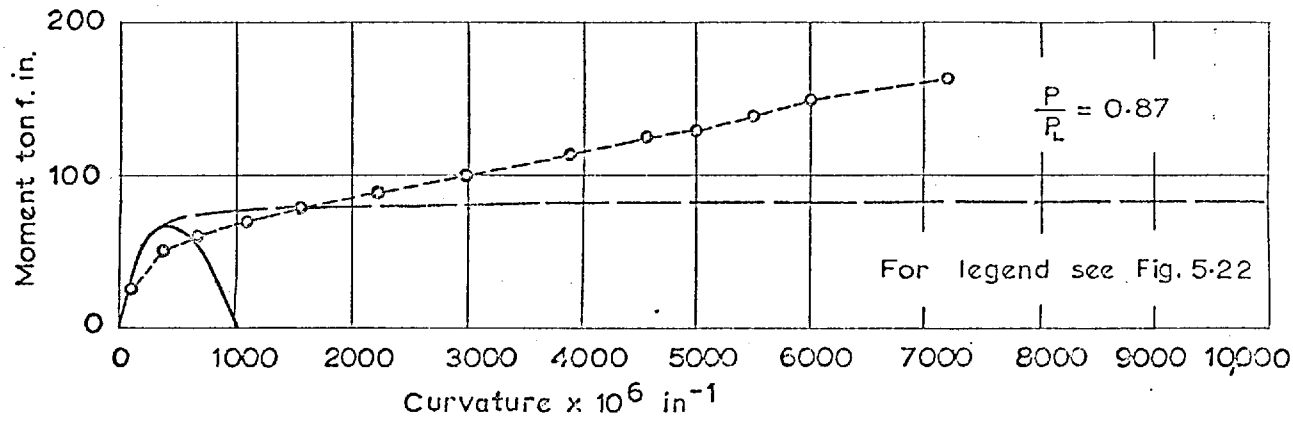

FIG. 5·21 COMPARISON BETWEEN EXPERIMENTAL AND CALCULATED MOMENT-CURVATURE RELATIONSHIPS FOR COLUMN E5.

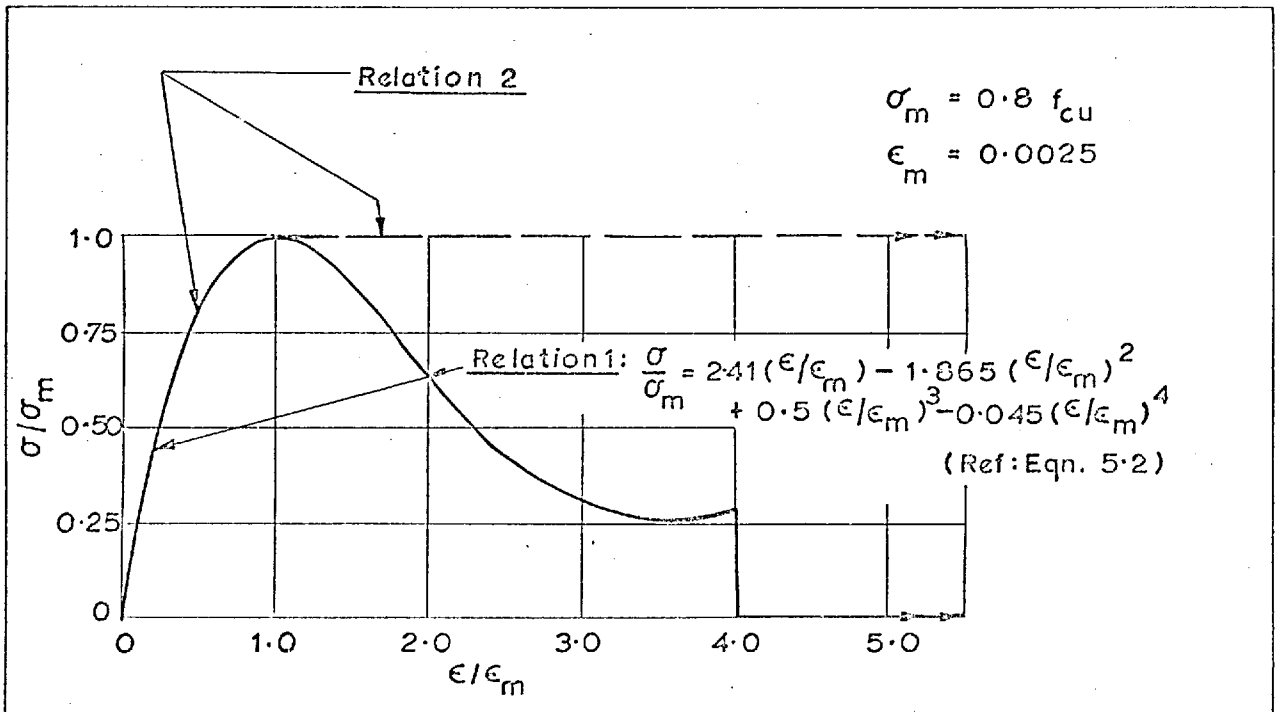

ASSUMED STRESS-STRAIN RELATIONSHIPS FOR CONCRETE.

Legend:

——— Moment-curvature relationship calculated from concrete stress-strain relation 1 (shown above) and a trapezoidal stress strain relation for steel.

— — — Same as above, except that stress-strain relation 2 is used for concrete.

-----o----- Experimental moment-curvature relationship.

FIG. 5·22. LEGEND USED IN FIGURES 5·7 TO 5·21

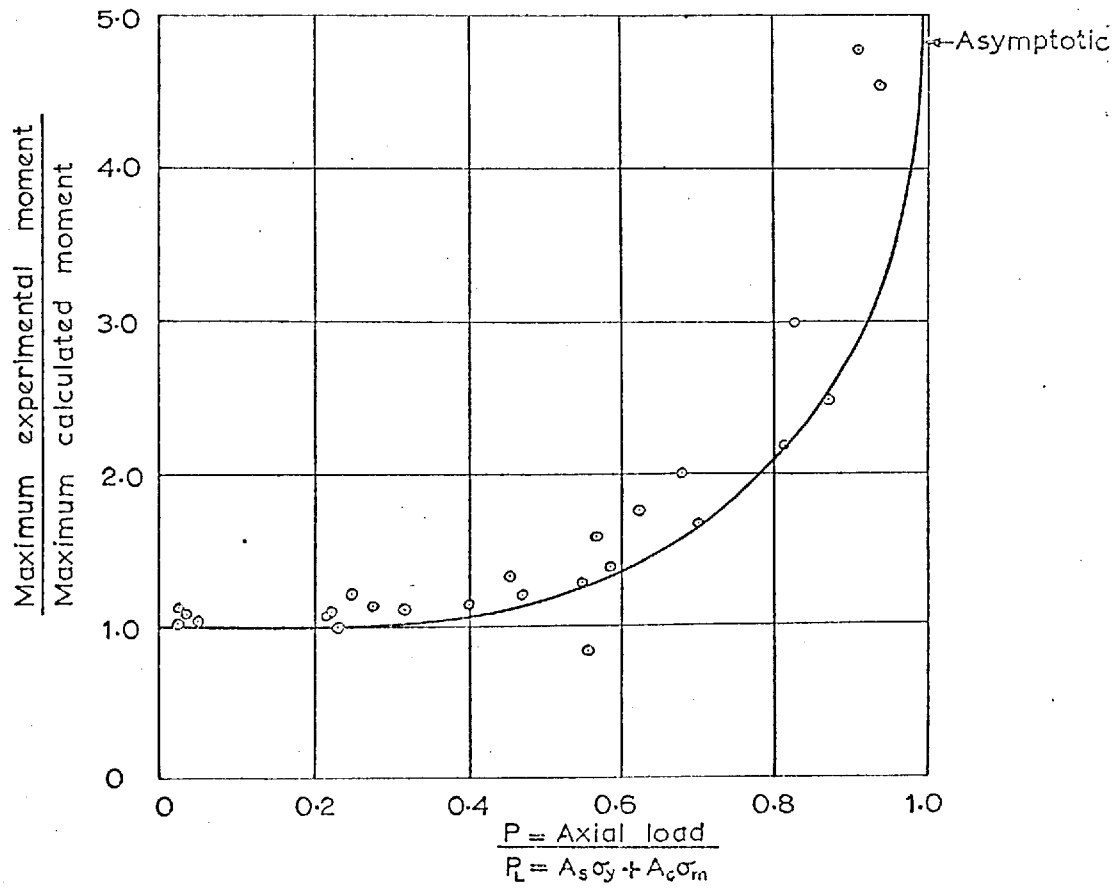

FIG. 5·23 COMPARISON BETWEEN TEST AND UNIAXIAL MOMENTS — IMPERIAL COLLEGE TESTS

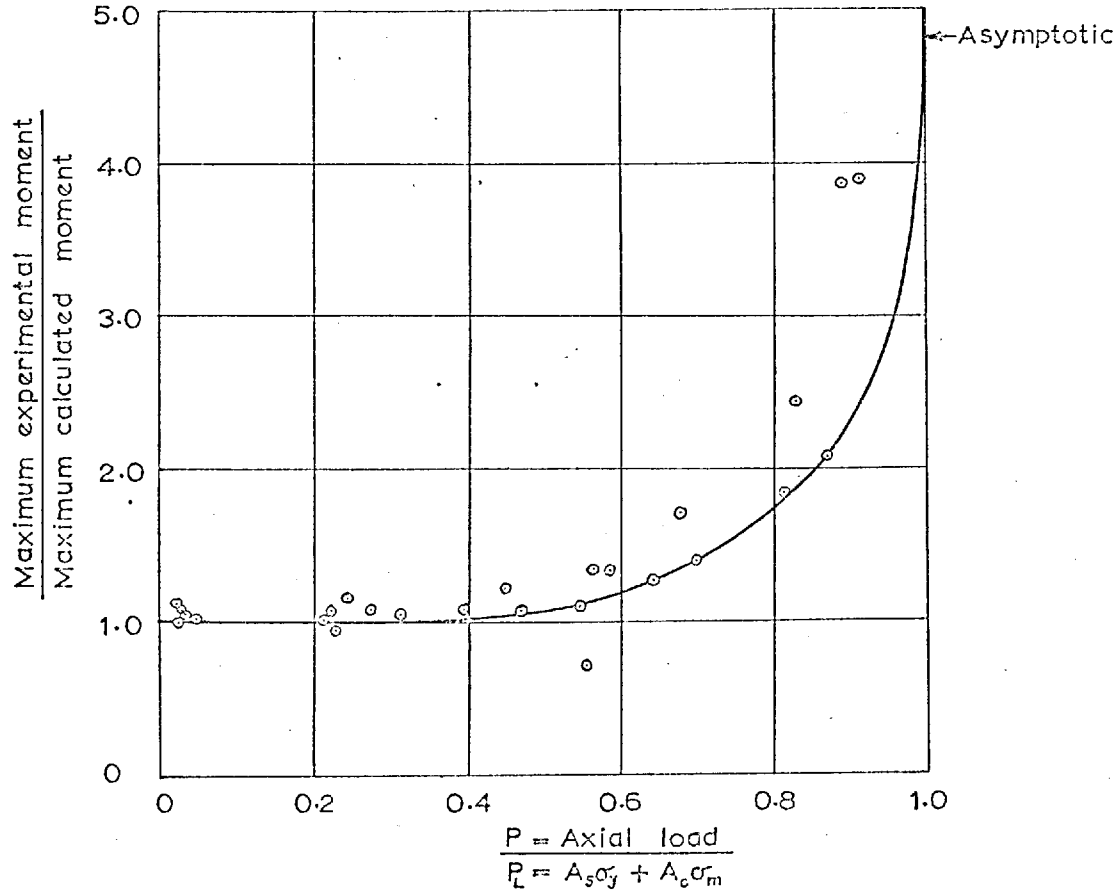

FIG. 5·24 COMPARISON BETWEEN TEST AND MODIFIED UNIAXIAL MOMENTS - IMPERIAL COLLEGE TESTS

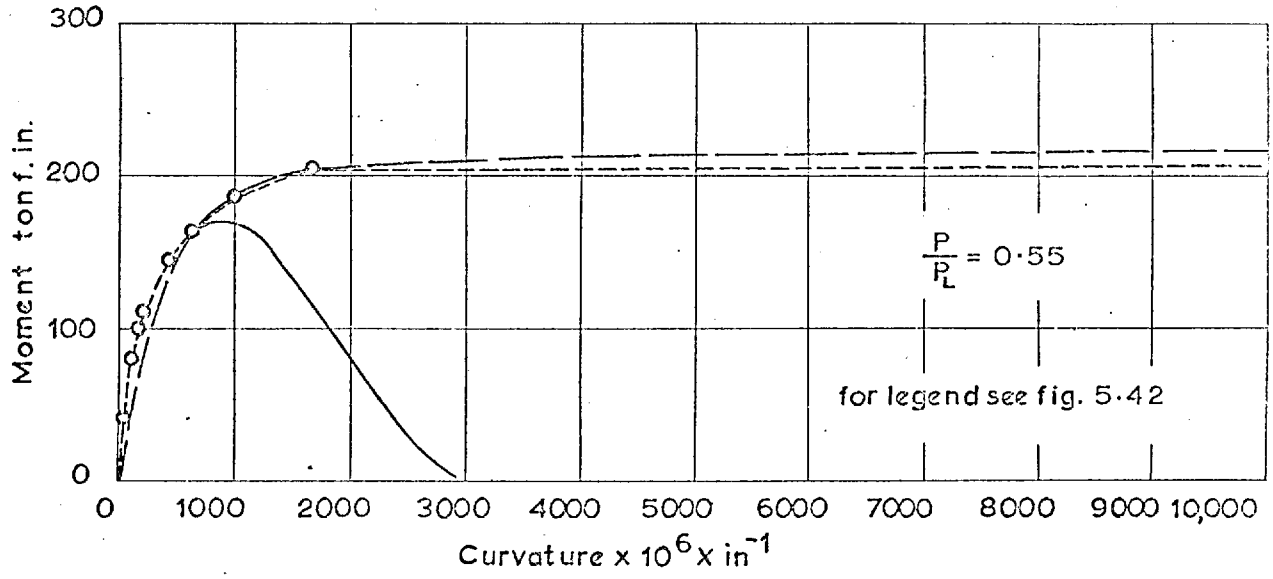

FIG.5·25 COMPARISON BETWEEN EXPERIMENTAL AND CALCULATED MOMENT-CURVATURE RELATIONSHIPS FOR COLUMN A3

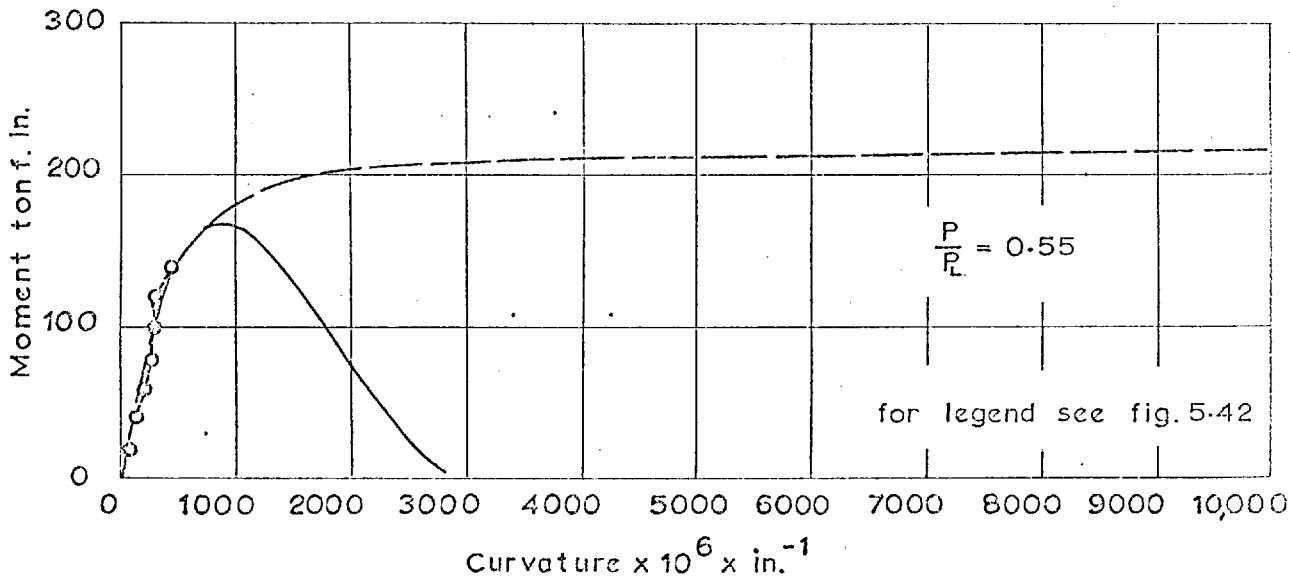

FIG.5·26 COMPARISON BETWEEN EXPERIMENTAL AND CALCULATED MOMENT-CURVATURE RELATIONSHIPS FOR COLUMN A4

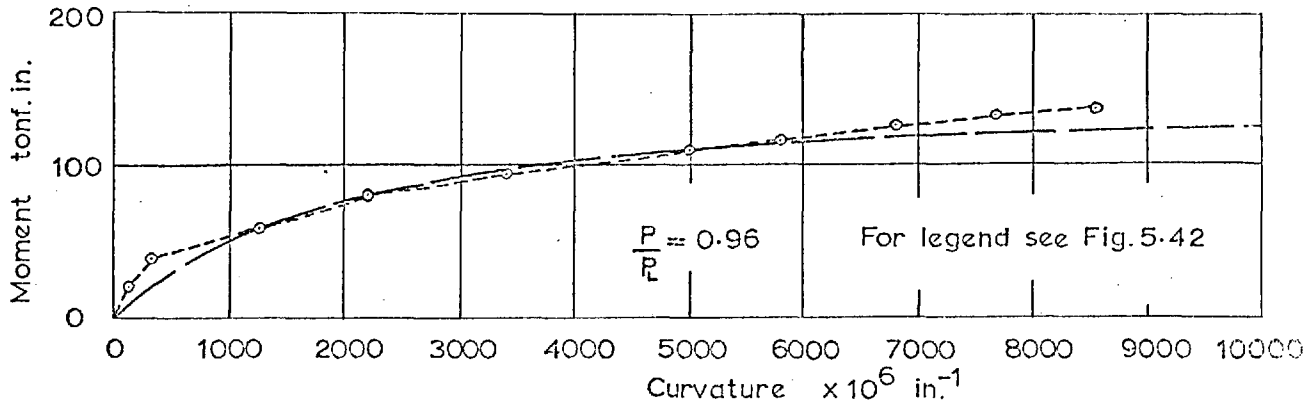

FIG. 5.27 COMPARISON BETWEEN EXPERIMENTAL AND CALCULATED MOMENT-CURVATURE RELATIONSHIPS FOR COLUMN A5

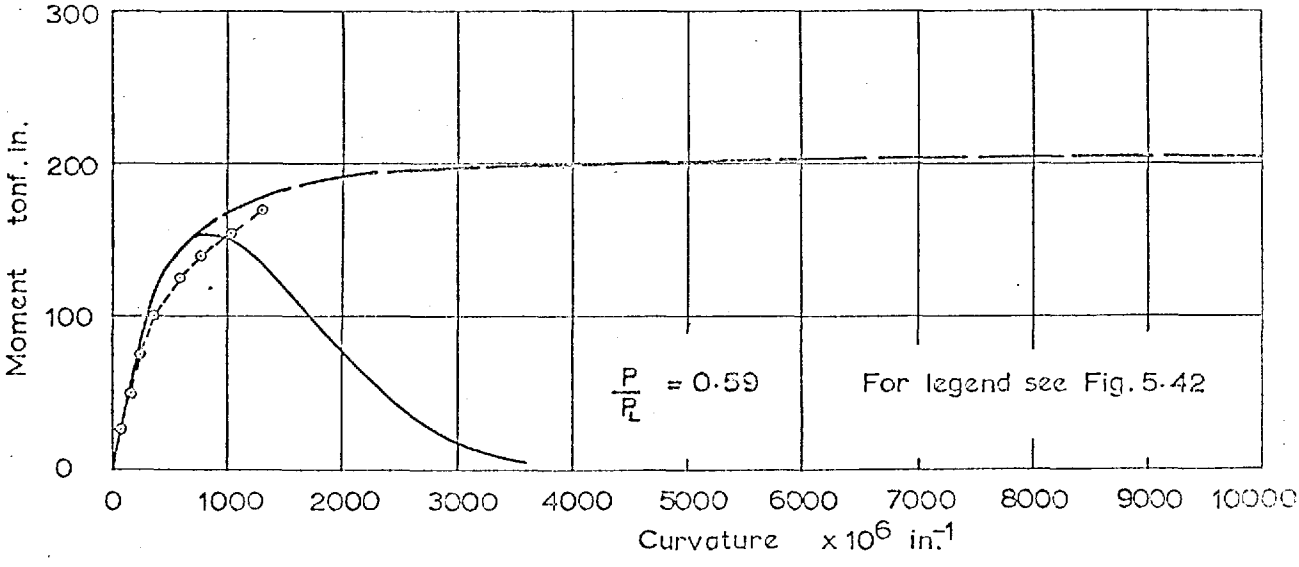

FIG. 5.28 COMPARISON BETWEEN EXPERIMENTAL AND CALCULATED MOMENT-CURVATURE RELATIONSHIPS FOR COLUMN B3

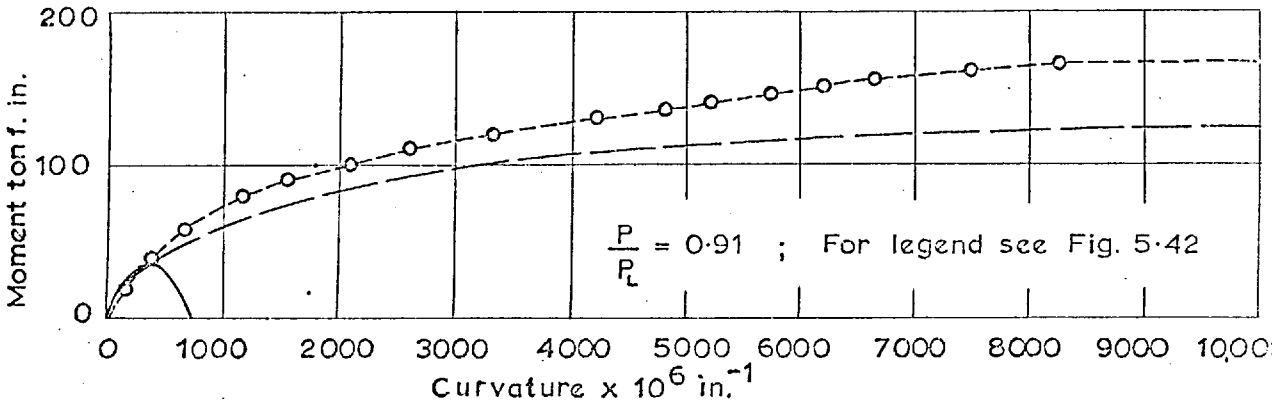

FIG. 5·29 COMPARISON BETWEEN EXPERIMENTAL AND CALCULATED MOMENT-CURVATURE RELATIONSHIPS FOR COLUMN B4

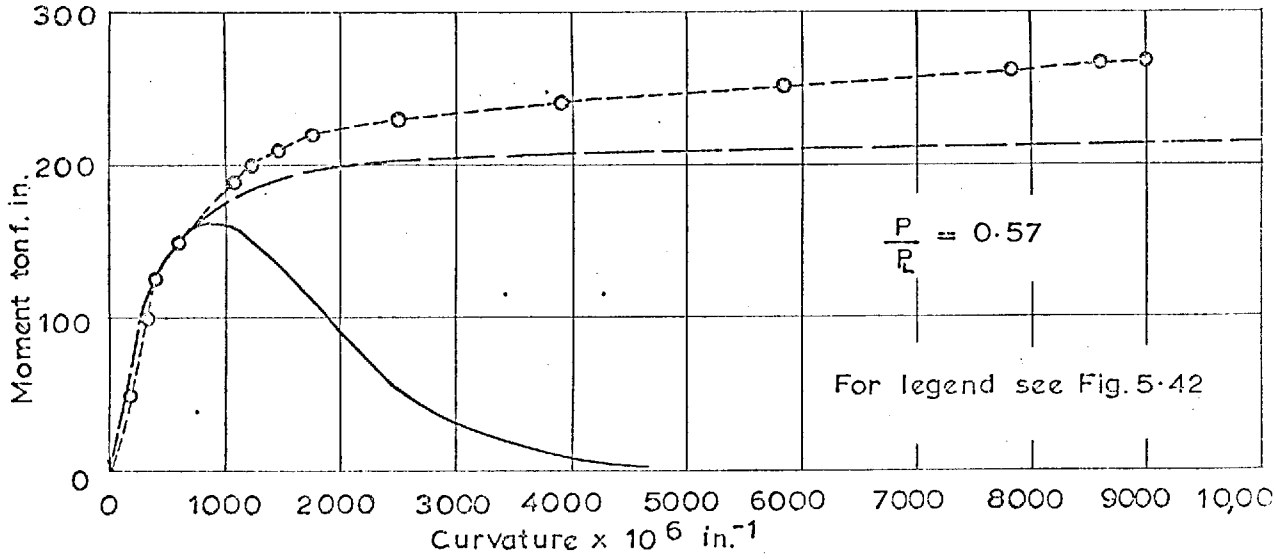

FIG. 5·30 COMPARISON BETWEEN EXPERIMENTAL AND CALCULATED MOMENT-CURVATURE RELATIONSHIPS FOR COLUMN C3

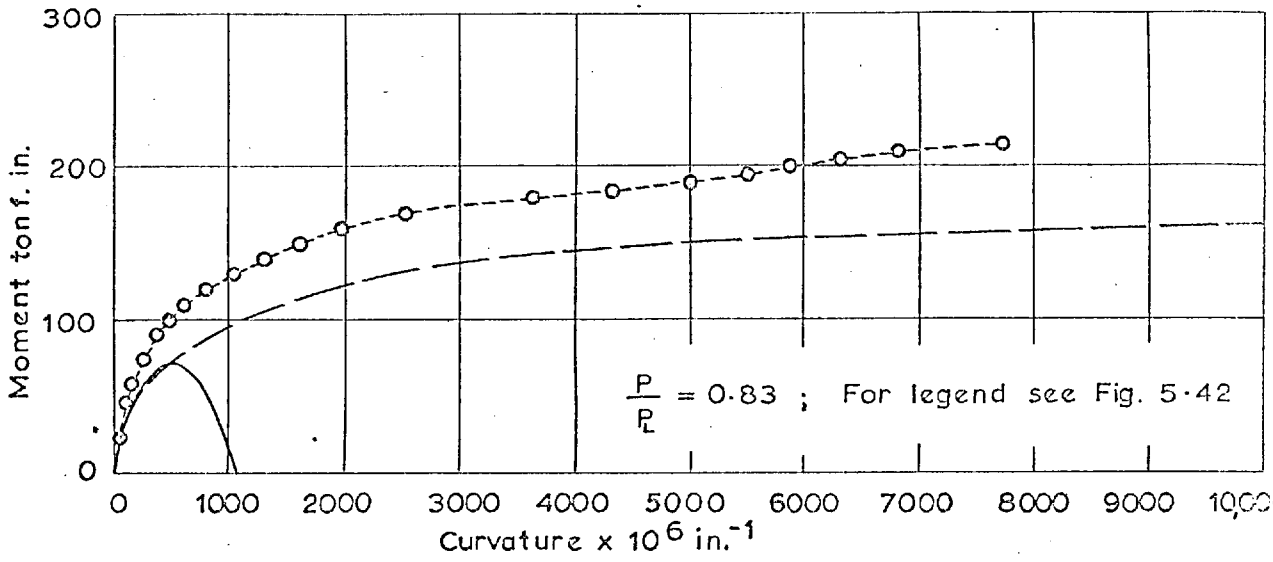

FIG. 5·31 COMPARISON BETWEEN EXPERIMENTAL AND CALCULATED MOMENT-CURVATURE RELATIONSHIPS FOR COLUMN C4.

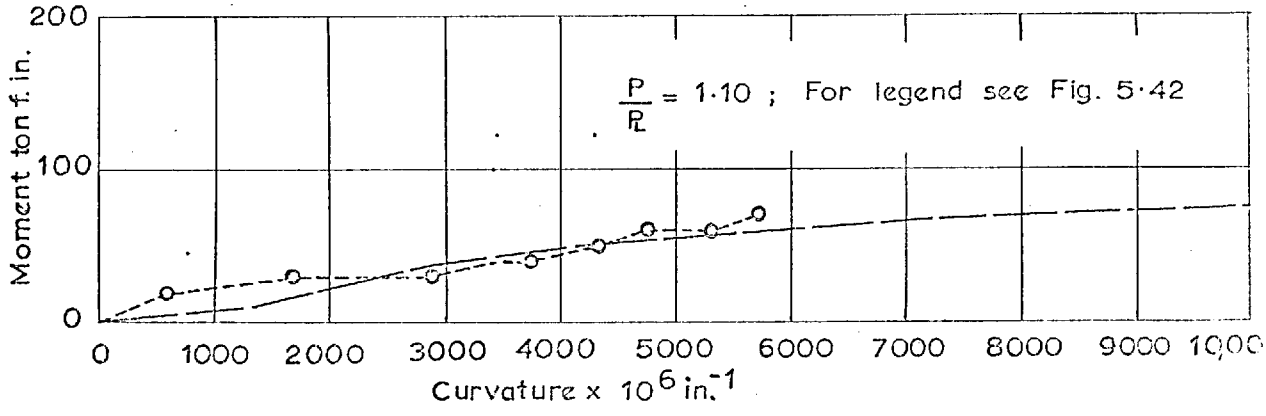

FIG. 5·32 COMPARISON BETWEEN EXPERIMENTAL AND CALCULATED MOMENT-CURVATURE RELATIONSHIPS FOR COLUMN C5.

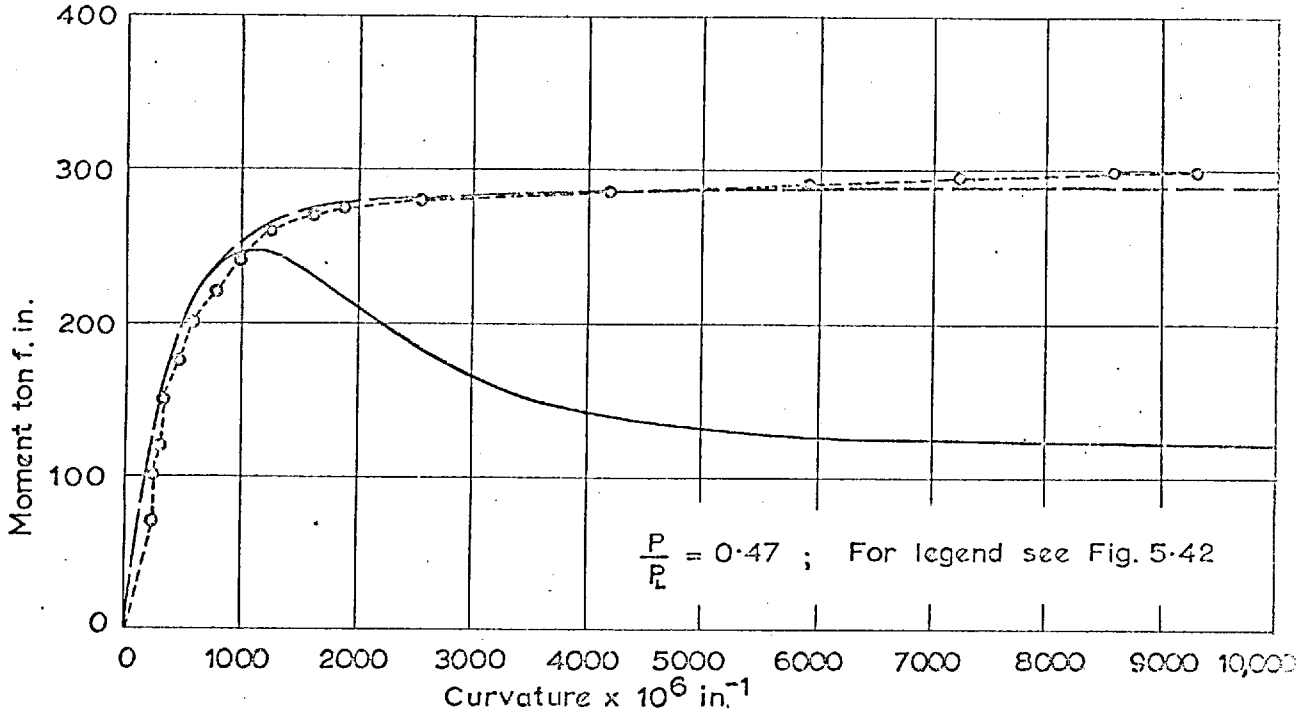

FIG. 5·33 COMPARISON BETWEEN EXPERIMENTAL AND CALCULATED MOMENT-CURVATURE RELATIONSHIPS FOR COLUMN E3

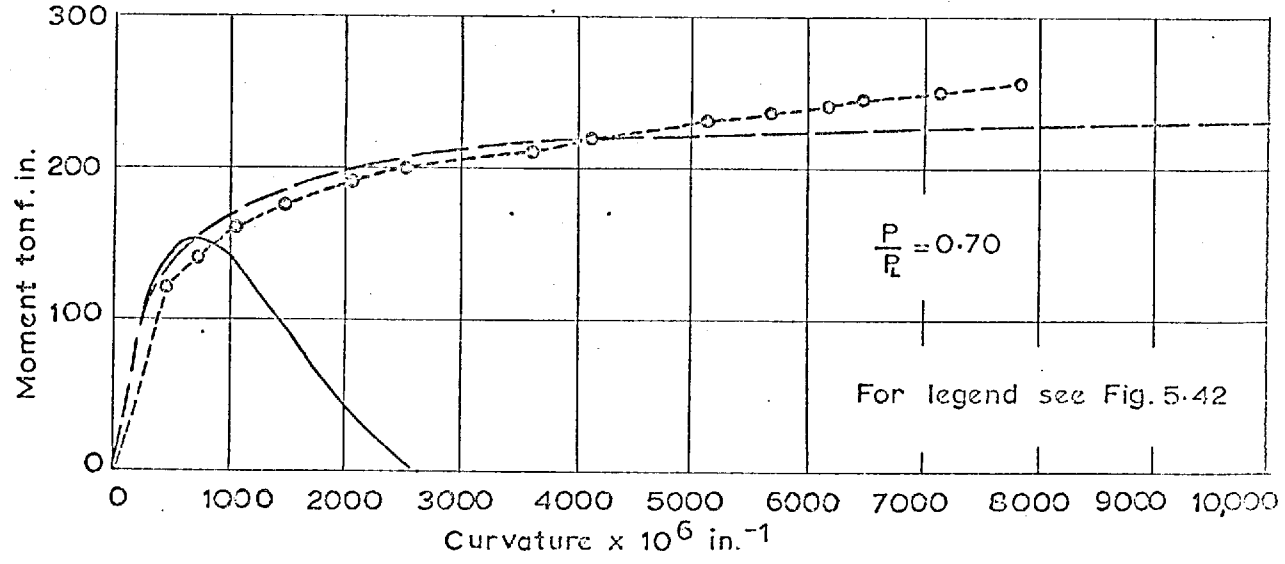

FIG. 5·34 COMPARISON BETWEEN EXPERIMENTAL AND CALCULATED MOMENT-CURVATURE RELATIONSHIPS FOR COLUMN E4

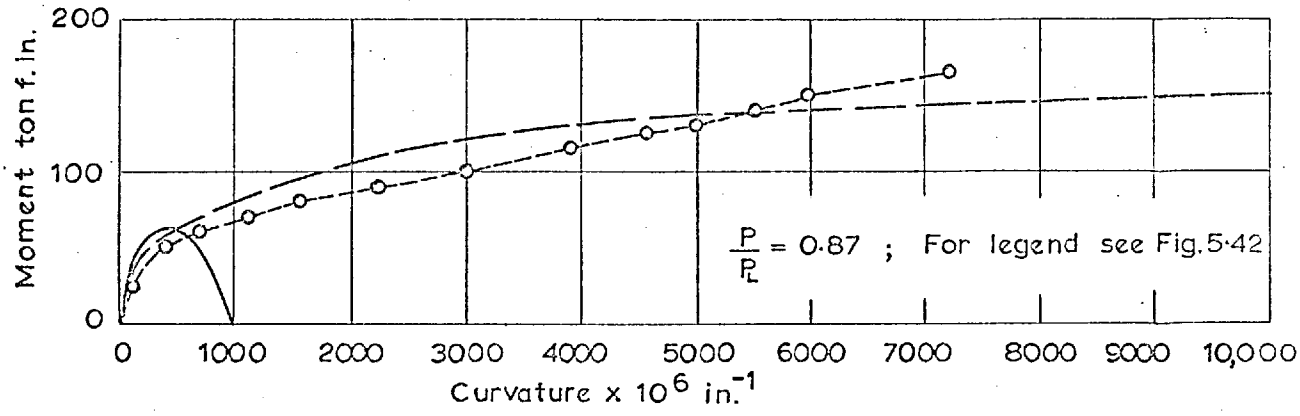

FIG. 5·35 COMPARISON BETWEEN EXPERIMENTAL AND CALCULATED MOMENT-CURVATURE RELATIONSHIPS FOR COLUMN E5

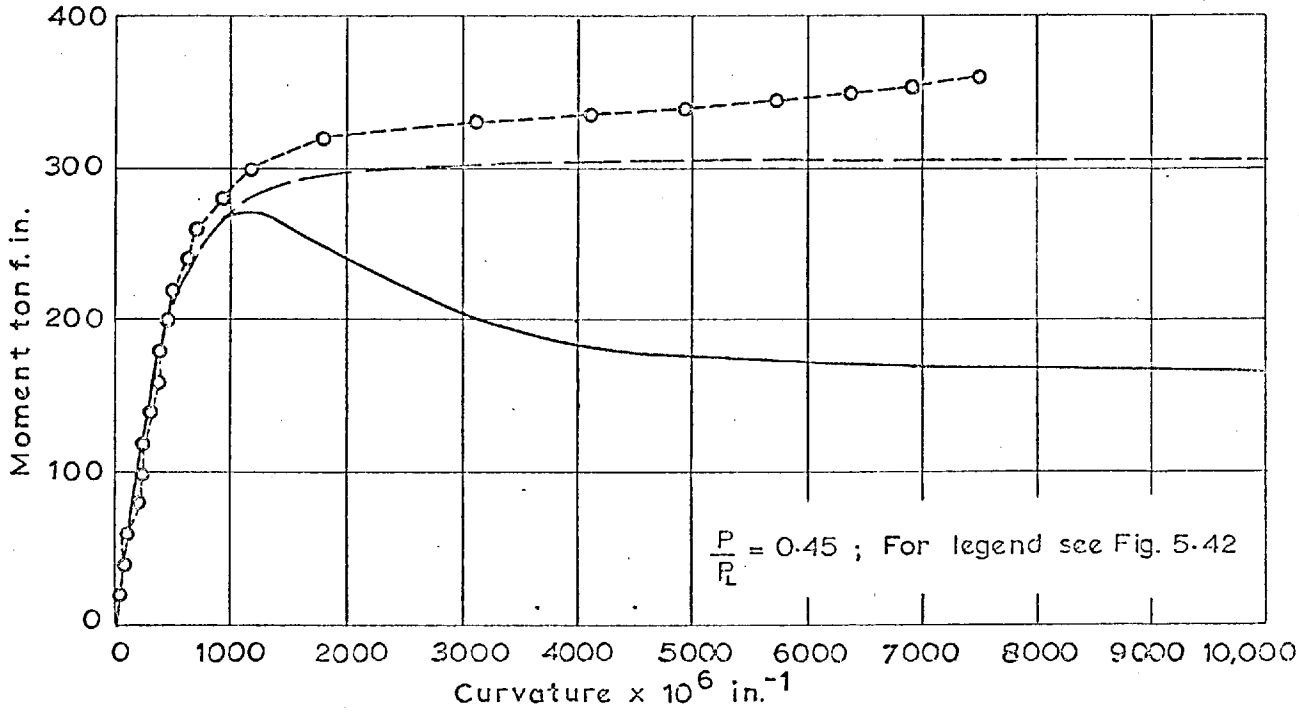

FIG. 5·36 COMPARISON BETWEEN EXPERIMENTAL AND CALCULATED MOMENT-CURVATURE RELATIONSHIPS FOR COLUMN F3.

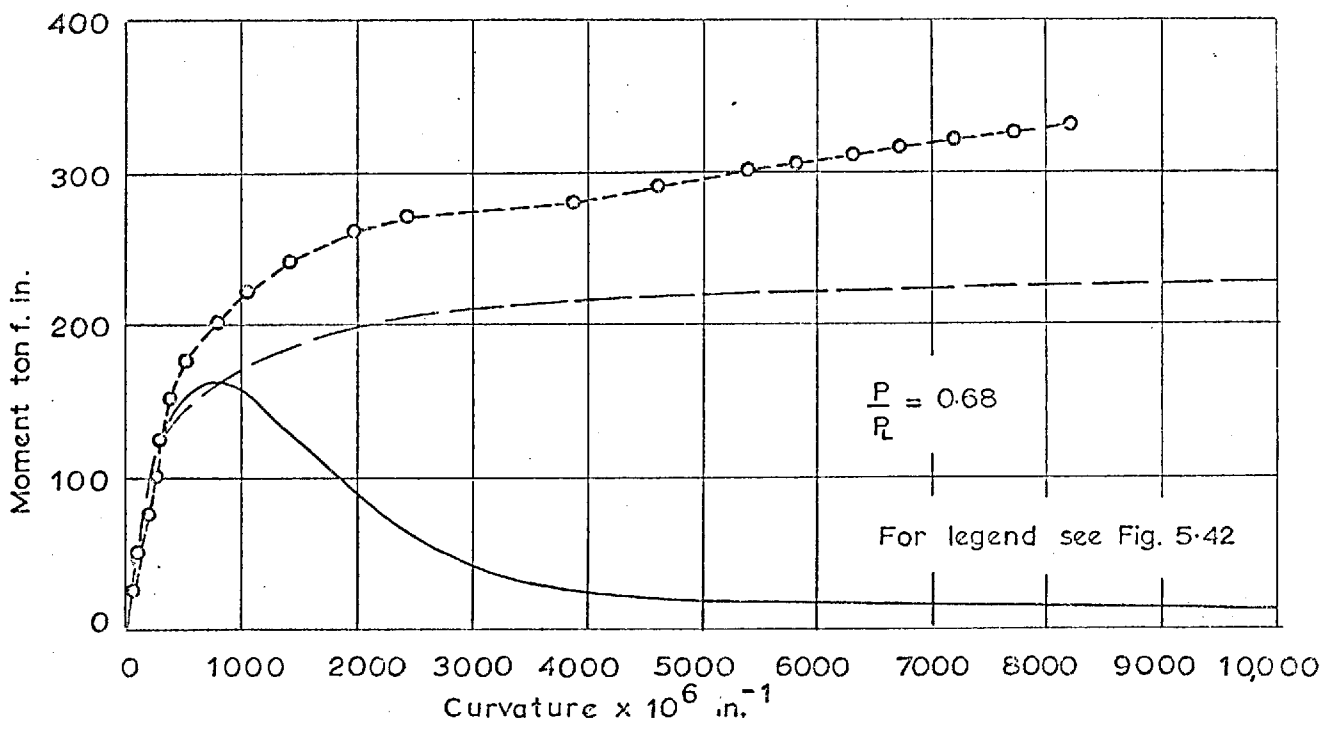

FIG. 5·37 COMPARISON BETWEEN EXPERIMENTAL AND CALCULATED MOMENT-CURVATURE RELATIONSHIPS FOR COLUMN F4

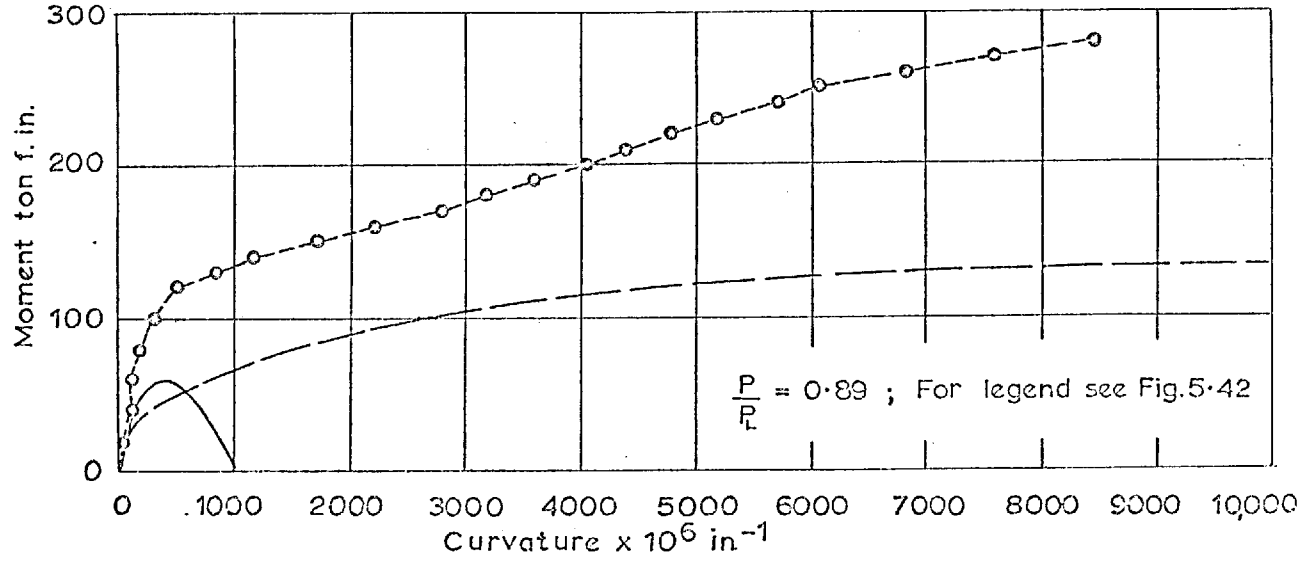

FIG. 5·38 COMPARISON BETWEEN EXPERIMENTAL AND CALCULATED MOMENT-CURVATURE RELATIONSHIPS FOR COLUMN F5

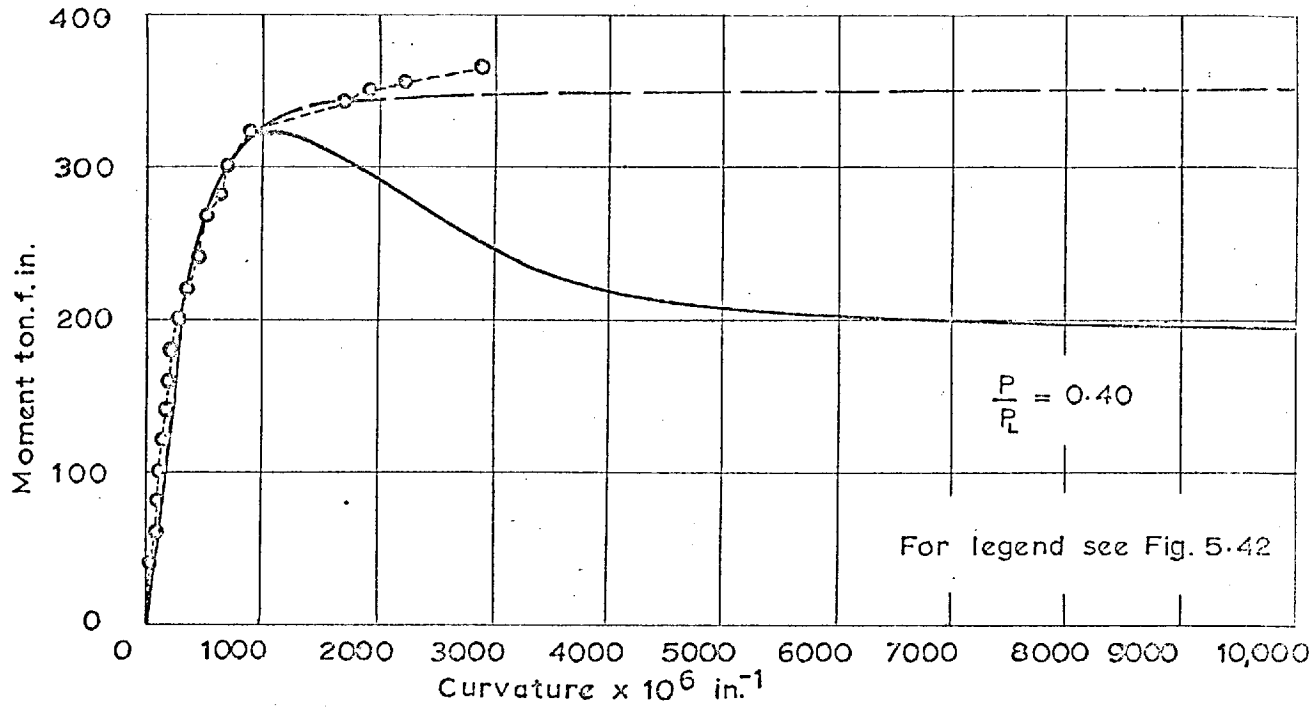

FIG. 5.39 COMPARISON BETWEEN EXPERIMENTAL AND CALCULATED MOMENT-CURVATURE RELATIONSHIPS FOR COLUMN G3.

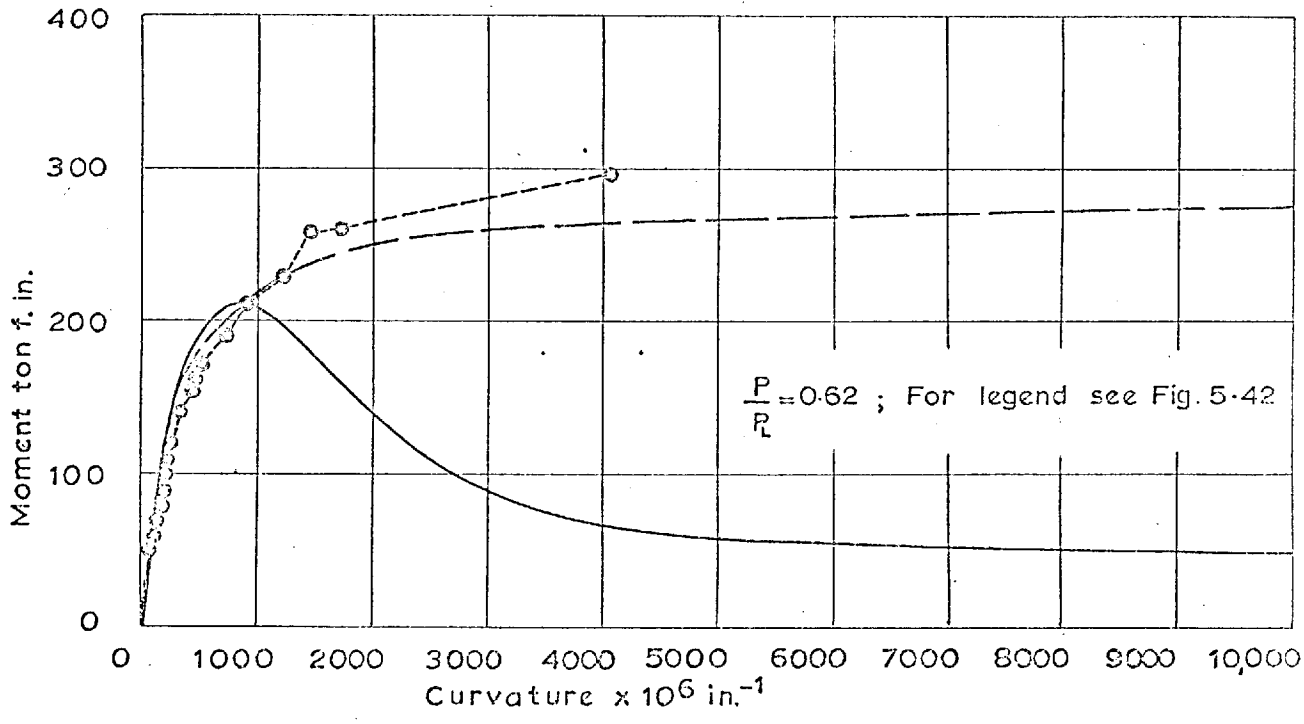

FIG. 5.40 COMPARISON BETWEEN EXPERIMENTAL AND CALCULATED MOMENT-CURVATURE RELATIONSHIP FOR COLUMN G4.

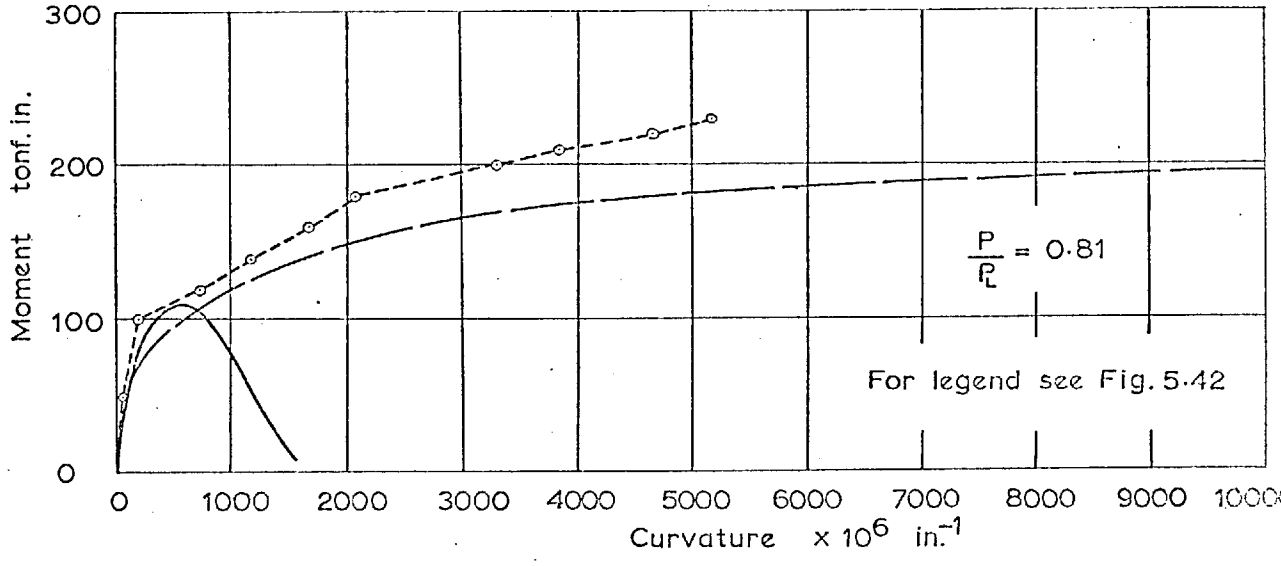

FIG. 5·41 COMPARISON BETWEEN EXPERIMENTAL AND CALCULATED MOMENT - CURVATURE RELATIONSHIPS FOR COLUMN G5

---o-----o--- Experimental moment-curvature relationship

———————— Uniaxial moment-curvature relationship, calculated by using stress-strain relationship 1 for the steel in both tension and compression, and stress-strain relationship 1 for the concrete in compression; concrete takes no tension.

———— ———— Triaxial moment-curvature relationship, calculated by using the following stress-strain relationships:

(1) For the steel:

(a) In compression -

(i) Relationship 1 when $P \leq 0.4\ P_L$

(ii) A linear interpolation for stress between relationships 1 and 2, as P varies between $0.4\ P_L$ and P_u

(b) In tension - Relationship 1 for all values of P

(2) For the concrete:

(a) In compression -

(i) Relationship 2 when $P \leq 0.4\ P_L$

(ii) A linear interpolation for stress between relationships 2 and 3, as P varies between $0.4\ P_L$ and P_u

(b) In tension - concrete takes no tension.

where, $P_L = A_S\ \sigma_y + A_c\ \sigma_m$

$P_u = 0.75\ A_s\ \sigma_y + 2.18\ A_c\ \sigma_m$

Stress-strain relationships are shown in Figure 5.1 for the steel, and in Figure 5.2 for the concrete.

FIG. 5.42 LEGEND USED IN FIGURES 5.25 TO 5.41